MODIFICATION OF FLY ASH STRUCTURE USING CYCLODEXTRIN FOR CONCRETE STRENGTH AND DURABILITY DEVELOPMENT

Bolanle Deborah Ikotun

A thesis submitted to the Faculty of Engineering and the Built Environment, University of Johannesburg, in fulfillment of the requirements for the degree of Doctor Ingeneriae (DIng).

Supervisor: Prof. G. C. Fanourakis

Co – Supervisor: Prof. S. B. Mishra

January, 2016

DECLARATION

I declare that this thesis is my own work. It is being submitted for the degree of Doctor Ingeneriae (DIng) to the University of Johannesburg. It has not been submitted before for any degree or examination in any other University.

(Signature of candidate)

---------- day of ---------- year ----------

ABSTRACT

Fly ash (FA) is a promising industrial waste, which has been used in concrete technology as a cement replacement. However, its utilization is still limited compared to the quantity (approximately 36 million tons per year) of the FA being generated by ESKOM (the major South African electricity producer) as industrial waste. There is a need to improve the utilisation of the large amount of unused FA (approximately 94% of ash generated). The exploitation of the unique chemistry of FA is needed to make it more applicable in concrete, especially with a view to improving early strength and early durability development when it is used in concrete. This study aimed at investigating the effectiveness of using FA-cyclodextrin (an enzymatic modification of starch) composite, a novel composite, to beneficially modify concrete's hydration products and hence increase FA usage in concrete technology.

Fly ash-cyclodextrin (FA-CD) composites were synthesized using two types of cyclodextrins (β and α) and two synthesis methods (physical mixtures and solution mixtures). The chemical structure and the microstructure of these composites were studied using X-ray diffraction (XRD), Fourier transform infrared spectroscopy (FT-IR) and Scanning electron microscope (SEM). In these studies, the additional peaks in the X-ray diffractogram and IR-spectra of the composite materials indicated interaction between the cyclodextrins and FA. The change in the surface morphology, particle size and pore size, between the composite materials and constituent materials were also observed. Since the use of these composites are relatively new in concrete technology, compressive strength, split tensile strength, permeability, water sorptivity and porosity were determined on samples made using two composites synthesis methods with different percentages of β-cyclodextrin (0.1%, 0.2% and 0.5%) and 30% FA on concrete strengths (compressive and split tensile) and durability (permeability, sorptivity and porosity). Based on these tests results, further

investigations were designed using the physical mixture composite, lower percentages of *β*-cyclodextrin (0.025%, 0.05% and 0.1%), 30% FA and 50% FA.

The effects of hydration on the microstructures and structures of FA, *β*-CD and FA-*β*-cyclodextrin (FA-*β*-CD) composite cement paste samples were also studied. The hydrated samples were subjected to XRD, SEM and FT-IR so as to monitor the changes that occurred as hydration progressed. The fresh cement paste viscosity and setting times were investigated to monitor the rheological behaviour of FA, *β*-CD and FA-*β*-CD composite cement paste samples. The effects of FA (30% and 50%), *β*-CD (0.025%, 0.05% and 0.1%) and FA-*β*-CD composite on concrete workability, compressive strength, split tensile strength and durability were studied using twenty four different concrete mixtures. The samples were cured for 7, 14, 28, 90 and 180 days before testing for the strength and cured for 28 and 90 days for durability tests. The durability indicator tests; oxygen permeability, sorptivity and chloride conductivity, were used to study the effects of FA, *β*-CD and FA-*β*-CD composites on concrete durability.

In general, the reaction of FA with cyclodextrin improved FA performance in concrete. The FA-*β*-CD composite at lower percentages of FA (30%) and *β*-CD (0.05%) improved properties such as, early compressive strength, permeability, sorptivity, porosity and chloride conductivity. The study contributed to the knowledge of FA performance using cyclodextrin and promoted the continued inclusion of FA in concrete, which in turn should reduce the environmental pollution resulting from FA on ash dams and carbon dioxide (CO_2) emitted during cement production.

LIST OF PUBLICATIONS

The following articles have been published from this thesis:

- **Ikotun B. D.,** Mishra S., Fanourakis G. C. (2014) **"*Study on the synthesis, morphology and structural analysis of fly ash–cyclodextrin composite"*** Publication in Journal of Inclusion Phenomena and Macrocyclic Chemistry, Imprint: Springer Volume79, pages 311-317.

- **Ikotun B. D.,** Mishra S., Fanourakis G. C. (2014) "***Structural Characterisation of four South African fly ashes and their structural changes with β-cyclodextrin"*** Publication in Particulate Science and Technology, Imprint: Taylor and Francis, Volume 32, Pages 360-365.

- **Ikotun B. D.,** Fanourakis G. C., Mishra S (2014) ***"Indicative tests on the effect of fly ash - β cyclodextrin composite on concrete workability and strength".*** Publication in the RILEM proceedings PRO 95 for the International RILEM Conference on Application of superabsorbent polymers and other new admixtures in concrete construction, at Germany from 14 September 2014 to 17 September 2014. ISBN 978-2-35158-147-6, pages 55 – 64.

- **Ikotun B. D.,** Fanourakis G. C., Mishra S (2014*) **"Indicative tests on the effect of fly ash - β cyclodextrin composite on mortar and concrete permeability, sorptivity and porosity"***. Publication in the proceedings of the first International Conference on Construction Materials and Structures, from 24 November to 26 November 2014, Johannesburg, South Africa. ISBN 978-1-61499-465-7, pages 825 – 834.

DEDICATION

I dedicate this thesis to the Trinity; God almighty for your reign over my life and the strength and grace you gave me to accomplish this research, Jesus Christ for your death on the cross of calvary that gives me access to be saved and the Holy Spirit for being the best friend I could ever have.

ACKNOWLEDGEMENTS

My profound appreciation goes to all the people that God brought my way during the journey of this project. The list is endless but my sincere appreciation goes to the following:

- My supervisors; Prof G.C Fanourakis and Prof S.B Mishra, for your support, encouragement and professional supervision of this work. I have drawn strength from your supervision skills and the constant word of encouragement you always shared with me during our meetings on this project, thank you so much.
- Mr Kayode Adams and Mr Opeoluwa Dada, for the selfless service you render in helping me with the laboratory activities. You are not just my friends you are indeed my brothers.
- The University of South Africa (UNISA), for sponsoring this programme and gave me chance to focus on my research during academic leave.
- My colleagues and supervisors at work (UNISA), I really appreciate your constant encouragement.
- AFRISAM, for the supply of all the aggregates used for this project and the facilities to do all the durability tests.
- Ash resources (Larfage), for the supply of fly ashes used for this project.
- Rolfes sand, for the supply of silica sand used for this project.
- PPC, for the supply of cement used for this project.
- Mr Nick Sfarnas, the laboratory manager of the Civil Engineering Technology Department, University of Johannesburg, for your constant readiness to render assistance in the laboratory, especially when new fabrications were needed to be made purposely for my research. Thank you so much.

- All the laboratory staff at the Civil Engineering Technology Department and Applied Chemistry Department, University of Johannesburg, especially Mr Collin Bulala; thank you for your assistance during the laboratory activities.

- Mr Benedict, Ms Lynda, Mr Bakang, Mr Jeffery and Mr Lucky of AFRISAM Roodeport, for your assistance in the durability and setting time tests.

- Mr M.P Mubiayi and Ms N. Baloyi of materials laboratory, University of Johannesburg, for your assistance in XRF, XRD and SEM analyses.

- To my Pastor and wife, Pastor Gbenga and Titi Ojo of The Pacesetters Church, thank you for your constant prayers.

- To all my friends, especially Mr & Mrs Adams, Mr Aladesanmi, Mr & Mrs Ogunmuyiwa, Mr Ewuola, Dr. Adeleke, Mr Thaimo, Mr & Mrs Adeagbo and Mr Adedokun, for your constant support and encouragement.

- My heartfelt appreciation goes to my wonderful mothers, Mrs E.O Ayeni and Mrs V. Ikotun, your prayers and faith in my success gave me the push that I needed.

- My siblings and in-laws, Mr & Mrs Ariyo, Mr & Mrs Bamitale, Mr & Mrs Ayeni and Mr & Mrs Alagbala, thank you for having so much faith in my success, you have already titled me before I even got the degree, your prayers and constant care have really fuelled my strength.

- To my lovely adopted sister, Angela Motaung, you always play the role of a mother to my kids whenever I had to work overnight. Thank you.

- To my wonderful kids, Queen and King Ikotun. Your hugs, kisses and happiness gave me the motivation that I needed.

Finally, to my lovely husband, Mr A.G Ikotun, You saw greatness in me, even at times when I didn't see myself there. You encouraged me throughout this programme, words are not enough to say thank you for the sacrifices you made to

make this a reality. Unfortunately, death snatched you away from me before I could receive the reward of this labour. Continue to rest in the bossom of the Almighty, your memory continually brings strength and hope to me.

Above all, I surrender all the glory and honour to God. This programme has indeed been a journey, but you saw me through every step of it. Thank you for fulfilling your word in my life that your thoughts toward me are thoughts of peace and not of evil, to give me an expected end. Thank you for the favour, which you bestowed upon me throughout this academic journey.

TABLE OF CONTENTS

LIST OF ABBREVIATIONS

FA	Fly ash
CD	Cyclodextrin
C_3S	Tricalcium silicate
C_2S	Dicalcium silicate
C_3A	Tricalcium aluminate
C_4AF	Tetracalcium aluminoferrite
CSH	Calcium silicate hydrate
W/B	Water-binder ratio
W/C	Water-cment ratio
α-CD	Alpha cyclodextrin
β-CD	Beta cyclodextrin
XRD	X-ray diffraction
FT-IR	Fourier transform infrared spectroscopy
SEM	Scanning electron microscopy
EDS	Energy dispersive X-ray spectrometry

LIST OF FIGURES

LIST OF TABLES

APPENDIX A TABLES

APPENDIX B TABLES

CHAPTER ONE

INTRODUCTION

Coal firing for power generation produces millions of tons of ash and related by–products. Current annual production of coal ash worldwide is estimated at around 600 million tones, with fly ash (FA) constituting about 500 million tons at 75-80 % of the total ash produced [1]. The main source of power generation in South Africa is the coal combustion at power stations [2, 3], which are located in close vicinity of the coalfields, all in the north of the country (Gauteng, Mpumalanga, Limpopo and Free State). A vast quantity of coal ash (3-6 million tons) arises at individual power stations [4]. Most South African power stations are owned and operated by ESKOM, and are responsible for 95% of all the electricity produced in South Africa. ESKOM generated approximately 36.01 million tons of ash in 2010, 36.2 million tons in 2011, 36.2 million tons in 2012, 35.3 million tons in 2013 and 34.97 million tons in 2014 of which 5.6%, 5.5%, 6.4%, 6.8% and 7.0% was used in the respective years [5]. The remaining ash is safely disposed of and managed at ash dams and dumps adjacent to the power stations. Considering the amount that remains unused, there is need to develop new applications for this material. Development of new applications will depend on the quality of the FA produced and the understanding of its chemistry.

Research on FA has been on-going worldwide. The approach used by South Africa was to first characterize FA from different sources in terms of chemical composition, morphology and mineralogy. The reported findings showed that the ash was high in alumina and silica with moderate amount of calcia and ferrate and low in alkalis [4]. According to the historical background on the utilization of coal ash in South Africa, done by Kruger and Krüeger [4], the initial tests in cement and concrete confirmed the pozzolanic potential of South African FA, which led to the introduction of blended cement in the country with between 15 and 35% (by mass), of classified FA.

In the polymer industry, it has also been shown that specially manufactured FA can be used to replace some of the functional filler used [6]. The synergistic effect of FA and other fillers forms a superior product in rubber. Also, addition of FA as a soil ameliorant has proven to significantly increase crop yield in agriculture [1]. In the mining industry, FA has been found useful in underground mine supports on gold mines. Fissure grouting also utilizes FA to reduce viscosity and enables more effective sealing. Its utilization for the neutralization of acid mine drainage and simultaneous manufacture of zeolite has also been established [2]. Research also indicated that FA could be used to replace or augment limestone for stone dusting in underground mining. The possible utilization of FA was attributed to its characteristics e.g. spherical shape, pozzolanicity, low alkali content and low carbon content.

Despite the wide range of research and interest that has gone into FA, the exploitation of its unique chemistry is needed to make it more applicable in concrete. Several researchers have explored the use of different polysaccharides in improving concrete rheology and late strength [7-11]. Research has shown that when polysaccharides are used optimally (0.5% of cement) in concrete, they retard setting time, improve fluidity and workability and give higher final concrete compressive strengths [7-9]. However, when not optimally used, polysaccharides can have a detrimental effect on concrete which is attributed to the adsorption of the polysacharrides (high carbohydrate contents) to the surfaces of the hydrated and/or anhydrous phases of cement [12-15]. Most of the research done in this area focused on using the polysaccharides as an organic admixture to normal concrete not to blended cement concrete. To improve FA usage in construction, extensive study is needed to explore the possibility of modifying FA structure through the modification of its hydration/pozzolanic products using a compound with less carbohydrate than a polysaccharide. Oligosaccharides, have a lesser carbohydrate content than polysaccharide and their effect on blended cement (FA) concrete was explored in this project. The oligosaccharide, which was used for this study is cyclodextrin. This

study was aimed at investigating the effectiveness of using FA-cyclodextrin composite to modify concrete's hydration products and hence concomitantly increasing FA usage in concrete technology.

Cyclodextrins (CDs) are cyclic oligosaccharides, formed by the enzymatic modification of starch. The three common types of cyclodextrins (α-CD, β-CD and γ-CDs) are referred to as the natives CDs [16-17]. α, β and γ-cyclodextrins are composed of six, seven and eight α-(1,4)-linked glycosyl units, respectively as shown in Figure 1.1 [16]. β-CD is commonly used because of its favourable complex-forming abilities and low cost [16-17]. The main property of cyclodextrins that has exposed them to variety of use and research is their ability to form inclusion complexes. Due to their inclusion-complex-forming capability (host–guest complexes) with a very wide range of solid, liquid and gaseous compounds by a molecular complexation, the properties of the materials with which they complex can be modified significantly [16]. Complexes can be formed either in solution or in the crystalline state and water is typically the solvent of choice. The fitness of the guest molecule into the cyclodextrin cavity is one of the decisive factors for the inclusion complexes [17]. Each year cyclodextrins are the subject of almost 1000 research articles and scientific abstracts, large numbers of which deal with drugs and drug-related products [16]. The application of cyclodextrin in modifying construction materials has been sparingly reported in open literature.

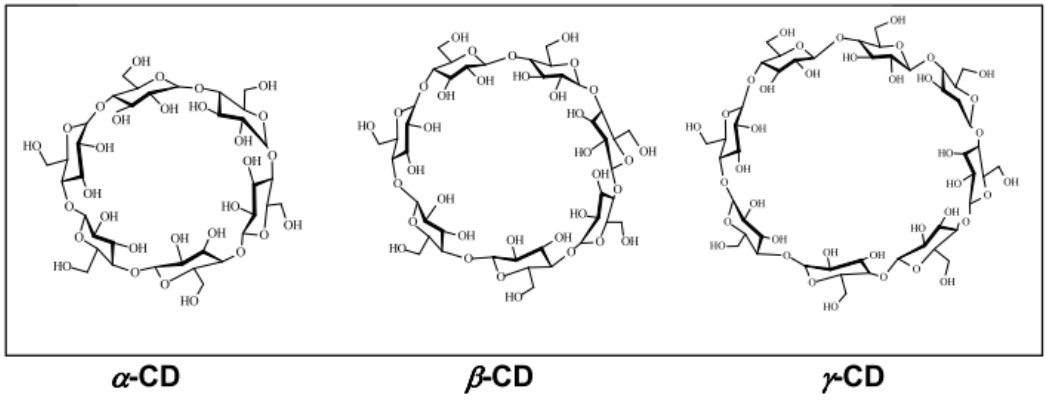

Figure 1.1: Cyclodextrin Structure [16]

1.1 BACKGROUND: WHY FLY ASH?

The focus of research on FA has both environmental relevance and industrial interest. Most of the FA produced is disposed as landfill, which is a cause of environmental concern. Findings by other researchers [1,3,18,19] have shown the potential use of FA in the cement and concrete industry, mining industry, agricultural sector and water engineering. The concrete industry is believed to contribute 5 % to 8 % of the CO_2 emissions [20, 21]. Cement production involves high energy consumption and the cement industry relies heavily on coal. The industry's heavy reliance on coal leads to high emission levels of CO_2, nitrous oxide, and sulfur, among other pollutants [20]. Calcination of limestone, which involves the breaking down of calcium carbonate when heated into calcium oxide (CaO) and carbon dioxide (CO_2) also contributes to 50% of the CO_2 emitted during cement production [22]. Hence, the need to investigate the use of industrial waste materials to achieve greenhouse gas reduction goals. One of the industrial wastes that is in abundance in South Africa and needs comprehensive research is coal FA. Fly does not need high energy consumption process for its usage as cement in concrete, therefore reduces the emission of CO_2 and other pollutants.

The study contributes to the knowledge of FA performance using cyclodextrin and promoted the continued inclusion of FA in concrete, which in turn will reduce the environmental pollution resulting from FA on ash dams and carbon dioxide (CO_2) that emits during cement production. This contribution is aligned with sustainable development principles.

1.2 AIM AND OBJECTIVES

The aim of this research was to explore the possibility of modifying concrete's hydration products using FA-β-cyclodextrin composite for optimum strength and durability development. The study was driven by the following objectives:

- To understand the chemical and mineral composition of Class F South African fly ashes.
- To study the compatibility of cyclodextrins and FA.
- To establish an appropriate cyclodextrin-fly ash composite sample preparation for optimum result.
- To characterize the properties of new formed composite (fly ash-cyclodextrin) using different microstructural and analytical test methods (scanning electron microscopy **(**SEM), X-ray diffraction (XRD) and Fourier transform infrared spectroscopy **(**FT-IR)).
- To optimize the dosages of cyclodextrin and fly ash present in the new-formed composite (fly ash-cyclodextrin).
- To determine the effect of FA, cyclodextrin and the new-formed composite on concrete hydration, viscosity, setting times, strength and durability.

1.3 ORGANISATION OF THESIS AND METHODOLOGY

The thesis is organised as follows:

Chapter 2 presents the literature review on concrete constituents, chemistry of FA, fly ash modification, *β*-cyclodextrin in concrete, properties of pozzolanic concrete and concrete microstructure.

Chapter 3 presents the analyses and discusses the characterisation of four South African fly ashes and their modification with *β*-cyclodextrin. This chapter gives the background of the composite formed as a result of FA and cyclodextrin interaction. The characterisation was based on XRD and FT-IR.

Chapter 4 presents the analyses and discusses the study on the synthesis, morphology and structural analysis of fly ash-cyclodextrin composite. Further study on the characteristics of FA-CD composite was looked into using a different fly ash from Matla power station. Further characterisation was done on two different composites mixtures procedure based on XRD, SEM and FT-IR.

Chapter 5 presents the analyses and discusses the indicative tests on the effect of fly ash-*β*-cyclodextrin (FA-*β*-CD) composites on mortar/concrete workability, strength and durability, which gave further guidance to the research due to the novelty of the composite.

Chapter 6 presents the analyses and discusses the effect of FA, *β*-CD and FA-*β*-CD composites on the structure and microstructure of hydrated cement paste samples. Hydrated samples were subjected to XRD, SEM and FT-IR analyses so as to monitor the structural and microstructural changes that had occurred as hydration progressed.

Chapter 7 presents the analyses and discusses the effect of FA, *β*-CD and FA-*β*-CD composites on cement paste viscosity and setting times. The rheological behaviour of cement paste samples was investigated.

Chapter 8 presents the analyses and discusses the effect of FA, *β*-CD and FA-*β*-CD composites on concrete workability and strength. Compressive and split tensile strengths were investigated on twenty four different concrete mixtures.

Chapter 9 presents the analyses and discusses the effect of FA, *β*-CD and FA-*β*-CD composites on concrete durability. Durabilty tests based on the three durability index tests; oxygen permeability, sorptivity and chloride conductivity were used.

Chapter 10 concludes the contributions of this research and suggests recommendations for future research work.

1.4 REFERENCES

[1] Ahmaruzzaman A.: Review on the utilization of fly ash. Progress in Energy and Combustion Science **36**, 327–363 (2010).

[2] Petrik L. F., White R.A, Klink M.J, Somerset V.S, Burgers C.L, Fey M.V.: Utilisation of South African fly ash to treat acid coal mine drainage and production of high quality zeolites from the residual solids. International Ash Utilisation symposium, oct 20-22, 2003, Center of Applied Energy research, University of Kentucky, USA.

[3] Bada S., Potgieter V.: Evaluation and treatment of coal ash for adsorption application. Leonardo Electronic Journal To Practices and Technologies **12**, 37 (2008).

[4] Kruger R. A., Krüeger J. E.: Historical development of coal ash utilization in South Africa. World of coal ash (WOCA), April 11-15, 2005, Lexington, Kentucky, USA.

[5] ESKOM 2014. ESKOM integrated report 2014, http://integratedreport.ESKOM.co.za/pdf/full-integrated.pdf (CITED: 28/11/2014).

[6] Merwe E. M. V., Prinsloo L. C., Kruger R. A., Mathebula L. C.: Characterisation of coal fly ash modified by sodium lauryl sulphate. World of coal ash (WOCA) conference, May 9-12, 2011, in Denver, co, USA.

[7] Peschard A., Govin A., Grosseau P., Guilhot B., Guyonnet R.: Effect of polysaccharides on the hydration of cement paste at early ages. Cement and Concrete Research **34**, 2153–2158 (2004).

[8] Peschard A., Govin A., Pourchez J., Fredon E., Bertrand L.: Maximilien S., Guilhot B.: Effect of polysaccharides on the hydration of cement suspension. Journal of the European Ceramic Society **26**, 1439–1445 (2006).

[9] Friedemann K., Stallmach F., Kärger J.: Carboxylates and sulfates of polysaccharides for controlled internal water release during cement hydration. Cement and Concrete Composites **31**, 244–249 (2009).

[10] Patural L., Marchal P., Govin A., Grosseau P., Ruo B., Devès O.: Cellulose ethers influence on water retention and consistency in cement-based mortars. Cement and Concrete Research **41**, 46–55 (2011).

[11] Lasheras-Zubiate M., Navarro-Blasco I., Fernández J.M., Álvarez J.I.: Effect of the addition of chitosan ethers on the fresh state properties of cement mortars. Cement and Concrete Composites **34**, 964–973 (2012).

[12] Pourchez J., Govin A., Grosseau P., Guyonnet R., Guilhot B., Ruot B.: Alkaline stability of cellulose ethers and impact of their degradation products on cement hydration. Cement and Concrete Research **36**, 1252–1256 (2006).

[13] Phan T.H., Chaouche M., Moranville M.: Influence of organic admixtures on the rheological behaviour of cement pastes. Cement and Concrete Research **36**, 1807–1813 (2006).

[14] Pourchez J., Grosseau P., Ruot B.: Changes in C_3S hydration in the presence of cellulose ethers. Cement and Concrete Research **40**, 179–188 (2010).

[15] Hua O.Z., Guo M.B., Wei J.S.: Influence of cellulose ethers molecular parameters on hydration kinetics of Portland cement at early ages, Construction and Building Materials **33**, 78–83 (2012).

[16] Martin Del Valle E.: Cyclodextrins and their uses: a review. Process Biochemistry **39**, 1033–1046 (2004).

[17] Castro E., Barbiric D.: Current theoretical methods applied to study cyclodextrins and their complexes. The journal of the Argentiane Chemical Society **90** (4/6), 1-44 (2002).

[18] Cetina B., Aydilek A.H., Guney Y.: Stabilization of recycled base materials with high carbon fly ash Resources. Conservation and Recycling **54**, 878–892 (2010).

[19] Rao C., Stehly R.D, Ahmad Ardani P.E.: IPRF Research Report Innovative Pavement Research Foundation Airport Concrete Pavement Technology Program Report IPRF-01-G-002-06-2 Handbook for Proportioning Fly Ash as Cementitious Material in Airfield Pavement Concrete Mixtures (2011).

[20] Wilson A.: Cement and Concrete: Environmental considerations. Environmental building news **2** No. 2 (1993).

[21] Malhotra V.M.: Role of supplementary cementing materials in reducing greenhouse gas emissions. Concrete Technology for a sustainable development in the 21st Century edited by O.E Gjorv and K. Sakai. Published by E and FN Spon, London EC4P 4EE, UK. ISBN: 0 419 25060 3, 226-236 (2000).

[22] Koch J., Dayan U., Mey-Marom A.: Inventory of emissions of greenhouse gases in Israel. Water, Air, and Soil Pollution **123**, 259–271 (2000).

CHAPTER TWO

LITERATURE REVIEW

The versatility of concrete stands it out as the most widely used construction material in the world. A composite material is produced when two or more constituent materials with different physical or chemical properties are combined together to make a material with different characteristics from the individual components. Concrete is a composite made up of cement, aggregates (fine and coarse) and water, while mortar is made up of cement, fine aggregate and water. The quality of concrete is directly connected to the quality of the constituent materials, mixing procedures and curing [1]. Cement, a binding material in concrete is manufactured from argillaceous limestone and requires extensive heat in its manufacturing. The extreme heat required for cement production makes it to account for about 5% to 8% of global carbon dioxide (CO_2) emissions [2-3]. The high emission of CO_2 generated from cement production has been of a great concern to researchers in concrete industry and has resulted in series of investigations into replacing part of the cement used in concrete production with extenders [4-16]. Pozzolans are alumino-silicate materials, which react with calcium hydroxide, when being used to replace cement, in the presence of water to produce compounds that possess cementitious properties [16-19]. This reaction is called pozzolanic reaction. Improved concrete strength and durability has been reported [6, 20-25] with pozzolans when use optimally in concrete. The most common pozzolans that have gained attention in South Africa and have been included in cements tagged "blended cements" are fly ash (FA) and condensed silica fume [26-32]. However, increasing accumulation of fly ash as landfills, with little usage requires further study on its chemistry to make it a better material for construction purposes. This chapter provides an overview of concrete constituents, chemistry of fly ash, fly ash modification, β-cyclodextrin in concrete, properties of pozzolanic concrete and concrete microstructure.

2.1 CONSTITUENTS OF CONCRETE

Concrete is made up of a mixture of cement, aggregates (fine and coarse) and water. Different cement types produced in South Africa are shown in Table 2.1 [33]. The percentages of siliceous fly ash in Portland-fly ash cements range between 6 – 35%. Concrete that included pozzolan in its production is referred to as pozzolanic concrete in this thesis. The organic admixture will also be discussed as part of concrete constituents.

2.1.1 Cement

Cement is the lime based, fine mineral powder material, which has the ability of bonding particles of solid matter into a compact whole in the presence of water. Cement in concrete, plays the major role of binding all other constituent materials together. The raw materials for producing cement are limestones (calcium carbonate) and argillaceous materials like shale and clay. A small quantity of gypsum (calcium sulphate) is added during the final grinding process of clinker to regulate the rate of hardening of the cement. The following are the major constituents of Portland cement [34 - 36], any calcium that remains unreacted is present as free lime (CaO):

- $4CaO.Al_2O_3.Fe_2O_3$ (C_4AF)
- $3CaO.Al_2O_3$ (C_3A)
- $2CaO.SiO_2$ (C_2S)
- $3CaO.SiO_2$ (C_3S)

The general Portland cement clinker composition is presented in Table 2.2.

Table 2.1: Common South African Cements [33]

Main types	Notation of products (types of common cement)		Composition, percentage by mass[a]										
			Clinker	Blast-furnace slag	Silica fume	Pozzolana		Fly ash		Burnt shale	Limestone		Minor additional constituents
			K	S	D[b]	Natural P	Natural calcined Q	Siliceous V	Calcareous W	T	L	LL	
CEM I	Portland cement	CEM I	95 - 100	-	-	-	-	-	-	-	-	-	0 - 5
CEM II	Portland-slag cement	CEM II A-S	80 - 94	6 - 20	-	-	-	-	-	-	-	-	0 - 5
		CEM II B-S	65 - 79	21 - 35	-	-	-	-	-	-	-	-	0 - 5
	Portland-silica fume cement	CEM II A-D	90 - 94	-	6 - 10	-	-	-	-	-	-	-	0 - 5
	Portland-pozzolana cement	CEM II A-P	80 - 94	-	-	6 - 20	-	-	-	-	-	-	0 - 5
		CEM II B-P	65 - 79	-	-	21 - 35	-	-	-	-	-	-	0 - 5
		CEM II A-Q	80 - 94	-	-	-	6 - 20	-	-	-	-	-	0 - 5
		CEM II B-Q	65 - 79	-	-	-	21 - 35	-	-	-	-	-	0 - 5
	Portland-fly ash cement	CEM II A-V	80 - 94	-	-	-	-	6 - 20	-	-	-	-	0 - 5
		CEM II B-V	65 - 79	-	-	-	-	21 - 35	-	-	-	-	0 - 5
		CEM II A-W	80 - 94	-	-	-	-	-	6 - 20	-	-	-	0 - 5
		CEM II B-W	65 - 79	-	-	-	-	-	21 - 35	-	-	-	0 - 5
	Portland-burnt shale cement	CEM II A-T	80 - 94	-	-	-	-	-	-	6 - 20	-	-	0 - 5
		CEM II B-T	65 - 79	-	-	-	-	-	-	21 - 35	-	-	0 - 5
	Portland-limestone cement	CEM II A-L	80 - 94	-	-	-	-	-	-	-	6 - 20	-	0 - 5
		CEM II B-L	65 - 79	-	-	-	-	-	-	-	21 - 35	-	0 - 5
		CEM II A-LL	80 - 94	-	-	-	-	-	-	-	-	6 - 20	0 - 5
		CEM II B-LL	65 - 79	-	-	-	-	-	-	-	-	21 - 35	0 - 5
	Portland-composite cement[c]	CEM II A-M	80 - 94	←				6 - 20			→		0 - 5
		CEM II B-M	65 - 79	←				21 - 35			→		0 - 5
CEM III	Blastfurnace cement	CEM III A	35 - 64	36 - 65	-	-	-	-	-	-	-	-	0 - 5
		CEM III B	20 - 34	66 - 80	-	-	-	-	-	-	-	-	0 - 5
		CEM III C	5 - 19	81 - 95	-	-	-	-	-	-	-	-	0 - 5
CEM IV	Pozzolanic cement[c]	CEM IV A	65 - 89	-	←		11 - 35		→	-	-	-	0 - 5
		CEM IV B	45 - 64	-	←		36 - 55		→	-	-	-	0 - 5
CEM V	Composite cement[c]	CEM V A	40 - 64	18 - 30	-	←	18 - 30	→		-	-	-	0 - 5
		CEM V B	20 - 39	31 - 50	-	←	31 - 50	→		-	-	-	0 - 5

Notes

(a) The values in the table refer to the sum of the main and minor additional constituents.

(b) The proportion of silica fume is limited to 10%.

(c) In portland-composite cements CEM II A-M and CEM II B-M, in pozzolanic cements CEM IV A and CEM IV B, and in composite cements CEM V A and CEM V B, the main constituents other than clinker shall be declared by designation of the cement.

Table 2.2: General composition of Portland cement clinker [37]

Oxide	% by mass in cement
CaO	63 – 69
SiO_2	19 – 24
Al_2O_3	4 – 7
Fe_2O_3	1 – 6
MgO	0.5 – 3.6
$Na_2O + 0{,}658\ K_2O$	0.2 – 0.8

Tricalcium silicate and dicalcium silicate compounds are responsible for the development of strength of cement paste [35, 38], while tricalcium silicate is the most important for strength development up to 28 days. Hydration reaction of cement compounds (C_3S and C_2S) with water produces calcium hydroxide and calcium silicate hydrate [36]. Calcium silicate hydrate (C-S-H) causes the stiffening of the paste, subsequent hardening and strength development. The presence of calcium hydroxide ($Ca(OH)_2$) causes high alkalinity of pore solution [39].

Tricalcium aluminate and gypsum have important influence on durability [40]. Hydration of calcium aluminate in the presence of gypsum produces ettringite and then monosulphate on further hydration [41]. Ettringite is voluminous and causes expansion and distress in concrete and is more detrimental with respect to strength and durability in hardened concrete. Therefore, cement with limited amounts of tricalcium aluminate is necessary to control further formation of ettringite in hardened concrete [40]. Hydration of tetracalcium aluminoferrite in the presence of gypsum is similar to that calcium aluminate, as the iron content increases, the rate of hydration decreases. The iron contents are the iron impurities, which are present in the raw materials. The rate of hydration is influenced majorly by the cement type, water/cement ratio (W/C) and curing temperature. The hydration reaction of individual cement compounds is represented by Equations (2.1) to (2.4).

Hydration reaction:

For tricalcium silicate,

$$\underbrace{2(3CaO.SiO_2)}_{C_3S} + \underbrace{6H_2O}_{H} \rightarrow \underbrace{3CaO.2SiO_2.3H_2O}_{C-S-H} + \underbrace{3Ca(OH)_2}_{C-H} \quad (2.1)$$

For dicalcium silicate,

$$\underbrace{2(2CaO.SiO_2)}_{C_2S} + \underbrace{4H_2O}_{H} \rightarrow \underbrace{3CaO.2SiO_2.3H_2O}_{C-S-H} + \underbrace{Ca(OH)_2}_{C-H} \quad (2.2)$$

For tricalcium aluminate,

$$\underbrace{3CaO.Al_2O_3}_{C_3A} + \underbrace{3CaSO_4.2H_2O}_{C_3\bar{S}H\,(gypsum)} + 26H_2O \rightarrow \underbrace{3CaO.Al_2O_3.3CaSO_4.32H_2O}_{Ettringite} \quad (2.3)$$

$$\underbrace{2(3CaO.Al_2O_3)}_{C_3A} + \underbrace{3CaO.Al_2O_3.3CaSO_4.32H_2O}_{Ettringite} + 4H_2O \rightarrow 3(\underbrace{3CaO.Al_2O_3.CaSO_4.12H_2O}_{monosulphate}) \quad (2.4)$$

From Equation 2.4, monosulphate is the final hydration product of C_3A.

The setting and hardening of cement paste is brought about by the formation of calcium silicate hydrate (C-S-H) gel during the hydration reaction [42], which fills the capillary pores and increases strength. Formation of calcium hydroxide ($Ca(OH)_2$) results in a high alkalinity of the pore solution. It has also been noted that calcium hydroxide will further react with carbon dioxide in air to form calcium carbonate [43].

2.1.2 Aggregates

Aggregates are natural sands or particles from crushed rock, which are mixed together with cement and water to produce concrete. Aggregates used in concrete fall in two categories; fine aggregate and coarse aggregate. Fine aggregate (sand) are

natural sand or crushed rock particles that pass through a 4.75 mm sieve, while coarse aggregates (stone) are particles greater than 4.75 mm but generally range between 9.5 mm and 37.5 mm. Aggregate helps to reduce the cost of concrete and improves the dimensional stability of the hardened concrete. Almost 75% of concrete is made up of aggregates, therefore their physical, thermal and chemical properties influence the strength and durability of concrete [1, 44]. The work done by Poon and Lam [45] on the effect of aggregate-to-cement ratio and type of aggregate on the properties of pre-cast concrete blocks showed that the strength of concrete was directly proportional to the crushing strength of the aggregate. The interfacial zone between aggregates and cement paste matrix is regarded as the most sensitive area within the concrete structure [46]. It is the weakest zone in a concrete mass. These zones are normally lower in density than the hydrated cement matrix. The aggregate characteristics that affect concrete properties as illustrated by Mehta and Monteiro [47] are as shown in Figure 2.1.

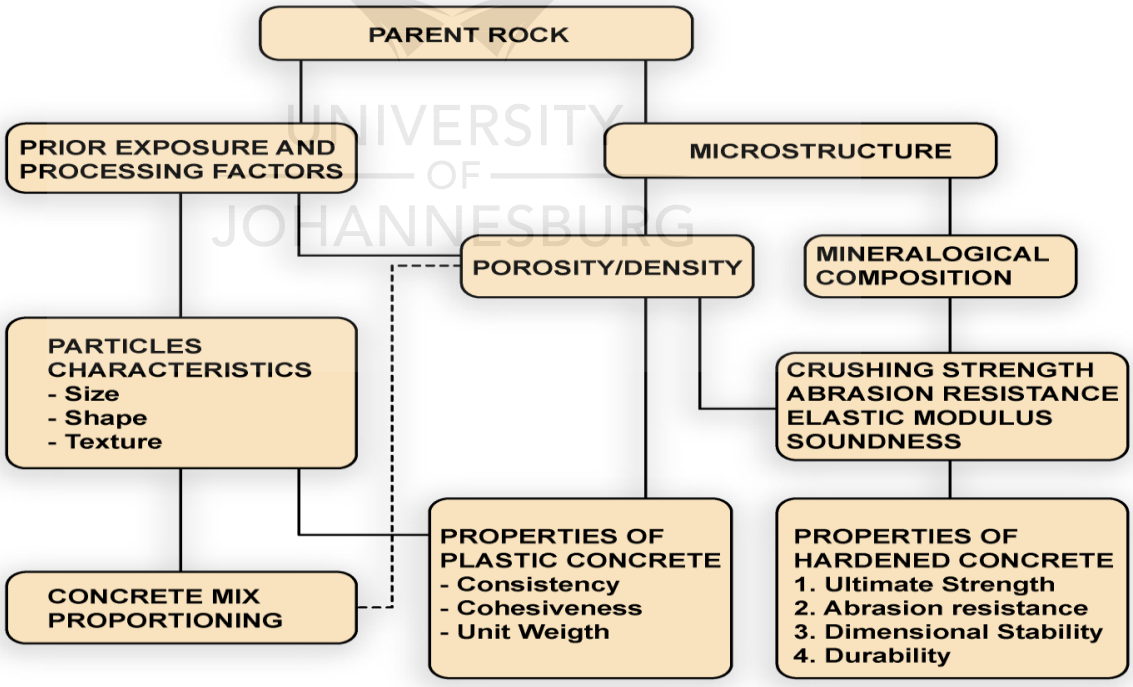

Figure 2.1: The aggregate characteristics that affect concrete properties [47]

The rock types used as aggregate in South Africa for concrete production are; quartzite (sandstone), basic igneous rocks (dolerite, gabbro and norite, basalt, andesite), granite, greywacke and tillite [48]. The effect of some of the South African aggregates on compressive strength of concrete with different cement/water ratio (C/W) was looked into by Alexander [49] in 1993. It was discovered that different aggregates have different influence on compressive strength of concrete. The graph as seen in Figure 2.2 showed that for the different South African aggregates tested, the compressive strength increased with increased C/W (decreased W/C).

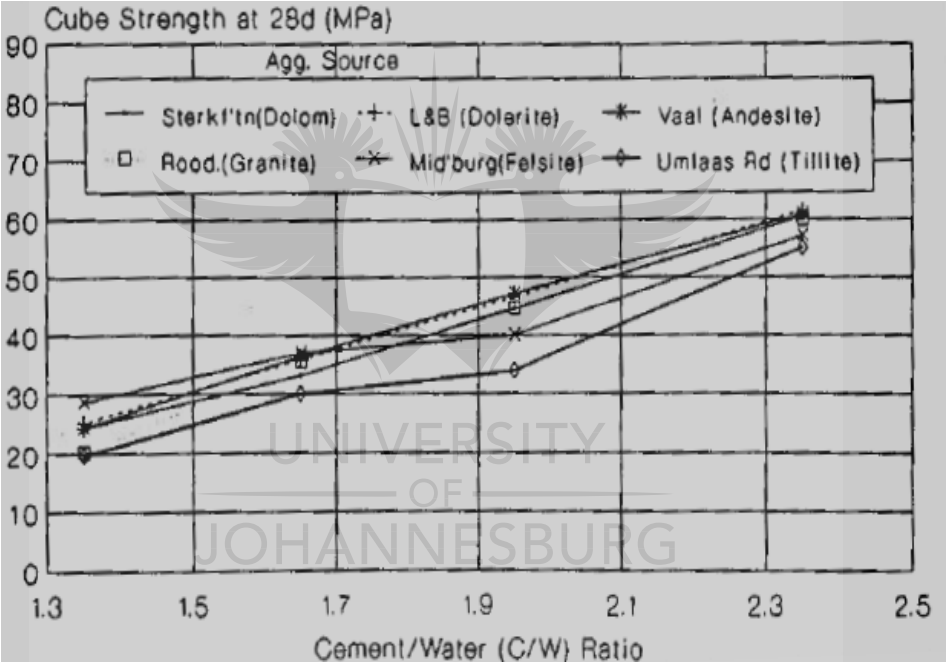

Figure 2.2: Effect of South African aggregates on compressive strength[49]

Granite, which is widespread in South Africa, was used as aggregate for this project. It consists essentially of quartz and feldspar together with differing amounts of mica, amphibole and iron oxides [48]. Crusher sand from granite, which is manufactured under controlled conditions to achieve uniformity of grading and minimization of being contaminated by deleterious substances such as clay minerals and organic

matter was also used as fine aggregate. The grading analysis of the crusher sand used in this project is as shown in Figure 2.3.

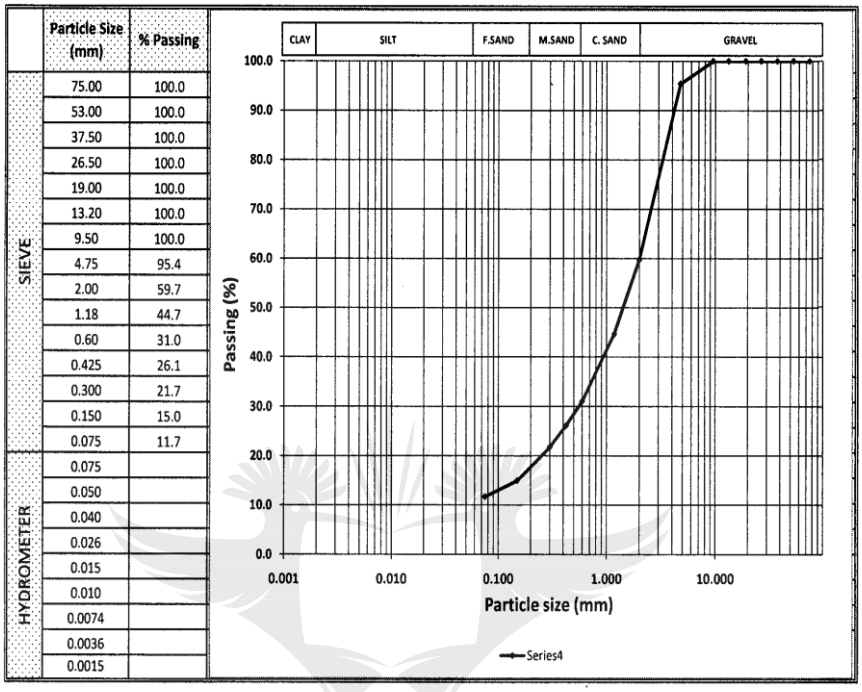

Figure 2.3: Particle size distribution of crusher sand used

2.1.3 Water

Water is essential for cement hydration; it aids the transformation of clinker ions through clinker phase to the reaction products. The suitability of water for concrete production is highly dependable on its composition and properties. Generally, potable water that has no pronounced taste or odour is suitable for concrete and has relatively little effect on the final concrete, and is seldom a source of problems [50]. However, non-potable water can be used for concrete production but such water must be verified for possible oils, grease, dissolved salts and acid. Non-potable water must comply with the requirements for mixing water presented in Table 2.3 as illustrated by Goodman [50]. Potable water supplied by the municipality was used throughout this project. The water to cement ratio (W/C) in concrete controls to a large extent

the workability, strength and durability of concrete. During the hydration reaction, free water is chemically bound to the hydrated cement; this bound water diffuses through the concrete or dries out under conditions of high temperature or dryness [51].

Table 2.3: Requirement for inspection of mixing water [50]

Item	Requirement
Oils and fats	No more than visible traces.
Detergents	Any foam should disappear within 2 minutes.
Colour	Water not recovered from processes in the concrete industry: The colour shall be assessed qualitatively as pale yellow or paler.
Suspended matter	Water from processes in the concrete industry.
	Water from other sources: Maximum 4 ml sediment.
Odour	Water from processes in the concrete industry: No smell, except the odour allowed for potable water and a slight smell of cement and where blast furnace slag is present in the water, a slight smell of hydrogen sulphide.
	Water from other sources: No smell, except the odour allowed for potable water. No smell of hydrogen sulphide after addition of hydrochloric acid.
Acids	pH greater than or equal to 4
Humic matter	The colour shall be assessed qualitatively as yellowish brown or paler, after addition of NaOH.

It is generally accepted that W/C is inversely proportional to concrete strength [24, 51-53]. Rahmani et al [53] studied the effect of W/C on compressive strength and abrasion of microsilica concrete. In the study [53], increased compressive strength

and abrasion strength of concrete were observed at lower W/C. Likewise, the investigation done by Wang et al [54] on the effect of water-binder ratio (W/B) and FA on the homogeneity of concrete showed decrease in homogeneity in concrete as the W/B increased, which resulted in a reduction in the compressive strength. It was further discussed that the addition of FA effectively improved the homogeneity of paste.

W/C also affects the properties of self-compacting concrete. Nikbin et al [55] did a comprehensive investigation into the effect of W/C and limestone powder content on mechanical properties of self-compacting concrete (SCC) using sixteen SCC mixes. The investigation showed that generally, with an increase of W/C ratio from 0.35 to 0.7, the value of compressive strength decreased by 66 %, concomitantly, the tensile strength decreased by 51%. Also, the effect of limestone powder content on the increase in compressive strength was more noticeable at a lower W/C. Beygi et al [56] reported related observation after they studied the effect of W/C on the fracture parameters and brittleness of self-compacting concrete (SCC). It was observed [56] that with a decrease of W/C ratio from 0.7 to 0.35 in SCC, the fracture toughness increases linearly, which can be attributed to the improved bond strength between the aggregates and the paste.

Theoretically, 0.25 W/C is required for complete hydration [1], but some of the water will be trapped in the gel pores in the hydrated paste and such concrete will be unworkable, difficult to compact and result in entrapped air in the concrete mix. In practice, to make allowance for bleeding and for water trapped in the gel pore in the hydration, a W/C greater than 0.38 is required for the complete hydration of the cement [1]. W/C's of 0.4 and 0.5-Were investigated for concrete in this project.

2.1.4 Pozzolans

Pozzolans are supplementary cementitious materials that can either occur naturally like zeolite, diatomaceous ash and volcanic ash or as industrial by-products like silica fume and FA or from agricultural wastes such as rice husk ash [57-59]. Pozzolans are alumino-silicate materials, which react with calcium hydroxide to form more calcium silicate hydrate and contribute to concrete strength [16-19, 59]. Pozzolans have more advantages than disadvantages in concrete. Some of the advantages of pozzolans among others in concrete include cost and CO_2 emission reduction, decreased permeability, increased chemical resistance and increased late strength [6, 20-25, 60]. Reduction in the early strength of concrete is the most obvious disadvantage of replacing Portland cement with pozzolans [21, 60], which is attributed to the slower pozzolanic reaction compared to the portland cement hydration reaction [10], in addition the amount of cement clinker is less.

During pozzolanic reaction, the setting takes place by the partial dissolution of alumino-silicate in alkali pore solution to produce silica in solution [1, 57]. Then, the dissolved silica reacts and consumes $Ca(OH)_2$ and increases the formation of C-S-H and subsequently increases strength. In a high pH environment, dissolution of alumina will also occur, the bulk of this will react to form calcium aluminate hydrate (C-A-H) and calcium aluminate sulphate hydrate (C-A-S-H) phases, while a small quantity will be incorporated in the C-S-H gel [57]. The chemical compositions of different pozzolans showing their high content of silica and alumina, as reported by different researchers and compiled by the author, are presented in Table 2.4. The pozzolanic activity of pozzolans can be measured by the rate of the reaction with $Ca(OH)_2$ and the total consumption of $Ca(OH)_2$ [61].

In the case of FA, a slow rate of dissolution of silica has been reported [57], which is responsible for the reduction of the early strength observed in FA pozzolanic concrete. With time, more of the silica goes into solution to form additional C-S-H gel, which leads to strength enhancement in the longer term [57]. To improve the

early strength development of FA pozzolanic concrete, possible investigation of its chemistry that can aid early dissolution of more silica in solution needs to be done. FA, being the pozzolan of interest in this project will be discussed further.

Table 2.4: Chemical compositions of various pozzolans

Pozzolans	Mass percentage								Reference
	SiO_2	Al_2O_3	Fe_2O_3	CaO	MgO	$Na_2O + K_2O$	SO_3	LOI	
Silica Fume 1	91.7	1.0	0.9	1.68	1.8	0.1	0.87	2.0	[23]
Biomass ash (palm oil fuel ash)	65.3	2.56	1.98	6.42	3.08	6.08	0.47	10.05	[24]
Natural zeolite	67.79	13.66	1.44	1.68	1.2	3.46	0.52	-	[58]
Silica Fume 2	88.10	5.39	0.84	1.49	1.50	0.60	0.06	1.70	[59]
Fly ash 1	56.95	25.76	6.5	4-10	2.5	0.28	0.35	1.28	[62]
Fly ash 2	41.5	37.2	2.45	9.95	2.27	1.36	0.5	-	[63]
Fly ash 3	55.2	23.3	6.9	4.0	2.5	4.5	0.4	1.9	[64]
Metakaolin	51.58	43.87	0.99	0.2	0.18	0.13	-	0.57	[65]
Silica Fume 3	93.16	1.13	0.72	-	1.6	-	0.05	1.58	[65]
Volcanic tuff from Uzuntarla-Turkey	63.96	12.5	4.00	3.40	2.45	-	0.2	11.00	[66]
Natural Algerian pozzolan	46.8	17.5	8.4	9.4	3.9	5.72	0.4	4.8	[67]
Rice husk ash 1	90.89	0.93	0.47	1.25	0.81	2.34	0.17	3.14	[68]
Rice husk ash 2	86.02	0.36	0.16	1.12	0.39	1.15	-	-	[69]
Coal bottom ash	57.76	21.58	8.56	1.58	1.19	1.22	0.02	5.80	[70]

2.1.4.1 Chemistry of fly ash

The non-combustible combustible residue, which represents the bulk mineral matter after carbon, oxygen, sulphur, and water has been driven off during coal combustion is referred to as FA [71]. FA can be classified as class C or F based on its chemical

composition. Class C FA is from lignite and sub-bituminous coals [72-74] and has free lime (CaO), which reacts with water and the glass content in the ash to allow for hydration and pozzolanic reactions, respectively [75]. This makes Class C FA both cementitious and Pozzolanic in nature [73]. Class F FA, on the other hand, is from anthracite and bituminous coals [74, 76] and needs additional lime to undergo the hydration and pozzolanic reactions, which makes it not cementitious in nature but pozzolanic because of its high content of glass. The pozzolanic reaction of FA is in operation between 4 and 150 days, after which the chemical reaction with calcium hydroxide to form calcium silicate hydrate would have almost completely, disintegrated the FA particles [1].

FA structure can be affected by the composition of coal, coal combustion technology used, and combustion and glassification process used at a particular power plant [77-79]. FA can be in glassy phase or crystalline phase. A glassy phase material is formed when the maximum temperature of the combustion process is above 1200 ^{0}C and the cooling time is short. Crystalline phase calcium compound is formed at gradual cooling of ash particles [80]. Crystalline phases contain minerals such as kaolinite, mullite, quartz and pyrite [76, 77, 79, 81-83]. The FA particles are generally spherical in shape [81, 82, 84-86] and usually silt size [73, 84, 85]. FA particles are generally characterized by low permeability, low density and a high specific surface area [84].

Investigation done by Brouwers and Van Eijk [81] on the cenosphere and solid sphere FA showed that the glass phase of FA consists of SiO_2, as well as the network formers, Al_2O_3, Fe_2O_3, TiO_2 and P_2O_5 and the network modifiers, CaO, MgO, Na_2O and K_2O. The glass components (Fe_2O_3, CaO, MgO, Na_2O and K_2O) are concentrated in the exterior (outer) hull of the FA [81]. The chemical composition and structure of FA are the main factors responsible for its cementitious behaviour. The possibility of increasing FA application in concrete technology will be explored in this project.

A comprehensive research findings on South African fly ash as a cement extender was compiled in a monograph by Kruger, 2003 [87]. The findings showed that South

African fly ashes consist of an aluminium silicate glass, mullite ($Al_6Si_2O_{13}$), quartz (SiO_2) and some quicklime (CaO). The glass phase consists of 21-100% SiO_2 and 0,1-49% Al_2O_3 with significant proportions of CaO, TiO_2, Fe_2O_3 and MgO as shown in Figure 2.4 [87]. This indicated that large content of SiO_2 in FA are in the glass phase.

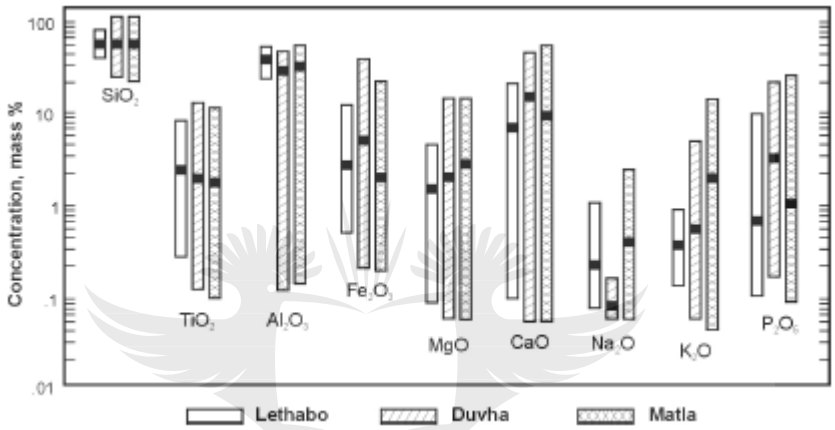

Figure 2.4: Concentration ranges of oxides determined in FA glass after Kruger [87]. Black squares on bars represent means.

The effect of FA on Portland cement systems was studied by Papadakis [88], using three different percentages of FA to replace cement in the mix. FLC1, FLC2, and FLC3, represented 10%, 20% and 30% replacement, respectively. Reduction of early strength was observed for all the FA replacement samples. This was attributed to lower pozzolanic activity at the early stage. However, after six months for FLC1 and FLC2 specimens, the strength exceeded that of the control (normal concrete without FA). Moreover, the FLC2 specimen presented the highest strength. This ultimate improvement was reported to be due to the higher active silica content (40%) of low-calcium FA in comparison with the cement (20%).

A research on the influence of two South African fly ashes on the engineering properties of concrete was done by Grieve [89]. It was reported that Matla and Lethabo fly ashes improve the flow characteristics of a cementitious mix when compared with the mix without FA. Increase in setting times was observed mostly for matla FA than lethabo FA when compared with cement paste without FA. The degree of retardation was reported to be proportional to the content of the FA. The higher the FA content, the greater the retardation observed. Reduction of early concrete compressive strength up to 28 days curing period was recorded with the incorporation of the two fly ashes in the concrete mixtures. 30% FA was recommended as the optimum percentage of FA to replace cement in blended concrete.

2.1.4.2 Fly ash modification

Different modification methods have been reported by researchers to improve the cementitious properties of FA, the most common being alkali activation, mechanical activation and thermal activation [21, 90-93].

The FA alkaline activation is similar to the chemistry involved in the synthesis of a large group of zeolites and totally differs from Portland cement hydration [91]. The alkaline activation produces alkaline aluminosilicate gel, which is structured around tetrahedrally co-ordinated silicon and aluminium, forming a polymer chain in which the Al^{3+} ions replace the Si^{4+} ions. The monovalent alkaline cations are being captured to compensate for the resulting net anionic charge [91].

FA was physically modified by grinding during the investigation done by Paya et al [90]. It was observed that grinding of FA broke down its coarse particles to finer particles comprising shell-shaped and solid fragments, compared to their original spherical shape. Lower workability was observed with ground FA (GFA) as compared to original FA.

Activation of pozzolanic reactivity of a natural pozzolan was examined by Shi and Day [21], using mechanical (grinding), thermal (increased curing temperature) and chemical methods. It was observed from their study [21] that mechanical activation did not show a significant effect on the ultimate strength, while thermal activation decreased the ultimate strength and chemical activation increased the ultimate strength of lime-pozzolan mixtures significantly.

2.1.5 Organic admixtures

Admixtures are materials other than water, aggregates and cement, which are added before or during concrete mixing to improve certain properties of the concrete. Concrete properties that can be improved by including certain admixture in concrete are workability, acceleration or retardation of setting time, strength development, and enhancement of resistance to frost action, thermal cracking, alkali-aggregate expansion, acidic and sulphate solutions [94]. The functionality process of chemicals used as admixtures on cement-water system can be explained in two ways. Firstly, some admixtures react immediately by influencing the surface tension and by being adsorbed on the surfaces of cement particles. Secondly, some admixtures affect the hydration reaction from several minutes to several hours after the addition, by breaking up into their ionic constituent [94].

An organic admixture can be referred to as a fluidizing agent, a water-reducing agent, a water retention agent or an air entraining-water-reducing agent [95, 96]. In cement paste, the electric charge on the surface of the particles generates van der Waals and electrostatic repulsive forces between the cement particles. When an organic admixture is added to cement paste, additional electrostatic forces will be applied between the particles due to the increased surface potential caused by the adsorption of the organic admixture on the surface of the cement particles. Also, osmotic pressure will be required to relieve the increase of density caused by overlapping of the adsorption layers of the admixture, which will generate steric repulsive force. Therefore, the improved fluidity of concrete caused by organic admixtures is as a

result of the dispersion of solid particles by the electrostatic repulsive force and by the steric repulsive force based on the interaction between the adsorption layers of admixture [95].

One of the most common organic admixtures, which have received research attention, is polysaccharide's based polymer [96-101]. Peschard et al [96] studied the effect of polysaccharides on the hydration of cement paste at early ages. The results showed increased retardation with higher polysaccharide-to-cement weight ratio (P/C). Low-molecular-weight starch showed enhanced retarding effect on the hydration of cement. Hua et al [101] observed similar behavior for cellulose ethers (CEs), they reported that the retardation effect of CEs with different molecular parameters is different, the lower the molecular weight of CEs or the hydroxyethyl content in HEMCs (hydroxyethyl methyl celluloses) or methyl content in HPMCs (hydroxypropyl methyl celluloses) and HEMCs is, the stronger the retardation ability is. A study done by Patural et al [100] on the influence of cellulose ethers on water retention and consistency in cement-based mortars showed that the molecular weight is crucial to control water retention and mortar consistency. It was noted that, as molecular weight increased, the yield stress was diminished, the consistency was increased and the water retention was improved.

Research done in this area focused attention on using the polysaccharides as organic admixture to normal concrete not to blended cement concrete [96-101]. Recent investigation done by Alonso et al [102] on the compatibility between polycarboxylate-based admixtures (PCE) and blended-cement pastes using fly ash, limestone and granulated blast furnace slag based blended cement showed that smaller amounts of admixture are adsorbed by both fly ash and blast furnace slag, and slightly larger amounts by limestone, than by the non-blended cement. It was also observed that the dispersing effect induced by PCE admixtures in CEM II/AV pastes, which contain fly ash, is similar to the effect observed in non-blended cement pastes.

Lastly, in cements containing fly ash, the delay in the hydration reactions induced by admixtures is similar to the delay observed in non-blended cement pastes.

Tkaczewska [103] studied the effect of the superplasticizer type on the properties of the fly ash blended cement using Portland fly ash cement concrete as a control sample. Three different super plasticizers were studied, which were; sulfonated melamine-formaldehyde condensate (SMF), sulfonated naphthalene-formaldehyde condensate (SNF), polycarboxylate (PC) and polycarboxylate ether (PCE). It was observed that a decrease in water content is needed to maintain consistency for all the added superplasiticisers samples compared to the control sample. The polycarboxylates were found to have a higher efficiency in improving the hydration heat evolution, setting time and mechanical properties of cement than that of traditional superplasticizers (SMF and SNF). It was also shown that the required reduction in water together with pozzolanic reactivity of ashes led to better mechanical properties of FA cement.

To improve FA usage in construction, extensive study is needed to explore the possibility of improving its chemistry using a compound of less carbohydrate than polysaccharide. Oligosaccharides, have a lesser carbohydrate content than polysaccharide and their effect on blended cement (pozzolan) concrete was explored in this project. Polysaccharides and oligosaccharides originate from the process of polymerisation. Generally, polymers do not behave as binders in concrete but they modify the pore structure. It is known that polymers change the setting properties of concrete by reducing the W/C as polymer to cement ratio increases, which eventually affects the mechanical properties of concrete [104].

2.2 *β*-CYCLODEXTRIN IN CONCRETE

Cyclodextrins (CDs) are crystalline, cyclic oligosaccharides derived from starch as explained in Chapter One. It is a solubility and stability agent, which has received

wide range of research in drug delivery systems [105-107]. *β*-cyclodextrin (*β*-CD) has a peculiar hollow truncated cone which is composed of seven α-(1,4)-linked glycosyl units forming a hydrophobic cavity and a hydrophilic wall [108] as shown in Figure 2.5, and was used in this project. The general physical characterisation of *β*-CD is shown in Table 2.5 [109]. Limited information is available on the compatibility of *β*-CD with FA and cementitious material for use in concrete technology. Therefore, the primary focus of this project was to investigate the compatibility of FA-*β*-CD interaction to form a composite that can improve the use of FA in concrete technology [110], as discussed in detail in Chapters Three and Four of this thesis.

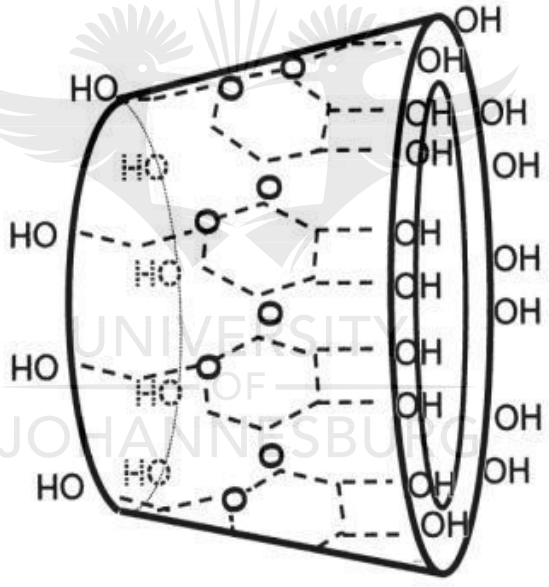

Figure 2.5: Hollow structure of *β*-cyclodextrin [108]

Table 2.5: General physical characterisation of *β*-cyclodextrin [109]

Empirical Formula	$C_{42}H_{70}O_{35}$
Molecular Weight	1135
Appearance	White fine crystalline powder
Odour	Odourless.
Taste	Slightly sweet taste
Density	0.523 g/cm^3
Melting point	255–265°C
Moisture content	13.0–15.0% w/w
Particle size distribution	7.0–45.0 μm
Stability	Stable in the solid state if protected from high humidity
Solubility	1 in 50 part of water at 20°C, 1 in 20 at 50°C; practically insoluble in acetone

Few investigations, which have only been done recently, on *β*-CD in the concrete environment, have looked into its usage as a superplasticiser. In 2012, Lv et al [108], synthesized a new PCM-*β*-CD superplasticizer through ring-opening polymerization of epoxy chloropropane and CM-*β*-CD using sodium hydroxide as the initiator. The chemical structure of PCM-*β*-CD was characterized by FT-IR and NMR spectra. The PCM-*β*-CD was used as the superplasticizer in cement and concrete, which showed a retardation effect based on its dosage. The results also showed that the fluidity of the cement paste increased with an increase in the PCM-*β*-CD dosage. The formation of complexes on the surface of cement particles, which thickened the solvation layer and prevented solid phase nucleation hydration reaction, and thus retarded the fluidity loss, was attributed to the carboxylic acid groups in PCM-*β*-CD and the hollow structure of *β*-CD. It was also reported that retardation caused using PCM-*β*-CD is likely due to the steric hindrance caused by the cone structure of *β*-CD and the hydrophilic functional groups, such as the hydroxyl and carboxyl groups, that act as "cement-anchoring" groups.

Li et al [111] also synthesized a new copolymer, PSDs, which is a novel functional comb-like copolymer, bearing pendant cyclodextrin (CD) group, based on the monovinyl functional monomers of β-CD and used as superplasticizer. Then, they evaluated the dispersion and adsorption mechanism of the PCDs in cement system. The results showed that PCDs copolymer showed excellent dispersion ability and a strong retarding effect. The retarding effect among others is attributed to the large number of hydroxyl group of the CD pendant, which affected the hydration reaction of cement.

2.3 PROPERTIES OF FLY ASH POZZOLANIC CONCRETE

FA pozzolanic properties will be discussed in two categories; fresh concrete properties and hardened concrete properties.

2.3.1 Properties of fresh fly ash concrete

The fresh properties of concrete affect the overall hardened concrete strength and durability. Fresh concrete properties include workability, air-entrainment, bleeding, segregation, pumpability, compactability, and finishability [112]. FA-pozzolanic-concrete workability is increased compared to normal concrete with the same water content due to the effect of FA on it. The increase in FA concrete workability has been assigned to the spherical shape and glassy surface of FA [113-115]. Due to its spherical shape, FA helps to reduce the internal friction between the ingredients of concrete, which results in a considerable increase in the fluidity of the concrete mix [116]. FA also increases the volume of paste in the concrete and this greatly improves workability [115]. Concrete consistency is an aspect of workability that gives an indication of concrete fluidity or wetness while concrete cohesiveness gives an indication as to whether the concrete is harsh, sticky or plastic. A harsh mix lacks plasticity and can result in segregation of the concrete constituents while sticky concrete requires a lot of water to achieve minimal workability, and therefore it tends

to develop excessive shrinkage cracking. A plastic concrete gives the desired cohesiveness without segregation or excessive shrinkage cracking. FA improves the plasticity of concrete due to reduced water quantity that is needed for minimum workability.

Properties of fresh concrete containing large amounts of FA were investigated by Ravina and Mehta [117] by replacing 35 to 50% of cement with FA. The workability of all the concrete mixtures containing FA was observed to be better than that of control mixtures without FA. The water requirement for all concrete mixtures containing FA was reported to have reduced by 5 to 10%. Setting time was also observed to be delayed at all levels of FA substitution, compared with control samples; the initial setting time was delayed from 20 minutes to up to 4 hours and the final setting time from 1 hour to 5 hours. Similar observations were reported by Duran-Herrera et al [118], who evaluated sustainable high-volume FA concretes. They [118] reported that higher water/binder ratio (W/B) and higher FA substitution in concrete resulted in increased setting times. A maximum retardation in final set of 6:32 (h:min) was obtained for W/B of 0.6 and FA substitution of 75%. According to Erdogdu et al [115], FA helps the consistency retention of concrete at higher percentage replacement. It was reported in their research that at 7% replacement of cement with FA, a higher rate of slump loss was observed when compared to 20% and 30% FA replacements.

Alvarez et al [119] observed while studying the properties of concrete made with FA that the effect of FA on concrete workability depends on the origin and the preparation of the FA. Two types of fly ashes of different origin were investigated in their study. Type A improved workability with increased FA content, while in Type B workability decreased with an increase in the amount of FA used. In this present project, fly ash from four different power stations were characterised but a single FA type was used for the main tests so as to limit the variables.

Properties of concrete incorporating high volumes of class F FA were studied by Siddique [114] using three replacement percentages (35%, 45% and 55%) of cement with class F FA. Both slump and vebe tests were performed to investigate the effect of the class F FA on concrete workability. The results of the investigation showed that an increase in the percentage of FA content resulted in an increase in workability (slump and vebe time).

The most widely and oldest used method, which measures only the consistency of concrete and gives indication of workability is slump test [94, 120]. There is a need for workability to also be defined in fundamental, scientific terms, such as fundamental flow properties, or rheology. Plastic viscosity and yield stress are the rheological properties of concrete based on Bingham model [120-123], which have effect on concrete placement and workability and eventually affect the mechanical and durability properties of concrete. Replacement of cement with FA in concrete has been reported to decrease the yield stress and plastic viscosity of the concrete [124]. Yield stress was observed to increase slightly at higher replacement levels while the change in plastic viscosity at higher replacement levels was insignificant [124]. The review done by Kovler and Roussel [125] on the properties of fresh and hardened concrete revealed that there is a relationship between the yield stress and setting time measurements when ultrasound spectroscopy and oscillating rheometer were used to measure the evolutions of both shear and bulk elastic moduli during setting of cement paste. It was reported that the initial setting time corresponded to a yield stress of the order of a couple hundred kPa when compared to the few Pascals (Pa) or tens of Pa of a freshly mixed cement paste.

In addition to the slump tests done in this project to monitor the workability of the concrete samples, viscosity and setting time of cement paste were also studied. It was envisaged that the inclusion of cyclodextrin (oligosaccharide**,** saccharide polymer) would increase the flow-ability of FA concrete due to its higher water solubility property.

2.3.2 Properties of hardened fly ash concrete

The transition from fresh concrete to hardened concrete involves three stages: The dormant stage, where the concrete remains plastic and workable. The setting stage, where the concrete becomes stiff and unworkable and the hardening stage, where the concrete is a rigid solid which gains strength with time. The graph relating concrete rigidity with hydration time, as illustrated by Mehta and Monteiro [126], is shown in Figure 2.6. This graph depicts the three stages involve in setting and hardening of concrete. According to Mehta and Monteiro [94], during the hydration reaction, the compounds first ionize and form hydrates in solution, which solidifies as hydration progresses. The stiffening, setting, and hardening of cement pastes are derived from the progressive hardening of the hydration products.

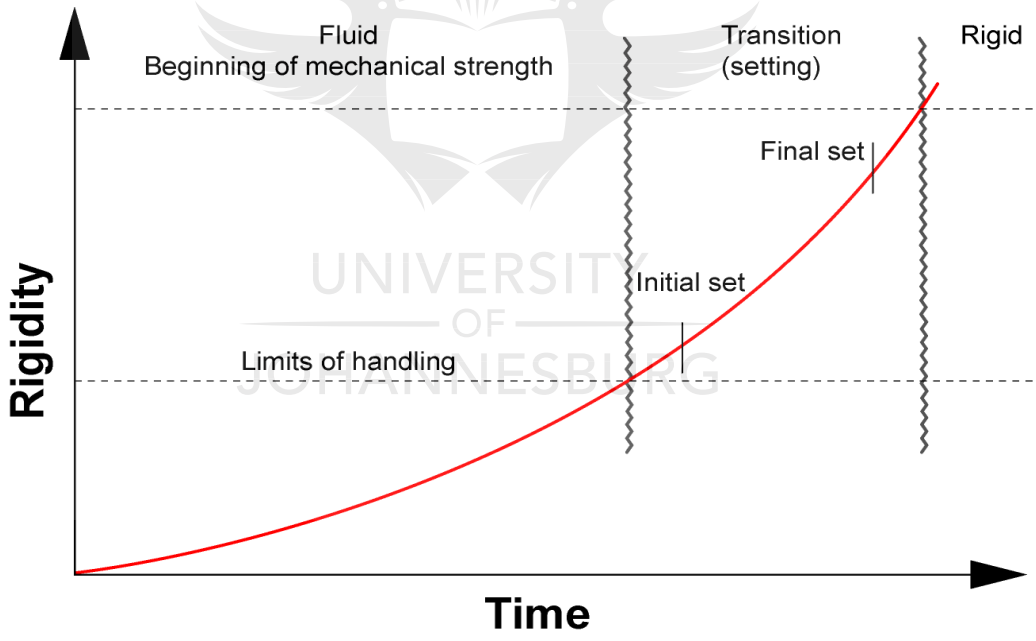

Figure 2.6: Setting and hardening of concrete [126]

Hardened concrete properties as related to strength and durability are the focus of this project. The effect of FA on concrete strength and durability will be discussed.

2.3.2.1 Strength

Strength is a concrete property that gives an indication of the overall view of concrete quality. As explained earlier, in Section 2.1.1, strength development starts with the hydration reaction that takes place between cement and water. Calcium silicate hydrate, a product of hydration reaction is responsible for strength development. During pozzolanic reaction, more calcium silicate hydrate is produced while calcium hydroxide is consumed. Pozzolanic reaction is a slow reaction compared to hydration reaction; therefore the effect of pozzolans on concrete strength takes time to manifest. FA has been reported to reduce the early strength of concrete but to increase late strength of concrete [127, 128]. The grade of the concrete is an important indication of the amount of FA to replace cement. According to Gopalan and Haque [129], the amount of FA required is progressively decreased as the required strength of the concrete increased.

Concrete strength can be measured by subjecting it to compressive, tensile or flexural loads. Compressive strength is the most commonly used concrete design parameter. Nonetheless, investigation of the other strength parameters is important to understand the behaviour of concrete in full because the relationship between tensile and compressive strength does not have a specific pattern [130].

Poon et al [131] studied high strength concrete (80 MPa) prepared with large volumes of low calcium FA. The experimental results revealed that FA contributed to a higher compressive strength at lower W/B. It was concluded that high strength concrete with 28 days compressive strength of 80 MPa could be obtained at a W/B of 0.24, and with a FA content of 45%. Such a concrete had a lower heat of hydration and chloride diffusivity when compared to the equivalent plain cement concrete.

In a study on the performance characteristics of high-volume Class F FA concrete conducted by Siddique [128], 40%, 45%, and 50% replacement of cement with FA were used. The study showed that the use of high volumes of Class F FA, as partial

replacement of cement, in concrete decreased its 28 days compressive strength, splitting tensile strength, flexural strength, modulus of elasticity, and abrasion resistance of the concrete. However, all these strength related properties and abrasion resistance showed continuous and significant improvement at the ages of 91 days and above. It was also observed that the compressive, splitting tensile and flexural strengths decreased with the increase in FA content. The same observation was reported by Kayali and Ahmed [132]. They showed in their work that replacing Ordinary Portland cement (OPC) with FA resulted in lower compressive strength, lower tensile strength and a lower modulus of elasticity. It was also reported that the compressive strength was shown to decrease as the ratio of FA replacement increased.

One of the disadvantages of FA pozzolanic concrete is the reduction of early strength of concrete. Since stiffening, setting, and hardening of cement pastes depend on the ionization of cement compounds and soldification of hydration products, it is reasonable to assume that adding certain soluble admixtures that can influence ionization of cement compounds and solidification of hydration products in the concrete mix will consequently influence the setting and hardening properties of the FA concrete.

2.3.2.2 Durability

Durability of concrete is the ability of concrete to resist weathering action, chemical attack, abrasion, or any other process of deterioration, while its desired engineering properties are maintained [94]. The agent of concrete deterioration, which is responsible for both physical and chemical processes of concrete degradation, is water. The ingress of chemicals in concrete, alkali silicate reaction, frost action, concrete volume change, and permeability are all affected by the movement and action of water in concrete. Water is capable of penetrating extremely fine pores or cavities, aids chemical decomposition of solid materials due to its ability to dissolve more substances than any other liquid and at ordinary temperatures, it has a tendency

to remain in a material in the liquid state, rather than to vaporize, because, it has highest heat of vaporization among the common liquids [94]. Environmental factors that can also have a detrimental effect on concrete are natural occurrences, weathering, abrasion and exposure to high temperature.

A durable concrete should have the ability to resist external penetration of ionic species such as sulphates and chloride and be dense and impermeable enough to limit the movement of liquids and gases into the concrete. Attempts to improve concrete durability have been made by several researchers. Some of the recent methods adopted are incorporating or engaging the following into cement mix; biotechnology [133, 134], corrosion inhibitors [10], glass powder [135, 136], epoxy [137, 138], nanocomposites [139, 140], modified starch [141], polymer [142, 143], synthetic fibre [144] and pozzolans [31, 145-150].

The most common method of improving concrete durability is the incorporation of pozzolans in concrete. Refinement of concrete pore structure and consequent improvement of concrete durability by pozzolans is one of the advantages of incorporating pozzolans into a concrete mix. The best way to study concrete durability is to study the parameters that influence the deterioration process than to study the process itself [151]. Relevant parameters that have great influence on concrete deterioration are the concrete accessibility to water and permeability to air. Heede et al [151] reported that a concrete mix with 50% FA, 400 kg/m^3 content of binder and 0.4-W/B had a lower capillary water uptake (-32.6%), water sorption under vacuum (-10.7%) and gas permeability (-78.9%) than normal concrete without FA. Incorporation of high volume of FA (30% and 40%) in concrete mixtures was also investigated by Nath and Sarker [146], they reported that a high volume of FA reduced sorptivity and chloride ion permeation significantly at 28 days and further reduction was recorded at 6 months.

According to Chindaprasirt et al [27, 152], the material transport properties, such as permeability, sorptivity and diffusivity, strongly influence the service life and durability of a concrete structure. This is associated with the material deterioration over the intended service life [153]. These transportation mechanisms are the main mechanisms leading to concrete deterioration. In this project, the samples durability properties were studied based on the three South Africa durability index approach; permeability, sorptivity and chloride conductivity [154-157]. The durability approach that was formulated in South Africa was aimed at achieving more realistic durability results that are site related. Most methods used previously by researchers to study concrete durability are useful mostly for research purposes and not for site use, also most of them require highly sophisticated equipment, and lengthy testing periods [135]. The significance of measuring parameters for the index tests are related to some transportation mechanisms; permeation for oxygen permeability, absorption for water sorptivity, and diffusion for chloride conductivity. The three durability index tests are further discussed below.

2.3.2.2.1 Oxygen permeability

Permeability is a major property affecting the durability of concrete in general. The movement of an aggressive chemical within the concrete is controlled by its permeability, which is influenced by the volume and size of the interconnected capillary pores in the cement paste. The intensity of the microcracks within cement paste and the interfacial zone between the aggregate and cement matrix also influences the permeability of concrete [158]. Pozzolans have shown in previous studies [151, 158] to improve the pore structure of concrete and as a result reduce the concrete permeability.

The oxygen permeability index (OPI) test is a gas permeability test that provides an indication of the degree of pore connectivity in a concrete matrix [32]. The OPI is the negative logarithm of the Darcy coefficient of permeability and values generally range from 8 to 11. The test is based on the falling head permeability in which an initial pressure is applied to concrete and allowed to decay as permeation proceeds

[157]. This approach maintains a high level of accuracy since pressure may be reliably monitored with time. The higher the OPI, the less permeable the concrete. The test procedure is described in Chapter Five.

The adequate protection of reinforcement steel against corrosion is dependent on the quality of the protection given by the concrete cover. The bulk of durability problem deals with the corrosion of reinforcement steel in reinforced concrete, which is aided by carbonation. The oxygen permeability index (OPI) can be used to predict the long-term performance of concrete against corrosion through carbonation. A strong correlation between OPI and carbonation has been established [157] as shown in Figure 2.7.

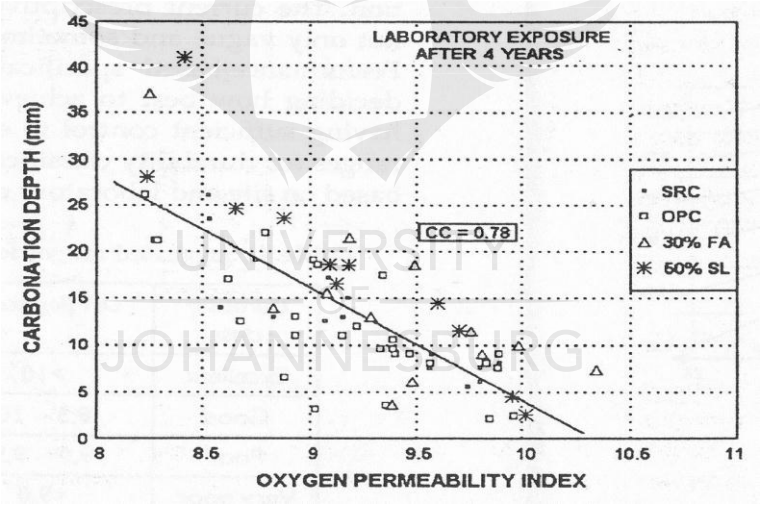

Figure 2.7: Oxygen permeability index versus carbonation depth [157]

2.3.2.2.2 Water sorptivity

The volume of open pores accessible to water by capillary suction is measured by sorptivity [42]. The water sorptivity index (WSI) test characterises the rate of movement of a penetrating wetting front through the exposure face of a concrete

specimen under capillary suction [32]. It is sensitive to the micro-structural properties of the near-surface zone of concrete and therefore reflects the nature and effectiveness of curing. The capillary suction is dependent on the pore geometry and the saturation level of the material [159]. The lower the water sorptivity index, the better the potential durability of the concrete. The test procedure is described in Chapter Five.

2.3.2.2.3 Chloride conductivity

Diffusion is the movement of liquid, gas or ion through a porous material under the action of a concentration gradient [157, 159]. Diffusion is an important transport mechanism for most concrete structures exposed to salt, which may occur in partially or fully saturated concrete. The chloride conductivity index (CCI) is related to the chloride diffusion properties of the concrete. It is an accelerated test used to measure the electrical conductance of a concrete's pore system which can in turn be related to resistance to chloride ion penetration [32]. The lower the chloride conductivity index, the better the potential durability of the reinforced concrete. The test procedure is described in Chapter Nine. Table 2.6 shows the durability classification of concrete based on the three durability index values as suggested by Alexander et al. [157].

Table 2.6: Suggested ranges of index values for concrete durability classification [157]

Durability	OPI (log scale)	Sorptivity	Chloride conductivity
Excellent	> 10.0	< 6.0	< 0.75
Good	9.5–10.0	6.0–10.0	0.75–1.50
Poor	9.0–9.5	10.0–15.0	1.50–2.50
Very poor	< 9.0	>15.0	> 2.50

2.4 CEMENT MICROSTRUCTURE

Cement transforms upon hydration from a powder form, after being mixed with water to form a high-viscuos, opaque slurry, which stiffens and solidifies. The solid product contains amorphous hydration products, unreacted clinker and unreacted water, which are difficult to characterize. Therefore, the chemistry and morphology of the hydration products are important because they affect the strength and durability of the paste and consequently, the concrete. The five–stage sequence of microstructure formation during setting and hardening of cement paste, as summarised by Janotka [36], are as follows:

- An immediate reaction with Ca^{2+} ions passing into solution.
- A "dormant" period specified by a slow rise in Ca^{2+} ion concentration up to the supersaturating of the solution.
- An accelerated period, characterized by the formation of C-S-H deposits and rapid $Ca(OH)_2$ crystallisation.
- A deceleration period that is a consequence of formed hydrate phase layers with decreased porosity.
- Diffusion controlled hydration process, due to decreased porosity and decreased transport of ionic species in the system.

A simplified illustration of cement hydration as presented by Moir [160], is as shown in Figure 2.8.

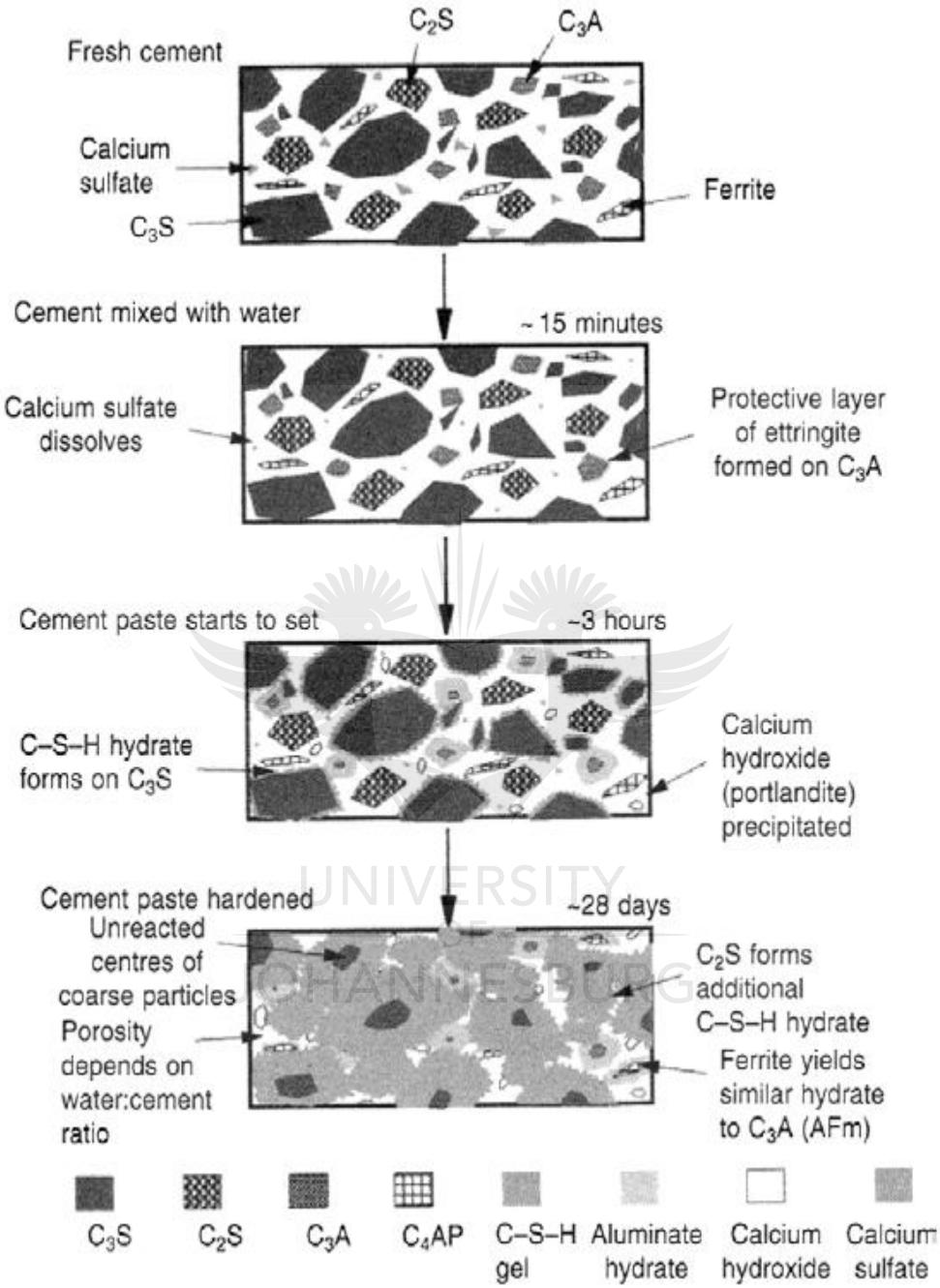

Figure 2 8: Simplified illustration of cement hydration [160]

A refined microstructure is envisaged for pozzolanic concrete due to the lower water content (compared to normal concrete) coupled with pore refinement through the

additional calcium silicate hydrate [59]. The microstructural features of concrete determine its transport mechanism properties, which aid or limit the ingress of aggressive chemicals and affect the total durability of concrete. The four principal solid phases in hydrated cement paste are calcium silicate hydrate, calcium hydroxide, ettringite and unhydrated clinker grains [94].

Calcium silicate hydrate (C-S-H) takes up to 50 to 60% of the volume of the completely hydrated cement paste. Its morphology varies from poorly crystalline fibres to reticular network. Figure 2.9 is an SEM image showing C-S-H formation in Portland limestone cement after 32 hours of hydration [161].

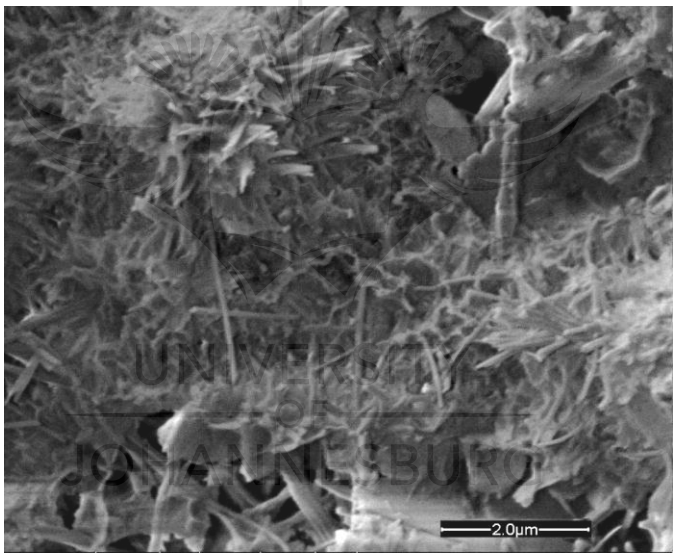

Figure 2.9: SEM image showing C-S-H formation in Portland limestone cement after 32 hours of hydration [161]

Calcium hydroxide is also known as portlandite, it takes up to 20 to 25% of the volume of the completely hydrated cement paste. It forms large crystals with distinctive hexagonal-prism morphology. Figure 2.10 shows the SEM micrograph of a hardened cement paste with urchin-like C-S-H, a portlandite crystal and, in the middle, a residual capillary pore [162].

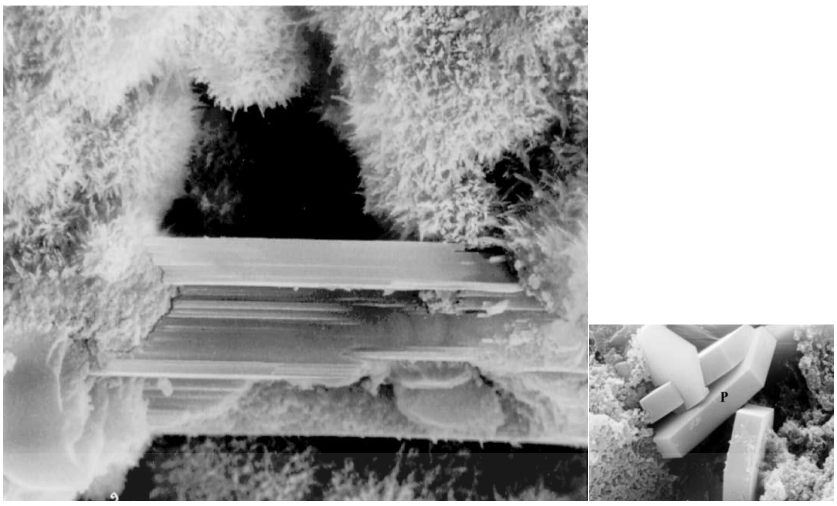

Figure 2.10: SEM micrograph of a hardened cement paste showing urchin-like C-S-H, a portlandite crystal and, in the middle, a residual capillary pore. Inset: well-crystallized hexagonal portlandite crystals [162]

Ettringite is formed during the early stage of hydration. It forms needle-shaped prismatic crystals that may restrict the ability of the fresh paste to flow [162]. Later during hydration, it eventually transforms to the monosulfate hydrate, which forms hexagonal-plate crystals, like portlandite, but much smaller. Figure 2.11 shows the SEM image of Portland limestone cement, with an aluminium sulfate accelerator added, hydrated for 8 hours, showing an ettringite cluster [161].

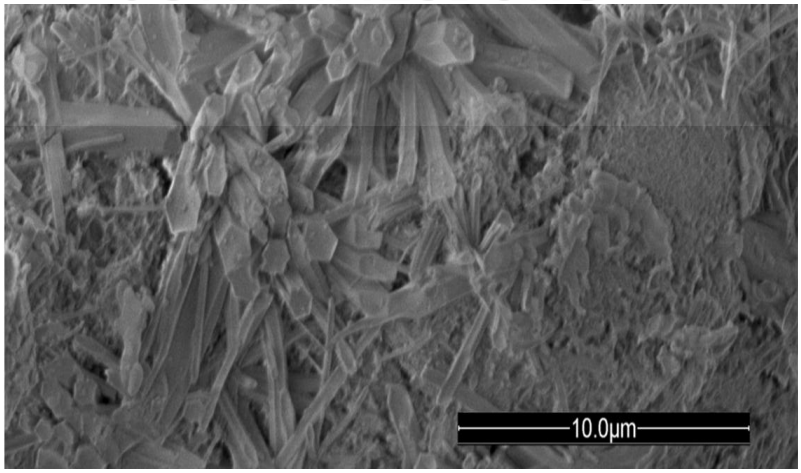

Figure 2.11: SEM image of Portland limestone cement, with an aluminium sulfate accelerator added, hydrated for 8 hours [161]

Some unhydrated clinker grains may be found in the microstructure of hydrated cement pastes, even long after hydration, depending on the particle size distribution of the anhydrous cement and the degree of hydration.

Apart from the solids phases, hydrated cement pastes also have some voids, which also influence their properties. Some of the voids are interlayer space between C-S-H, capillary voids and air voids [94]. Interlayer space between C-S-H varies from 5 to 25 Å. This void size is too small to have an adverse effect on the strength and permeability of the hydrated cement paste. Capillary voids are the spaces that are not filled by the solid component of hydrated cement paste. These voids are irregular in shape. Air entrapped in the cement paste during mixing operation result in air voids in the paste. They are generally spherical in shape. Purposely entrained air due to certain admixture in cement paste also accounts for air voids.

The morphological effect of FA on concrete is due to its morphology, structure and surface properties of its particles as well as the particle size distribution. This effect comprises of three roles as explained by Wang et al [163]. These roles are the filling role, which is relative to the particle size; the surface role, which is relative to the specific surface area and the water affinity and the lubricating role, which is relative to the shape of particle. Wang et al [163] concluded that in pozzolanic concrete, smaller FA particles can reduce the filling water by occupying the space between the particles of cement. Larger surface area due to finer FA will demand more surface layer water, but the inclusion of superplasticizer in the pozzolanic concrete can reduce the surface layer water effectively. Smaller spherical particles have a stronger lubrication effect.

Different techniques are available for assessing the microstructure and structure of cement matrix. The techniques used in this project were X-ray diffraction (XRD), Scanning electron microscopy (SEM) and Fourier transform infrared spectroscopy (FT-IR**),** they are briefly discussed below.

2.4.1 X-ray diffraction (XRD)

X-ray powder diffraction is a powerful tool for studying phase identification of crystalline materials. Cement phases and some hydration products are crystalline in structure and have unique X-ray diffraction patterns [164]. The scattering of the X-rays is as a result of the radiation interaction with the orbital electrons as X-rays pass through different types of matter. The procedure of the XRD used in this project is given in Chapter Three.

2.4.2 Scanning electron microscopy (SEM)

SEM uses electrons to produce images of samples under vacuum conditions by scanning them with a focused beam of electrons. The electron beam travels through the microscope, where a series of magnetic lenses and apertures focus the electron beam. As the electron beam hits the sample, it will scan the surface in a raster scan pattern [161]. With secondary electrons for imaging, the morphology and surface topography of a sample will be shown. SEM attached with Energy dispersive X-ray spectroscopy (EDS) also gives information of the chemical composition of the interested part of the sample. The procedure of the SEM used in this project is given in Chapter Three.

2.4.3 Fourier transform infrared spectroscopy (FT-IR)

The FT-IR is a useful tool for studying the hydration of cement. Cement's chemical components contain various functional groups, which are infrared active [161]. The chemical surroundings of the functional groups influence the absorbed infrared wavelengths leading to the shifts of the absorption bands of the functional groups. A molecule or specific groups present in a compound or sample can be identified by the characteristic frequencies resulting from the electromagnetic radiation absorbed by the molecules. Sending electromagnetic radiation of known frequency through the sample and measuring the change in intensity of the radiation provides the characteristic wave numbers of an infrared (IR) Spectrum [161]. The IR spectra are

presented as plots of intensity versus wave number. The procedure of the (ATR) FT-IR spectroscopy used in this project is given in Chapter Three.

2.5 REFERENCES

[1] Gani M.S.J.: Concrete, Chapter 5, Cement and concrete, published by Chapman and Hall, 2-6 boundary row, London SEI 8HN, UK, first edition. ISBN 0 412 79050 5, 56-69 (1997).

[2] Wilson A.: Cement and Concrete: Environmental considerations. Environmental building news 2 No. **2** (1993).

[3] Malhotra V.M.: Role of supplementary cementing materials in reducing greenhouse gas emissions. Concrete Technology for a sustainable development in the 21st Century edited by O.E Gjorv and K. Sakai. Published by E and FN Spon, London EC4P 4EE, UK. ISBN: 0 419 25060 3, 226-236 (2000).

[4] Yu L.H, Ou H., Lee L.L.: Investigation on pozzolanic effect of perlite powder in concrete. Cement and Concrete Research **33,** 73–76 (2003).

[5] Shayan A., Xu A.: Performance of glass powder as a pozzolanic material in concrete: A field trial on concrete slabs. Cement and Concrete Research **36,** 457–468 (2006).

[6] Chusilp N., Jaturapitakkul C., Kiattikomol K.: Utilization of bagasse ash as a pozzolanic material in concrete. Construction and Building Materials **23**, 3352–3358(2009).

[7] Rosell-Lam M., Villar-Cociña E., Frías M.:Study on the pozzolanic properties of a natural Cuban zeolitic rock by conductometric method: Kinetic parameters. Construction and Building Materials **25,** 644–650 (2011).

[8] Yildirim H., Ilica T., Sengul O.: Effect of cement type on the resistance of concrete against chloride penetration. Construction and Building Materials **25,** 1282–1288 (2011).

[9] Jain N.: Effect of nonpozzolanic and pozzolanic mineral admixtures on the hydration character of ordinary Portland cement. Construction and Building Materials **27**, 39–44 (2012).

[10] Zeng Q., Li K., Fen-chong T., Dangla P.: Determination of cement hydration and pozzolanic reaction extents for fly-ash cement pastes. Construction and Building Materials **27** 560–569 (2012).

[11] Zhou S., Zhang X., Chen X.: Pozzolanic activity of feedlot biomass (cattle manure) ash, Construction and Building Materials **28,** 493–498 (2012).

[12] Bajare D., Bumanis G., Upeniece L.: Coal combustion bottom ash as microfiller with pozzolanic properties for traditional concrete. Procedia Engineering **57,** 149 – 158 (2013).

[13] Jamil M., Kaish A.B.M.A., Raman S.N., Zain M.F.M.: Pozzolanic contribution of rice husk ash in cementitious system. Construction and Building Materials **47,** 588–593 (2013).

[14] Van V., Rößler C., Bui D., Ludwig H.: Mesoporous structure and pozzolanic reactivity of rice husk ash in cementitious system. Construction and Building Materials **43,** 208–216 (2013).

[15] Hassan A.A.A., Abouhussien A.A., Mayo J.: The use of silica-breccia as a supplementary cementing material in mortar and concrete. Construction and Building Materials **51,** 321–328 (2014).

[16] Kanning R.C., Portella K.F., Braganca M.O.G.P., Bonato M.M., Dos Santos J.C.M.: Banana leaves ashes as pozzolan for concrete and mortar of Portland Cement. Construction and Building Materials **54,** 460–465 (2014).

[17] Setina J., Gabrene A., Juhnevica I.: Effect of pozzolanic additives on structure and chemical durability of concrete. Procedia Engineering **57**, 1005 – 1012 (2013).

[18] Tironi A., Trezza M.A., Scian A.N., Irassar E.F.: Assessment of pozzolanic activity of different calcined clays. Cement and Concrete Composites **37,** 319–327 (2013).

[19] Wong L.S., Hashim R., Ali F.: Utilization of sodium bentonite to maximize the filler and pozzolanic effects of stabilized peat. Engineering Geology **152,** 56–66 (2013).

[20] Massazza F.: Pozzolanic cements. Cement and Concrete Composites **15**, 185-214 (1993).

[21] Shi C., Day R.L.: Comparison of different methods for enhancing reactivity of pozzolans. Cement and Concrete Research **31**, 813-818 (2001).

[22] Isaia G.C., Gastaldini A.L.G., Moraes R.: Physical and pozzolanic action of mineral additions on the mechanical strength of high-performance concrete. Cement and Concrete Composites **25,** 69–76 (2003).

[23] Behnood A., Ziari H.: Effects of silica fume addition and water to cement ratio on the properties of high-strength concrete after exposure to high temperatures. Cement and Concrete Composites **30,** 106–112 (2008).

[24] Sata V., Tangpagasit J., Jaturapitakkul C., Chindaprasirt P.: Effect of W/B ratios on pozzolanic reaction of biomass ashes in Portland cement matrix. Cement and Concrete Composites **34**. 94–100 (2012).

[25] Yio M.H.N., Phelan J.C., Wong H.S., Buenfeld N.R.: Determining the slag fraction, water/binder ratio and degree of hydration in hardened cement pastes. Cement and Concrete Research **56,** 171–181 (2014).

[26] Hou W., Chang K., Hwang C.: A study on anticorrosion effect in high-performance concrete by the pozzolanic reaction of slag. Cement and Concrete Research **34,** 615–622 (2004).

[27] Chindaprasirt P., Jaturapitakkul C., Sinsiri T.: Effect of fly ash fineness on compressive strength and pore size of blended cement paste. Cement and Concrete Composites **27**, 425–428 (2005).

[28] Binici H., Temiz H., Kose M.M.: The effect of fineness on the properties of the blended cements incorporating ground granulated blast furnace slag and ground basaltic pumice. Construction and Building Materials **21**, 1122–1128 (2007).

[29] Pipilikaki P., Katsioti M.: Study of the hydration process of quaternary blended cements and durability of the produced mortars and concretes. Construction and Building Materials, **23**, 2246–2250 (2009).

[30] Ogawa S., Nozaki T., Yamada K., Hirao H., Hooton R.D.: Improvement on sulfate resistance of blended cement with high alumina slag. Cement and Concrete Research **42(**2), 244–251(2012).

[31] Uysal M., Akyuncu V.: Durability performance of concrete incorporating Class F and Class C fly ashes. Construction and Building Materials **34**, 170–178 (2012).

[32] Githachuri K., Alexander M.G.: Durability performance potential and strength of blended Portland limestone cement concrete. Cement and Concrete Composites **39**, 115–121 (2013).

[33] The concrete institute, leaflet publication, http://www.theconcreteinstitute.org.za/#!leaflets/cg0k, CITED on 25/07/2105

[34] Bogue R.H.: The chemistry of Portland cement, Reinhold Publishing, New York, USA. pp. 148-160 (1947).

[35] Gani M.S.J.: Production of Portland cement, Chapter 2, Cement and concrete, published by Chapman and Hall, 2-6 boundary row, London SEI 8HN, UK, first edition. ISBN 0 412 79050 5, 56-69 (1997).

[36] Janotka I.: Hydration of the cement paste with Na_2CO_3 addition. Ceramics Silikáty **45,** (1) 16-23 (2001).

[37] Grieve G.: Cementitious materials, Fulton's Concrete Technology, Edited by Gill Owens, 9th edition, Cement and Concrete Institute Midrand, South Africa. ISBN 978-0-9584779-1-8, pp. 1-16 (2009).

[38] Brooks J.J., Johari M.A.M., Mazloom M.: Effect of admixtures on the setting times of high-strength concrete. Cement and Concrete Composites **22** 293-301 (2000).

[39] Muller H.S., Rubner K.: High-strength concrete-microstructural characteristics and related durability aspects. PRO 1: International RILEM Workshop on Durability of High Performance Concrete, 23-27 (1995).

[40] Ficcadenti S.J.: Effects of cement type and water to cement ratio on concrete expansion caused by sulphate attack, Structural Engineering. Mechanics and Computation **2,** 1607- 1614 (2001).

[41] Weerdt K.D., Haha M.B., Saout G.L., Kjellsen K.O., Justnes H., Lothenbach B.: Hydration mechanisms of ternary Portland cements containing limestone powder and fly ash. Cement and Concrete Research **41,** 279–291(2011).

[42] Soroka I.: Portland cement paste and concrete, Published by the Macmillan Press Limited, ISBN 0-333-24231-9, pp. 30-34 (1979).

[43] Temuujin J., Riessen A., Williams R.: Influence of calcium compounds on the mechanical properties of fly ash geopolymer pastes. Journal of Hazardous Materials **167**, 82–88 (2009).

[44] Yasar E., Erdogan Y., Kılıc A.: Effect of limestone aggregate type and water–cement ratio on concrete strength. Materials Letters **58,** 772– 777 (2004).

[45] Poon C.S., Lam C.S.: The effect of aggregate-to-cement ratio and types of aggregates on the properties of pre-cast concrete blocks. Cement and Concrete Composites **30,** 283–289 (2008).

[46] Prokopski G., Langier B.: Effect of water/cement ratio and silica fume addition on the fracture toughness and morphology of fractured surfaces of gravel concretes. Cement and Concrete Research **30,** 1427-1433 (2000).

[47] Mehta and Monteiro (a): Aggregates for concrete, CITED on 25th, June, 2014 http://www.ce.berkeley.edu/~paulmont/165/aggregate.pdf.

[48] Grieve G.: Aggregates for concrete, Fulton's Concrete Technology, Edited by Gill Owens, 9th edition, Cement and Concrete Institute Midrand, South Africa. ISBN 978-0-9584779-1-8, pp. 25-61. (2009)

[49] Alexander M.G.: Properties of aggregates in concrete; report on phase 2 testing of concretes made with aggregates from a further 10 different quarries, and associated design recommendations. Prepared for HIPPO quarries, pp. 61 (1993).

[50] Goodman J.: Mixing water, Fulton's Concrete Technology, Edited by Gill Owens, 9th edition, Cement and Concrete Institute Midrand, South Africa. ISBN 978-0-9584779-1-8, pp. 63-70 (2009)

[51] Kharita M.H., Yousef S., AlNassar M.: The effect of the initial water to cement ratio on shielding properties of ordinary concrete. Progress in Nuclear Energy **52,** 491–493 (2010).

[52] Fu X., Chung D.D.L.: Improving the bond strength between steel rebar and concrete by increasing the water/cement ratio. Cement and Concrete Research. 27(12), 1805-1809 (1997).

[53] Rahmani K., Shamsai A., Saghafian B., Peroti S.: Effect of Water and Cement Ratio on Compressive Strength and Abrasion of Microsilica Concrete. Middle-East Journal of Scientific Research **12** (8): 1056-1061 (2012).

[54] Wang G., Kong Y., Sun T., Shui Z.: Effect of water–binder ratio and fly ash on the homogeneity of concrete. Construction and Building Materials **38**, 1129–1134 (2013).

[55] Nikbin I.M., Beygi M.H.A., Kazemi M.T., Amiri J.V., Rabbanifar S., Rahmani E., Rahimi S.: A comprehensive investigation into the effect of water to cement ratio and powder content on mechanical properties of self-compacting concrete. Construction and Building Materials **57** 69–80 (2014).

[56] Beygi M.H.A., Kazemi M.T., Nikbin I.M., Amiri J.V.: The effect of water to cement ratio on fracture parameters and brittleness of self-compacting concrete. Materials and Design **50** 267–276 (2013).

[57] Sabir B.B., Wild S., Bai J.: Metakaolin and calcined clays as pozzolans for concrete: a review. Cement and Concrete Composites **23,** 441-454 (2001).

[58] Najimi M., Sobhani J., Ahmadi B., Shekarchi M.: An experimental study on durability properties of concrete containing zeolite as a highly reactive natural pozzolan. Construction and Building Materials **35,** 1023–1033 (2012).

[59] Senhadji Y., Escadeillas G., Mouli M., Khelafi H., Benosman: Influence of natural pozzolan, silica fume and limestone fine on strength, acid resistance and microstructure of mortar. Powder Technology **254,** 314–323(2014).

[60] Habert G., Choupay N., Montel J.M., Guillaume D., Escadeillas G.: Effects of the secondary minerals of the natural pozzolans on their pozzolanic activity. Cement and Concrete Research **38**, 963–975 (2008).

[61] Grist E.R., Paine K.A., Heath A., Norman J., Pinder H.: Compressive strength development of binary and ternary lime–pozzolan mortars. Materials and Design **52,** 514–523 (2013).

[62] Nili M., Salehi A.M.: Assessing the effectiveness of pozzolans in massive high-strength concrete. Construction and Building Materials **24** 2108–2116 (2010).

[63] Foner H.A., Robl T.L., Hower J.C., GrahamU.M.: Characterization of fly ash from Israel with reference to its possible Utilization. Fuel **78** 215–223(1999).

[64] Moreno N., Querol X., Andres J.M., Stanton K., Towler M., Nugteren H., Janssen-Jurkovicova M., Jones R.: Physico-chemical characteristics of European pulverized coal combustion fly ashes. Fuel **84** 1351–1363(2005).

[65] Valipour M., Pargar F., Shekarchi M., Khani S.: Comparing a natural pozzolan, zeolite, to metakaolin and silica fume in terms of their effect on the durability characteristics of concrete: A laboratory study. Construction and Building Materials **41,** 879–888 (2013).

[66] Pekmezci B.Y., Akyuz S.: Optimum usage of a natural pozzolan for the maximum compressive strength of concrete. Cement and Concrete Research **34**, 2175–2179 (2004).

[67] Nguyen V., Leklou N., Aubert J., Mounanga P.: The effect of natural pozzolan on delayed ettringite formation of the heat-cured mortars. Construction and Building Materials **48**, 479–484 (2013).

[68] Sargın S., Saltan M., Morova N., Serin S., Terzi S.: Evaluation of rice husk ash as filler in hot mix asphalt concrete. Construction and Building Materials **48** 390–397 (2013).

[69] Hesami S., Ahmadi S., Nematzadeh M.: Effects of rice husk ash and fiber on mechanical properties of pervious concrete pavement. Construction and Building Materials **53**, 680–691 (2014).

[70] Siddique R.: Compressive strength, water absorption, sorptivity, abrasion resistance and permeability of self-compacting concrete containing coal bottom ash. Construction and Building Materials **47**, 1444–1450 (2013).

[71] Speight J.G.: Coal analysis: The chemistry and technology of coal, published by Taylor and Francis and the CRC press, ISBN: 978-1-4398-3646-0, pp 229 (2013).

[72] Iyer R.: The surface chemistry of leaching coal fly ash. Journal of Hazardous Materials **B93,** 321–329 (2002).

[73] Ahmaruzzaman A.: Review on the utilization of fly ash. Progress in Energy and Combustion Science **36**, 327–363 (2010).

[74] Temuujin J., Riessen A., MacKenzie K.J.D.: Preparation and characterisation of fly ash based geopolymer mortars. Construction and Building Materials **24** 1906–1910 (2010).

[75] Misra A., Biswas D., Upadhyaya S.: Physico-mechanical haracter of self-cementing class C fly ash–clay mixtures. Fuel **84,** 1410–1422(2005).

[76] Gomes S., François M., Abdelmoula M., Refait P., Pellissier C., Evrard O.: Characterization of magnetite in silico-aluminous fly ash by SEM, TEM, XRD, magnetic susceptibility, and Mössbauer spectroscopy. Cement and Concrete Research **29,** 1705–1711(1999).

[77] Sarbak Z., Kramer-Wechowiak M.: Porous structure of waste fly ashes and their chemical modifications. Power Terchnology **123**, 53-58 (2002).

[78] Sarkar A., Rano R., Udaybhanu G., Basu A.K.: A comprehensive characterization of fly ash from a thermal power plant in Eastern India. Fuel Processing Technology **87,** 259 – 277 (2006).

[79] Chancey R.T., Stutzman P., Juenger M.C.G., Fowler D.W.: Comprehensive phase characterization of crystalline and amorphous phases of a Class F fly ash. Cement and Concrete Research **40**, 146–156 (2010).

[80] Smith R.D.: The trace element chemistry of coal during combustion and the emissions from coal-fired plants, Prog. Energy Combust. Sci., **6**, 53-119 (1980).

[81] Brouwers H.J.H., Van Eijk R.J.: Chemical Reaction of Fly Ash, Proceedings of the 11th International Congress on the Chemistry of Cement (ICCC), 11 – 16 May 2003, Durban, South Africa, .Cement.s Contribution to the Development in the 21st Century. ISBN Number: 0-9584085-8-0, Hosted by: The Cement and Concrete Institute of South Africa (2003).

[82] Fernandez-Jimenez A., Palomo A.: Characterisation of fly ashes. Potential reactivity as alkaline cements. Fuel **82,** 2259–2265(2003).

[83] Wang S., Ma Q., Zhu Z.H.: Characteristics of coal fly ash and adsorption application. Fuel **87**, 3469–3473(2008).

[84] Yeheyis M.B., Shang J.Q., Yanful E.K.: Chemical and mineralogical transformations of coal ash after landfilling, World of coal ash (WOCA) conference, May 4-7, 2009, in Lexington, KY, USA.

[85] Sakorafa V., Michailidis K., Burragato F.: Mineralogy, geochemistry and physical properties of fly ash from the Megalopolis lignite fields, Peloponnese, Southern Greece. Fuel **75(4)**, 419-423 (1996).

[86] Dudas M.J., Warren C.J.: Submicroscopic model of fly ash particles. Geoderma **40**, 101-114 (1987).

[87] Kruger J.E.: South African Fly Ash: A cement Extender, Published by The South African Coal Ash Association, ISBN 0-958-45349-7.

[88] Papadakis V.G.: Effect of fly ash on Portland cement systems Part I. Low-calcium fly ash. Cement and Concrete Research **29,** 1727–1736 (1999).

[89] Grieve G.R.H.: The influence of two South African fly ashes on the engineering properties of concrete. Thesis submitted to the faculty of engineering, University of the Witwatersrand, Johannesburg, in fulfilment of the requirements for the degree of Doctor of Philosophy. (1991).

[90] Paya J., Monzo J., Borrachero M.V., Peris-Mora E., Gonzalez-Lopez E.: Mechanical treatment of Fly ashes Part II: Particle morphologies in Ground Fly ashes (GFA) and workability of GFA-Cement mortars**.** Cement and Concrete Research **26** (2) 225-235 (1996).

[91] Criado M., Palomo A., Ferna´ndez-Jime´nez A.: Alkali activation of fly ashes. Part 1: Effect of curing conditions on the carbonation of the reaction products. Fuel **84,** 2048–2054 (2005).

[92] Hela R., Orsáková D.: The mechanical activation of Fly ash. Procedia Engineering **65** 87 – 93 (2013).

[93] Rashad A.M.: A comprehensive overview about the influence of different admixtures and additives on the properties of alkali-activated fly ash. Materials and Design **53** 1005–1025 (2014).

[94] Mehta P.K., Monteiro P.J.M.: Concrete: Microstructure, Properties, and Material Edition: 2nd , published by McGraw-Hill Professional ISBN-071462899, ISBN-9780071462891, pp 25-29, 61-82, 123-135,151(2001).

[95] Uchikawa H., Hanehara S., Sawaki D.: The role of steric repulsive force in the dispersion of cement particles in fresh paste prepared with organic admixture. Cement and Concrete Research **27** (1), 37-50 (1997).

[96] Peschard A., Govin A., Grosseau P., Guilhot B., Guyonnet R.: Effect of polysaccharides on the hydration of cement paste at early ages. Cement and Concrete Research **34**, 2153–2158 (2004).

[97] Vieira M.C., Klemm D., Einfeldt L.: G. Albrecht, Dispersing agents for cement based on modified polysaccharides. Cement and Concrete Research **35**, 883– 890 (2005).

[98] Peschard A., Govin A., Pourchez J., Fredon E., Bertrand L.: Maximilien S., Guilhot B.: Effect of polysaccharides on the hydration of cement suspension. Journal of the European Ceramic Society **26**, 1439–1445 (2006).

[99] Friedemann K., Stallmach F., Kärger J.: Carboxylates and sulfates of polysaccharides for controlled internal water release during cement hydration. Cement and Concrete Composites **31**, 244–249 (2009).

[100] Patural L., Marchal P., Govin A., Grosseau P., Ruo B., Devès O.: Cellulose ethers influence on water retention and consistency in cement-based mortars. Cement and Concrete Research **41**, 46–55 (2011).

[101] Hua O.Z., Guo M.B., Wei J.S.: Influence of cellulose ethers molecular parameters on hydration kinetics of Portland cement at early ages. Construction and Building Materials **33**, 78–83 (2012).

[102] Alonso M.M., Palacios M., Puertas F.: Compatibility between polycarboxylate-based admixtures and blended-cement pastes. Cement and Concrete Composites **35** 151–162 (2013).

[103] Tkaczewska E.: Effect of the superplasticizer type on the properties of the fly ash blended cement. Construction and Building Materials **70,** 388–393 (2014).

[104] Fink J.K.: Cement additives (Chapter 10), Petroleum Engineer's Guide to Oil Field Chemicals and Fluids, 311-359 (2012).

[105] Cirri M., Bragagni M., Mennini N., Mura P.: Development of a new delivery system consisting in ‘‘drug – in cyclodextrin – in nanostructured lipid carriers’’ for ketoprofen topical delivery. European Journal of Pharmaceutics and Biopharmaceutics **80,** 46–53 (2012).

[106] Rocha de Freitas M., Rolim L.A., Soares M.F., Rolim-Neto P.J., Muniz de Albuquerque M., Soares-Sobrinho J.L.: Inclusion complex of methyl-cyclodextrin and olanzapine as potential drug delivery system for schizophrenia. Carbohydrate Polymers **89**, 1095– 1100 (2012).

[107] Hernandez-Montelong O., Naveas N., Degoutin S., Tabary N., Chai F., Spampinato V., Ceccone G., Rossi F., Torres-Costa V., Manso-Silvan M., Martel

B.: Porous silicon-cyclodextrin based polymer composites for drug delivery applications. Carbohydrate Polymers **110,** 238–252 (2014).

[108] Lv S., Gao R., Cao Q., Li D., Duan J.: Preparation and characterization of poly-carboxymethyl-β-cyclodextrin superplasticizer. Cement and Concrete Research **42,** 1356–1361 (2012).

[109] Pandya S.J., Mansuri J.S., Patel P.: Compatible Polymer used as complexes in various drug delivery systems : β-Cyclodextrin. Pharmaceutical Reviews **6**(2) (2008).

[110] Ikotun B.D., Mishra S., Fanourakis G.C.: Study on the synthesis, morphology and structural analysis of fly ash–cyclodextrin composite. Journal of Inclusion Phenomena and Macrocyclic Chemistry **79**, 311-317 (2014).

[111] Li Y., Guo H., Zhang Y., Zheng J., Li Z., Yang C., Lu M.: Synthesis of copolymers with cyclodextrin as pendants and its end group effect as superplasticizer. Carbohydrate Polymers **102**, 278– 287 (2014).

[112] Siddique R., Khan M.I.: Supplementary cementing materials, published by Springer-Verlag Berlin Heidelberg, ISBN 978-3-642-17865-8 (2011).

[113] Joshi R.C., Lothia R.P.: Fly ash in concrete: Production, Properties and Uses, published by Gordon and Breach Science Publishers, ISBN 90-5699-580-4, pp 69 (1997).

[114] Siddique R.: Properties of concrete incorporating high volumes of class F fly ash and san fibers. **34**(1), 37- 42 (2004).

[115] Erdogdu S., Arslanturk C., Kurbetci S.: Influence of fly ash and silica fume on the consistency retention and compressive strength of concrete subjected to prolonged agitating. Construction and Building Materials **25,** 1277–1281 (2011).

[116] Garbacz A., Sokołowska J.J.: Concrete-like polymer composites with fly ashes – Comparative study. Construction and Building Materials **38**, 689–699 (2013).

[117] Ravina D., Mehta P.K.: Properties of fresh concrete containing large amounts of fly ash. Cement and concrete research **16,** 227-238 (1986).

[118] Durán-Herrera A., Juárez C.A., Valdez P., Bentz D.P.: Evaluation of sustainable high-volume fly ash concretes. Cement and Concrete Composites **33,** 39-45 (2011).

[119] Alvarez M., Salas J., Veras J.: Properties of concrete made with fly ash. The international Journal of Cement Composites and Lightweight concrete **10** (2), 109-120 (1988).

[120] Wallevik O.H., Wallevik J.E.: Rheology as a tool in concrete science: The use of rheographs and workability boxes. Cement and Concrete Research **41,** 1279–1288 (2011).

[121] Banfill P. F. G.: Rheology of fresh cement and concrete. Rheology Reviews, 61 – 130 (2006).

[122] Chidiac S.E., Mahmoodzadeh F.: Plastic viscosity of fresh concrete – A critical review of predictions methods. Cement and Concrete Composites **31,** 535–544 (2009).

[123] Xie H., Liu F., Fan Y., Yang H., Chen J., Zhang J., Zuo C.: Workability and proportion design of pumping concrete based on rheological parameters. Construction and Building Materials **44,** 267–275 (2013).

[124] Laskar A.I., Talukdar S.: Rheological behavior of high performance concrete with mineral admixtures and their blending. Construction and Building Materials **22,** 2345–2354 (2008).

[125] Kovler K., Roussel N.: Properties of fresh and hardened concrete. Cement and Concrete Research **41** 775–792 (2011).

[126] Mehta and Monteiro: properties of fresh concrete, CITED on 11th, August, 2014. http://www.ce.berkeley.edu/~paulmont/165/early_age2.pdf.

[127] Ravina D., Mehta P.K.: Compressive strength of low cement/high fly ash concrete. Cement and concrete research **18**, 571-583 (1988).

[128] Siddique R.: Performance characteristics of high-volume Class F fly ash concrete. Cement and Concrete Research **34,** 487–493 (2004).

[129] Gopalan M.K., Haque M.N.: Mix design for Optimal Strength Development of Fly ash concrete. Cement and Concrete Research **19** 634-641 (1989).

[130] Addis B.J.: Portland cement and cement extenders, Fulton's Concrete Technology, Edited by Addis, B.J, 7th edition, Cement and Concrete Institute Midrand, South Africa. ISBN 0-620-18227-X, pp. 2-7 (1994).

[131] Poon C.S., Lam L., Wong Y.L.: A study on high strength concrete prepared with large volumes of low calcium fly ash. Cement and Concrete Research **30** 447-455 (2000).

[132] Kayali O., Ahmed M.S.: Assessment of high volume replacement fly ash concrete – Concept of performance index. Construction and Building Materials **39**, 71–76 (2013).

[133] Achal V., Pan X., Özyurt N.: Improved strength and durability of fly ash-amended concrete by microbial calcite precipitation. Ecological Engineering **37,** 554-559 (2011).

[134] Pacheco-Torgal F., Labrincha J.A.: Biotech cementitious materials: Some aspects of an innovative approach for concrete with enhanced durability. Construction and Building Materials **40**, 1136–1141 (2013).

[135] Schwarz N., Cam H., Neithalath N.: Influence of a fine glass powder on the durability characteristics of concrete and its comparison to fly ash. Cement and Concrete Composites **30**, 486-496 (2008).

[136] Castro S., Brito J.: Evaluation of the durability of concrete made with crushed glass aggregates. Journal of Cleaner Production **41** 7-14 (2013).

[137] Colak A., Cosgun T., Bakırcı A.E.: Effects of environmental factors on the adhesion and durability characteristics of epoxy-bonded concrete prisms. Construction and Building Materials **23**, 758–767 (2009).

[138] El-Hawary M.M., Abdul-Jaleel A.: Durability assessment of epoxy modified concrete. Construction and Building Materials **24**, 1523–1528 (2010).

[139] Shekari A. H., Razzaghi M.S.: influence of nano particles on durability and mechanical properties of high performance concrete. Procedia Engineering 14, 3036–3041(2011).

[140] Peyvandi A., Soroushian P., Balachandra A.M., Sobolev K.: Enhancement of the durability characteristics of concrete nanocomposite pipes with modified graphite nanoplatelets. Construction and Building Materials **47,** 111–117 (2013).

[141] Saboktakin A., Saboktakin M.R.: Improvement of reinforced concrete properties based on modifiedstarch/polybutadiene nanocomposites. International Journal of Biological Macromolecules **70**, 381–384 (2014).

[142] Beushausen H., Gillmer M., Alexander M.: The influence of superabsorbent polymers on strength and durability properties of blended cement mortars. Cement and concrete composites **52**, 73-80 (2014).

[143] Heidari-Rarani M., Aliha M.R.M., Shokrieh M.M., Ayatollahi M.R.: Mechanical durability of an optimized polymer concrete under various thermal cyclic loadings – An experimental study. Construction and Building Materials **64,** 308-315 (2014).

[144] Richardson A.E., Coventry K.A., Wilkinson S.: Freeze/thaw durability of concrete with synthetic fibre additions. Cold Regions Science and Technology **83–84** , 49–56 (2012).

[145] Vejmelková E., Pavlíková M., Keppert M., Keršner Z., Rovnaníková P., Ondrácek M., Sedlmajer., Cerny R.: High performance concrete with Czech metakaolin: Experimental analysis of strength, toughness and durability characteristics. Construction and Building Materials **24**, 1404-1411 (2010).

[146] Nath P., Sarker P.: Effect of Fly Ash on the Durability Properties of High Strength Concrete. Procedia Engineering **14,** 1149–1156 (2011).

[147] Hadjsadok A., Kenai S., Courard L., Michel F., Khatib J.: Durability of mortar and concretes containing slag with low hydraulic activity. Cement and concrete composites **34,** 671-677 (2012).

[148] Ramezanianpour A.A., Jovein H.B.: Influence of metakaolin as supplementary cementing material on strength and durability of concretes. Construction and Building Materials **30**, 470-479 (2012).

[149] Duan P., Shui Z., Chen W., Shen C.: Enhancing microstructure and durability of concrete from ground granulated blast furnace slag and metakaolin as cement replacement materials. Journal of Materials Research and Technology **2**(1), 52-59 (2013).

[150] Teng S., Lim T.Y.D., Divsholi B.S.: Durability and mechanical properties of high strength concrete incorporating ultra fine Ground Granulated Blast-furnace Slag. Construction and Building Materials **40**, 875-881 (2013).

[151] Heede P.V., Gruyaert E., Belie N.D.: Transport properties of high-volume fly ash concrete: Capillary water sorption, water sorption under vacuum and gas permeability. Cement and Concrete Composites **32**, 749–756 (2010).

[152] Chindaprasirt P., Jaturapitakkul C., Sinsiri T.: Effect of fly ash fineness on microstructure of blended cement paste. Construction and Building Materials **21**, 1534–1541 (2007).

[153] Ballim Y., Alexander M.G.: Towards a performance-based specification for concrete durability. African Concrete Code Symposium, 206-218 (2005).

[154] Ballim Y.A.: Low cost, falling head permeameter for measuring concrete gas permeability, Concrete/Beton, Journal of the Concrete Society of Southern Africa **61**, 13-18 (1991).

[155] Streicher P.E., Alexander M.G.: A chloride conduction test for concrete, Cement and Concrete Research **25**, 1284-1294 (1995).

[156] Streicher P.E., Alexander, M.G.: Towards standardisation of a rapid chloride conduction test for concrete. Cement, Concrete and Aggregates **21**, 23-30 (1999).

[157] Alexander M.G., Mackechnie J.R., Ballim Y.: Guide to the use of durability indexes for achieving durability in concrete structures, Research monograph no 2, published by the Department of Civil Engineering, University of Cape Town in collaboration of University of the Witwatersrand, pp. 5-25 (2001).

[158] Guneyisi E., Gesoglu M., Ozturan T., Ozbay E.: Estimation of chloride permeability of concretes by empirical Character: Considering effects of cement type, curing condition and age. Construction and Building Materials **23,** 469–481(2009).

[159] Olorunsogo F.T., Padayachee N.: Performance of recycled aggregate concrete monitored by durability indexes. Cement and Concrete Research **32** 179–185 (2002).

[160] Moir G.: Cement, Advanced Concrete Technology Set, 3–45 (2003).

[161] Ylmén E.R.: Early Hydration of Portland Cement - An Infrared Spectroscopy Perspective Complemented by Calorimetry and Scanning Electron Microscopy, thesis for the degree of doctor of technology, Chalmers University of Technology, Gothenburg, Sweden 2013 ISBN 978-91-7385-853-3.

[162] Damme H.V., Gmira A.: Chapter 13.3 Cement hydrates, Handbook of Clay Science Edited by F. Bergaya, B.K.G. Theng and G. Lagaly Developments in Clay Science, Vol. 1, Elsevier Ltd, pp 1113- 1127 (2006).

[163] Wang A., Zhang C., Sun W.: Fly ash effects: I. The morphological effect of fly ash. Cement and Concrete Research **33,** 2023–2029 (2003).

[164] Hema J.: The Effects of Liquid Nitrogen on Concrete Hydration, Microstructure and Properties, thesis for the degree of Doctor of Philosophy, University of Texas at Austin (2008).

CHAPTER THREE

CHARACTERISATION OF FOUR SOUTH AFRICAN FLY ASHES AND THEIR MODIFICATION WITH *β*-CYCLODEXTRIN

3.1 INTRODUCTION

The use of industrial waste as construction materials has attracted the interest of many researchers due to the benefits attached such as, reduction of environmental pollution, availability of land use for purposes other than dumping industrial waste and reduction in construction materials cost [1-3]. Industrial wastes that are of abundance in South Africa include fly ash (FA). FA is produced from the coal firing for power generation, which is the main source of electricity in South Africa. ESKOM, the main South African electricity producer produces approximately thirty six million tons of FA per annum [4] while approximately two million tons of the FA per year is sold for reuse. The remaining fly ash is normally dumped on landfill adjacent to the power stations. Researchers have found use for fly ash in the area of construction, agriculture and mining [5], but large quantities (approximately thirty four million tons) are still left unused and there is need to expand its usage. The understanding of the characteristics of fly ash will help to identify new areas of construction in which FA can be utilised effectively.

Structural characterisation analysis helps to characterise a material based on its structural features. Almost all engineering materials exhibit structural features that are characteristic of them; these features may need a low-powered optical microscope to reveal them or may be visible [6]. Structural features of most engineering materials dictate their properties and their study can reveal casually the relationship between a particular feature and a specific physical, chemical or engineering property [6]. In this chapter, X-ray diffraction (XRD) and Fourier transform infrared spectroscopy (FT-IR) are used to characterise four South African fly ashes and to study their modification with *β*-cyclodextrin (*β*-CD).

3.2. MATERIALS AND MIXES

Fly ashes used were obtained from four different South African power stations; Matla, Kendal, Lethabo and Majuba through ash resources, South Africa. *β*-CD from Wacker Chemie was obtained from Industrial Urethanes (Pty) Ltd, South Africa. The characteristics of the *β*-CD as supplied by the producer are presented in Table 3.1. FA samples were subjected to XRF, particle size distribution, FT-IR and XRD analysis. XRD and FT-IR analyses were used to study the structural changes and functional groups of FA-*β*-CD composites.

Table 3.1: Characterisation of the *β*-cyclodextrin used

Property	***β* -CD**
Empirical formula	$C_{42}H_{70}O_{35}$
Bulk density	400-700 kg/m^3
Solubility in water at 25 ^oC	18.5 g/l
Content (on dry basis)	Min. 95 %

FA-*β*-CD composite mixes were prepared by co-grinding a pre-weighed amount of *β*-CD with each FA in a mortar at a mass ratio of 1:9 (10%*β*-CD-90%FA); the composite samples were heated in the oven at 40 ^0C for 20 minutes.

3.3 EXPERIMENTAL PROCEDURE

3.3.1 X-ray fluorescence (XRF) analysis

XRF analysis was done on all the FA samples to obtain their chemical composition. The samples were oven-dried overnight at 105 ^0C. One gram of the dried sample was placed in a porcelain crucible and put in an oven at 930 ^0C for 30 minutes to calculate the loss of ignition (LOI). XRF analysis of the ignited sample was done by fusion with lithium tetraborate at 1200 ^0C in a platinum crucible. The casting procedure was

used to produce the flat glass discs, which were placed directly on the XRF machine for elemental analysis.

3.3.2 Particle size distribution

The particle size distribution was determined by using both sieve and hydrometer (sedimentation process) methods because most of the particles were less than 0.075 mm. Samples were first placed in an oven at 100 ^{0}C for 12 hours after which they were each split in two. The first part was weighed and soaked in water then washed through 0.075 mm sieve. The portion retained on the 0.075 mm sieve was oven dried again for 12 hours at 100 ^{0}C. This dried portion was weighed and allowed to pass through a series of sieves with the 0.075 mm sieve as the smallest. The percentage of the total sample (by mass) passing through each sieve was recorded, the procedure followed was according to Method A1 (b) of TMH 1 [7]. The sedimentation process was followed using a hydrometer for the second part after being sieved in a 0.425 mm sieve as described in Method A6 of TMH 1 [8], with a modification to the dispersing agent. TMH 1 Method A6 [8] prescribes the use of the mixture of sodium silicate and sodium oxalate solution as the dispersing agent. The solution used in this project comprised of 8.75 g sodium carbonate and 41.25 g of sodium hexametaphosphate in distilled water, to make up a volume of one litre. The test was done at the Civil Engineering Technology laboratory, University of Johannesburg.

3.3.3 X-ray diffraction (XRD) analysis

XRD analysis was done to determine the minerals present in the powdered samples using a PW1710 Philips powder diffractometer with monochromatic Cu Kα radiation at 40 kV and 40 mA. Diffractograms were collected over a range of 2θ between 10-80^o, with a step size of 0.017. The XRD samples were prepared using front loading technique. The test was done at the Chemistry laboratory, University of Johannesburg.

3.3.4 Fourier transform-infrared spectroscopy (FT-IR) analysis

FT-IR analysis was done using a Perkin Elmer 100 Spectrometer incorporated with diamond attenuated total reflectance (ATR). The diamond ATR instrument was installed securely on the spectrometer. The samples were analysed in their powder form using a ZnSe/diamond composite as the key component of the universal ATR sample holder with the characteristic peaks in wavenumbers from 650 to 4000 cm^{-1}. Spectra were collected and recorded with nitrogen gas at 20 ml/min flow rate and a temperature range between 30 and 800 ^{0}C at 10.00 ^{0}C/min. The test was done at the Chemistry laboratory, University of Johannesburg.

3.4 RESULTS AND DISCUSSION

3.4.1 XRF analysis

The chemical compositions of the fly ashes are shown in Table 3.2. All the samples are in class F with $SiO_2 + Al_2O_3 + Fe_2O_3$ greater than 70 %, SO_3 less than 5 %, alkalis ($Na_2 + K_2O$) less than 1.5 % and loss of mass on ignition (LOI) less than 6 % according to ASTM C618 [9]. The main oxide content of all the four samples was SiO_2 followed by Al_2O_3, which makes FA generally a potential pozzolan in concrete technology as proven in different literatures [4, 10-13]. FA has also been discovered to be a good source of producing aluminosilicate gel in geopolymer chemistry [14-16], because of its high contents of SiO_2 and Al_2O_3.

Table 3.2: Chemical composition of fly ashes

Content in oxide form.	% mass			
	Matla	**Majuba**	**Lethabo**	**Kendal**
SiO_2	50.95	52.05	49.13	52.07
Al_2O_3	29.69	30.42	34.48	29.97
Fe_2O_3	2.51	4.29	3.02	4.62
MgO	1.87	1.54	1.04	1.47
CaO	6.15	6.10	3.88	5.53
Na_2O	0.54	0.11	0.22	0.20
K_2O	0.79	0.81	0.59	0.76
TiO_2	1.70	1.75	1.70	1.61
SO_3	0.29	0.17	0.10	0.12
LOI	2.30	0.40	0.60	1.70
SiO_2/Al_2O_3	1.72	1.71	1.42	1.74
TOTAL	96.79	97.64	94.76	98.05

3.4.2 Particle size distributions

The particle size distribution of the FA samples is represented in Figure 3.1a, b, c, d. All the samples were finely graded with most particles passing the 0.075 mm sieve. Lethabo FA (Figure 3.1c) was the finest with an average particle size of 0.0152 mm as shown in Table 3.3. The Kendal FA had the highest average particle size of 0.0538 mm (Table 3.3), which is still less than 0.075 mm. All the samples were finely graded within the acceptable range.

Table 3.3: Average particle size of Matla, Majuba, Lethabo and Kendal fly ashes samples from grading analysis

Samples	Average Particle size from grading analysis (mm)
Matla fly ash	0.0160
Majuba fly ash	0.0379
Lethabo fly ash	0.0152
Kendal fly ash	0.0538

	Particle Size (mm)	% Passing
SIEVE	75.00	100.0
	53.00	100.0
	37.50	100.0
	26.50	100.0
	19.00	100.0
	13.20	100.0
	9.50	100.0
	4.75	100.0
	2.00	100.0
	1.18	100.0
	0.60	100.0
	0.425	100.0
	0.300	100.0
	0.150	99.9
	0.075	97.0
HYDROMETER	0.075	97.0
	0.050	92.0
	0.040	89.0
	0.026	80.0
	0.015	64.0
	0.010	52.0
	0.0074	42.0
	0.0036	27.0
	0.0015	16.0

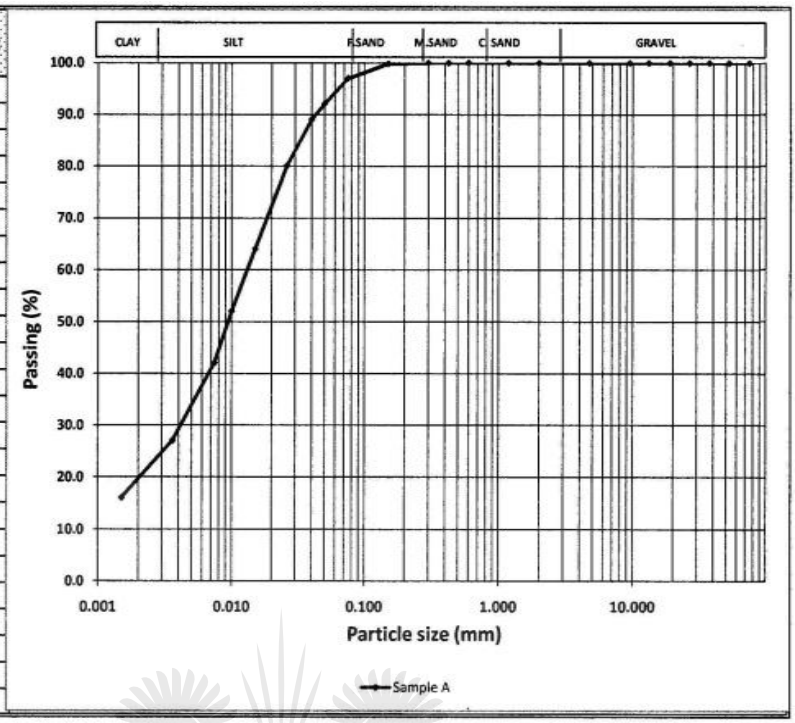

(a) Matla

	Particle Size (mm)	% Passing
SIEVE	75.00	100.0
	53.00	100.0
	37.50	100.0
	26.50	100.0
	19.00	100.0
	13.20	100.0
	9.50	100.0
	4.75	100.0
	2.00	100.0
	1.18	100.0
	0.60	100.0
	0.425	100.0
	0.300	99.8
	0.150	94.9
	0.075	80.0
HYDROMETER	0.075	80.0
	0.050	70.0
	0.040	64.0
	0.026	55.0
	0.015	44.0
	0.010	36.0
	0.0074	30.0
	0.0036	20.0
	0.0015	15.0

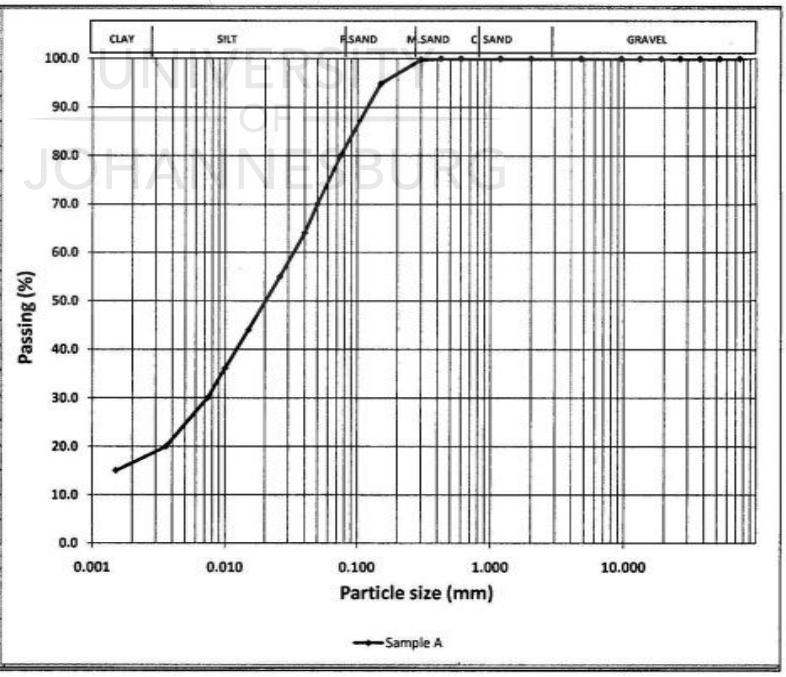

(b) Majuba

	Particle Size (mm)	% Passing
SIEVE	75.00	100.0
	53.00	100.0
	37.50	100.0
	26.50	100.0
	19.00	100.0
	13.20	100.0
	9.50	100.0
	4.75	100.0
	2.00	100.0
	1.18	100.0
	0.60	100.0
	0.425	100.0
	0.300	100.0
	0.150	100.0
	0.075	99.0
HYDROMETER	0.075	99.0
	0.050	96.0
	0.040	94.0
	0.026	86.0
	0.015	50.0
	0.010	34.0
	0.0074	28.0
	0.0036	20.0
	0.0015	15.0

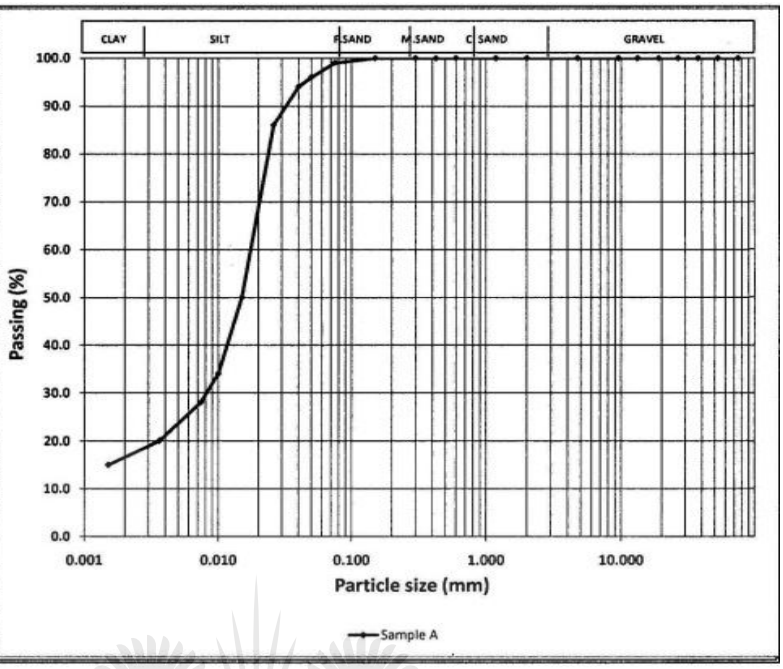

(c) Lethabo

	Particle Size (mm)	% Passing
SIEVE	75.00	100.0
	53.00	100.0
	37.50	100.0
	26.50	100.0
	19.00	100.0
	13.20	100.0
	9.50	100.0
	4.75	100.0
	2.00	100.0
	1.18	99.9
	0.60	99.7
	0.425	99.4
	0.300	98.4
	0.150	87.5
	0.075	73.5
HYDROMETER	0.075	73.5
	0.050	63.6
	0.040	57.6
	0.026	47.7
	0.015	37.8
	0.010	29.8
	0.0074	25.8
	0.0036	18.9
	0.0015	13.9

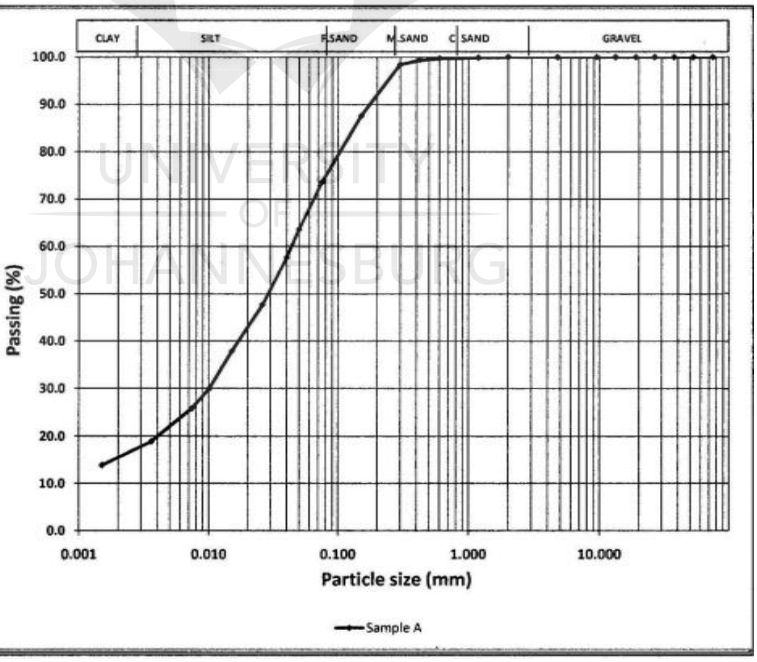

(d) Kendal

Figure 3.1: Particle size distribution of: (a) Matla fly ash (b) Majuba fly ash (c) Lethabo fly ash (d) Kendal fly ash

3.4.3 XRD analysis

The β-CD revealed intense crystalline peaks in Figure 3.2 at approximately diffraction angles $2\theta = 12.74^0$, 22.74^0 and 34.86^0 as also reported by Roik and Belyakova [17]. The major peaks of all the FA samples were obtained at approximate diffraction angles of $2\theta = 26.5^0$, 35.2^0, 40.8^0 and 60.6^0 as shown in Figure 3.3a, b, c & d. These peaks were attributed to quartz (SiO_2), hematite (Fe_2O_3), sillimanite (Al_2SiO_5) and mullite ($Al_6Si_2O_{13}$), respectively. This is in agreement with other researchers [18-20].

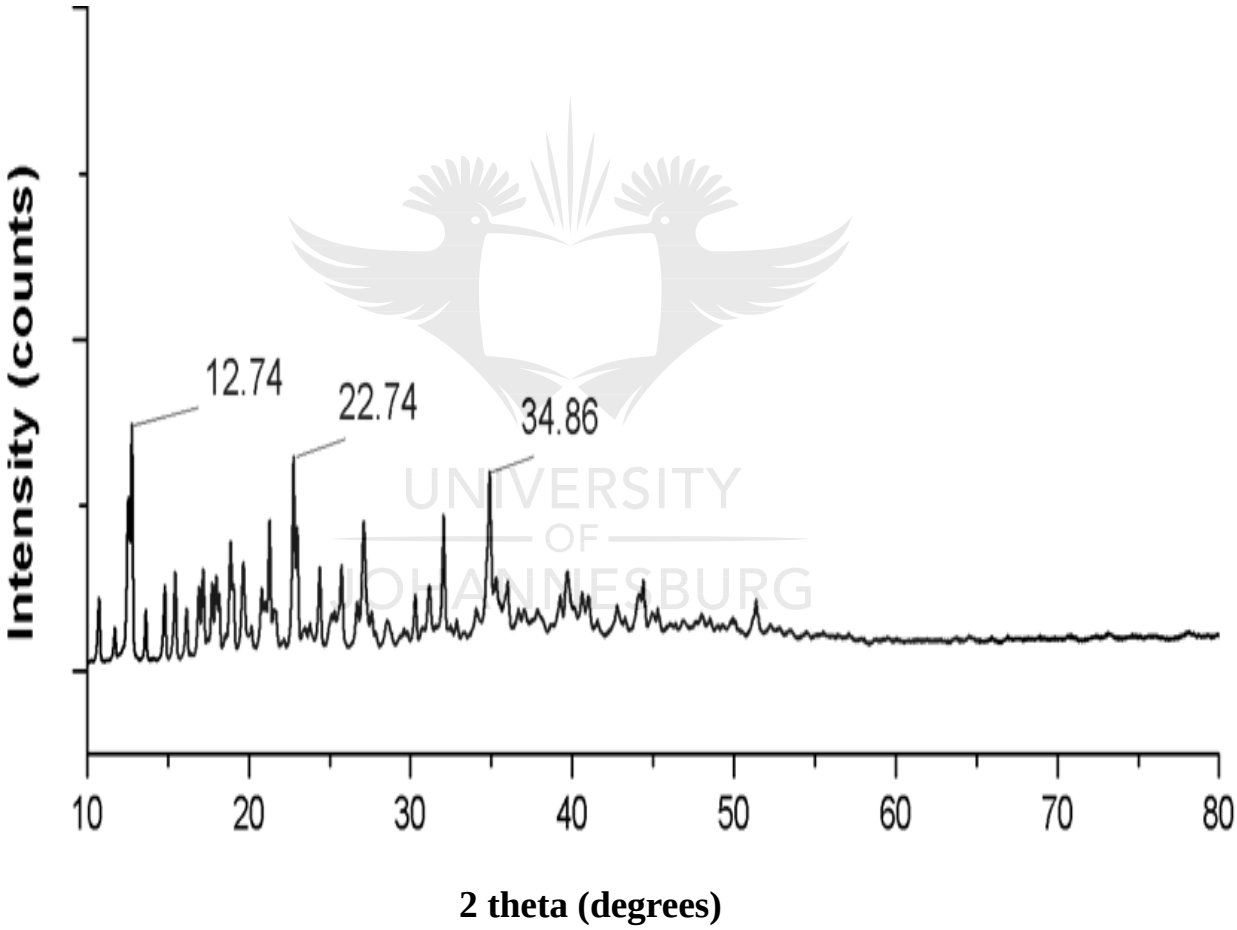

Figure 3.2: X-ray diffractogram of β-CD

Kendal FA had the highest intensity of quartz (SiO_2) followed by Majuba FA as confirmed with the XRF results (Table 3.2). In addition, Lethabo FA had the highest intensity of sillimanite (Al_2SiO_5) and mullite ($Al_6Si_2O_{13}$) followed by Majuba FA; this is also in agreement with the XRF results (Table 3.2) with Lethabo FA having the highest content of Al_2O_3.

The XRD diffractograms of the FA-β-CD composites are shown in Figure 3.4a, b, c, d. All the composites formed with the four fly ashes and β-CD revealed additional peaks at approximately 12.6^0 and 22.7^0 diffraction angles (2θ), which were not in their raw fly ashes. These peaks are attributed to CD. The crystalline structure of β-CD and FA were observed in all the composite samples. However, all the diffractograms conformed more to their raw fly ashes.

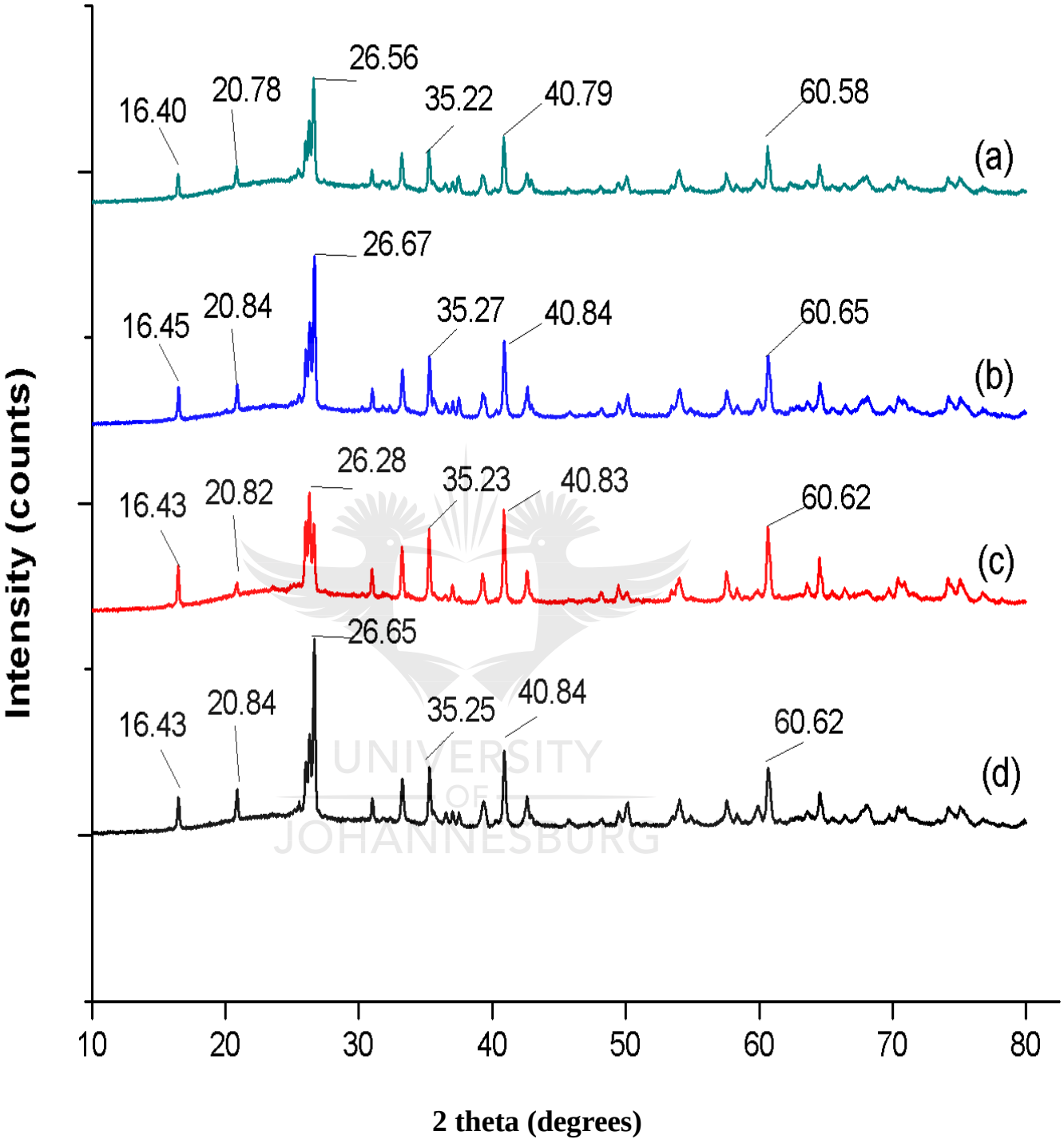

Figure 3.3: XRD diffractograms of: (a) Matla Fly ash (b) Majuba fly ash (c) Lethabo fly ash (d) Kendal fly ash

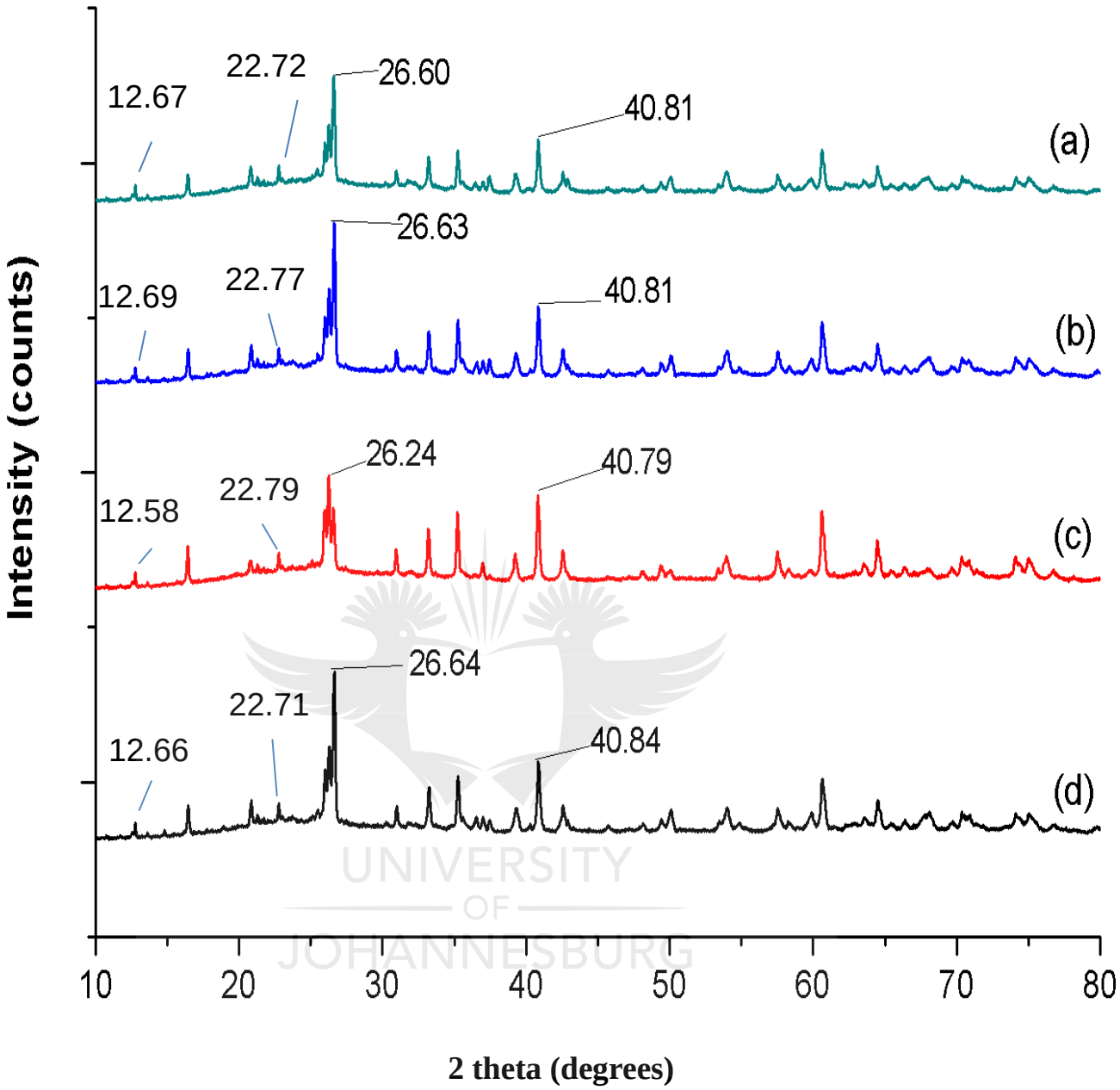

Figure 3.4: XRD diffractograms of: (a) Matla Fly ash-*β*-CD (b) Majuba fly ash-*β*-CD (c) Lethabo fly ash-*β*-CD (d) Kendal fly ash-*β*-CD composites

3.4.4 FT-IR analysis

Figure 3.5 shows the FT-IR spectra of β-CD, broad peaks associated with O-H stretching vibration were observed at approximately 3316 cm^{-1} and 2928 cm^{-1}. Sharp IR bands associated with C-O-H deformation vibration were also observed at approximately 1657 cm^{-1} and 1550 cm^{-1} while C-O deformation was seen at approximately 1220 cm^{-1}, 1078 cm^{-1}, 1023 cm^{-1} and 999 cm^{-1}. The peak at approximately 775 cm^{-1} was attributed to C-H deformation band.

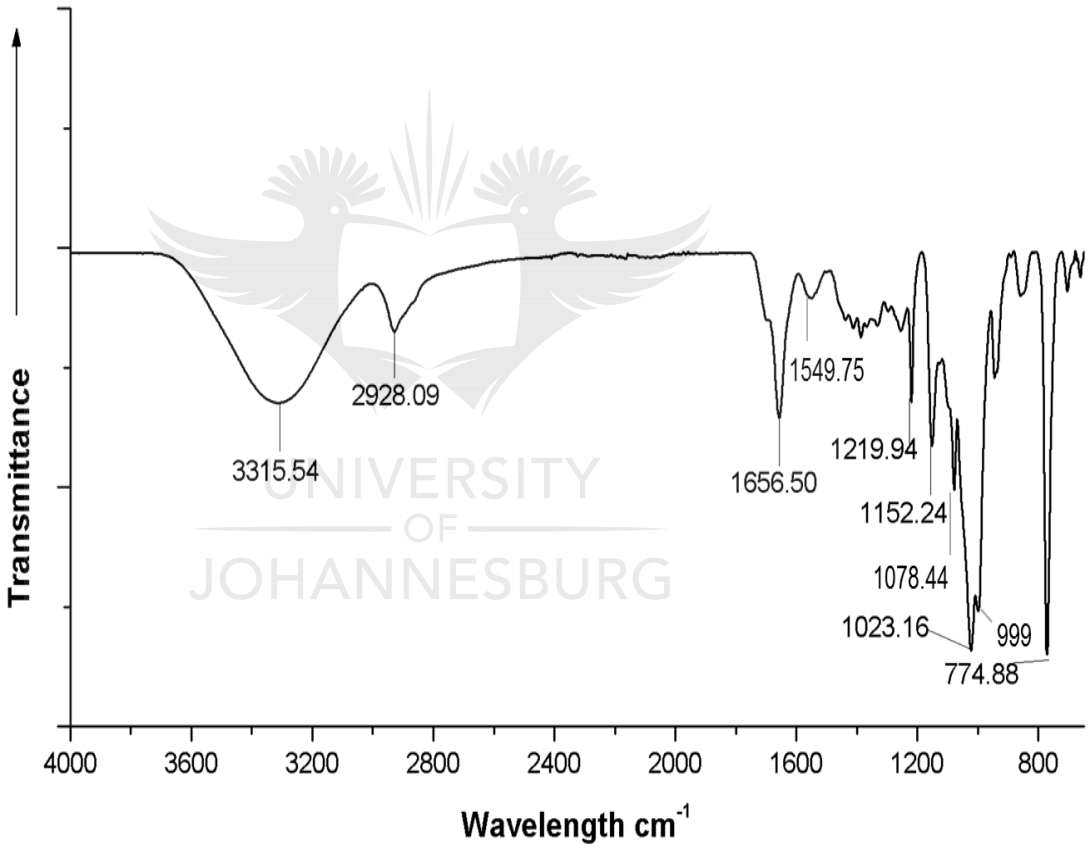

Figure 3.5: FT-IR spectra of β-CD

A strong and broad band, between the range 1074 cm^{-1} and 1096 cm^{-1}, due to Si-O-Si asymmetric stretching vibration [21, 22] was observed in the FT-IR spectrum of all the fly ashes (Figure 3.6a, b, c & d). The peaks observed between the range 2180 cm^{-1} and 2236 cm^{-1} as shown in Figure 3.6a, b, c & d, were attributed to asymmetric stretching of Si–O–Si in the silicate framework structures [23]. The peak at approximately between 796 cm^{-1} and 918 cm^{-1} could be attributed to Al-O symmetric stretching vibration.

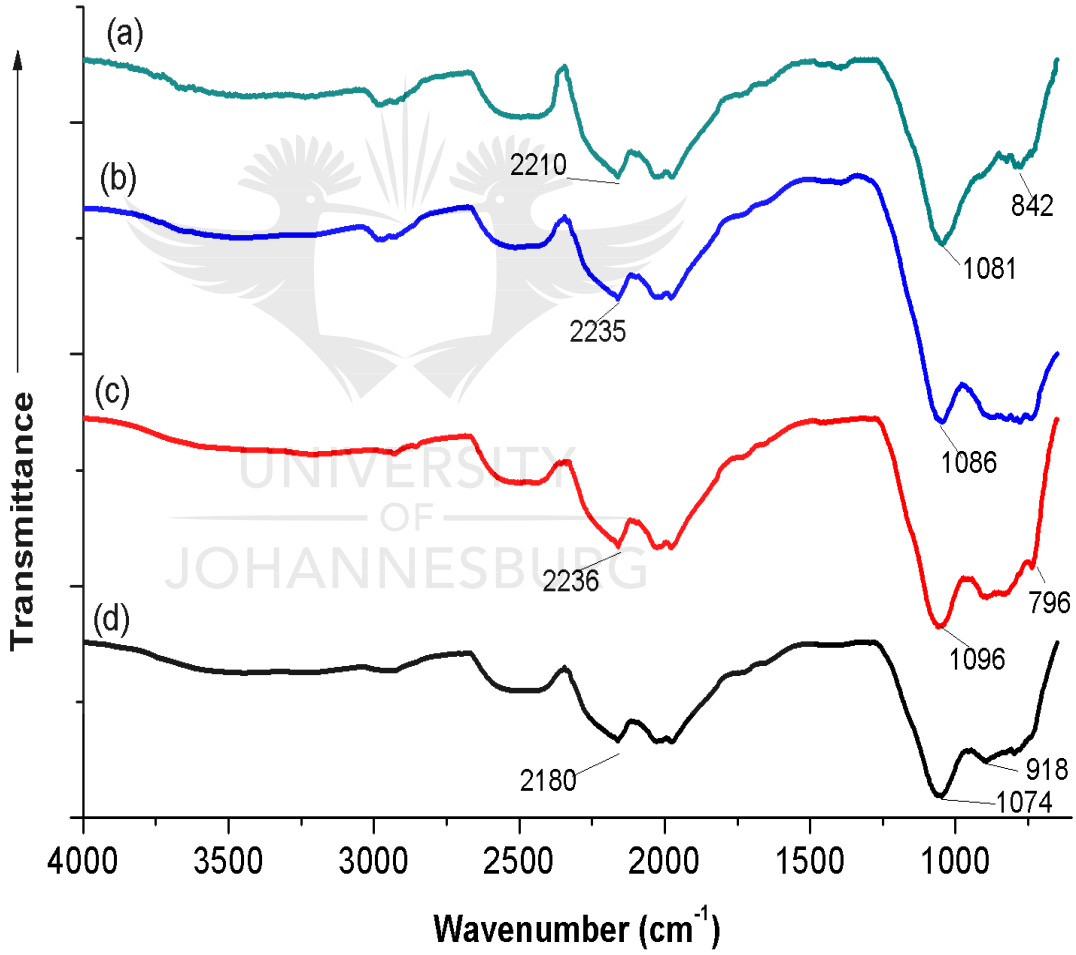

Figure 3.6: FT-IR spectra of: (a) Matla Fly ash (b) Majuba fly ash (c) Lethabo fly ash (d) Kendal fly ash

Changes were observed in the FT-IR Spectra of all the composite samples as represented in Figure 3.7a, b, c, d. An additional peak, at approximately 1155 cm^{-1}, attributed to O-Si-O bending vibration was observed in all the composite samples, which was not present in the raw fly ashes. The stronger intensity of Si-O-Si peak between 1052 cm^{-1} and 1084 cm^{-1} on the spectra of all the composite samples was evidence of the contribution of the C-O deformation vibration peak at approximately 1023 cm^{-1} in β-CD (Figure 3.5). Frequencies shift from the range between 1074 cm^{-1} and 1096 cm^{-1} to the range between 1052 cm^{-1} and 1084 cm^{-1} was observed in all the composite samples.

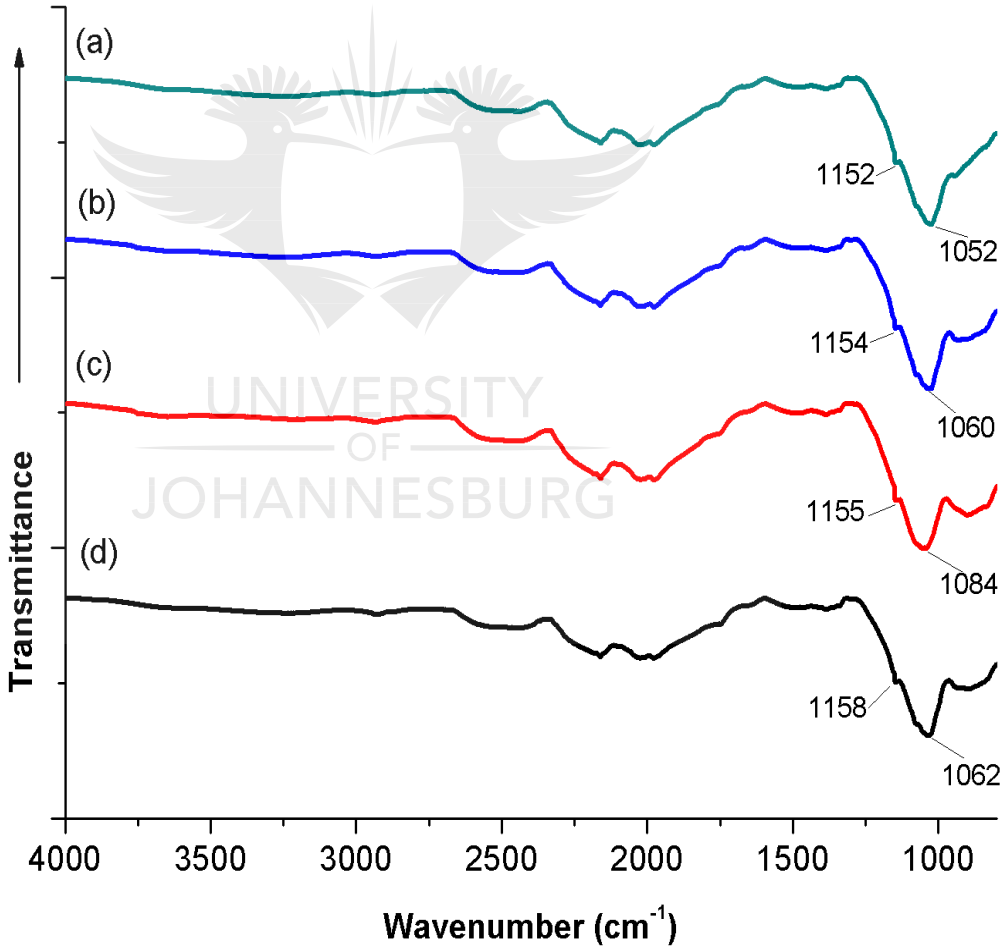

Figure 3.7: FT-IR spectra of: (a) Matla Fly ash-β-CD (b) Majuba fly ash-β-CD (c) Lethabo fly ash-β-CD (d) Kendal fly ash-β-CD composites

3.5 CONCLUSIONS

Structural characterisation of four South African fly ashes and the effect of their composites with β-CD were studied. The four South African class F fly ashes investigated have similar characteristics. Both β-CD and FA contributed similarly to the changes in all the composites with the evidence of additional peaks at approximately 12.6^0 and 22.7^0 of the X-ray diffraction angles (2θ), shift in FT-IR spectra frequencies and additional IR peak at approximately 1155 cm^{-1} (attributed to O-Si-O bending vibration).

3.6 REFERENCES

[1] Yun W.C., Yong J.K., Ook C., Kwang M.L., Mohamed L.: Utilization of tailings from tungsten mine waste as a substitution material for cement. Construction and Building Materials **23**, 2481–2486 (2009).

[2] Sen T., Mishra U.: Usage of industrial waste products in village road construction. International Journal of Environmental Science and Development **1(2)**, 122- 126 (2010).

[3] Zhao Y., Zhang Y., Chen T., Chen Y., Bao S.: Preparation of high strength autoclaved bricks from hematite tailings. Construction and Building Materials **28**, 450–455 (2012).

[4] ESKOM 2011. Partnering for a sustainable future integrated report, http://financialresults.co.za/2011/ESKOM_ar2011/gb_coal03.php (CITED: 20/10/2013).

[5] Ahmaruzzaman A. M.: Review on the utilization of fly ash. Progress in Energy and Combustion Science **36**, 327–363 (2010).

[6] Brandon D., Kaplan W.D.: Microstructural Characterisation of Materials. 2nd ed. John Wiley and Sons ISBN 9780470027851 (2008).

[7] TMH 1 Method A1 (b).: Standard Methods of Testing Road Construction Materials: The dry preparation and sieve analysis of gravel, sand and soil samples, 1986. Published by National Institute for Transport and Road Research (NITRR), South Africa.

[8] TMH 1 Method A6.: Standard Methods of Testing Road Construction Materials: The determination of the grain size distribution in soils by means of a hydrometer, 1986. Published by National Institute for Transport and Road Research (NITRR), South Africa.

[9] ASTM C618: 2012 Standard Specification for Coal Fly Ash and Raw or Calcined Natural Pozzolan for Use in Concrete.

[10] Paya J, Borrachero M.V., MonzoÂ J., Peris-Mora E., Amahjour F.: Enhanced conductivity measurement techniques for evaluation of fly ash pozzolanic activity. Cement and Concrete Research **31**, 41- 49 (2001).

[11] Jatuphon T., Raungrut C., Chai J., Kraiwood K.: Packing effect and pozzolanic reaction of fly ash in mortar. Cement and Concrete Research **35,** 1145– 1151 (2005).

[12] Uzal B., Turanlı L., Yücel H., Göncüoğlu M.C., Çulfaz A.: Pozzolanic activity of clinoptilolite: A comparative study with silica fume, fly ash and a non-zeolitic natural pozzolan. Cement and Concrete Research **40,** 398–404 (2010).

[13] Frías M., García R., Vigil de la Villa R., Villar E.: The effect of binary pozzolan mix on the mineralogical changes in the ternary activated paper sludge–fly ash–$Ca(OH)_2$ system. Construction and Building Materials **38**, 48-53 (2013).

[14] Kong D.L.Y., Sanjayan J.G.: Effect of elevated temperatures on geopolymer paste, mortar and concrete. Cement and Concrete Research 40:334–339 (2010).

[15] Al Bakri M.M., Mohammed H., Kamarudin H., Khairul Niza I., Zarina Y.:. Review on fly ash-based geopolymer concrete without Portland Cement. Journal of Engineering and Technology Research **3(1),** 1-4 (2011).

[16] Nuruddin M.F., Kusbiantoro A., Qazi S., Darmawan M.S., Husin N.A.: Development of Geopolymer Concrete with Different Curing Conditions. The Journal for Technology and Science 22**(1)**, 24-28 (2011).

[17] Roik N.V., Belyakova L.A: IR Spectroscopy, X-Ray Diffraction and Thermal Analysis Studies of Solid "b-Cyclodextrin - Para-Aminobenzoic Acid" Inclusion Complex. Physics and Chemistry of Solid State **12(1)**, 168-173 (2011).

[18] Fernandez-Jimenez A., Palomo A.: Characterisation of fly ashes. Potential reactivity as alkaline cements. Fuel **82**, 2259–2265 (2003).

[19] Ayanda O.S., Fatoki O.S., Adekola F.A., Ximba. B.J.: Characterization of Fly Ash Generated from Matla Power Station in Mpumalanga, South Africa. E-Journal of Chemistry **9(4)**, 1788-1795 (2012).

[20] Yilmaz G.: Structural characterization of glass–ceramics made from fly ash containing SiO_2–Al_2O_3–Fe_2O_3–CaO and analysis by FT-IR–XRD–SEM methods. Journal of Molecular Structure 1019: 37–42 (2012).

[21] Fernandez-Jimenez A., Palomo A.: Composition and microstructure of alkali activated fly ash binder: Effect of the activator. Cement and Concrete Research **35,** 1984 – 1992 (2005).

[22] Celik O., Damci E., Piskin S.: Characterization of fly ash and it effects on the compressive strength properties of Portland cement. Journal of Engineering and Materials Sciences **15(5)**, 433-440 (2008).

[23] Zhang Z., Wang H., Provis J.L.: Quantitative study of the reactivity of fly ash in geopolymerization by FT-IR. Journal of Sustainable Cement-Based Materials **1(4)**, 154–166 (2012).

CHAPTER FOUR

SYNTHESIS, MORPHOLOGY AND STRUCTURAL ANALYSIS OF FLY ASH-CYCLODEXTRIN COMPOSITE

4.1 INTRODUCTION

In order to have an in depth study and to ascertain that a new composite was formed with the interaction of fly ash (FA) and cyclodextrin, the morphology and structural analysis of a FA from Matla ESKOM power station, supplied by Ash Resources, was done on two different types of cyclodextrins; α-cyclodextrin (α-CD) and β-cyclodextrin (β-CD) using two different mixtures. α-cyclodextrin (α-CD) was incorporated in this study so as to compare the structural changes of FA with two different types of cyclodextrins.

4.2 MATERIALS AND MIXES

Fly ash (FA), α-cyclodextrin (α-CD) and β-cyclodextrin (β-CD) were the raw materials used in this study. A FA from Matla ESKOM power station supplied by Ash Resources (South Africa), was used, while α-CD and β-CD from Wacker Chemie were obtained from Industrial Urethanes (Pty) Ltd, South Africa. The characteristics of the cyclodextrins as supplied by the producer are presented in Table 4.1. Two sample preparation procedures were followed. In the first procedure, physical mixtures were prepared by co-grinding a pre-weighed amount of α-CD and β-CD with FA, respectively, at a mass ratio of 10:90 (10%CD-90%FA). The mixed samples were heated in the oven at 40 ^{0}C for 20 minutes. In the second procedure, a specified quantity of cyclodextrin was placed in a mortar; water was added slowly to obtain 0.881M β-CD and 1.02 M α-CD solutions. These solutions were mixed with pre-weighed FA by grinding at cyclodextrin solution/FA mass ratio of 10:90. The mixture was dried in an oven at 100 ^{0}C for 20 minutes. Seven samples were analysed in all, which were: Fly ash (FA), α-cyclodextrin (α-CD), β-cyclodextrin (β-CD), FA + α-CD

(90%FA-10% α-CD), FA + β-CD (90%FA-10% β-CD), FA + α-CD solution (90%FA-10% α-CD (solution)) and FA + β-CD (90%FA-10% β-CD (solution)). The chemical analysis of FA as obtained from ESKOM is presented in Table 4.2, the FA used is classified as "Class F" since it has a sum of SiO_2, Al_2O_3, and Fe_2O_3 contents greater than 70% by mass as specified in ASTM C 618 [1]. The samples were characterised using: X-ray diffraction (XRD) analysis, scanning electron microscopy (SEM) analysis with energy dispersive X-ray spectrometry (EDS) and Fourier transform-infrared spectroscopy (FT-IR) analysis. The samples descriptions are shown in Table 4.3.

Table 4.1: General characterisation of α and β-cyclodextrins used

Property	**α-CD**	**β-CD**
Empirical formula	$C_{36}H_{60}O_{30}$	$C_{42}H_{70}O_{35}$
Bulk density	400-700 kg/m^3	400-700 kg/m^3
Solubility in water at 25 ^oC	145 g/l	18.5 g/l
Content (on dry basis)	Min. 90 %	Min. 95 %

Table 4.2: Chemical composition of the fly ash (Matla)

Content in oxide form.	**% mass**
SiO_2	50.26
Al_2O_3	31.59
Fe_2O_3	3.08
MgO	2.04
CaO	6.78
Na_2O	0.56
K_2O	0.81
TiO_2	1.64
SO_3	0.55
LOI	1.42
SiO_2/Al_2O_3	1.59
TOTAL	98.73

Table 4.3: Samples description

COMPOSITION	DESCRIPTION
FA	Fly ash
α-CD	α- cyclodextrin
β-CD	β - cyclodextrin
90%FA-10%α-CD	90 % fly ash and 10 % α- cyclodextrin, dry mix
90%FA-10% β-CD	90 % fly ash and 10 % β - cyclodextrin, dry mix
90%FA-10% α-CD+H_2O	90 % fly ash and 10 % α- cyclodextrin, solution mix
90%FA-10%β-CD+H_2O	90 % fly ash and 10 % β - cyclodextrin, solution mix

4.3 EXPERIMENTAL PROCEDURE

4.3.1 X-ray diffraction (XRD) analysis

Formation of a new composite material from fly ash-cyclodextrin interaction was studied using powder XRD. The XRD analysis was performed on the powdered samples to determine the mineral composition. The procedure explained in Section 3.3.3 was followed.

4.3.2 Scanning electron microscopy (SEM) and energy dispersive X-ray spectrometry (EDS) analysis

The seven samples were subjected to scanning electron microscopy (SEM) (PHILIPS Environmental Scanning Electron Microscope XL30). The SEM was coupled with an energy dispersive X-ray spectrometer (EDS) in order to determine the composition of individual particles. The samples were mounted on the SEM and irradiated with a beam of electrons at 15 kV. The particle size, pore size and porosity of the samples were calculated from SEM images using imageJ software.

4.3.3 Fourier transform-infrared analysis spectroscopy (FT-IR)

FT-IR was used to analyze the functional group of the samples. The procedure explained in Section 3.3.4 was followed.

4.4 RESULTS AND DISCUSSIONS

4.4.1 XRD analysis

The change in diffraction patterns of the individual materials and prepared mixes indicate composite formation. The α and β-cyclodextrins showed intense crystalline peaks at $2\theta = 11.96^0$, 14.34^0 and 21.72^0 and $2\theta = 12.74^0$, 22.74^0 and 34.86^0, respectively (Figures 4.1a and 4.1b), which conforms with the findings by Roik and Belyakova [2]. The diffractogram of FA contains major peaks at diffraction angles $2\theta = 26.25^0$, 35.29^0, 40.86^0 and 60.65^0 (Figure 4.2a), which can be attributed to quartz (SiO_2), hematite (Fe_2O_3), sillmanite (Al_2SiO_5) and mullite ($Al_6Si_2O_{13}$) respectively. This is in agreement with some findings in the literature [3-5]. The observed peaks in α-CD, β-CD and FA are reflected in the mixtures of the composite materials [6] (Figures 4.2b, c), conforming more to FA diffraction pattern with additional peaks at $2\theta = 11.93^0$ and 21.71^0 for 90%FA-10%α-CD and $2\theta = 12.76^0$ and 22.76^0 of 90%FA-10%β-CD. α-CD and β-CD peaks totally disappear in the CD solution samples (Figures 4.2d, e). The combinations of the diffraction pattern of the individual materials in the physical mixtures of the mixtures and formation of additional peaks indicate composite formation between FA and both cyclodextrins.

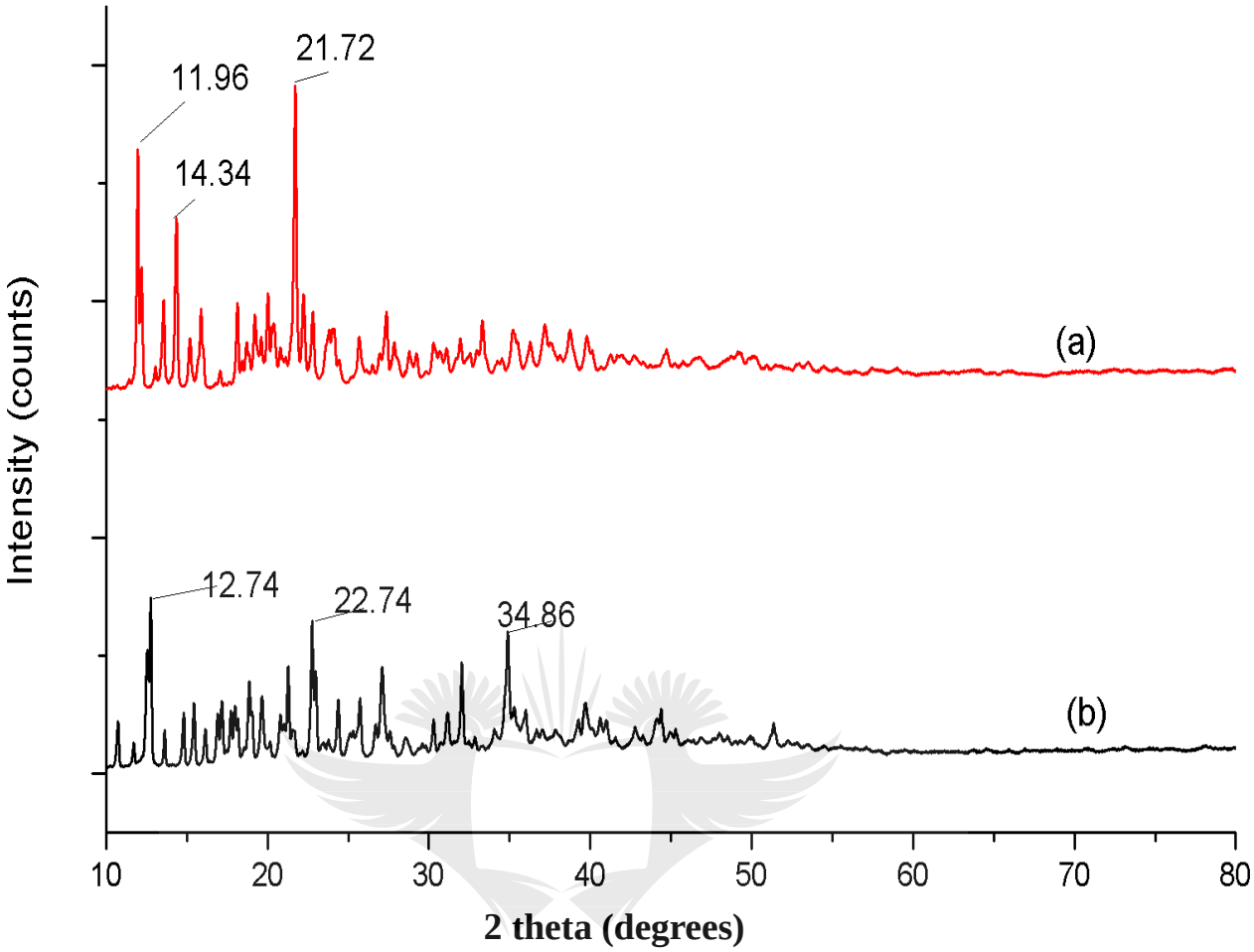

Figure 4.1: X-ray diffractograms of (a) α-CD and (b) β-CD

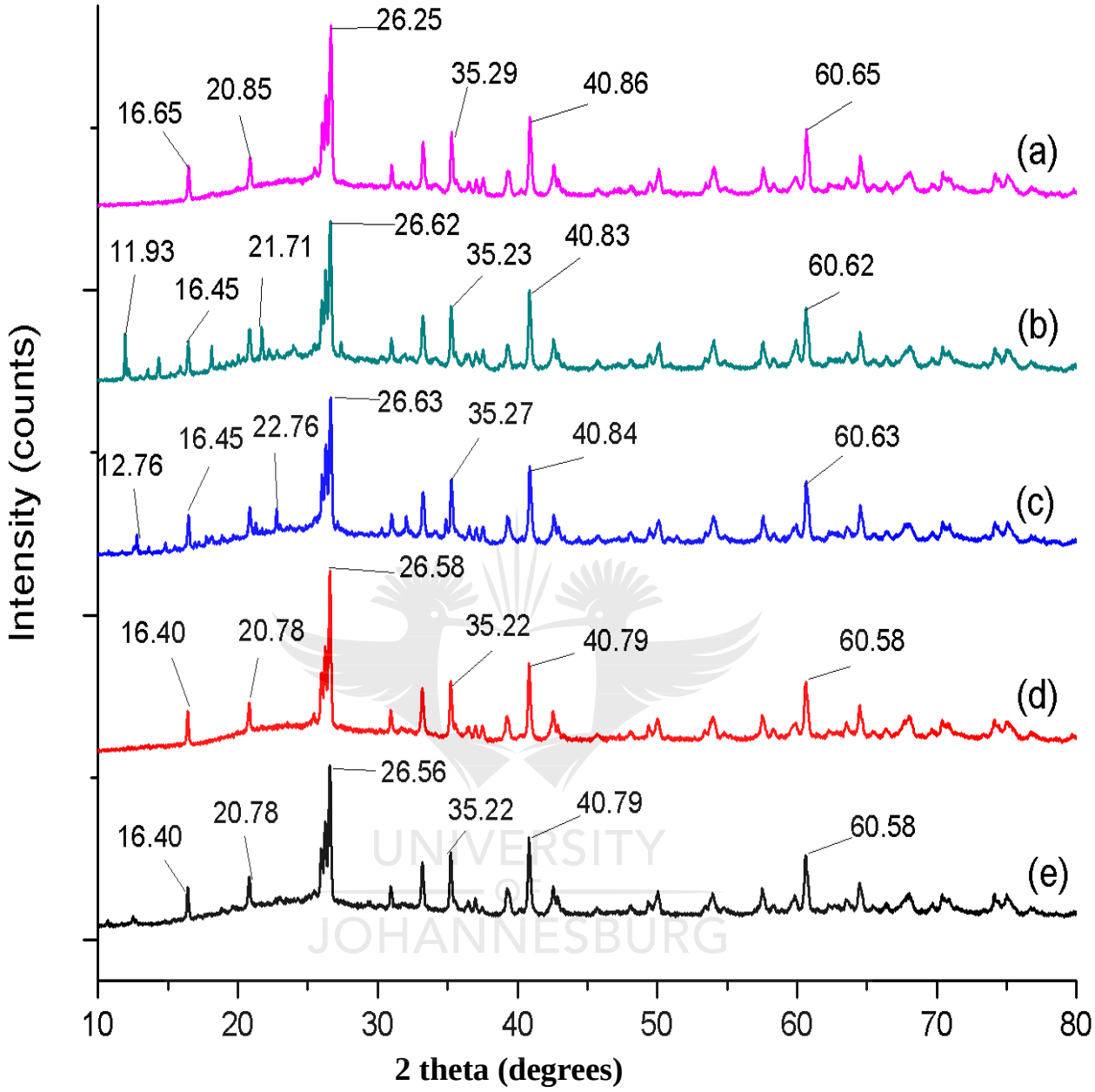

Figure 4 2: X-ray diffractograms of: (a) FA; (b) 90%FA-10%α-CD, (c) 90%FA-10%β-CD; (d) 90%FA-10% α-CD+H_2O; (e) 90%FA-10%β-CD+H_2O

4.4.2 SEM/EDS analysis

The changes in particle morphology that occurred are indicated in the SEM study. The SEM micrographs of α-CD and β-CD are similar as shown in Figures 4.3a and b. The materials are crystalline as confirmed by the XRD results (Figure 4.1a and b). The EDS results (Figures 4.3c, d) show that both cyclodextrins consist of mainly carbon and oxygen, this is expected being glucose molecules and informs their ability to form numerous hydrogen bonds with surrounding water molecules [7]. Hydrogen was not detected because EDS cannot detect lightest elements below the atomic number of Na.

The FA particles are predominantly spherical with a smooth surface texture as observed in the SEM image in Figure 4.4a. The sample is made up of both small and big semi-spherical particles. Agglomeration of small particles was observed whereas big particles are independent with smaller particles clustering around them. The EDS result (Figure 4.5a) reveals a high content of aluminium and silicon. The results are consistent with the XRD data where the most prominent peaks are quartz (SiO_2), mullite ($Al_6Si_2O_{13}$) and sillimanite (Al_2SiO_5) (Figure 4.2a). The dissolved surfaces were observed with the interaction between FA and α-CD (Figure 4.4b) showing a change in the composite material morphology compared to the morphology of the constituent materials (FA and CD). It is also noticeable that the spherical shape of the FA is slightly distorted. The carbon and oxygen contents in α and β-cyclodextrins contributed to their (carbon and oxygen) high contents in the composite samples (Figures 4.5b, c, d, e). The deformation of FA spherical shape is more evident in 90%FA-10%β-CD (Figure 4.4c) than 90%FA-10%α-CD (Figure 4.4b) with additional slightly punched surfaces. In Figure 4.4d, the FA spherical shape is gradually disintegrating for 90%FA-10%α-CD+H_2O. Unique effect of composite dissolution is observed with 90%FA-10%β-CD+H_2O (Figure 4.4e). The morphology shows the surface breaking of FA solid spherical shape sphere. The change in morphology indicates composite formation.

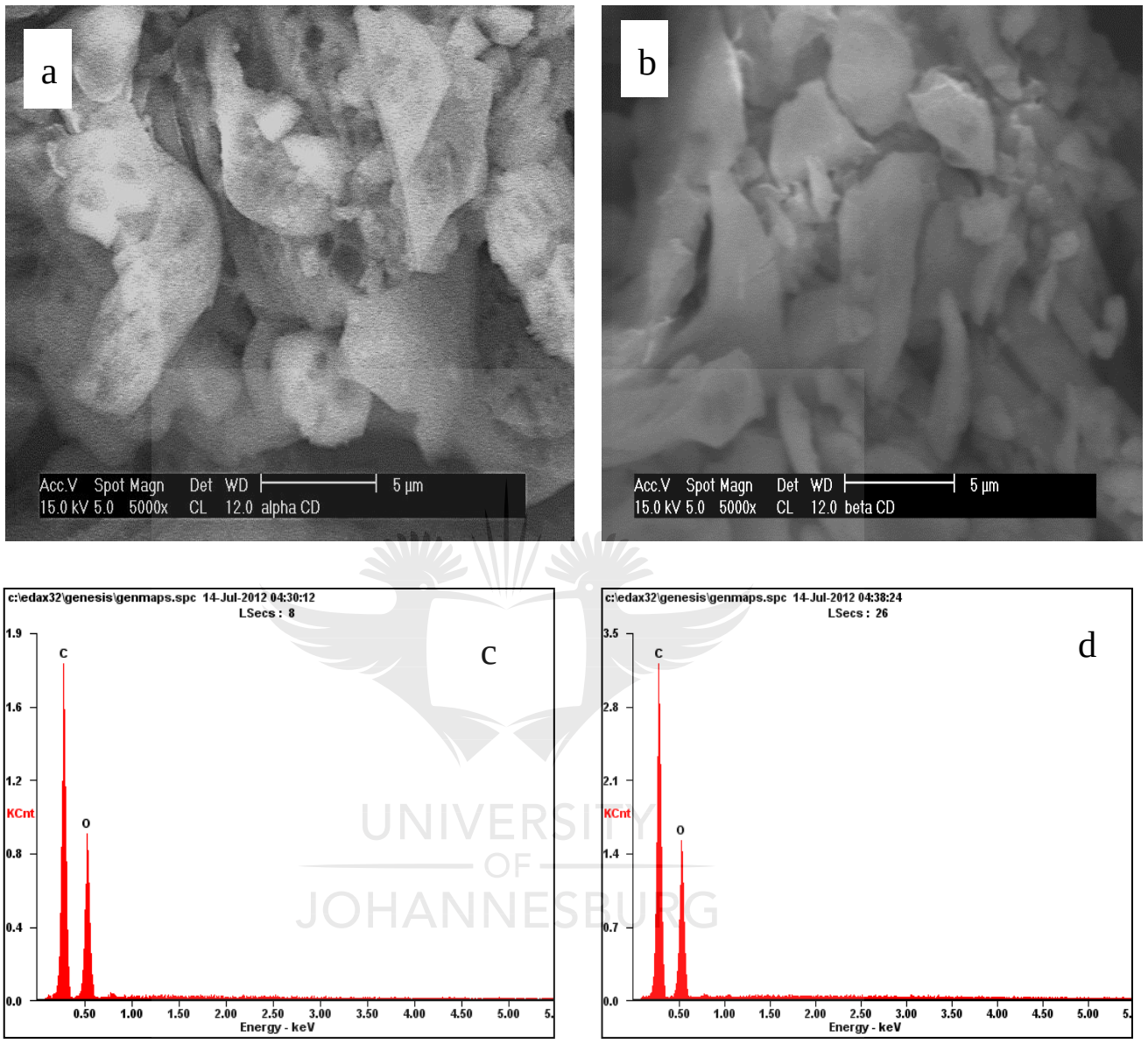

Figure 4 3: (a) SEM of α-CD; (b) SEM of β-CD; (c) Overall EDS-spectrum of α-CD ; (d) Overall EDS-spectrum of β-CD

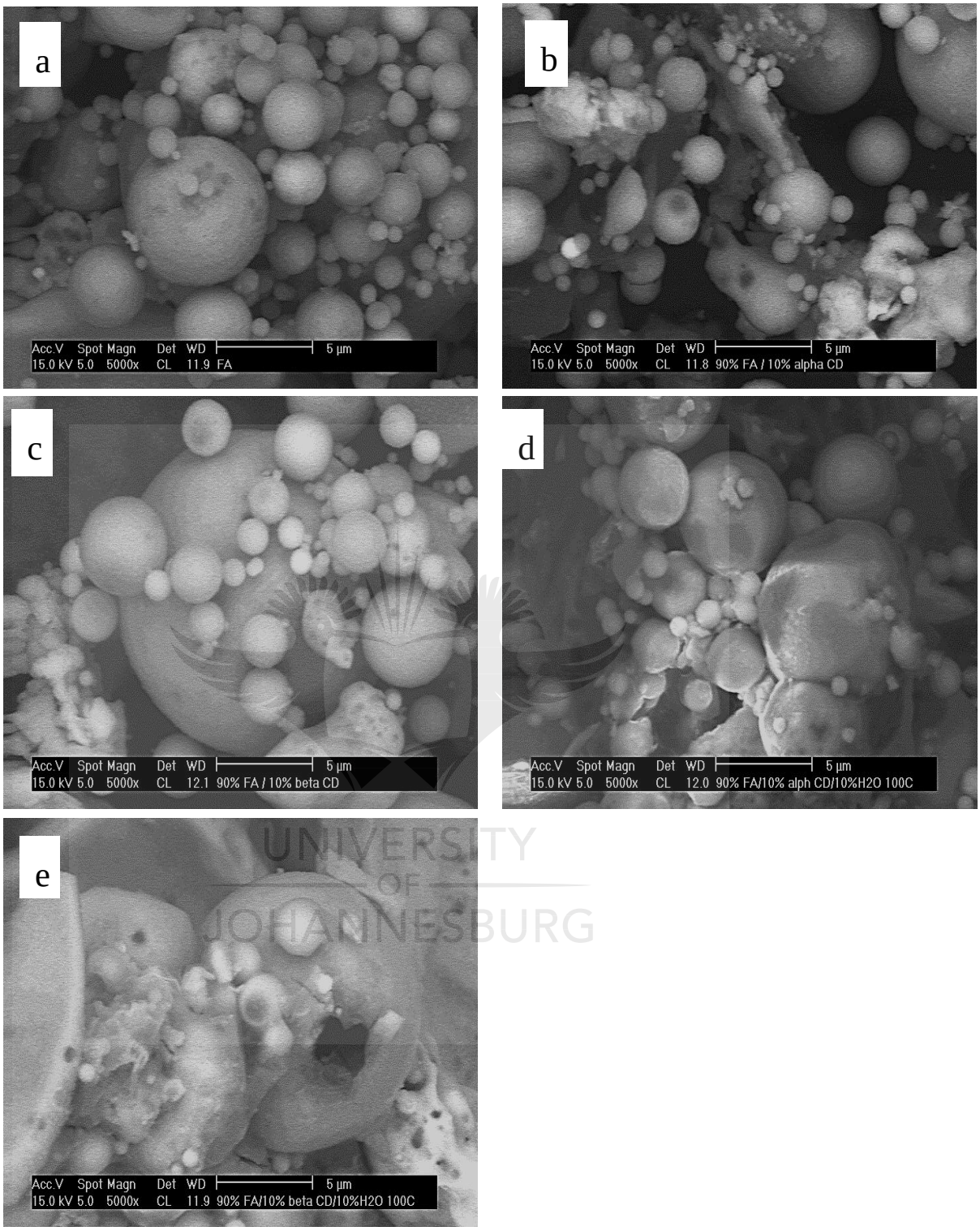

Figure 4 4: (a) SEM of FA; (b) SEM of 90 %FA-10 % α-CD; (c) SEM of 90 %FA-10 % β-CD; (d) SEM of 90 %FA-10 % α-CD + H_2O; (e) SEM of 90 %FA-10 % β-CD + H_2O

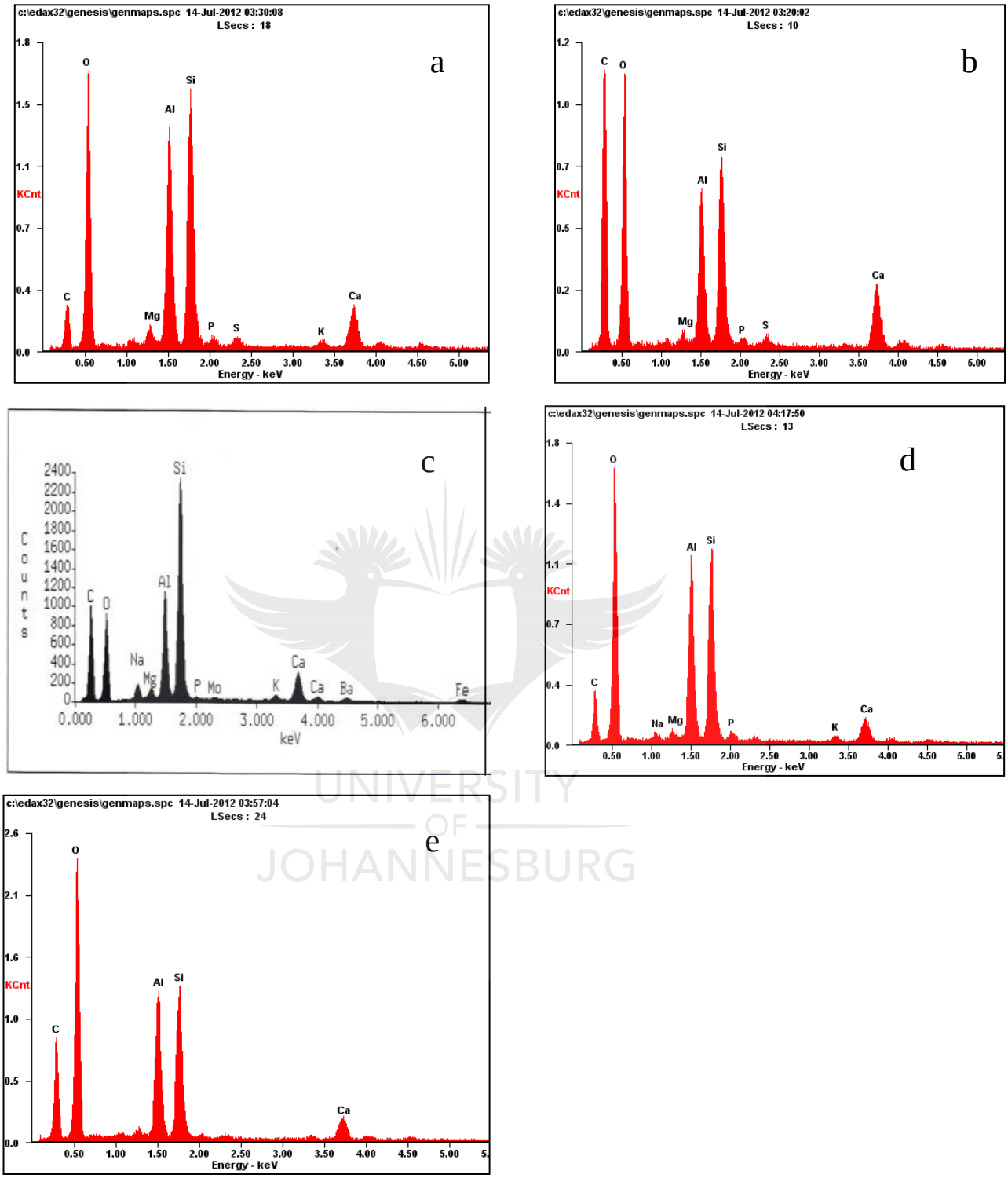

Figure 4 5: (a) Overall EDS-spectrum of FA; (b) Overall EDS-spectrum of 90 %FA-10 % α-CD; (c) Overall EDS-spectrum of 90 %FA-10 % β-CD; (d) Overall EDS-spectrum of 90 %FA-10 % α-CD + H_2O; (e) Overall EDS-spectrum of 90 %FA-10 % β-CD + H_2O

4.4.3 Particle size, pore size and porosity

The particle size analyses obtained from SEM images using imageJ software show that the composite formed for both α and β-cyclodextrins with FA reduced the particle size and pore size of the samples as shown in Table 4.4. Further reduction in both particle size and pore size was also observed for samples prepared with both α-CD and β-CD solution. This may be due to the fact that cylcodextrins in solution will try to occupy the pores thereby reducing the pore size. In the case of the dry mix method, the pore size of the FA will not be able to accommodate the cyclodextrins effectively. The reduction in particle size of the FA can be attributed to the dispersion of its particles in the solution whereas in case of the dry mix, these particles coalesce to form aggregate which affects the overall size of the particle. This is an indication that the new composite materials formed have different physical properties in terms of particle size and pore size than the original FA. However, the effect of both cyclodextrins on the porosity of the FA was not significant.

Table 4.4: Particle size, pore size and porosity of fly ash and blended samples (mean ± SD, n = 3)

Samples	Particle size (µm)	Pore Size (µm)	Porosity (%)
FA	4.32 ± 1.68	2.22 ± 0.47	27.88 ± 0.21
90%FA-10%α-CD (dry mix)	3.60 ± 1.21	2.06 ± 0.36	28.40 ± 0.28
90%FA-10%β-CD (dry mix)	4.17 ± 1.59	2.19 ± 0.46	28.12 ± 0.12
90%FA-10%α-CD (solution)	2.32 ± 0.96	1.63 ± 0.35	28.00 ± 0.33
90%FA-10%β-CD (solution)	1.74 ± 0.48	1.42 ± 0.20	27.80 ± 0.24

4.4.4 FT-IR

Figure 4.5 shows the α-CD peaks associated with C-O deformation vibration at approximately 1154 cm^{-1}, 1076 cm^{-1}, 1023 cm^{-1} and 998 cm^{-1} (Figure 4.5). On the other hand, broad peaks associated with O-H stretching vibration are observed at

approximately 3316 cm^{-1} and 2928 cm^{-1} for β-CD. Sharp IR bands associated with C-O-H deformation vibration are also observed at approximately 1657 cm^{-1} and 1550 cm^{-1} in β-CD, while C-O deformation vibration seen in α-CD also appears in β-CD at approximately 1220 cm^{-1}, 1078 cm^{-1}, 1023 cm^{-1} and 999 cm^{-1}.

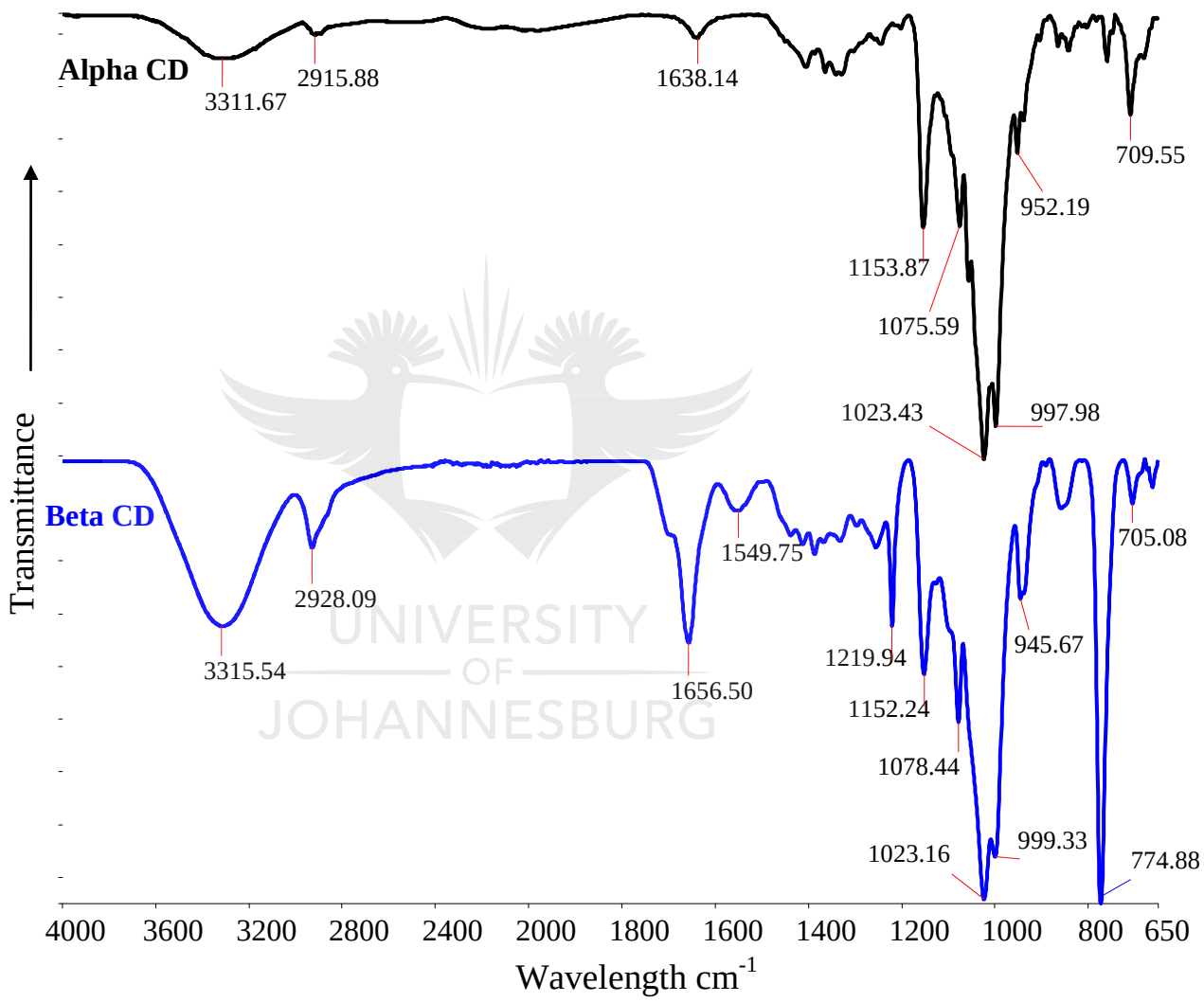

Figure 4 6: FT-IR spectra of α-CD and β-CD

The FT-IR spectrum of the FA shown in Figure 4.6 indicates strong and broad band at 1082 cm^{-1} due to Si-O-Si asymmetric stretching vibration [8-9]. The two upcoming peaks at 1338 cm^{-1} and 763 cm^{-1} can be attributed to Si-O and Al-O vibrations respectively. Most of the characteristic bands of the FA are also present in the FT-IR spectra of the composite materials with additional peaks and frequencies shift as a result of FA-CD interaction. The spectra peak (1082 cm^{-1}) of Si-O-Si asymmetric stretching is found to be of stronger intensities in composite materials than in FA (Figure 4.6). The C-O deformation vibration peak at approximately 1023 cm^{-1} in both cyclodextrins contributed to the sharpness of Si-O-Si peak of the composite materials. Frequencies shift of Si-O-Si peak from wavelength 1082 cm^{-1} in FA to approximately 1037 cm^{-1} in composite materials can also be attributed to the presence of Al-O-Si bonding in the materials. The upcoming peaks at approximately 1335 cm^{-1} and 772 cm^{-1} in the composite materials can be attributed to Si-OH and Al-OH hydroxl group stretching vibrations respectively. Additional peak at approximately 1160 cm^{-1} attributed to O-Si-O bending vibration is observed in all the composite materials, which is not present in the FA. The sharpness of Si-O-Si peak, frequencies shift and new peak formed during FA-CD interaction are indication of the formation of new composite materials. The FT-IR results agree with the XRD observation, which reveals the formation of new peaks in the diffraction pattern of the physical mixtures of FA-CD interaction. The changes in morphology of FA-CD interaction materials as shown in SEM results (Figure 4.4a-j), also indicate the formation of the composite.

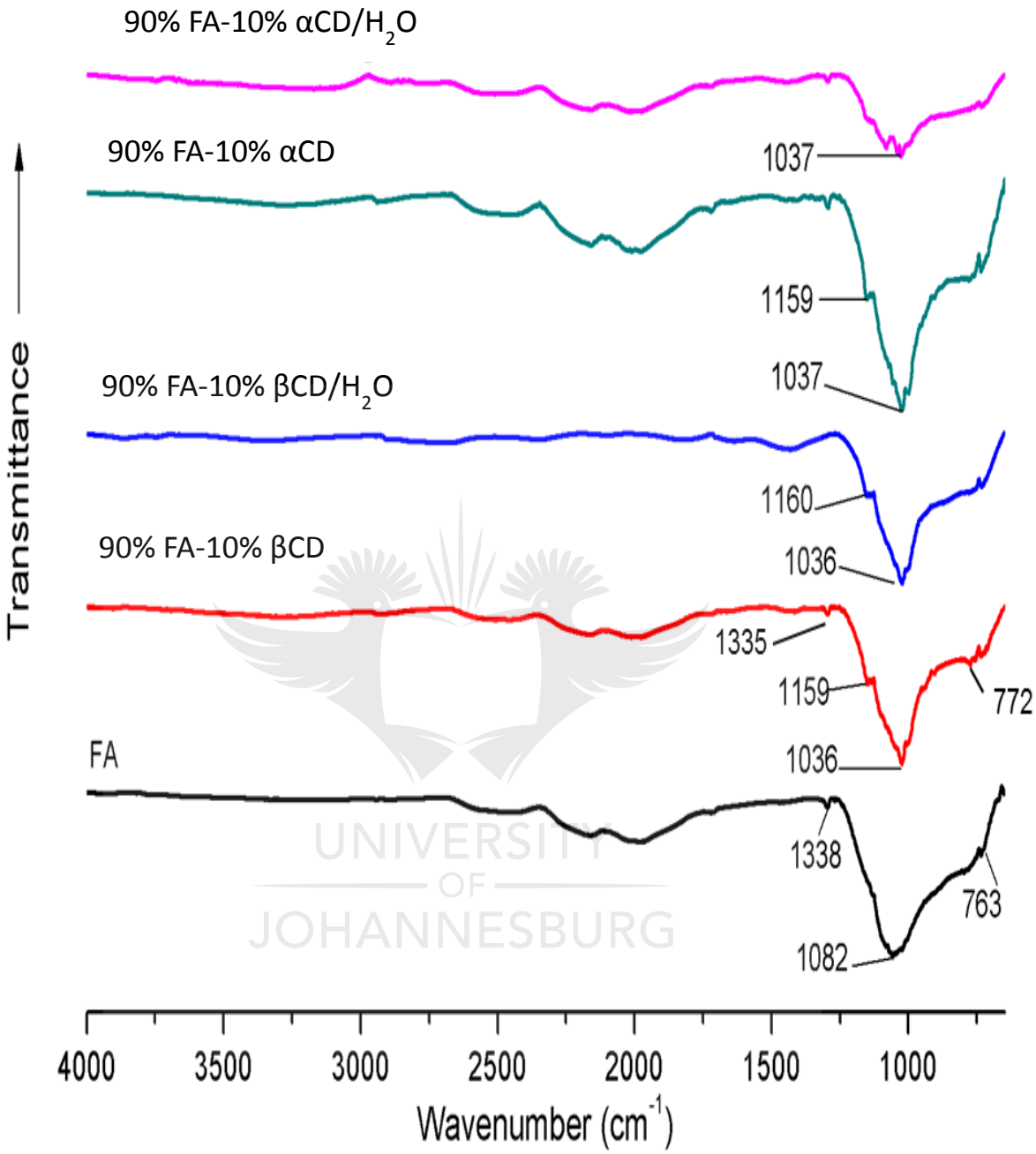

Figure 4 7: FT-IR spectra of FA, 90%FA-10% α-CD, 90%FA-10% α-CD+H_2O, 90%FA-10% β-CD and 90%FA-10% β-CD+H_2O

4.5 CONCLUSIONS

The formation of a new composite material with FA-CD interaction was studied using XRD, SEM and FT-IR. The additional peaks at the X-ray diffractogram and IR-spectra of the composite materials indicated interaction between cyclodextrins and FA. Changes in surface morphologies, particle size and pore size between the composite materials and constituent materials were also observed. β-cyclodextrin will be used in the subsequent chapters because of its availability and low cost.

4.6 REFERENCES

[1] ASTM C618: 2012 Standard Specification for Coal Fly Ash and Raw or Calcined Natural Pozzolan for Use in Concrete.

[2] Roik N.V., Belyakova L.A.: IR Spectroscopy, X-Ray Diffraction and Thermal Analysis Studies of Solid "b-Cyclodextrin - Para-Aminobenzoic Acid" Inclusion Complex. Physics and Chemistry of Solid State **12 (1),** 168-173 (2011).

[3] Fernandez-Jimenez A., Palomo, A.: Characterisation of fly ashes. Potential reactivity as alkaline cements. Fuel **82**, 2259–2265 (2003).

[4] Alvarez-Ayuso E., Querol X., Plana F., Alastuey A., Morenoa N., Izquierdo M.: Environmental, physical and structural characterisation of geopolymer. Journal of Hazardous Materials **154**, 175–183 (2008).

[5] Yilmaz G.: Structural characterization of glass–ceramics made from fly ash containing SiO2–Al2O3–Fe2O3–CaO and analysis by FT-IR–XRD–SEM methods. Journal of Molecular Structure **1019**, 37–42 (2012).

[6] Singh R., Bharti N., Madan J., Hiremath S.N.: Characterization of Cyclodextrin Inclusion Complexes – A Review. Journal of Pharmaceutical Science and Technology **2(3)**, 171-183 (2010).

[7] Micle L.M., Vlaia A., Vlaia V., Hadaruga D.I., Mircioiu C.: Preparation and characterisation of inclusion complexes of meloxicam and α-cyclodextrin and β-cyclodextrin. FARMACIA **58**, 583-593 (2010).

[8] Fernandez-Jimenez A., Palomo A.: Composition and microstructure of alkali activated fly ash binder: Effect of the activator. Cement and Concrete Research **35**, 1984 – 1992 (2005).

[9] Celik O., Damci E., Piskin S.: Characterization of fly ash and it effects on the compressive strength properties of Portland cement. Journal of Engineering and Materials Sciences **15 (5)**, 433-440 (2008).

CHAPTER FIVE

INDICATIVE TESTS ON THE EFFECT OF FLY ASH-*β*-CYCLODEXTRIN COMPOSITES ON MORTAR/ CONCRETE WORKABILITY, STRENGTH AND DURABILITY.

5.1 INTRODUCTION

The main properties of concrete that define its quality and serviceability are strength and those related to its durability [1-3]. The strength of concrete indicates the concrete's ability to resist stress and therefore it is an important parameter for concrete design. Strength of concrete indicates the overall view of concrete quality and it is regarded as the foremost property of concrete. However, in some practical cases, other properties like durability and impermeability may be more important. The key durability assessment of concrete is based on the factors that affect concrete transport mechanisms [4-7]. According to Gameiro et al [4] and Chindaprasirt et al [8], the material transport properties, such as permeability, sorptivity and diffusivity, strongly influence the service life and durability of a concrete structure. This is associated with the material deterioration over the intended service life [9].

Fly ash–*β* cyclodextrin (FA-*β*-CD) interaction has been shown in Chapters Three and Four to have formed a composite that will be useful in concrete technology. Since this is a novel composite and its use in concrete technology has not been previously researched, indicative tests were run, which gave further guidance to the research. This chapter presents and discusses the results of the indicative tests of the effect of FA-*β*-CD composite on concrete workability, compressive strength, split tensile strength and durability. The durability performance of mortar and concrete was assessed from the measurement of oxygen gas permeability, sorptivity and porosity using the South Africa durability index approach [9]. Permeation and absorption are the two major transportation mechanisms parameters, which aid these tests. As a

result of the indicative tests (strength and durability), optimum percentages of the compositions were used to design appropriately detailed research test program.

5.2 MATERIALS AND MIXES

Fly ash (FA) and Portland cement (CEM I 52.5 N) were considered as binding materials in this study. The FA obtained from Matla ESKOM power station used in Chapter Four was used. *β*-cyclodextrin (*β*-CD) from Wacker Chemie (Munich, Germany) was obtained from Industrial Urethanes (Pty) Ltd, South Africa. The cement type (CEM I 52.5 N) was obtained from Pretoria Portland Cement Company (PPC), South Africa. The composition of the FA and the cement used is presented in Table 5.1 and the *β*-cyclodextrin composition is presented in Table 3.1. Granite crusher sand and coarse aggregate with a nominal size of 22 mm were used in concrete mixtures. These aggregates were obtained from Afrisam, South Africa. Silica sand sized within the ranges of 0.8-1.8 mm (coarse), 0.4–0.85 mm (medium) and 600 µm (fine), produced by Rolfes Silica, South Africa, was used in mortar mixtures. Standard silica sand was prepared with the available size ranges in accordance with the SANS 50196-1 [10] and used for mortar mixtures. The characteristics of *β*-CD as supplied by the producer are presented in Table 3.1. The FA used is classified as "Class F" since it has a sum of SiO_2, Al_2O_3, and Fe_2O_3 contents greater than 70% by mass as speculated in ASTM C 618 [11].

Two sample preparation procedures were followed for the FA-*β*-CD composites mixtures. In the first procedure, physical mixtures of a pre-weighed amount of *β*-CD and FA were adopted for the dry mixtures and in the second procedure, 0.0103M, 0.0206M and 0.0516M *β*-CD solutions were added to the concrete at the mixing stage. A proportion of 30% FA was maintained in the mixtures. Furthermore, 0.1%, 0.2% and 0.5% *β*-CD were used together with FA in both dry and solution mixtures.

Table 5.1: Chemical composition of the fly ash and cement used

Content in oxide form.	% mass FA	% mass Cement
SiO_2	50.26	18.8
Al_2O_3	31.59	3.77
Fe_2O_3	3.08	3.83
MgO	2.04	1.68
CaO	6.78	66.70
Na_2O	0.56	0.09
K_2O	0.81	0.26
TiO_2	1.64	0.45
SO_3	0.55	4.53
LOI	1.42	-
SiO_2/Al_2O_3	1.59	-

5.2.1 Mortar mixtures and curing

A total of six mortar mixtures were prepared, in accordance with the mixture proportions shown in Table 5.2. The mortar samples were prepared and mixed in accordance with SANS 50196-1 [10] in a rotating mixer with a 100 litre capacity. In the case of the dry mixtures, water was added to the CEM I 52.5 N, FA and β-CD over a period of 30 seconds, whilst mixing at a low speed. Thereafter, standard silica sand was added over a 30 seconds period, after which, the mixer was stopped and the mix was allowed to stay for one minute, while the mortar adhering to the wall of the mixer was scraped into the main mortar in the mixer. The mixing then continued for a further minute at medium speed.

In the case of the solution mixtures, the 0.0103M and 0.0206M β-CD solutions for F-0.1CD-S and F-0.2CD-S samples, respectively, were added after the standard silica sand had been introduced to the mix. Immediately after each mixture was produced, 100 mm cubes were cast and compacted (using a vibrating table). The moulds containing the samples were covered with polythene sheets and left for 24 hours at room temperature of about 20 ^{0}C before demoulding. As documented in SANS 5861-3 [12] that in case the retarding effect of a material such that the pre-demoulding

time lapse of 20 to 24 hours is not suitable, the time may be extended for a suitable period. Hence, specimens with β-CD were kept covered with polythene sheets for three days before demoulding. After demoulding, the samples were cured in a water bath maintained at 23 ^{o}C ± 2 ^{o}C until testing.

To maintain relative consistency as the control sample, the samples were prepared with varying water/binder ratio (W/B). This approach was adopted to assess the behaviour of β-CD on fresh mortar and to establish a relationship that formed a basis for proper mixture design for the project. The flow test was conducted on mortars according to ASTM C 1437 [13] immediately after mixing.

Table 5.2: Mixture proportion per 1 m^3 of indicative mortar samples

Samples	Cement (kg)	Silica sand (kg)	Fly ash (kg)	CD (kg)	β-CD solution (litres)	Water (kg)	W/B	Flow (mm)
Control	586.00	1758.00	0.00	0.00	0.00	293.00	0.5	101
FA-C	410.20	1758.00	175.80	0.00	0.00	293.00	0.5	106
F-0.1% β-CD-D	410.20	1758.00	175.21	0.59	0.00	275.42	0.47	115
F-0.2% β-CD-D	410.20	1758.00	174.63	1.17	0.00	246.12	0.42	120
F-0.1% β-CD-S	410.20	1758.00	174.63	0.00	50.00	226.01	0.47	120
F-0.2% β-CD-S	410.20	1758.00	172.87	0.00	50.00	197.29	0.42	125

Note: Control (100 % Cement), FA-C (30%FA + Cement), F-0.1% β-CD-D (29.9% FA + 0.1% β-CD dry + Cement), F-0.2 β-CD-D (29.8% FA + 0.2% β-CD dry + Cement), F-0.1 β-CD-S (29.9% FA + 0.1% β-CD in solution (0.0103M) + Cement), F-0.2 β-CD-S (29.8% FA + 0.2% β-CD in solution (0.0206M) + Cement).

5.2.2 Concrete mixtures and curing

The concrete was mixed according to SANS 5861-1:2006 [14]. During mixing, the rotary mixer with a 100 litre capacity was charged with coarse aggregate, fine aggregate, cement, FA and *β*-CD, respectively. These materials were mixed in their dry state for one minute. Thereafter, water was introduced into the mix over the period of one minute and mixing continued for one more minute. In the case of the solution mixtures, the *β*-CD solution was added, over a 30 second period, after the dry material was mixed for one minute. Thereafter, the remaining water was added after a period of 30 seconds and mixing continued for one more minute. Immediately after each mixture was produced, the slump test was performed according to SANS 5862-1:2006 [15] and 100 mm cubes and cylinders (with a diameter and length of 150 mm and 300 mm) were cast and compacted (using a vibrating table).

Table 5.3 presents the eight mixtures used for the production of the concrete cubes and cylinders. Each batch catered for twelve 100 mm cubes and nine cylinders (with a diameter and length of 150 mm and 300 mm, respectively). A total of 96 cubes and 72 cylinders were produced for compressive and split tensile strength tests, respectively, while 32 cubes were produced for durability tests.

The mixture design for the control sample was maintained for all the samples, at the same time the effect of water content on workability was monitored, since the behaviour of *β*-CD on concrete had not been established previously. This approach was used to observe the behaviour of *β*-CD on fresh concrete and to establish a relationship that will form a basis for proper mixture design for the actual mixtures (discussed in Chapters Eight and Nine). The moulds containing the samples were covered with polythene sheets and left for 24 hours at room temperature before demoulding. As done in the case of the mortar samples, specimens with *β*-CD were kept covered with polythene sheets for three days before demoulding because of the nature of the material. After demoulding, the samples were placed in a water bath maintained at 23 ^{o}C ± 2 ^{o}C for curing until the testing ages.

Table 5.3: Mixture proportions per 1 m^3 of indicative concrete samples

Samples	Cement	Crusher sand (kg)	Coarse aggregate (kg)	FA (kg)	β-CD (kg)	β-CD solution (litres)	Water (Kg)	W/B	Slump (mm)
Control	410.00	788	980	0.00	0.00	0.00	205	0.5	50
FA-C	287.00	788	980	123.00	0.00	0.00	205	0.5	90
F-0.1% β-CD-D	287.00	788	980	122.59	0.41	0.00	192.7	0.47	95
F-0.2% β-CD-D	287.00	788	980	122.18	0.82	0.00	172.2	0.42	120
F-0.5 %β-CD-D	287.00	788	980	120.95	2.05	0.00	172.2	0.42	130
F-0.1%β-CD-S	287.00	788	980	122.59	0.00	35.00	192.29	0.47	150
F-0.2% β-CD-S	287.00	788	980	122.18	0.00	35.00	171.38	0.42	150
F-0.5% β-CD-S	287.00	788	980	120.95	0.00	35.00	161.95	0.42	160

Note: F-0.5 β-CD-D (29.5% FA + 0.5% β-CD dry + Cement), F-0.5 β-CD-S (29.5% FA + 0.5% β-CD in solution (0.0516M) + Cement).

5.3 EXPERIMENTAL PROCEDURE

5.3.1 Compressive strength tests

The compressive strength tests were performed according to SANS 5863: 2006 [16] at 7, 14, 28, 90 and 180 curing days. Three samples were tested for each mixture at each age. The average of the three results, calculated in N/mm^2 from Equation (5.1), was recorded as the strength at the relevant age. An Amsler compression testing machine, with a load capacity of 2000 kN was used. A uniaxial load was applied to the centrally placed sample, perpendicular to the direction of casting. The load was applied at a rate of 150 kN/minute. Figure 5.1 shows a concrete cube being loaded during testing.

$$R_c = \frac{F_c}{A} \quad (5.1)$$

where:

R_c is the compressive strength in Newtons per square millimeter (N/mm^2);

F_c is the maximum load at fracture, in Newtons (N);

A is the area of the load-bearing plates, in square millimeter (mm^2).

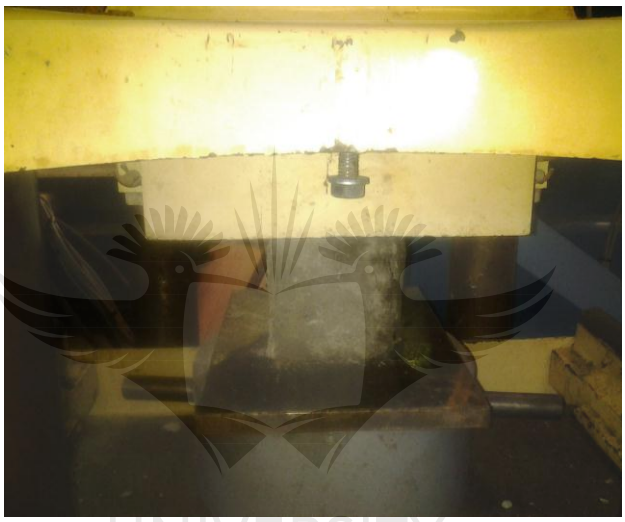

Figure 5.1: Concrete cube being loaded for compressive strength testing

5.3.2 Split tensile strength tests

The split tensile test on the cylinders was performed, according to SANS 6253: 2006 [17] on each sample at 14, 28 and 90 days curing ages. Three samples were tested for each mixture at each curing age. The average of the triplicate results, calculated from Equation (5.2), was recorded as the strength at the relevant age. Figure 5.2 shows a cylindrical concrete sample being loaded during testing.

$$F = \frac{2P}{\pi dl} \quad (5.2)$$

where:

F is the tensile strength in Newtons per square millimeter (N/mm^2)

P is the maximum load at fracture, in Newtons (N)

d is the diameter of the cylinder (mm)

l is the height of the cylinder (mm)

Figure 5.2: Cylindrical concrete sample being loaded for split tensile strength testing

The percentage decrease or increase in compressive strength or split tensile strength (CSt) was calculated using Equation (5.3), to determine the effect of β-CD on the strength of FA pozzolanic concrete (FA-C). A positive value indicates an increase in the compressive strength or split tensile strength (CSt) while a negative value indicates a decrease in the compressive strength or split tensile strength (CSt).

$$\%increase/decrease\,(ref.\,FA\ pozzolanic) = \frac{FA-\beta\,CD\ composite\ CSt - FA\ pozzolanic\ CSt}{FA\ pozzolanic\ CSt}\,x\,100 \qquad (5.3)$$

5.3.3 Permeability, sorptivity and porosity tests

The oxygen permeability and sorptivity tests were performed at the AFRISAM laboratory in Roodepoort, South Africa. The South African durability index approach which was developed by Ballim and Alexander [18-20] was adopted in this study. The approach was developed to cater for the practical durability tests that could be site-applicable. Three durability index test methods were developed namely; sorptivity, oxygen permeability and chloride conductivity. The approach used the concept of characterizing concrete quality cover by parameters related with transport mechanisms, such as gaseous and ionic diffusion, and water absorption. Measurements of oxygen permeability and sorptivity/porosity were used in this study to assess the durability performance of the indicative samples. The oxygen permeability index (OPI) test gives an indication of the degree of pore connectivity in a concrete matrix, while sorptivity measures the rate of movement of a water front through the concrete under capillary suction. The higher the OPI value, the lower the permeabilty of the sample.

These tests were conducted on discs samples with a diameter of 68 mm and thickness of 30 ± 2 mm which were core drilled from the cover zone of the 100 mm cubes samples, after being cured for 14 and 28 days. The disc samples were preconditioned in an oven at 50 ^{0}C for 7 days before testing. The detailed procedures, documented by other researchers [19, 21-25], were followed. Brief descriptions of the tests are given below:

5.3.3.1 Permeability

Disc samples were allowed to cool down for 2 hours in a room maintained at 23 ^{o}C, after being preconditioned in an oven at 50 ^{0}C for 7 days. The thickness of each sample was measured at 4 points while the diameter was measured at 2 points. After the measurement, the samples were then placed in a compressible collar with the test face (outer face) facing the bottom. The collar was placed in a PVC sheath to form a

unit. This unit was placed in the permeameter chamber, covered with a wooden ring and tightened. Initial time and pressure were recorded after the oxygen pressure in the permeameter chamber had been increased to 100 kPa and the inlet valve had been closed. Pressure decay was recorded at intervals of approximately 5 kPa and test stopped when pressure reached approximately 60 kPa or 6 hours from start of test. The test setup is shown in Figure 5.3a and b. After the permeability test, the disc samples were removed from the collar and later used for sorptivity test.

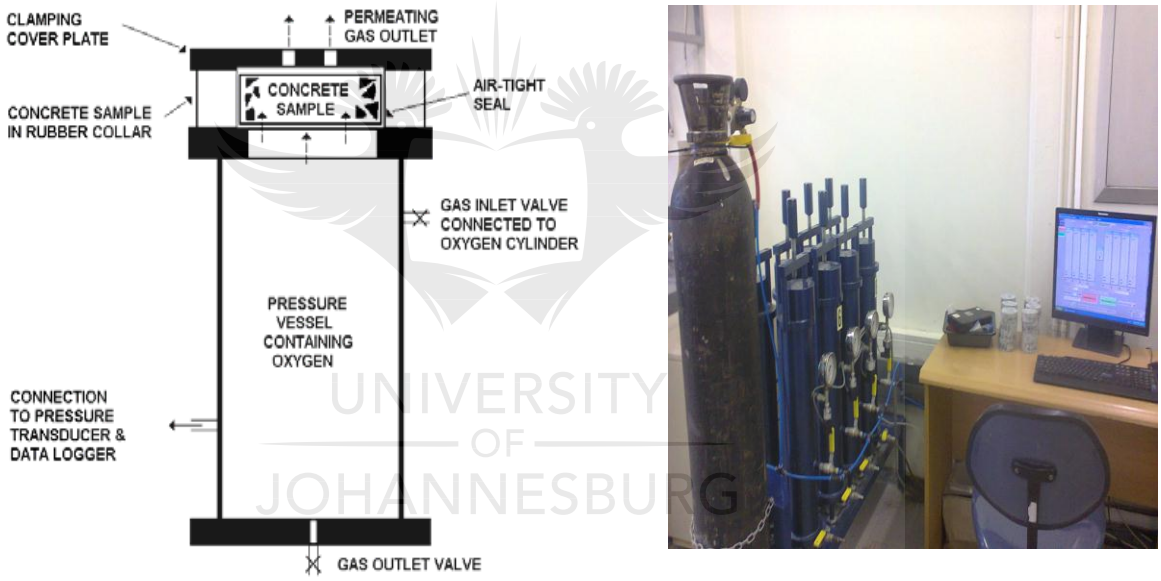

Figure 5.3: (a) Oxygen permeability apparatus [19] (b) Oxygen permeability apparatus setup used

The coefficient of permeability (m/s) was calculated using the Equation (5.4):

$$K = \frac{WVg}{RA}\left(\frac{d}{\theta.t}\right)\ln\left(\frac{P_o}{P}\right) \qquad (5.4)$$

where:

K = coefficient of permeability in m/s

W = molecular mass of oxygen, 32 g/mol

V = volume of oxygen under pressure in permeameter (m^3)

g = acceleration due to gravity, 9.81 m/s^2

R = universal gas constant, 8.313 Nm/Kmol

A = superficial cross- sectional area of sample (m^3)

d = average sample thickness (m)

θ = absolute temperature (K)

t = time (s) for pressure to decrease from P_o to P

P_o = pressure at the beginning of test (kPa)

P = pressure at the end of test

Results recorded were the average of four discs.

5.3.3.2 Sorptivity and porosity tests

After the permeability test, the curved surface of the disc samples was sealed with tape up to 5 mm above the test face to allow only one directional capillary flow of water. The test face of disc samples was placed in lime-saturated solution contained in a tray such that the final level of solution was slightly above the edge of sample. These samples were weighed for a period of up to 25 minutes at regular intervals of 3, 5, 7, 9, 12 minutes. The samples were then vacuum saturated by applying -75 kPa suction for 3 hours to samples in an empty desiccator. Thereafter, the samples were subjected to vacuum suction in $Ca(OH)_2$ saturated water for 5 hours. The samples were allowed to soak for 18 hours after the vacuum suction and weighed. Porosity was calculated using Equation (5.5) and sorptivity was calculated following Equations (5.6) to (5.7). The test setup is shown in Figure 5.4.

$$n = \frac{M_{sv} - M_{so}}{A.d.\rho_w} \qquad (5.5)$$

where:

M_{sv} = vacuum saturated mass of the samples to the nearest 0.01 g

M_{so} = initial mass of the specimen to the nearest 0.01 g

A = cross-sectional area of the samples to the nearest 0.02 m^2

d = average samples thickness to the nearest 0.02 mm

P_w = density of water

Then the mass of the water absorbed at each weighing period was calculated using:

$$M_{wt} = M_{st} - M_{so} \quad (5.6)$$

where:

M_{st} = mass to the nearest 0.01 g of the sample at time t

Sorptivity was calculated from the slope of graph of water absorbed (M_{wt}) versus the square root of time (in hr).

$$S = \frac{F.d}{M_{sv} - M_{so}} \quad (5.7)$$

where:

F = the slope of the best fit line obtained by plotting M_{wt} against $t^{½}$

S = sorptivity

Results recorded were the average of four discs.

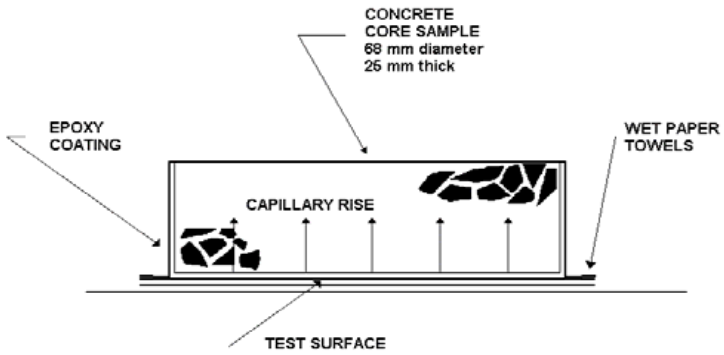

Figure 5.4: Water sorptivity test apparatus [19]

The percentage decrease or increase in permeability, sorptivity or porosity (PSP) was calculated using Equation (5.8). A positive value indicates an increase in the permeability, sorptivity or porosity (PSP) while a negative value indicates a decrease in the permeability, sorptivity or porosity (PSP).

$$\%increase/decrease\ (ref.\ FA\ pozzolanic) = \frac{FA-\beta CD\ composite\ PSP - FA\ pozzolanic\ PSP}{FA\ pozzolanic\ PSP} x\,100 \quad (5.8)$$

5.4 RESULTS AND DISCUSSION

5.4.1 Flow of mortar and workability of concrete samples

The flow of mortar and concrete samples shown in Tables 5.2 and 5.3, respectively, revealed that β-CD increased both flow and workability with reduced water content. The characteristic of β-CD of enhancing wettability in water [26-27] contributed to this behaviour, with a higher dissolution being experienced in the solution mixed samples. Table 5.4 shows the variation in slump of the samples at different W/B as observed in this study. At a W/B of 0.5, a collapse slump was observed in the case of samples with a β-CD content of 0.2% or greater. In the case of W/Bs lower than 0.5, the workability of the concrete increased with an increase in β-CD content. Furthermore, mixtures containing higher contents (0.5%) of β-CD exhibited higher increase in slump with small increase in water. Mixtures comprising β-CD solutions yielded higher increase in slump corresponding to small increase in water compared with samples made with powdered β-CD. The slump was maintained between 50 and 160 mm for all samples (Table 5.3).

It was observed that for samples containing β-CD (both powdered and solution), curing in water could not take place after 24 hours of casting. A few samples from these sets that were cured in water after 24 hours of casting collapsed in the curing tank. Samples with β-CD contents of 0.2% and higher were left to cure in the mould and covered with a polythene sheet for three days (after casting) before being cured in water. The observation was in agreement with the fact that organic admixture (e.g

polysaccharides) act as retarders in concrete, which is attributed to the adsorption of the admixture to the surfaces of the hydrated and/or anhydrous phases of clinker [28-30]. This slows down hydration and consequently retards setting [31]. The retarding effect observed will aid delay in the initial setting of concrete when special placement is required such as placing concrete in large piers, foundations or over considerable distances [32] and consequently might reduce early strength. However, longer concrete retardation than necessary might virtually prevent setting of concrete [30, 32]. The degree of retardation depends on the dosage of the admixture, method of application and curing conditions [32]. Lower contents of *β*-CD (0.025% and 0.05%) were investigated for the actual tests, which are reported in the subsequent chapters, so as to limit the effect of longer retardation of concrete, and also the direct effect of *β*-CD on concrete without FA were studied.

Table 5.4: Concrete slump test details

Samples	W/B					
	0.5 (Slump, mm)	**0.47 (Slump, mm)**	**0.46 (Slump, mm)**	**0.42 (Slump, mm)**	**0.4 (Slump, mm)**	**0.35 (Slump, mm)**
Control	50	-	No slump	No slump	-	-
FA-C	90	-	-	-	-	-
F-0.1CD-D	-	95	80	No slump	-	-
F-0.2CD-D	Collapsed	-	-	120	30	-
F-0.5CD-D	Collapsed	-	-	130	40	-
F-0.1CD-S	-	150	-	-	-	-
F-0.2CD-S	Collapsed	-	-	150	40	-
F-0.5CD-S	Collapsed	-	-	160	60	25

- Not measured

-

5.4.2 Compressive strength of indicative samples

Figure 5.5 shows the relationship between the compressive strength of the samples and curing age. With the exception of the control sample, compressive strength increased with curing age up to 180 days. The control sample with no FA yielded a higher compressive strength at earlier curing ages than the other samples. From a curing age of approximately 125 days, the FA-β-CD composite samples exhibited a higher compressive strength than the control and FA-C samples, except for composite samples with 0.5% β-CD. The mixtures containing the highest content of β-CD (0.5%) yielded the lowest compressive strength at all the curing ages. This might be as a result of the reduction in concrete cohesiveness at higher content of β-CD, which resulted in longer setting time and loss of strength. The highest compressive strength were observed with the samples containing 0.1% β-CD. No trend was identified regarding the strength of the concrete mixtures containing the dried β-CD versus the solution β-CD composite samples. The variations in the mixture W/Bs and workabilities might also have affected the overall strength results. Lower W/B and higher workability generally aid compressive strength. Further research on this investigation, reported in Chapter Eight, adopted lower contents of β-CD so as to maintain the W/B ratio of the mixtures.

The percentage increase in the compressive strength of FA-β-CD composite samples as compared to the compressive strength of FA-C sample is shown in Figure 5.6. From Figure 5.5, it is obvious that the strengths of F-0.5CD-D and F-0.5CD-S samples were far lower than the strength of FA-C; therefore these samples were excluded from further discussion. One of the characteristics of pozzolans is the reduced compressive strength at early age [33, 34]. The incorporation of the FA-β-CD composite in the mixture improved early compressive strength, with the highest increase of 45.05% observed for the F-0.1CD-D sample at 7 days age as compared to the FA-C samples (Figure 5.6). The results indicated that FA-β-CD composite might have boosted the pozzolanic reaction with evidence of increased compressive strength at all ages. This might be as a result of reduced pore sizes of FA-β-CD composite

compared to FA, as reported in Section 4.4.3, lower water content of FA-*β*-CD composite samples and higher workability. Also, there is an interaction between FA and *β*-CD according to the FT-IR results discussed in Section 4.4.4. The FT-IR results, showed stronger intensities of Si-O-Si asymmetric stretching in the composite formed between FA and *β*-CD, which was claimed to be as a result of the C-O deformation vibration in *β*-CD. The presence of Al-O-Si bonding was also observed in the composite. The positive effect of *β*-CD on final strength can be attributed to improved pozzolanic reaction due to stronger Si-O-Si and Al-O-Si bonding present in the composite, which allows more active SiO_2 to react with $Ca(OH)_2$ to form more C-S-H (Calcium Silicate Hydrate) that is responsible for strength formation. Finally, in general, the longer the curing age (from 28 days onwards), the less the effect of the *β*-CD on the increase in compressive strength relative to the FA-C mixtures.

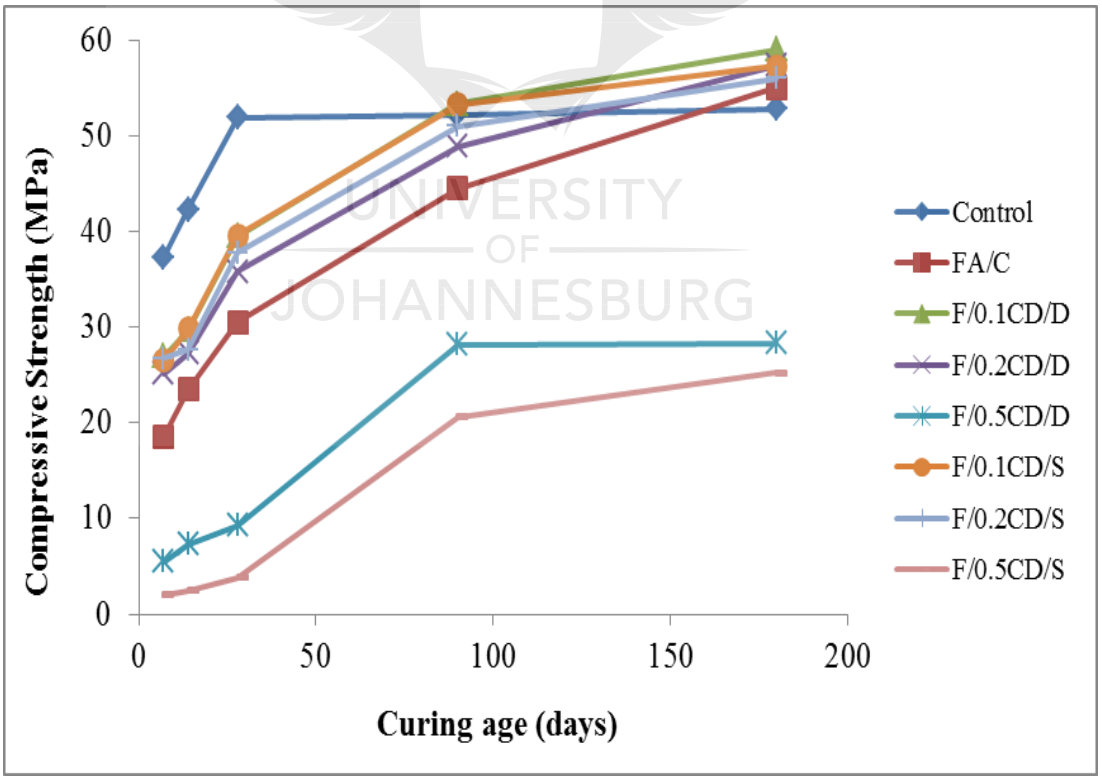

Figure 5.5: Compressive strength of samples at different curing ages

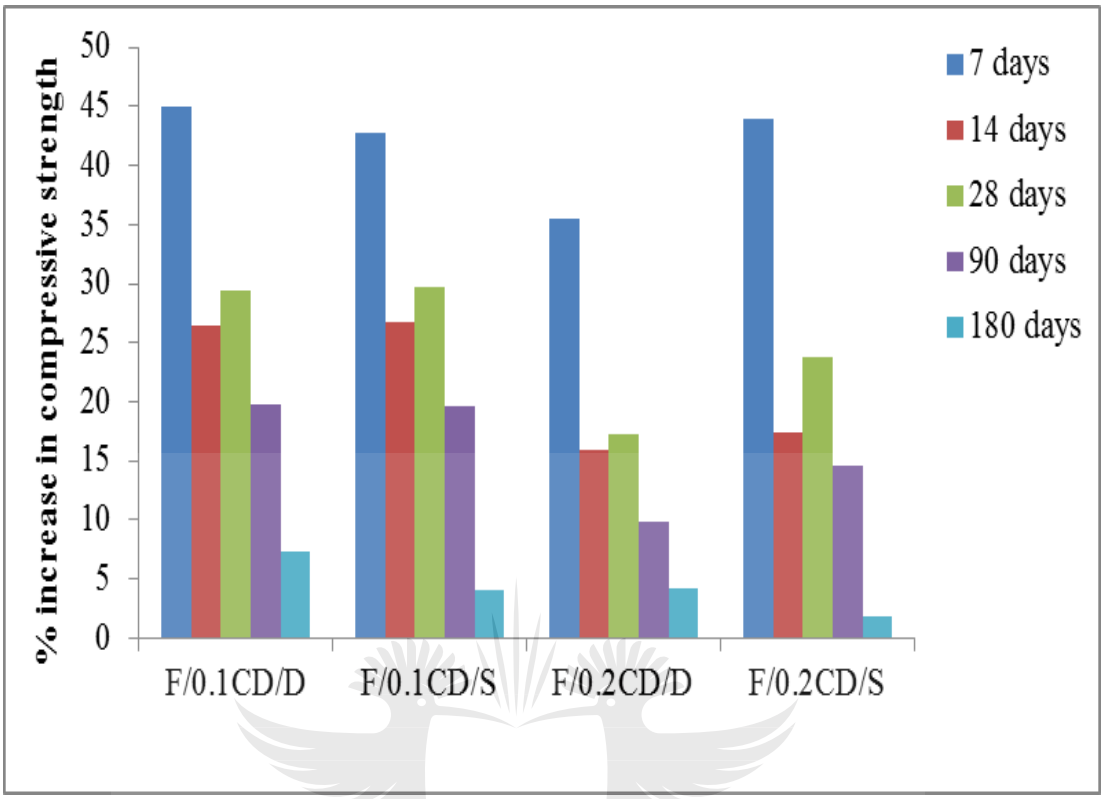

Figure 5.6: Percentage increase in the compressive strength of FA-*β*-CD composite samples compared to the compressive strength of pozzolanic sample (FA-C)

5.4.3 Split Tensile strength of indicative samples

Concrete is generally weak in tension and strong in compression, therefore, it is expected to have a lower split tensile strength than compressive strength, as revealed in Figure 5.7 for all the samples. The FA-*β*-CD composite samples with a relatively low content of *β*-CD (0.1% and 0.2%) exhibited a higher split tensile strength than the pozzolanic samples (FA-C) for all curing ages (up to 90 days). Furthermore, these samples yielded higher split sample strength than the control sample at a curing age of 90 days. As also observed for compressive strength, a higher content of *β*-CD (0.5%) in the mixture resulted in unsatisfactory lower split tensile strength. The split tensile strength of dried mixed composites samples and solution mixed composite samples were closely related.

When comparing the pozzolanic sample (FA-C) split tensile strength and the FA-*β*-CD composite samples with lower content of *β*-CD (0.1% and 0.2%) split tensile strengths, it was observed that at 14 days curing period, the FA-C samples generally exhibited a higher split tensile strength than FA-*β*-CD composite samples as presented in Figure 5.8. However, the percentage increase in the split tensile strength for FA-*β*-CD composite samples was higher than that of FA-C samples at curing ages of 28 and 90 days, resulting in an increase in split tensile strength of up to 28.74% as observed for F-0.1CD-D sample at 90 days curing period. Hence, in general, the longer the curing period, the greater the effect of the *β*-CD in increasing the split tensile strength of the concrete. In addition, the inclusion of 0.1% *β*-CD in the mixtures resulted in an improved tensile strength compared to the strength achieved when including 0.2% of *β*-CD.

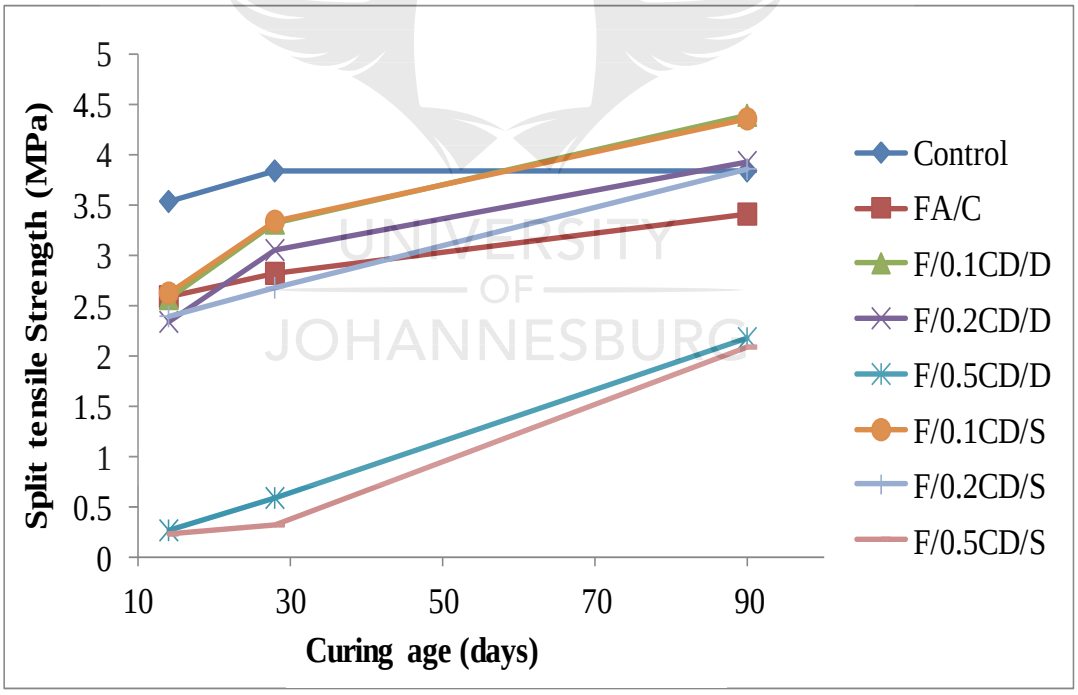

Figure 5.7: Split tensile strength of samples at different curing ages

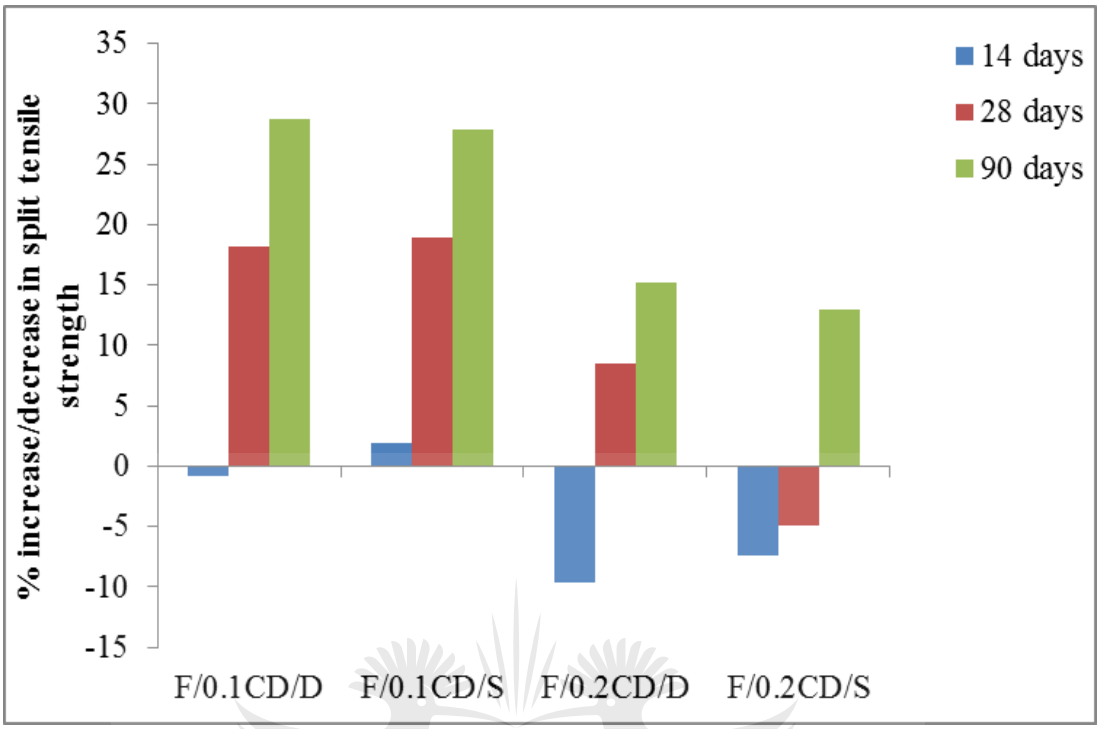

Figure 5.8: Percentage increase/decrease in the split tensile strength of FA-*β*-CD composite samples compared to the split tensile strength of pozzolanic sample (FA-C)

5.4.4 Permeability of indicative mortar samples

The oxygen permeability index (OPI) test is sensitive to the amount and continuity of larger pores and voids where most of the flow will occur [9]. The coefficient of permeability (k) and oxygen permeability index (OPI) values for mortar samples are presented in Figures 5.9 and 5.10, respectively. The permeability results for concrete samples were not reported because of some anomalous values. It is evident from Figure 5.9 that all the samples showed decrease in permeability at increased curing age. The highest permeability was exhibited by the FA-C sample at 14 days curing age. However, a decrease in permeability was observed in the case of the FA-C mortar sample relative to the control sample at 28 days curing age. The samples containing the FA-*β*-CD composite exhibited a lower permeability than the control sample and the FA-C sample, for both curing ages. The *β*-CD solution was more effective in decreasing permeability, compared to the dry *β*-CD. When considering

dry and solution β-CD mortar mixtures, no general trend was established between the quantity of β-CD and its effectiveness in reducing permeability.

Figure 5.11 shows the percentage decrease in FA-β-CD mortar permeability, relative to the FA-C mixture permeability, with the inclusion of the different β-CD composites. From this Figure, it is evident that the mixtures containing the β-CD solutions resulted in the greatest relative reductions in permeability, being 64.8 % and 62.8 % in the case of the F-0.2 CD-S and F-0.1 CD-S, respectively. This showed that despite the dissolution observed with the solution mixed samples, a positive effect on sample permeability was observed. Generally, the results indicated that FA-β-CD composite might have boosted the pozzolanic reaction with evidence of permeability reduction at both 14 and 28 days curing period, compared to control sample.

When comparing Figures 5.10 and 5.11, it is evident that, in general, the higher the OPI, the less permeable the mortar. This is in agreement with the findings of Ballim and Alexander [9], who stated that the OPI provides an indication of the degree of pore connectivity in the matrix and the permeability of the samples.

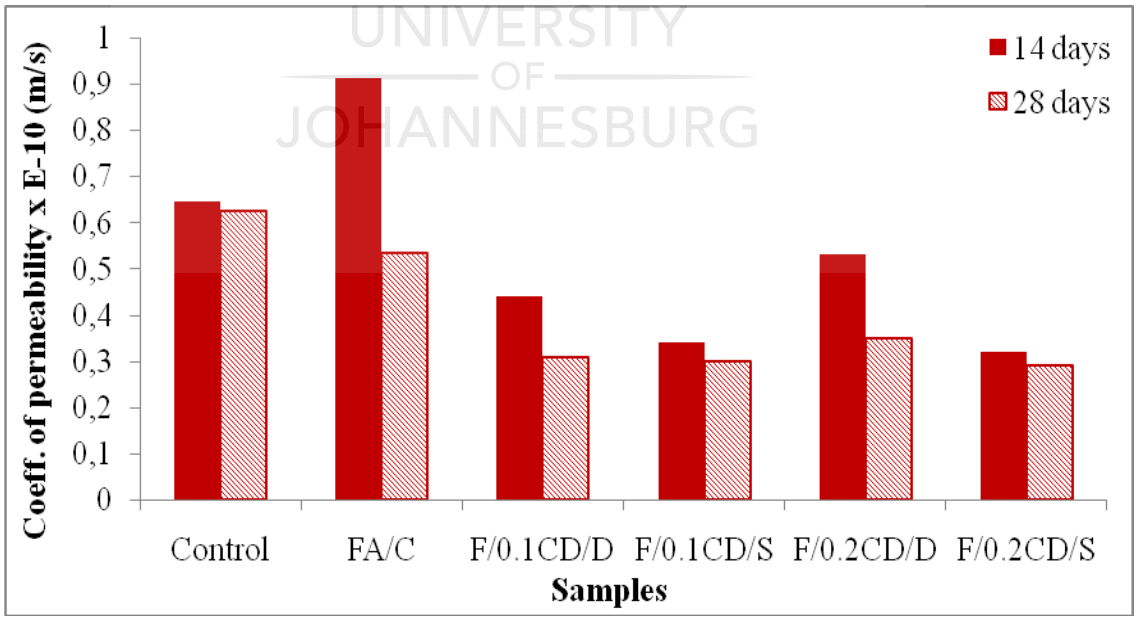

Figure 5.9: Permeability of mortar samples

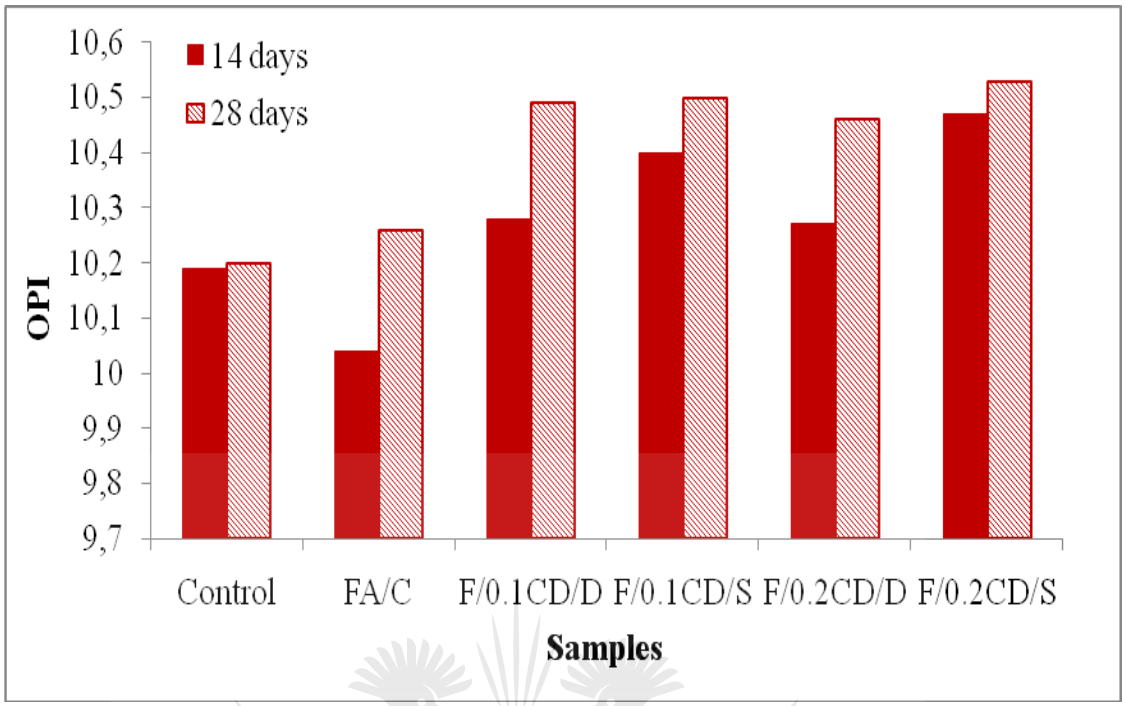

Figure 5.10: Oxygen permeability index (OPI) values of mortar samples

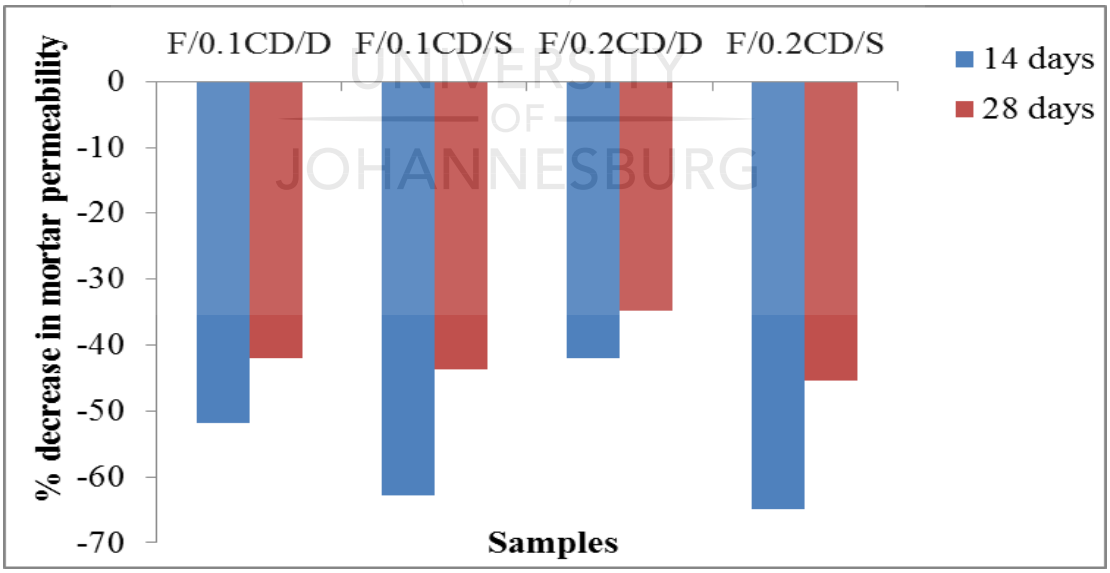

Figure 5.11: Percentage decrease in the permeability of FA-*β*-CD composite mortar compared to the permeability of FA-C mortar

5.4.5 Sorptivity of indicative mortar and concrete samples

The water sorptivity test measures the rate of movement of a water front through the exposed face of the mortar or concrete samples, under capillary suction. It reflects the effectiveness of curing. The lower the water sorptivity index, the better the potential durability of the concrete [9]. Figures 5.12 and 5.13 present the sorptivity results of mortar and concrete samples, respectively.

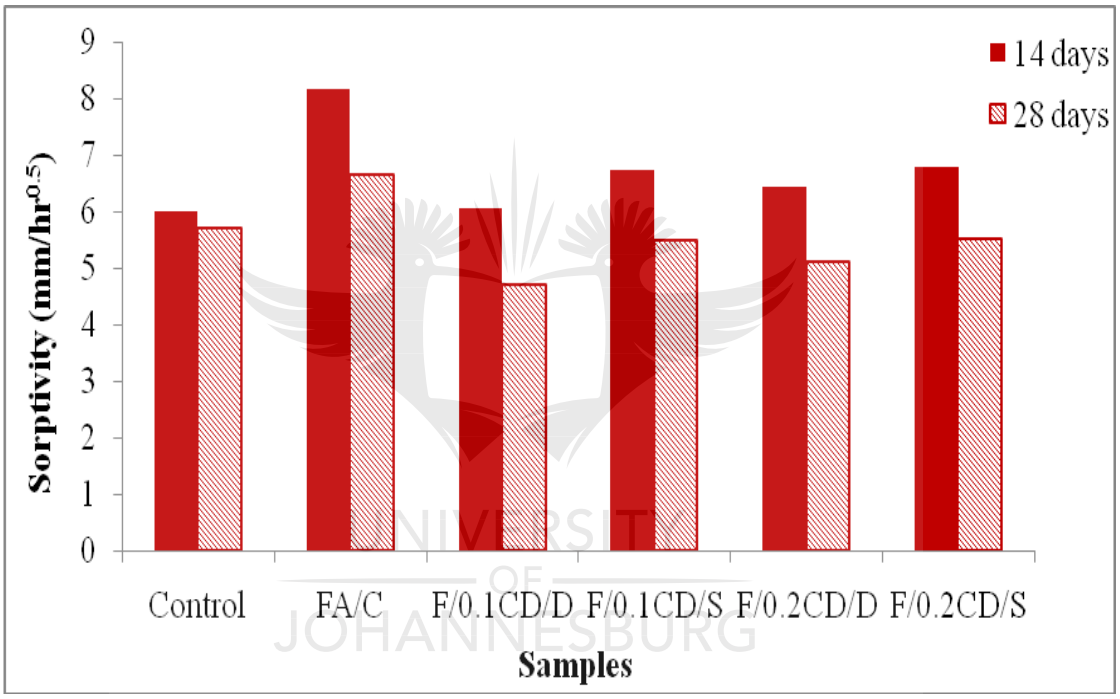

Figure 5.12: Sorptivity of mortar samples

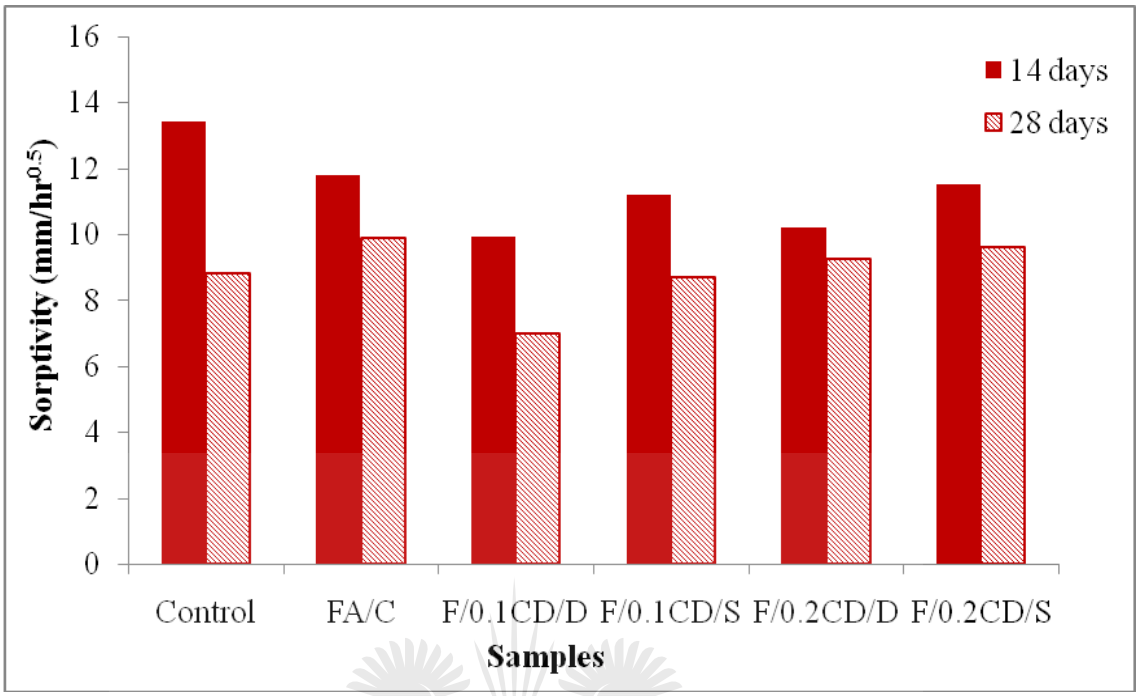

Figure 5.13: Sorptivity of concrete samples

A decrease in sorptivity was observed with an increase in curing age for all samples for both mortar and concrete. The reason for this is that as the curing age increased; the mortar or concrete became denser, which resulted in decrease in sorptivity. A higher sorptivity was observed for FA-C mortar compared to the control samples at both curing ages due to the slow pozzolanic reaction, which might have not been completed to result in a denser mortar at these ages. However, a lower sorptivity was observed for FA-C concrete relative to the control sample at a curing age of 14 days. However, the slower pozzolanic reaction resulted in higher soptivity of FA-C concrete relative to the control sample at a curing age of 28 days.

The mortar and concrete samples with FA-β-CD composites, exhibited a lower sorptivity than the FA-C sample at both curing ages. Figures 5.14 and 5.15 show the percentage decrease in FA-β-CD mortar and concrete sorptivity, relative to the FA-C mixture sorptivity, with the inclusion of the different β-CD composites. From Figures

5.14 and 5.15, it is evident that the F-0.1CD-D sample exhibited the highest reduction in sorptivity compared with FA-C, with approximately 29% reduction at 28 days curing period. Furthermore, the FA-*β*-CD composite dry mixes proved to be more effective in reducing the sorptivity than their corresponding solution mixes, in the case of both curing ages. In general, the sorptivity results agree with the permeability results in that FA-*β*-CD composite might have modified the composition and morphology of the hydration products.

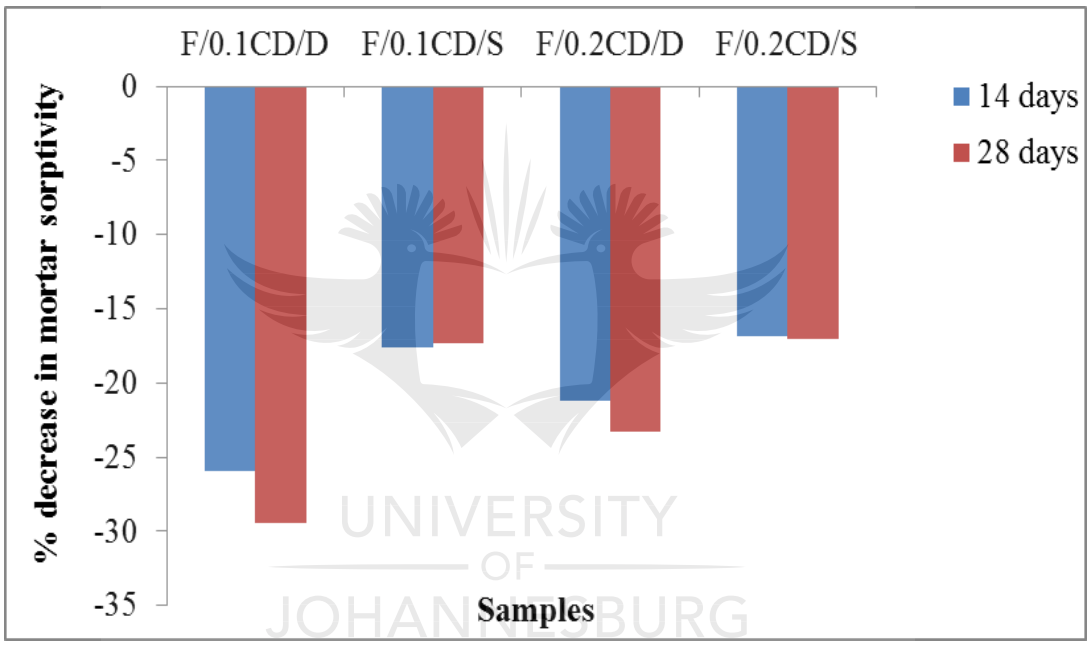

Figure 5.14: Percentage decrease in the sorptivity of FA-*β*-CD composite mortar compared to the sorptivity of FA-C mortar

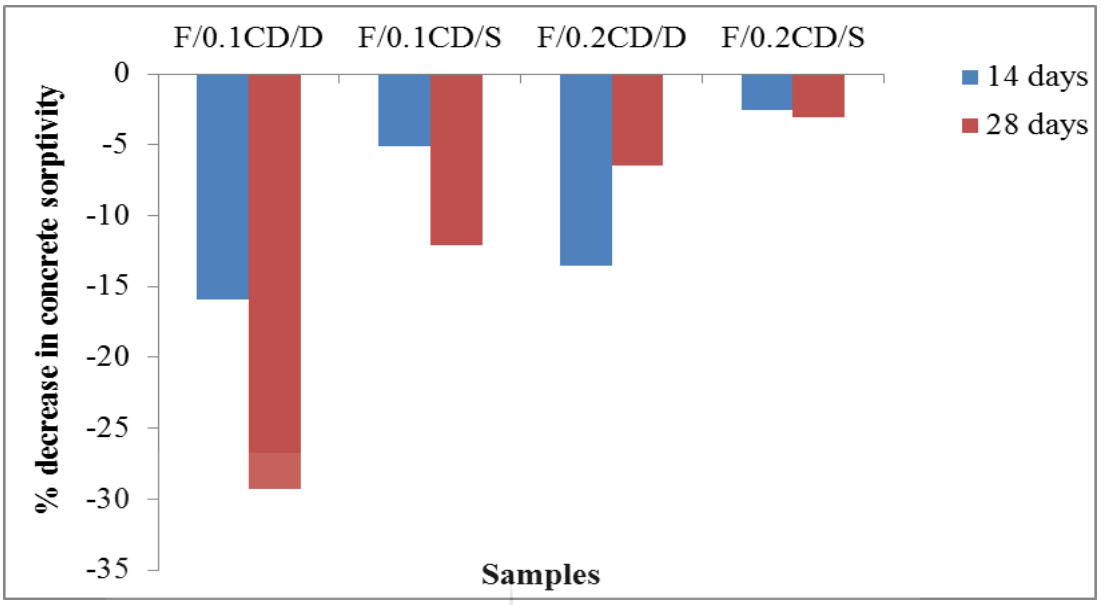

Figure 5.15: Percentage decrease in the sorptivity of FA-*β*-CD composite concrete compared to the sorptivity of FA-C concrete

5.4.6 Porosity of indicative mortar and concrete samples

The trend of results observed in sorptivity was also observed in porosity results as shown in Figures 5.16, 5.17, 5.18 and 5.19. As curing age increased, porosity decreased. The samples with FA-*β*-CD composite exhibited lower porosity than the control sample and FA-C sample for both curing ages. A higher porosity was observed for FA-C mortar relative to the control samples at both curing ages, due to the slow pozzolanic reaction. In the case of the concrete samples, a lower porosity was observed for FA-C mix compared to the control sample at a curing age of 14 days, while higher porosity was observed for FA-C concrete compared to the control sample at a curing age of 28 days. As reflected in sorptivity results, the FA-*β*-CD composite dried mix samples showed lower porosity compared to FA-C sample than their corresponding solution mix samples for both curing ages. The above observations might be as a result of the explanation given for sorptivity results. The porosity results further buttressed the fact that FA-*β*-CD composite might have boosted the pozzolanic reaction.

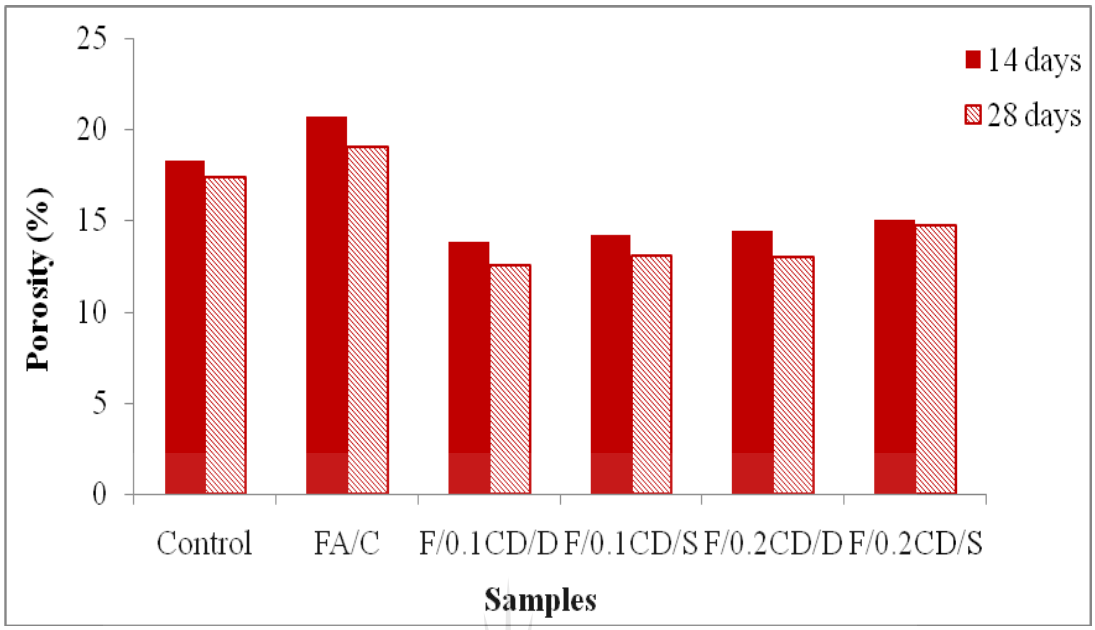

Figure 5.16: Porosity of mortar samples

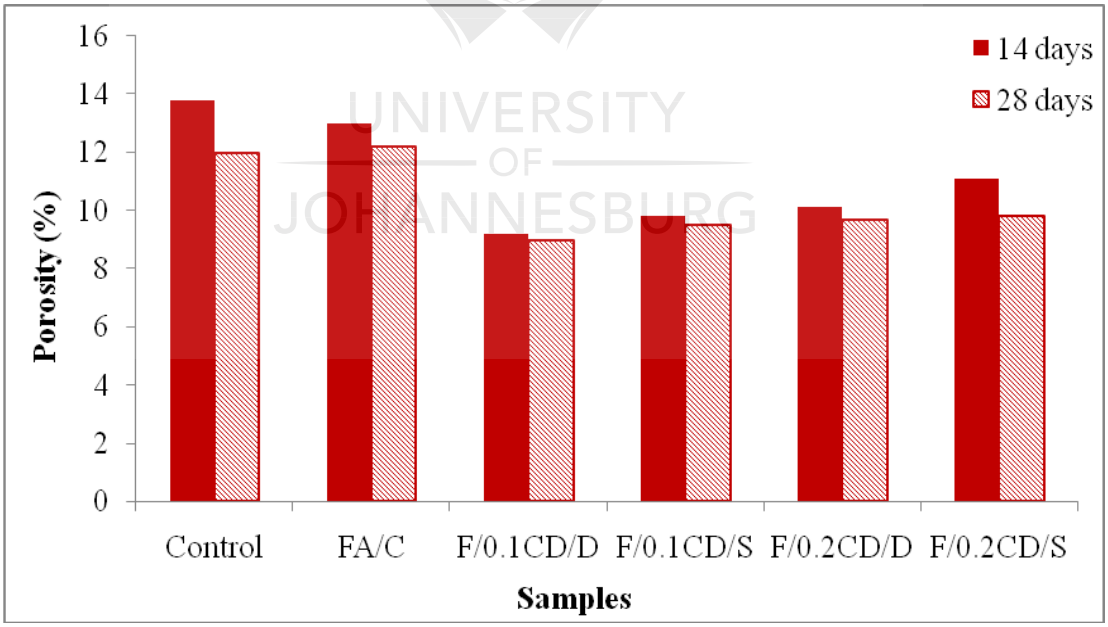

Figure 5.17: Porosity of concrete samples

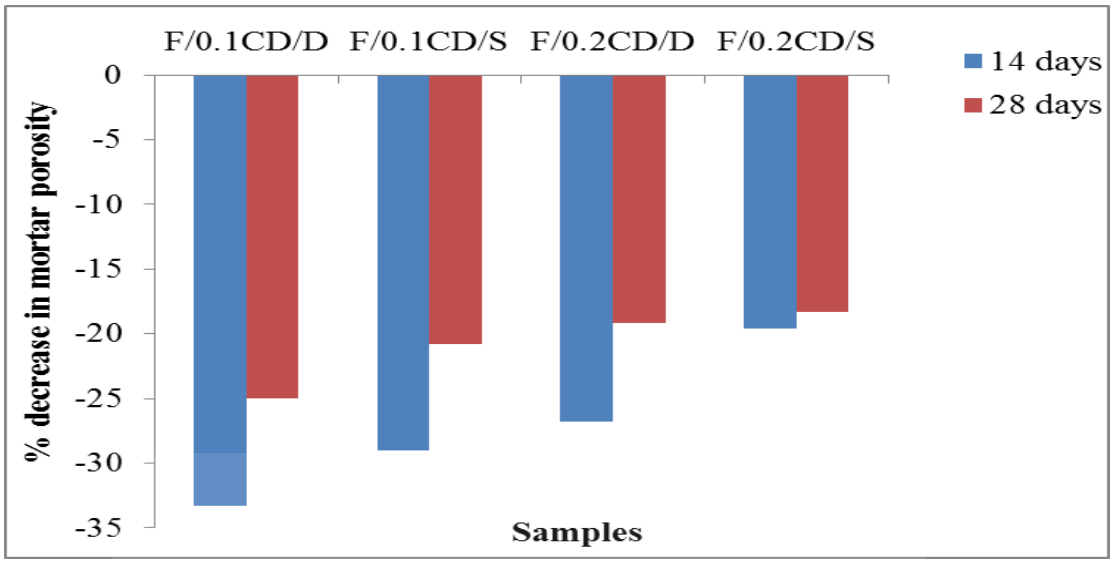

Figure 5.18: Percentage decrease in the porosity of FA-*β*-CD composite mortar compared to the porosity of FA/C mortar

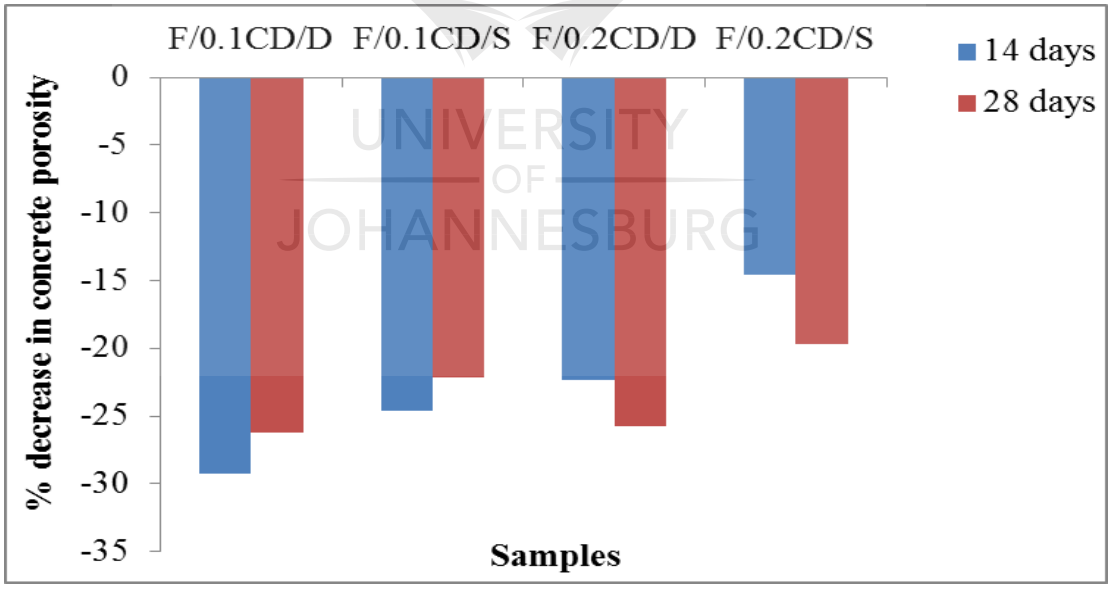

Figure 5.19: Percentage decrease in the porosity of FA-*β*-CD composite concrete compared to the porosity of FA/C concrete

5.5 CONCLUSIONS

The indicative tests results on the effect of fly ash-*β*-cyclodextrin composite on concrete workability, strength, oxygen permeability, water sorptivity and porosity presented in this chapter provided guidance for the development of an appropriately detailed research test program. The FA-*β*-CD composite improved the flow of mortars and workability of concrete. The results showed that higher content of *β*-CD (0.5%) in concrete has a detrimental effect on strength for both dry and solution mixtures. However, lower percentages of *β*-CD (0.1% and 0.2%) improved workability without reducing the cohesiveness of concrete, increased compressive strength at all ages compared to the pozzolanic samples and increased split tensile strength at curing ages of 28 and 90 days when compared to the pozzolanic samples. The durability results indicated that FA-*β*-CD composite might have modified the composition and morphology of the hydration products. The positive compatibility of FA and *β*-CD at lower percentages of *β*-CD (0.1% and 0.2%) to produce better pozzolanic concrete is advantageous towards utilizing FA more in concrete, which in turn will reduce construction cost and environmental pollution arising from dumping FA. The effect of *β*-CD on the pozzolanic samples is attributed to the stronger Si-O-Si and Al-O-Si bonding present in the FA-*β*-CD composite as seen in Chapter Four, which allows more active SiO_2 to react with $Ca(OH)_2$ to form more C-S-H (Calcium Silicate Hydrate) that is responsible for strength formation.

Further research, which is documented in the subsequent chapters, investigated the effect of lower contents of *β*-CD (0.025%, 0.05% and 0.1%) on hydration reactions. Focus was placed on the structure/microstructure (XRD, SEM and FT-IR), fresh properties (viscosity, setting times and workability) and hardened properties (compressive strength, split tensile strength, oxygen permeability, water sorptivity, porosity and chloride conductivity) of cement paste/concrete.

5.6 REFERENCES

[1] Chindaprasirt P., Jaturapitakkul C., Sinsiri T.: Effect of fly ash fineness on compressive strength and pore size of blended cement paste. Cement and Concrete Composites **27**, 425–428 (2005).

[2] Nath P., Sarker P.: Effect of Fly Ash on the Durability Properties of High Strength Concrete. Procedia Engineering **14,** 1149–1156 (2011).

[3] Yılmaz M., Tugrul A.: The effects of different sandstone aggregates on concrete strength. Construction and Building Materials **35**, 294–303 (2012).

[4] Gameiro F., Brito J. de, Correia da Silva D.: Durability performance of structural concrete containing fine aggregates from waste generated by marble quarrying industry. Engineering Structures **59**, 654–662 (2014).

[5] Kubissa W., Jaskulski R.: Measuring and Time Variability of The Sorptivity of Concrete, 11th International Conference on Modern Building Materials. Structures and Techniques, MBMST 2013, Procedia Engineering **57**, 634 – 641 (2013).

[6] Sideris K.K., Anagnostopoulos N.S.: Durability of normal strength self-compacting concretes and their impact on service life of reinforced concrete structures. Construction and Building Materials **41**, 491–497 (2013).

[7] Wang W., Liu J., Agostini F., Davy C.A., Skoczylas F., Corvez D.: Durability of an ultra high performance fiber reinforced concrete (UHPFRC) under progressive aging. Cement and Concrete Research **55**, 1–13 (2014).

[8] Chindaprasirt P., Jaturapitakkul C., Sinsiri T.: Effect of fly ash fineness on microstructure of blended cement paste. Construction and Building Materials **21**, 1534–1541 (2007).

[9] Ballim Y., Alexander M.G.: Towards a performance-based specification for concrete durability. African Concrete Code Symposium, 206-218 (2005).

[10] SANS 50196-1:2006: South African national standard. Methods of testing cement Part 1: Determination of strength, ISBN 0-626-17596-8. Edition 2.

[11] ASTMC 618: 2012 Standard Specification for Coal Fly Ash and Raw or Calcined Natural Pozzolan for Use in Concrete.

[12] SANS 5861-3: 2006: South African national standard. Concrete tests, Part 3: Making and curing of test specimens, ISBN 978-0-626-27130-5. Edition 2.1.

[13] ASTM C 1437. Standard Test Method for Flow Table for Flow of Hydraulic Cement Mortar. Annual Book of ASTM Standards **4(1),** 614-615 (2006).

[14] SANS 5861-1: 2006: South African national standard. Concrete tests, Part 1: Mixing fresh concrete in the laboratory, ISBN 978-0-626-27128-2. Edition 2.1.

[15] SANS 5862-1:2006, Concrete tests-consistence of freshly mixed concrete – slump test, Pretoria: South Africa Bureau of Standards.

[16] SANS 5863:2006 Concrete tests-compressive strength of hardened concrete, Pretoria: South Africa Bureau of Standards.

[17] SANS 6253:2006 Concrete tests-tensile splitting strength of concrete. Pretoria: South Africa Bureau of Standards.

[18] Alexander M.G., Ballim Y., Mackechnie J.M.: Concrete durability index testing manual, Research monograph no. 4, Departments of Civil Engineering, University of Cape Town and University of the Witwatersrand (1999).

[19] Alexander M.G., Mackechnie J.R., Ballim Y.: Guide to the use of durability indexes for achieving durability in concrete structures, Research monograph no 2, published by the Department of Civil Engineering, University of Cape Town in collaboration of University of the Witwatersrand, 5-25 (2001).

[20] Alexander M. G.: Durability indexes and their use in concrete engineering, International RILEM Symposium on Concrete Science and Engineering: A Tribute to Arnon Bentur. Print-ISBN**:** 2-912143-46-2, e-ISBN**:** 2912143586, Publisher**:** RILEM Publications SARL, 9 – 22 (2004).

[21] Ballim Y.A.: Low cost, falling head permeameter for measuring concrete gas permeability, Concrete/Beton. Journal of the Concrete Society of Southern Africa **(61)** 13-18 (1991).

[22] Streicher P.E., Alexander M.G.: A chloride conduction test for concrete, Cement and Concrete Research **(25),** 1284-1294 (1995).

[23] Streicher P.E., Alexander M.G.: Towards standardisation of a rapid chloride conduction test for concrete. Cement, Concrete and Aggregates **(21),** 23-30 (1999).

[24] Gouws S.M., Alexander M.G., Maritz G.: Use of durability index tests for the assessment and control of concrete quality on site. Concrete Beton **(98),** 5-16 (2001)**.**

[25] Alexander M. G., Ballim Y., Stanish K.: A framework for use of durability indexes in performance based design and specifications for reinforced concrete structures. Materials and Structures **(41),** 921–936 (2008).

[26] Bajor T., Szente L., Szejtli J., Methods for Characterization of the Wettability of Cyclodextrin Complexes, Proceedings of the Fourth International Symposium on Cyclodextrins. Advances in Inclusion Science, **(5),** 237-241 (1988).

[27] Singh R., Bharti N., Madan J., Hiremath S. N.: Characterization of Cyclodextrin Inclusion Complexes – A Review. Journal of Pharmaceutical Science and Technology **2(3),** 171-183(2010).

[28] Pourchez J., Govin A., Grosseau P., Guyonnet R., Guilhot B., Ruot B.: Alkaline stability of cellulose ethers and impact of their degradation products on cement hydration. Cement and Concrete Research **36**, 1252–1256 (2006).

[29] Phan T.H., Chaouche M., Moranville M.: Influence of organic admixtures on the rheological behaviour of cement pastes. Cement and Concrete Research **36**, 1807–1813 (2006).

[30] Khan B., Baradan B.: The effect of sugar on setting-time of various types of cements. Quarterly science vision **8(1)** (2002).

[31] Abalaka A.E.: Effects of Sugar on Physical Properties of Ordinary Portland Cement Paste and Concrete. AU Journal of Technology **14(3),** 225-228 (2011).

[32] Khan B., Ullah M.: Effect of a Retarding Admixture on the Setting Time of Cement Pastes in Hot Weather. JKAU: Engineering Science, **15(1),** 63-79 (2004).

[33] Grieve G.: Cementitious materials, Fulton's Concrete Technology, Edited by Gill Owens, 9th edition. Cement and Concrete Institute Midrand, South Africa. ISBN 978-0-9584779-1-8, 1-16 (2009).

[34] Siddique R.: Compressive strength, water absorption, sorptivity, abrasion resistance and permeability of self-compacting concrete containing coal bottom ash. Construction and Building Materials **(47),** 1444–1450 (2013).

CHAPTER SIX

THE EFFECT OF FLY ASH, *β*-CYCLODEXTRIN AND FLY ASH-*β*-CYCLODEXTRIN COMPOSITE ON THE STRUCTURE AND MICROSTRUCTURE OF CEMENT PASTE DURING THE HYDRATION PROCESS

6.1 INTRODUCTION

The process of setting and hardening of cement paste during the hydration reaction causes changes in the structure and microstructure as the process progresses. Observation of these changes helps to understand the behaviour of the final product. During the hydration period, cement compounds react to produce calcium hydroxide ($Ca(OH)_2$) and calcium silicate hydrate (C-S-H). C-S-H is responsible for strength development. During pozzolanic reaction, calcium hydroxide is consumed to form more C-S-H. In the process of hydration and pozzolanic reactions, changes in the different crystalline phases of tricalcium silicate (C_3S), dicalcium silicate (C_2S), tricalcium aluminate (C_3A), tetracalcium aluminoferrite (C_4AF), ettringite (calcium sulfoaluminate), calcium hydroxide ($Ca(OH)_2$), the amorphous phase of C-S-H and the morphology changes of these different phases help to understand the strength development from the mixing stage to the hardened stage. These changes are affected by different factors, such as the composition of cement, curing temperature, the solid/solution ratio and admixtures [1-3].

To understand the effect of fly ash (FA), *β*-cyclodextrin (*β*-CD) and fly ash- *β*-cyclodextrin (FA-*β*-CD) composite on concrete properties, the study of their effect on the structure and microstructure of cement paste as hydration progresses is important. FA dilutes the cement, such that less C-S-H from clinker is formed. It has been reported that in the presence of FA, hydration reaction slows down and leads to low early strength [4]. According to Aimin and Sarkar [5], the relatively slow gain of early strength due to FA, requires the need for an additional component to activate the

hydrolysis ability of low calcium FA. Aimin and Sarkar [5] also added that the possibility of FA activation lies in breaking down of its glass phases. This chapter presents and discusses the effect of FA, β-CD and FA-β-CD composites on the structure and microstructure of cement paste samples during the hydration process. XRD, SEM and FT-IR were employed for the investigation. Possible assignment of FT-IR bands as reported by Hughes et al [6] is shown in Table 6.1. This chapter does not limit the assignment of FT-IR bands to Table 6.1. The studies were monitored at different ages of hydration.

Table 6.1: Possible assignment of FT-IR absorption bands [6]

Mineral	Fundamentals			Overtones	O-H Stretch	O-H Bend
Sulfates	ν_1	ν_3	ν_4			
Gypsum	1005	1117	669, 604	2500–1900	3553, 3399	1686, 1618
Bassanite	1009	1152, 1117, 1098	660, 629, 600	2500–1900	3611, 3557	1618
Syngenite	1001	1192, 1130, 1113	658, 644, 604	2500–1900	3309	1678
Anhydrite	1015	1163	677, 615, 600	2500–1900		
Carbonates Hydroxides	ν_2	ν_3	ν_4			
Calcium Carbonate	876, 849	1458	714	2980–2500, 1794		
Calcium Hydroxide					3646	
Magnesium Hydroxide					3696	
Clinker phases		Unassigned Fundamentals				
C_3S	Si–O	935, 521		2000–1600		
C_2S	Si–O	991, 879, 847, 509		2060–1600		
C_3A	Al–O	889, 860, 812, 785, 762, 621, 586, 518, 506				
C_4AF	Fe–O	700–500				

6.2 MATERIALS AND MIXES

The cement (CEM 1 52.5N), FA and *β*-CD used were the same as in Section 5.2. The composition of the FA and the cement used are presented in Table 5.1 and the *β*-CD composition is presented in Table 3.1. Twelve cement paste samples were prepared with a W/B of 0.3. Physical FA-*β*-CD mixtures were prepared by co-grinding a pre-weighed amount of *β*-CD and FA. FA was used at the percentages of 30 and 50, while *β*-CD was used at 0.025, 0.05 and 0.1 percentages. These percentages were based on the total percentage of cement. The samples were labelled as described in Table 6.2. The percentages of *β*-CD used were based on the indicative strength and durability tests that were done on FA-*β*-CD composite concrete, which are fully detailed in Chapter Five.

Table 6.2: Description of samples used

SAMPLE	COMPOSITION	DESCRIPTION
a	Control (100% C)	Reference sample with cement
b	C30FA	Sample with cement and 30% fly ash
c	C50FA	Sample with cement and 50% fly ash
d	C0.025CD	Sample with cement and 0.025% *β*-cyclodextrin
e	C0.05CD	Sample with cement and 0.05% *β*-cyclodextrin
f	C0.1CD	Sample with cement and 0.1% *β*-cyclodextrin
g	C30FA0.025CD	Sample with cement and 30% fly ash-0.025% *β*-cyclodextrin
h	C30FA0.05CD	Sample with cement and 30% fly ash-0.05% *β*-cyclodextrin
i	C30FA0.1CD	Sample with cement and 30% fly ash-0.1% *β*-cyclodextrin
j	C50FA0.025CD	Sample with cement and 50% fly ash-0.025% *β*-cyclodextrin
k	C50FA0.05CD	Sample with cement and 50% fly ash-0.05% *β*-cyclodextrin
l	C50FA0.1CD	Sample with cement and 50% fly ash-0.1% *β*-cyclodextrin

The structure of the hydrated cement paste samples was studied by XRD and FT-IR. The surface morphology of the hydrated samples was studied using SEM. For these tests, cement paste samples were cast in 40 x 40 x 160 mm moulds and were covered with polythene and left for 24 hours before demoulding. Samples with β-CD were left under polythene for 48 hours before demoulding. These samples were still soft and could not be handled after 24 hours. SANS 5861-3 [7], stipulated that due to retarding effect of a material such that the pre-demoulding time lapse of 20 to 24 hours is not suitable, the time may be extended for a suitable period. After the samples were demoulded, they were sliced into approximately 8 mm thick slices using a slow speed cut-off saw with a diamond-wafering blade. The sliced samples were well labelled and placed in a water bath maintained at 23 ^{o}C ± 2 ^{0}C for curing until the testing ages. At each testing age, a slice of each sample was placed in an excess of cold acetone for 2 hours to stop hydration. This time period was intended to facililitate acetone to completely be exchanged with the pore water. Acetone had been previously used by several researchers [8-12] to stop hydration. Since cyclodextrin is practically insoluble in acetone [13], the use of acetone to stop hydration had no effect on the stability of the cement paste.

After 2 hours in acetone, the samples were put in the oven maintained at 60 ^{0}C for 24 hours to avoid hydrate decomposition. For XRD and FT-IR, the samples were then pulverised with pestle in a porcelain mortar and sieve on the 75 µm sieve and kept in a desiccator, ready for testing. Samples were tested after 24 hours, 7 days, 28 days and 90 days hydration periods. The XRD samples were prepared using front loading technique. For SEM, the samples, after being removed from the oven were put in a desiccator and tested after 7 days, 28 days and 90 days hydration periods. Immediately prior to testing, samples were broken to reveal fresh surfaces for examination.

6.3 EXPERIMENTAL PROCEDURE

6.3.1 X-ray diffraction (XRD)

The procedure explained in Section 3.3.3 was followed.

6.3.2 Scanning electron microscope (SEM)

The procedure explained in Section 4.3.2 was followed.

6.3.3 Fourier transform-infrared analysis (FT-IR)

The procedure explained in Section 3.3.4 was followed.

6.4 RESULTS AND DISCUSSIONS

6.4.1 XRD

6.4.1.1 XRD analysis after 24 hours hydration period

XRD was used to monitor the evidence and extent of hydration in the samples by studying the consumption of the crystalline anhydrous phases of the samples (C_3S, C_2S, C_3A and C_4AF), the formation of the crystalline hydrates (CH) and the formation of amorphous C–S–H (this is indicated by the change from the crystalline anhydrous phases to amorphous phases of the diffractogram). The most prominent crystalline peaks observed after 24 hours hydration, as shown in Figure 1(a-l), were of calcium hydroxide (CH), tricalcium silicate (C_3S) and dicalcium silicate (C_2S). Quartz (SiO_2) and mullite ($Al_6Si_2O_{13}$) were evident in samples containing FA (Figure 1 b, c, g, h, i, j, k, l). A little peak of cyclodextrin (CD) was observed in some of the samples containing β-CD (Figure 1 e, f, h, i, j, k, l).

It is evident from Figure 6.1(e, f, h, i, k, l) that the samples with 0.05CD and 0.1CD have a higher C_3S/C_2S intensity than other samples. The peaks observed for the control sample (Figure 6.1a) are similar to those reported by other researchers [3, 5, 8, 14-16]. Delayed hydration was evident for samples containing β-CD (Figure 6.1d, e,

f, g, h, i, j, k, l) at 24 hours hydration period as seen from the high content of C_3S and C_2S and little formation of CH at the region approximately 18.3^0 as compared to the control sample. As expected, pozzolanic reaction is a slow reaction, therefore at this hydration stage, formation of CH was still in process so no consumption of CH by FA was observed. Further delay in the formation of CH was observed for C50FA and FA-β-CD composites samples than in the C30FA sample. The higher the content of FA and β-CD, the lower the formation of CH observed, which might be as a result of dilution effect. The addition of FA reduced the clinker content and therefore less CH developed.

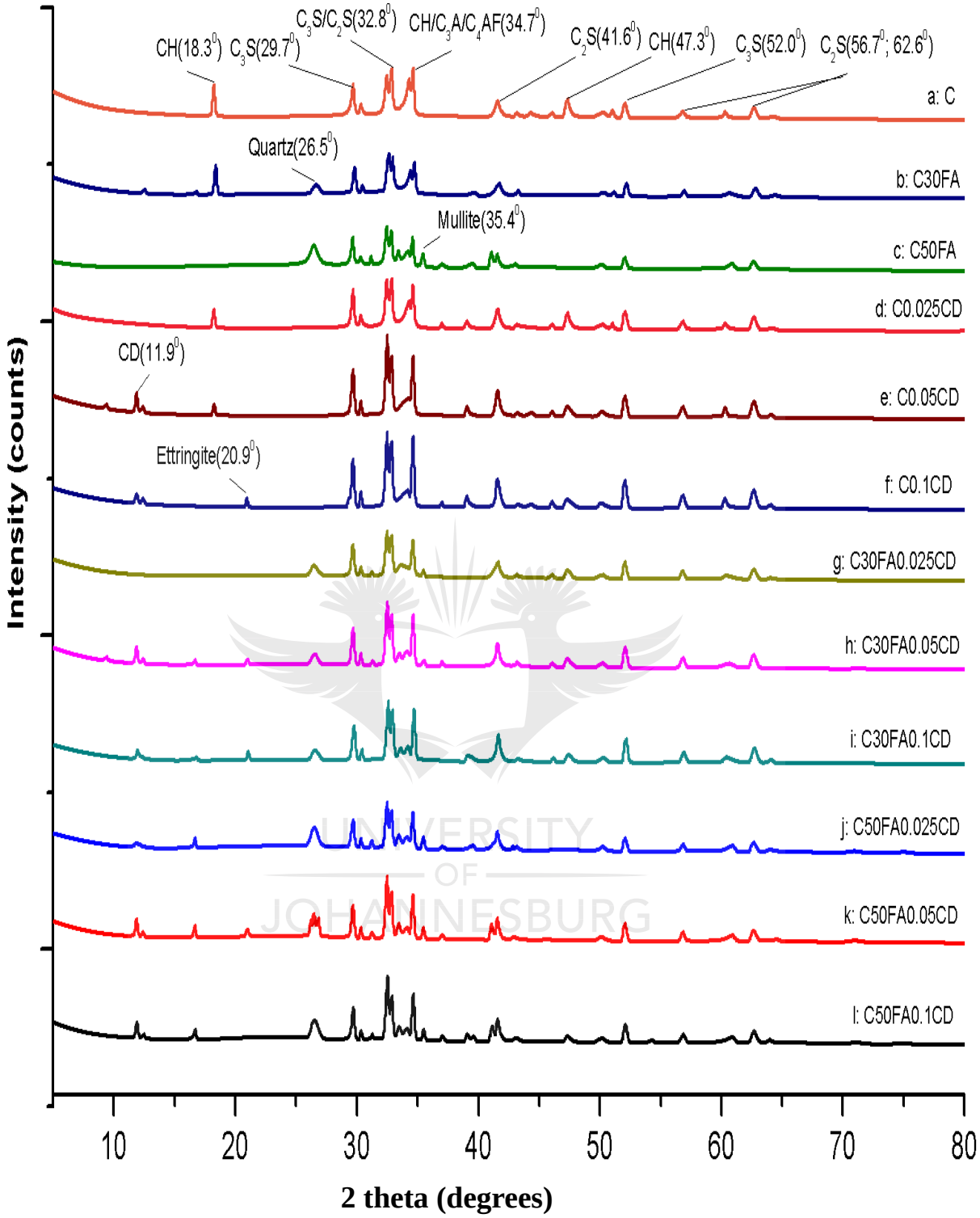

Figure 6.1: X-ray diffractograms (XRD) of cement paste samples hydrated for 24 hours

6.4.1.2 XRD analysis after 7 days hydration period

Figure 6.2(a-l) shows the diffractograms of the cement paste samples hydrated for 7 days. At this hydration period, the intensity of C_3S and C_2S peaks were reduced for all the samples due to the formation of calcium silicate hydrate gel (C-S-H) and calcium hydroxide (CH), as is evidenced by a high peak for CH. *β*-CD increased the dissolution of C_3S and C_2S and aided the formation of CH (Figure 6.2d, e, g, h, j, k) and amorphous C-S-H at 0.025% and 0.05% *β*-CD replacements compared to the control, C30FA and C50FA samples. These samples (samples containing 0.025% and 0.05% *β*-CD) are envisaged to have an increased strength at this early hydration period following the observation reported by Khater [12] that an increased early formation of C-S-H would lead to an increase in strength. A higher growth rate of the hydrates (CH) was observed for the samples with 0.025% *β*-CD than for the samples with 0.05% *β*-CD.

A lower formation of CH was observed in the samples with 0.1% *β*-CD replacement (Figure 6.2f, i, l) compared to the 0.025% and 0.05% *β*-CD replacements samples. This observation for the 0.1% *β*-CD replacement samples might be an indication of setting retardation, which will result in a delay of early formation of hydration products. Slower pozzolanic reaction was observed in the FA and FA-*β*-CD composite samples (Figure 6.2b, c, g, h, i, j, k, l). A higher content of quartz and crystalline phase of mullite was observed in samples containing 50% FA (Figure 6.2c, j, k, l).

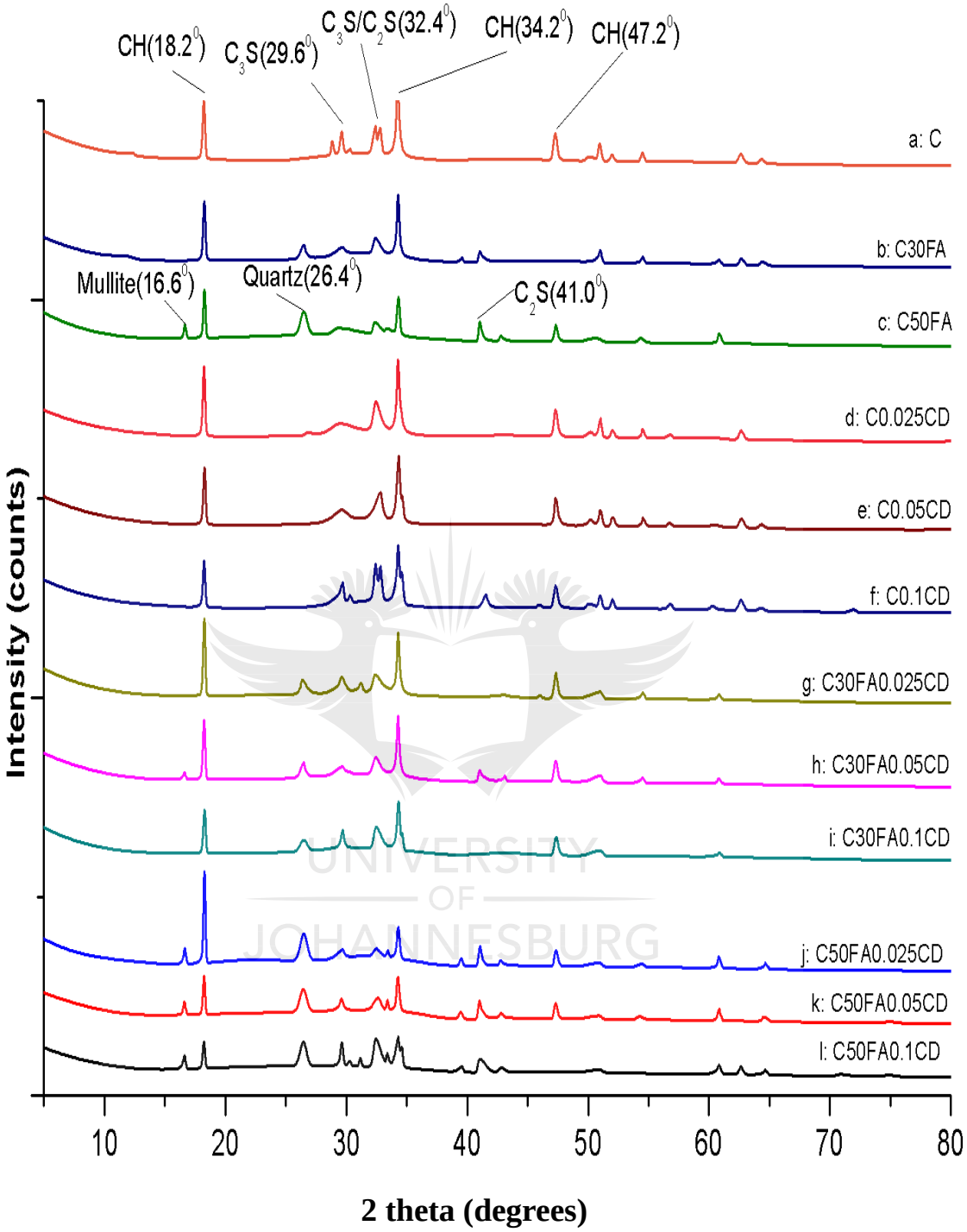

Figure 6.2: X-ray diffractograms (XRD) of cement paste samples hydrated for 7 days

6.4.1.3 XRD analysis after 28 days hydration period

The diffractograms of the cement paste samples hydrated for 28 days are shown in Figure 6.3(a-l). In all the samples, the crystalline anhydrous phases were further consumed at the 28 days hydration period to form more amorphous C–S–H. There was little difference between the levels of dissolution of anhydrous phases in the control sample (Figure 6.3a) compared to samples with *β*-CD (Figure 6.3d, e, f). The reduction of the CH peak in all the FA and FA-*β*-CD composite samples (Figure 6.3b, c, g, h, i, j, k, l) at the 28 days hydration period compared to the 7 days hydration period was evidence of pozzolanic reaction, which allowed the consumption of some of the CH to produce more C-S-H. The higher the FA content, the greater the reduction in the CH peak observed.

Further dissolution of silica in FA and FA-*β*-CD composite samples at 28 days hydration, as compared to 7 days hydration period, confirmed that pozzolanic reaction was taking place between the SiO_2 and calcium hydroxide (CH). Higher contents of quartz (compared to the samples containing 30% FA) and mullite were still left in samples containing 50% FA (Figure 6.3c, j, k, l).

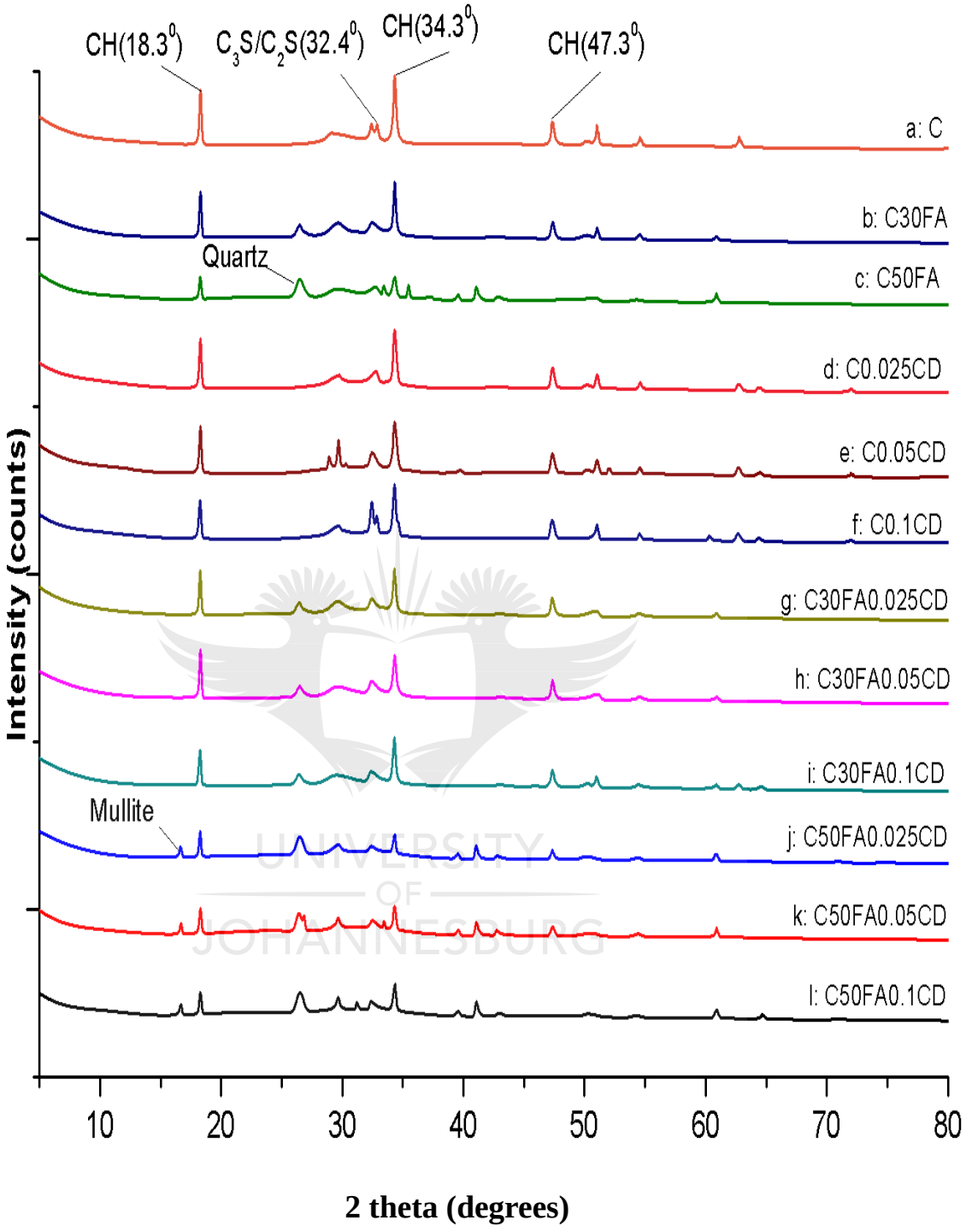

Figure 6.3: X-ray diffractograms (XRD) of cement paste samples hydrated for 28 days

6.4.1.4 XRD analysis after 90 days hydration period

Hydration reaction was envisaged to have been completed by the 90 days. The diffractograms of the cement paste samples at this hydration period are presented in Figure 6.4 (a-l). The anhydrous phases of cement compounds have completely formed crystalline CH and amorphous C-S-H (Figure 6.4a, d, e, f). The higher formation of CH and greater dissolution of the anhydrous phases observed in β-CD samples (Figure 6.4d, e, f), as compared to the control sample (Figure 6.4 a), are evidence that the β-CD aided the hydration reaction. A greater CH peak was observed for samples with 0.025% β-CD (Figure 6.4d) than the other samples.

At the 90 days hydration period, a greater pozzolanic reaction had taken place in FA samples resulting in the reduction of CH peak (Figure 6.4b, c). A higher content of FA resulted in a greater consumption of CH. Reduced CH peaks were also observed for the FA-β-CD composite samples containing 0.05% and 0.1% β-CD replacements (Figure 6.4h, i, k, l) at 90 days hydration period, compared to 28 days hydration period as a result of the pozzolanic reaction. At 0.025% β-CD replacements in the FA-β-CD composite samples (Figure 6.4g, j), increased CH peaks (at approximately 18.3^0) were observed, especially for the sample with 50% FA at 90 days hydration period compared to 28 days hydration period. The 0.025% β-CD replacements had little effect on the pozzolanic reaction.

In general, the XRD results showed the changes that occurred in the phases as hydration progressed. Highly crystalline anhydrous phases in the 24 hours hydration samples gradually formed the hydration products phases (CH and C-S-H). β-CD showed a delay in the 24 hours hydration, which was an indication of the retarding effect of the β-CD. Early hydration reaction was observed for control samples from the 24 hours hydration period. β-CD generally improved the hydration reaction of the control sample from the 7 days hydration period. The effect of β-CD on pozzolanic reaction was revealed from the 28 days hydration period. The 0.025% β-CD had little effect on pozzolanic reaction.

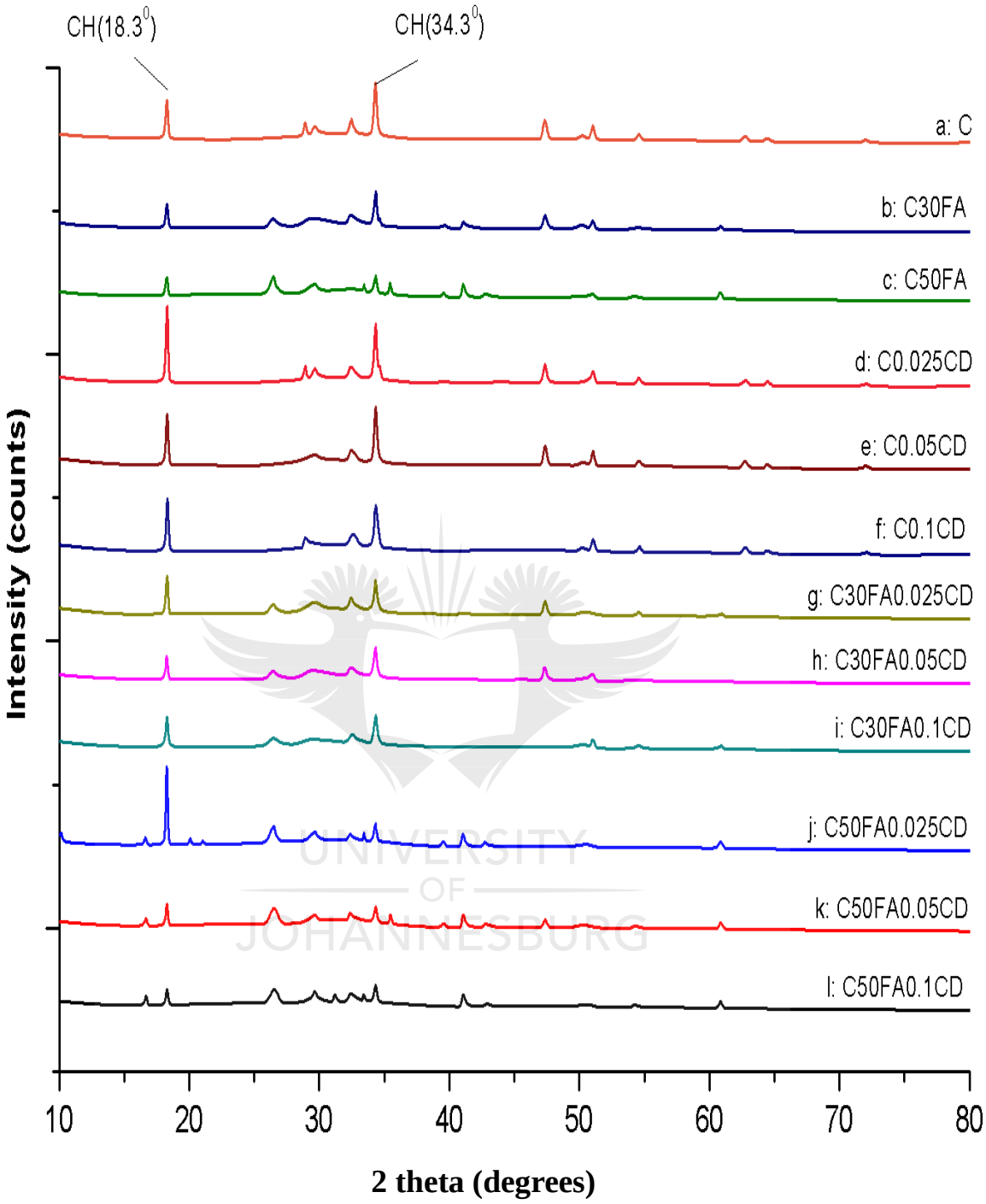

Figure 6.4: X-ray diffractograms (XRD) of cement paste samples hydrated for 90 days

6.4.2 SEM

6.4.2.1 SEM analysis after 7 days hydration period

At the 7 days hydration period, hydration reaction would have started while pozzolanic reaction was still delayed as seen in the XRD results. Figure 6.5(a-l) shows the SEM micrograghs of cement paste samples hydrated for 7 days. The control sample (Figure 6.5a) showed a spongy structure, revealing early formation of C-S-H with smaller particles coagulating together around unhydrated cement grains. Some pockets of capillary pores were also revealed. Unhydrated spherical particles of FA are shown in the C30FA sample (Figure 6.5b). At lower magnification, which is inserted, evidence of tiny needle shaped ettringite formation can be seen. The C50FA sample (Figure 6.5c) showed a semi-amorphous structure with more obvious and brighter evidence of needle-like-shaped ettringite at lower magnification (inserted).

The formation of primary crystalline structure of portlandite (CH) is evident in the C0.025CD sample (Figure 6.5d); a better view can be seen in lower magnification (inserted). This confirms the XRD observation for samples containing 0.025% β-CD (Figure 6.2d), which showed a greater peak of CH at 7 days hydration compared to the control sample. A cloudy surface was also observed for this sample, which is attributed to the adsorption of β-CD at the surface of the hydrates. With the 0.05% β-CD sample (Figure 6.5e), more evidence of cloudy surface was seen, with coagulation of tiny particles revealing early formation of C-S-H, due to the dissolution of the anhydrous phase of the cement paste. The cement paste sample containing 0.1% β-CD (Figure 6.5f) revealed a semi-amorphous surface revealing unhydrated cement grains, with lower evidence of hydration products in this sample compared to 0.025% and 0.05% β-CD samples. These observations confirmed the XRD results.

For the FA-β-CD composite samples, layered deposition of stacked CH primary crystals was observed for C30FA0.025CD sample (Figure 6.5g) with early micro

crystalline C-S-H formation around the FA particles. Breaking of FA particles into flaky/spongy like structure was observed in the C30FA0.05CD sample (Figure 6.5h), revealing improved reaction between FA and the hydrates. Improved flaky/spongy, less compacted like structure, with evidence of unhydrated particles of cement grains and FA can be seen in C30FA0.1CD sample (Figure 6.5i).

The C50FA0.025CD sample (Figure 6.5j) revealed coagulation of particles with little evidence of hydration products. The cloudy surface showing the adsorption of β-CD and FA on the surface of the hydrates is shown for C50FA0.05CD sample (Figure 6.5k). Unhydrated cement grains and FA particles with larger capillary pore were revealed for the C50FA0.1CD sample (Figure 6.5l).

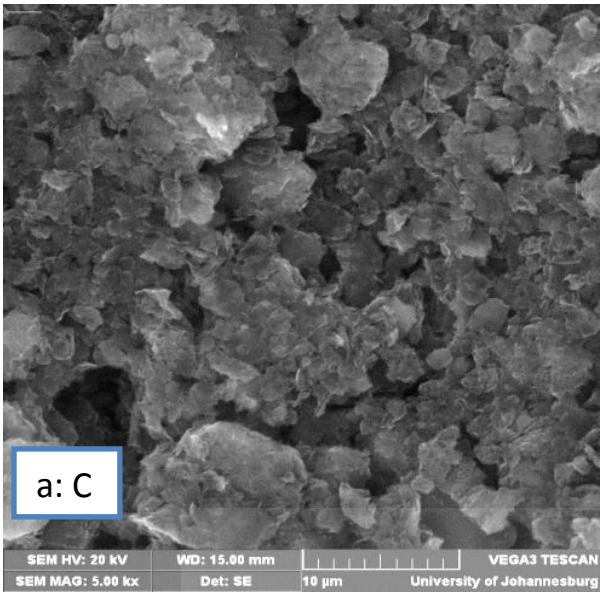

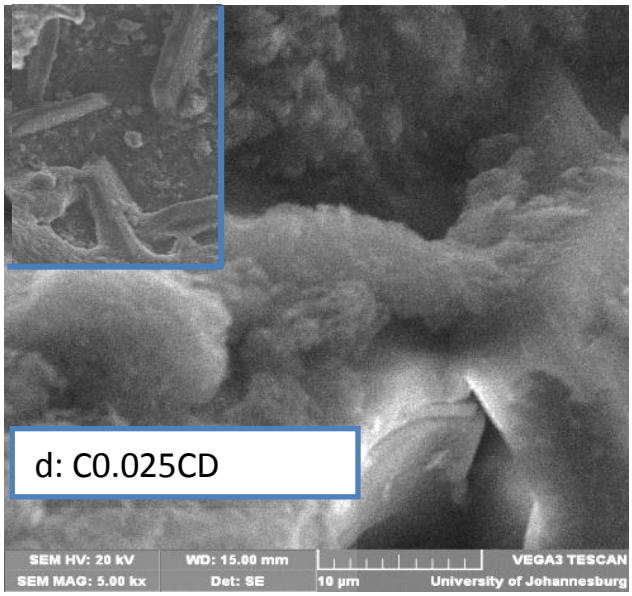

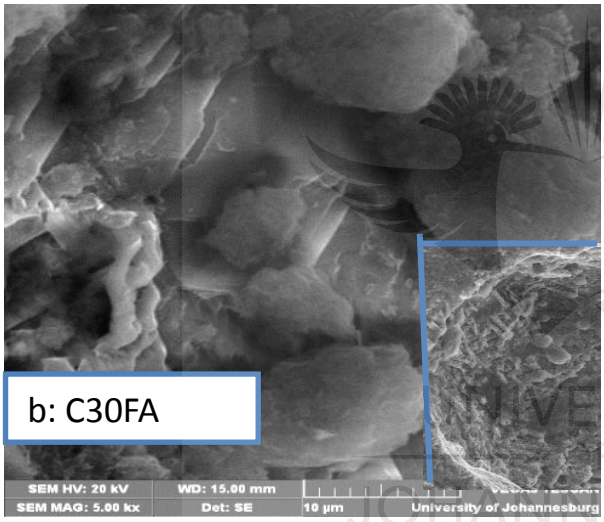

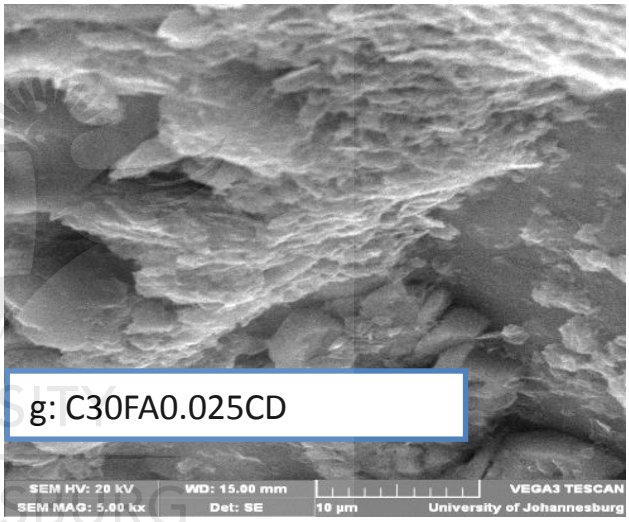

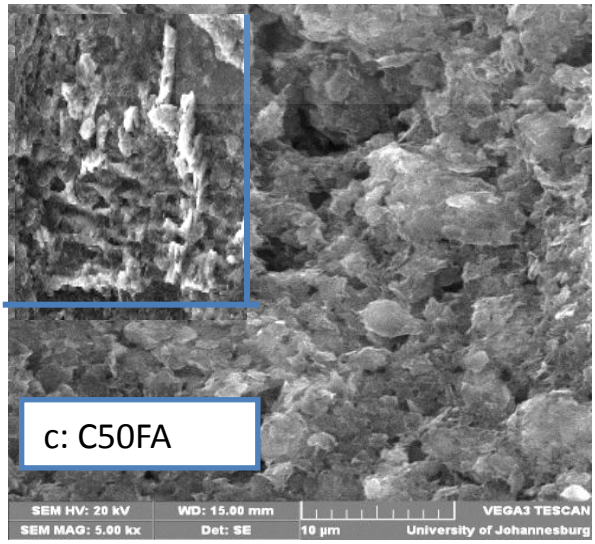

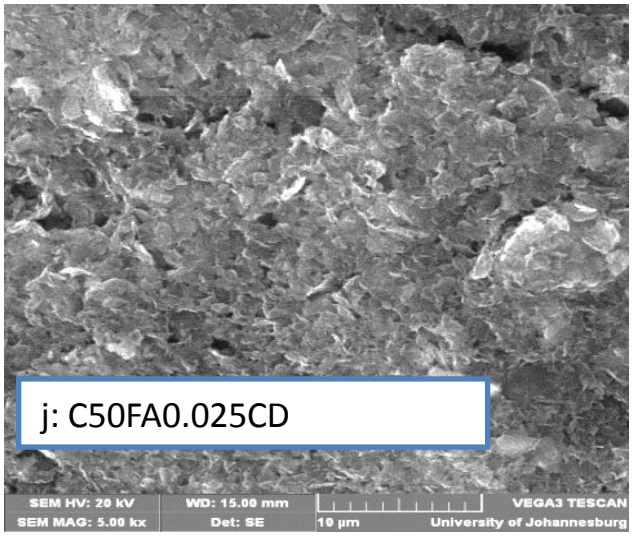

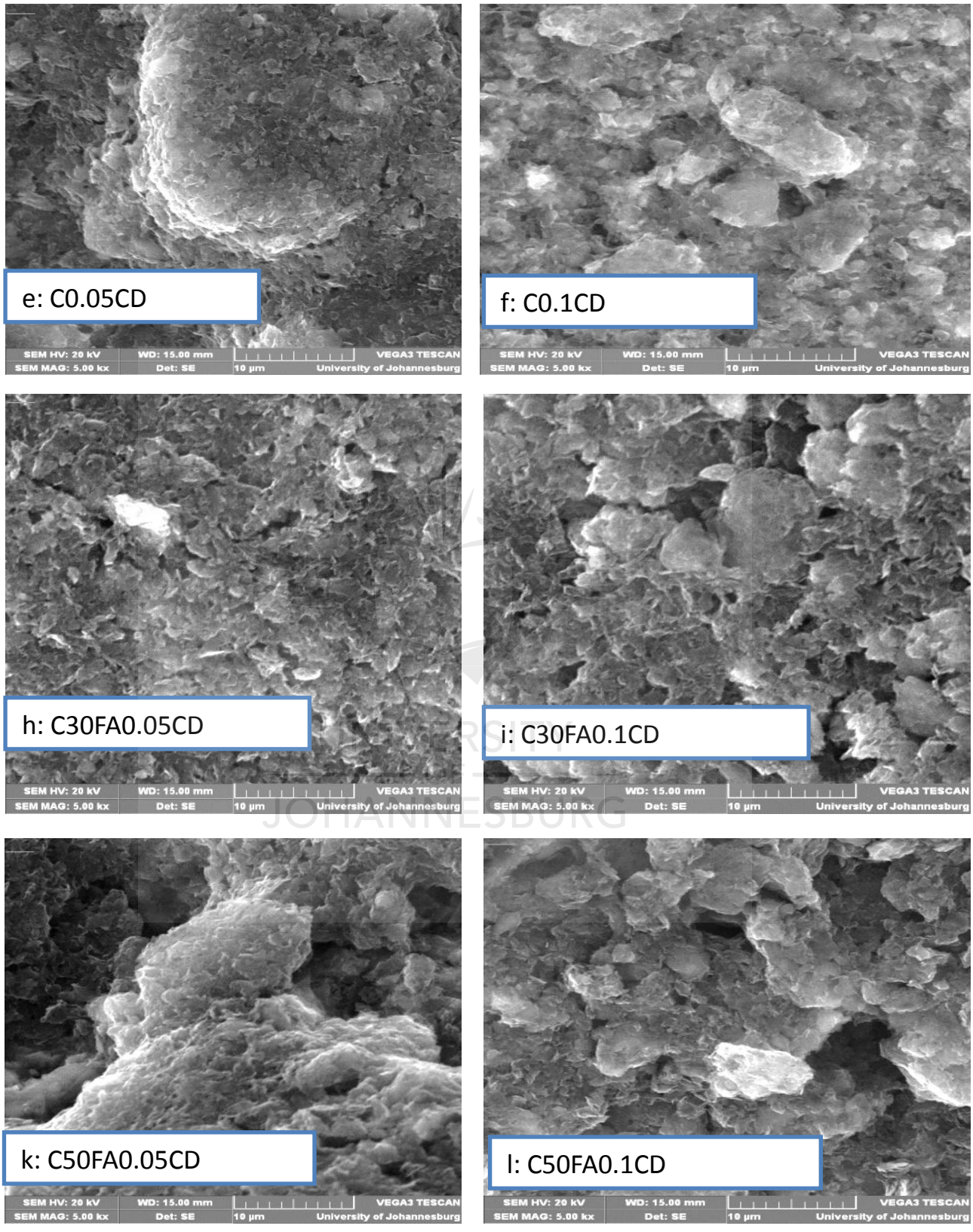

Figure 6.5: SEM of samples (a-l) hydrated for 7 days at 5000x magnification

6.4.2.2 SEM analysis after 28 days hydration period

The SEM micrographs of the samples hydrated for 28 days are shown in Figure 6.6 (a-l). Denser morphology structures were observed for all the samples revealing improved hydration and pozzolanic reactions. Formation of C-S-H gel, which filled the pores and resulted in a more dense surface and compact particles was observed for the control sample (Figure 6.6a), especially at lower magnification (inserted). Breaking of FA particles, resulting in smaller particle sizes and a denser surface was evidence of pozzolanic reaction as seen in the C30FA sample (Figure 6.6b). Less crystalline structure revealed the gradual formation of C-S-H gel. A spongy, less compacted structure was observed for the C50FA sample (Figure 6.6c) revealing a slower pozzolanic reaction than for the C30FA sample.

More improved denser surfaces were observed for samples containing *β*-CD (Figure 6.6d, e, f) when compared to control sample (Figure 6.6a). The improved denser surface of *β*-CD samples revealed greater hydration reaction at this hydration period than at 7 days. A less compacted surface was revealed for the C0.1CD sample (Figure 6.6f) than for the C0.025CD and C0.05CD samples (Figure 6.6 d, e). Reduced cloudy surfaces showing that more of *β*-CD and FA have been utilized in the reaction were observed for all FA-*β*-CD composite samples (Figure 6.6g, h, i, j, k, l) than 7 days hydration samples. This revealed improved pozzolanic reactions. The C30FA0.05CD sample (Figure 6.6h) showed a denser and more compact particle structure than the C30FA0.025CD and C30FA0.1CD samples (Figure 6.6g, i). Improved pozzolanic reaction showing the transformation of FA particles into the hydrate was obvious in the C50FA0.025CD sample (Figure 6.6j). The C50FA0.05CD and C50FA0.1CD samples (Figure 6.6k, l) showed similar features of spongy morphology revealing gradual formation of C-S-H. The C50FA0.05CD sample (Figure 6.6k) was more compacted than the C50FA0.1CD sample (Figure 6.6l).

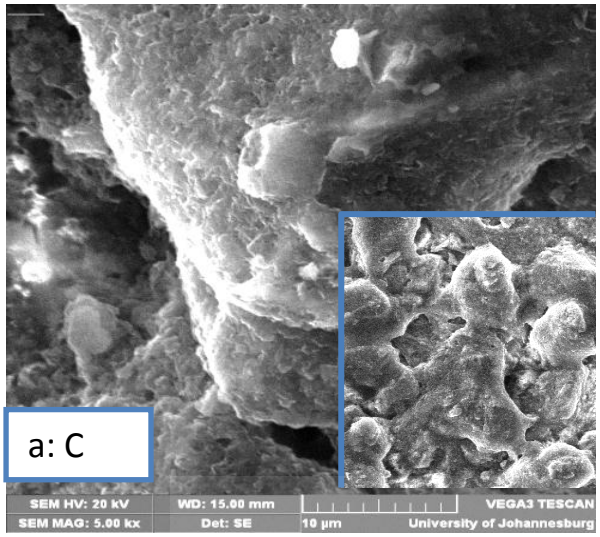
a: C
SEM HV: 20 kV
WD: 15.00 mm
VEGA3 TESCAN
SEM MAG: 5.00 kx
Det: SE
10 µm
University of Johannesburg

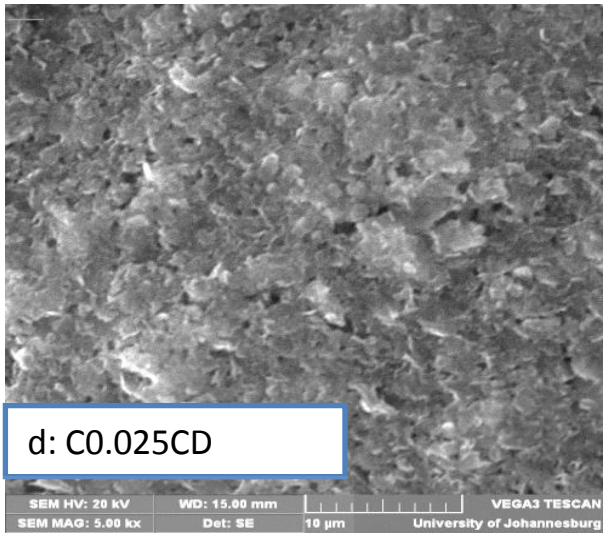
d: C0.025CD
SEM HV: 20 kV
WD: 15.00 mm
VEGA3 TESCAN
SEM MAG: 5.00 kx
Det: SE
10 µm
University of Johannesburg

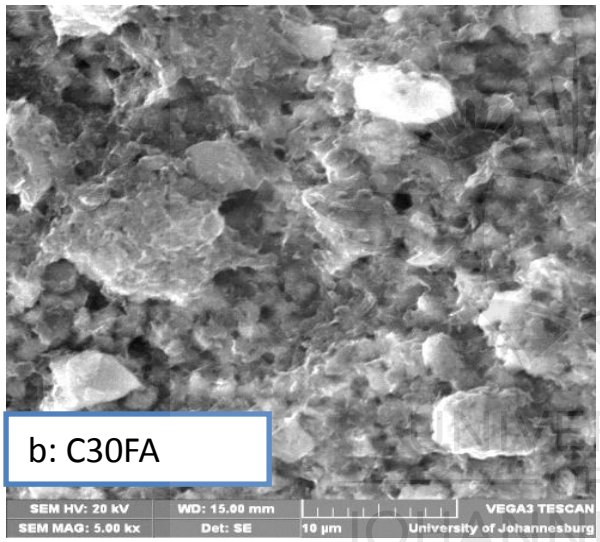
b: C30FA
SEM HV: 20 kV
WD: 15.00 mm
VEGA3 TESCAN
SEM MAG: 5.00 kx
Det: SE
10 µm
University of Johannesburg

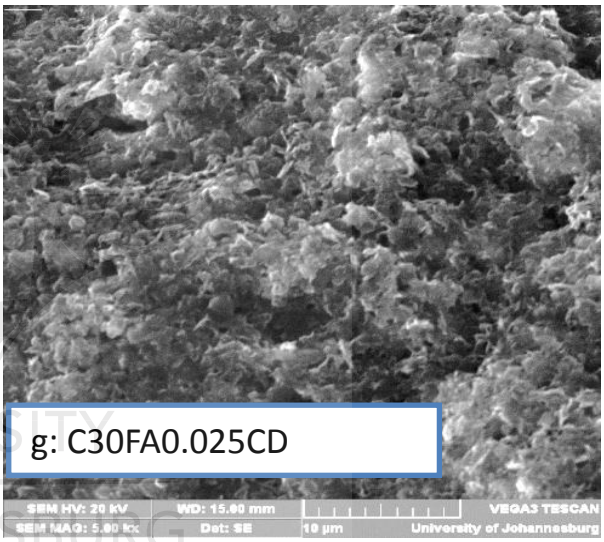
g: C30FA0.025CD
SEM HV: 20 kV
WD: 15.00 mm
VEGA3 TESCAN
SEM MAG: 5.00 kx
Det: SE
10 µm
University of Johannesburg

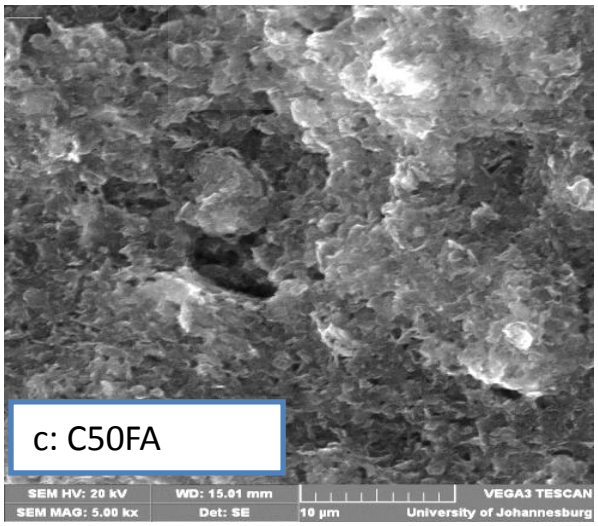
c: C50FA
SEM HV: 20 kV
WD: 15.01 mm
VEGA3 TESCAN
SEM MAG: 5.00 kx
Det: SE
10 µm
University of Johannesburg

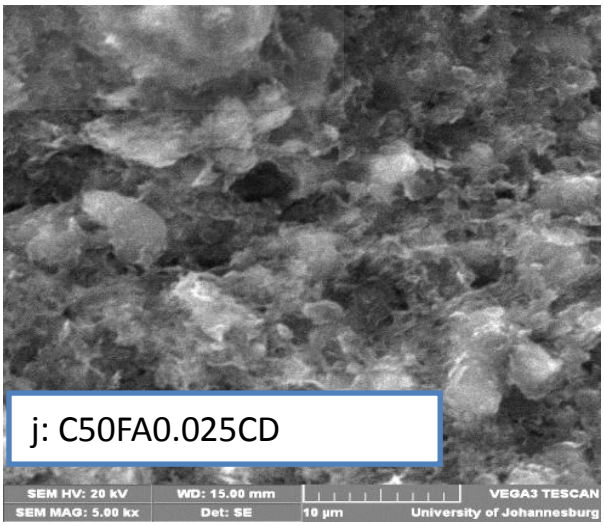
j: C50FA0.025CD
SEM HV: 20 kV
WD: 15.00 mm
VEGA3 TESCAN
SEM MAG: 5.00 kx
Det: SE
10 µm
University of Johannesburg

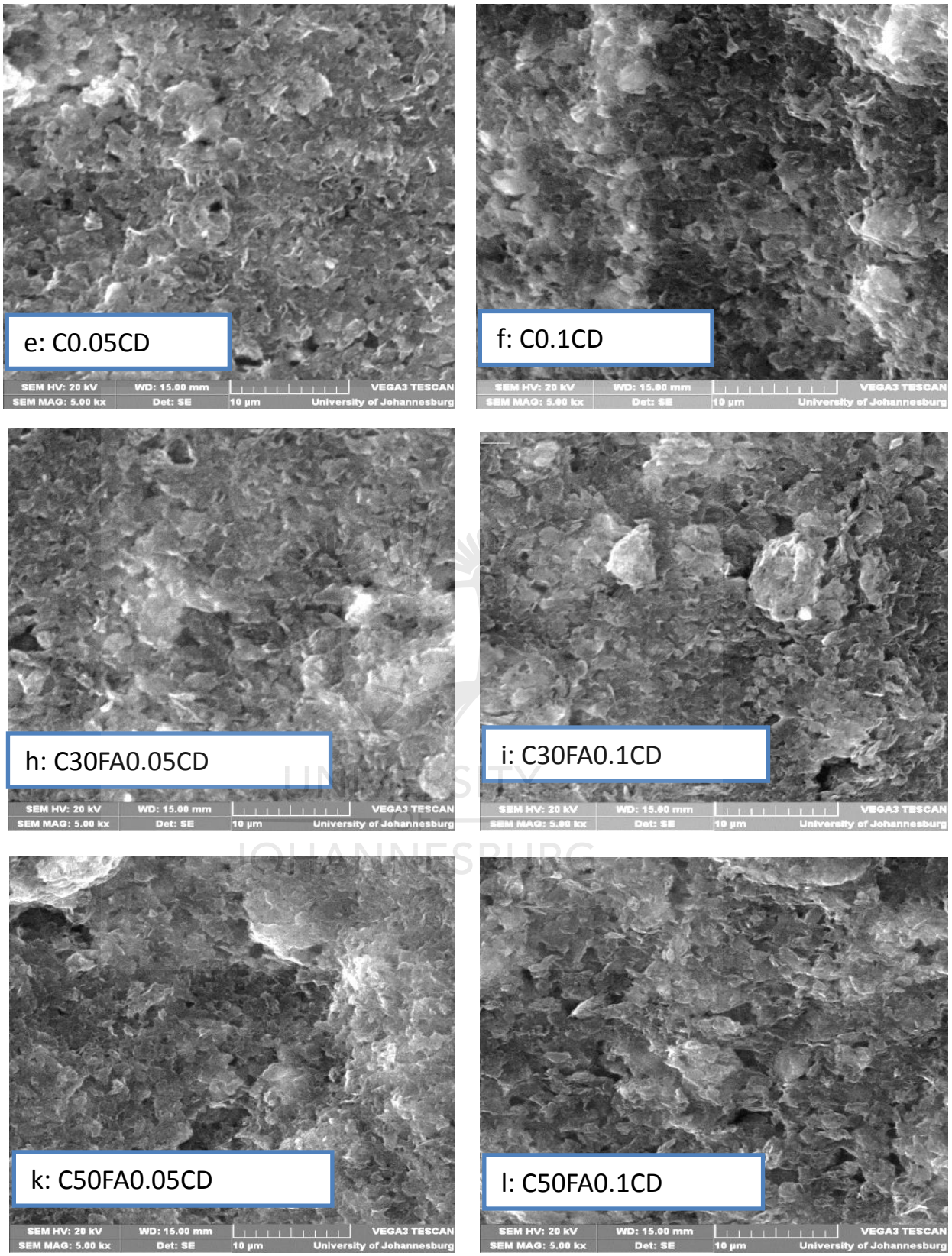

Figure 6.6: SEM of samples (a-l) hydrated for 28 days at 5000x magnification

6.4.2.3 SEM analysis after 90 days hydration period

Well hydrated morphology was revealed for all the samples after 90 days hydration period as shown in Figure 6.7 (a-l). The control sample's morphology (Figure 6.7a) showed flowered flaky particles that have been coagulated together; no further hydration reaction process was evident. Capillary pores were also shown. More flaky particles with evidence of some C-S-H gel covering the particles were revealed for the C30FA sample (Figure 6.7b). Reduced capillary pores are evident in the C30FA sample compared to the control sample. Large particles undergoing further pozzolanic reaction are seen in the morphology of the C50FA sample (Figure 6.7c).

The samples containing *β*-CD (Figure 6.7d, e, f) showed an improved denser surface and reduced continuous capillary pores compared to the control sample (Figure 6.7a). A more improved surface was revealed for the C0.025CD sample (Figure 6.7d). The C0.05CD sample (Figure 6.7e) showed greater flaky particles morphology than the C0.025CD and C0.1CD samples, these flaky particles were better packed than for the control sample. The C0.1CD sample (Figure 6.7f) showed evidence of C-S-H gel covering the particles. This could be attributed to the increased amount of *β*-CD in C0.1CD sample, which showed evidence of delayed hydration.

Compacted morphologies are seen for C30FA0.025CD and C30FA0.05CD composite samples (Figure 6.7g, h). A less compacted, porous flaky morphology was revealed for the C30FA0.1CD sample (Figure 6.7i). Reduced particle sizes were observed for the C30FA0.05CD sample (Figure 6.7h) than for the C30FA, C30FA0.025CD and C30FA0.1CD samples (Figure 6.7 b, g, i). Evidence of C-S-H gel was seen on the surface of C50FA0.025CD and C50FA0.05CD composite samples (Figure 6.7 j, k) particles. The dissolving surface of the C50FA0.025CD and C50FA0.05CD samples was evidence of the delayed pozzolanic reaction of the FA-*β*-CD composite samples with 50% FA compared to the FA-*β*-CD composite samples with 30% FA. An improved denser surface was observed for respective FA-*β*-CD composite samples when compared to their original C30FA and C50FA samples.

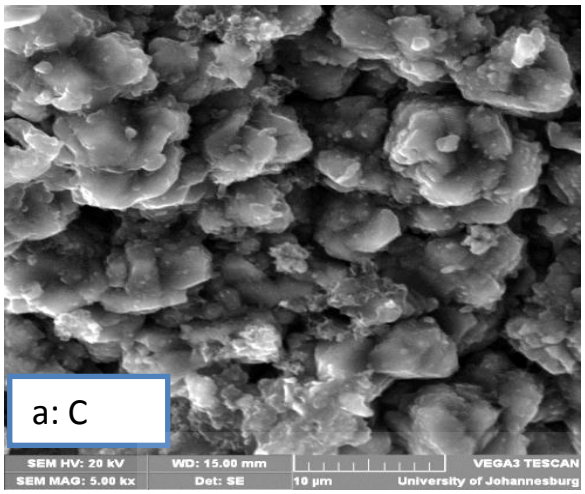

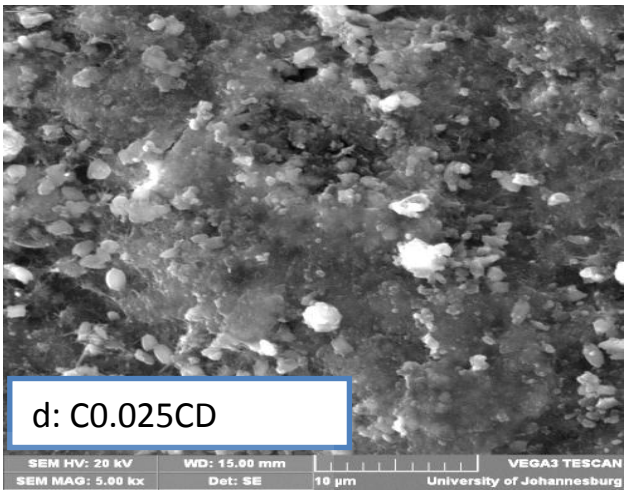

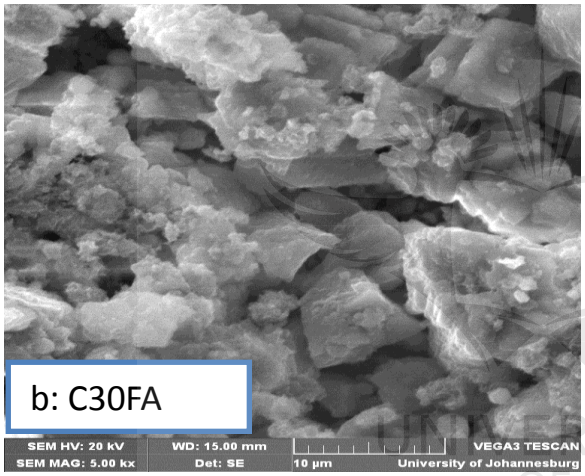

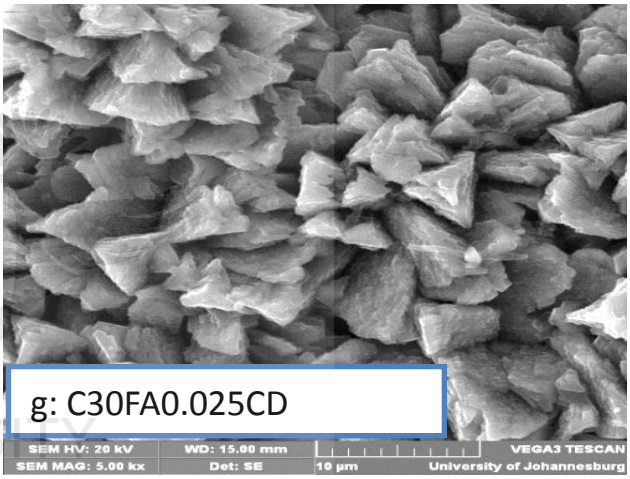

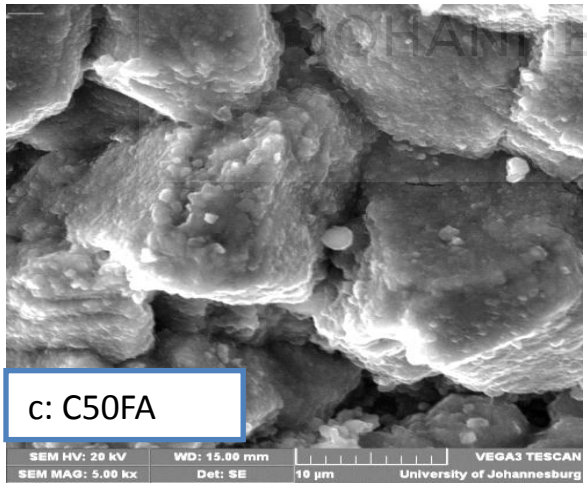

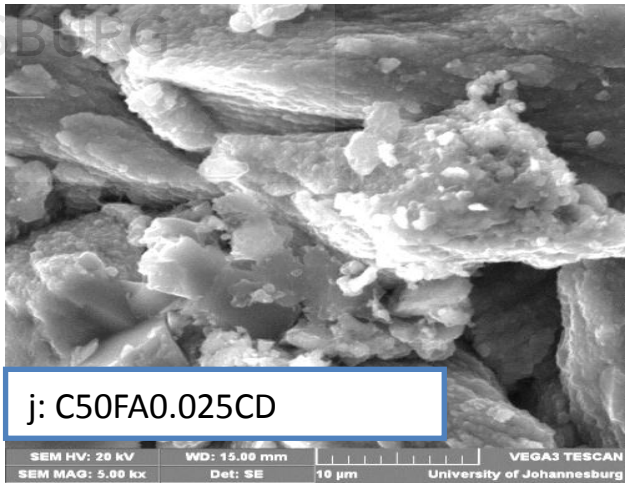

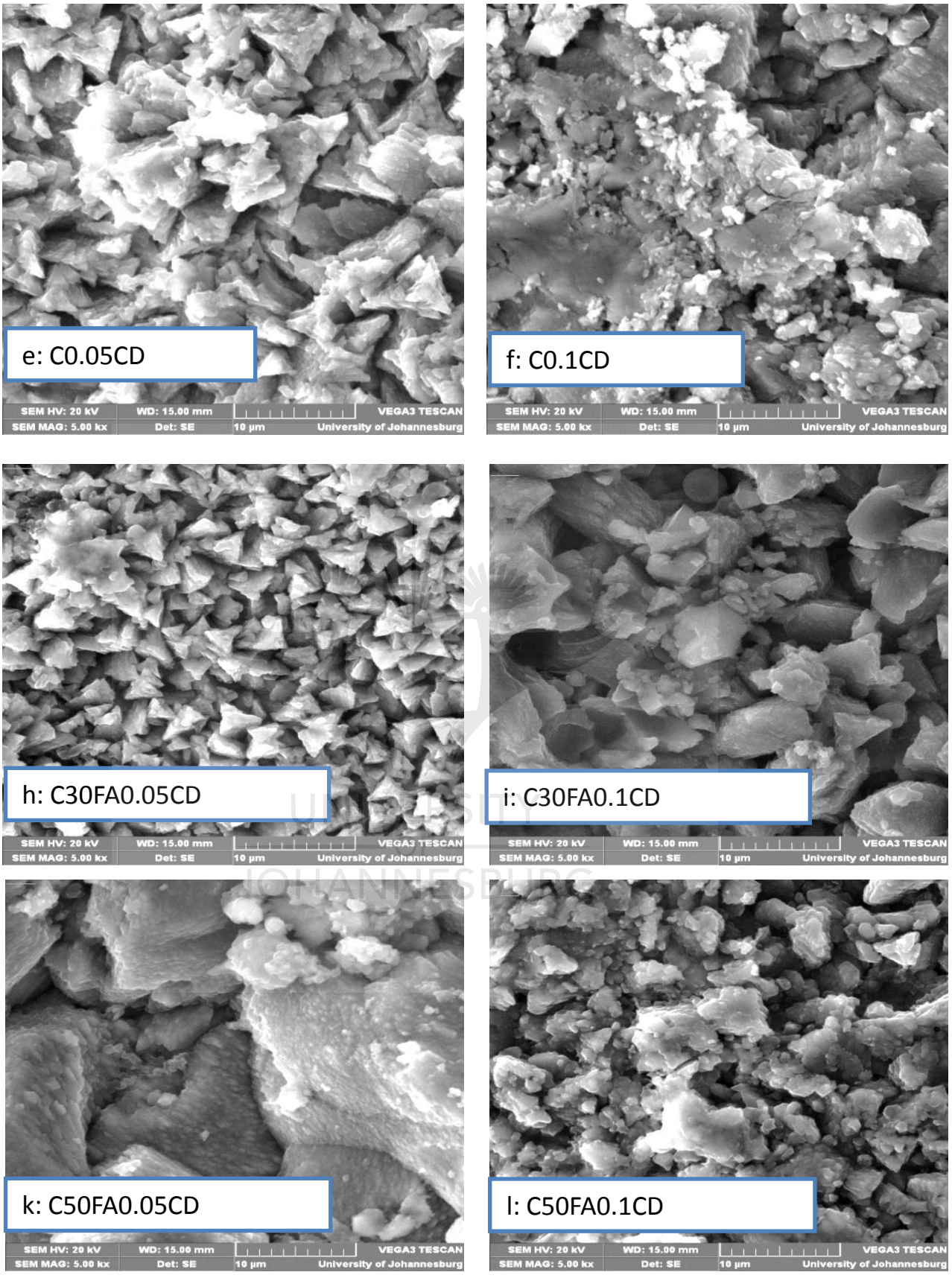

Figure 6.7: SEM of samples (a-l) hydrated for 90 days at 5000x magnification

6.4.3 FT-IR

6.4.3.1 FT-IR analysis after 24 hours hydration period

The FT-IR spectra of the samples hydrated for 24 hours are shown in Figure 6.8(a-l). The control sample (Figure 6.8a) showed Si-O asymmetric stretching band (υ_3) at 962 cm^{-1} due to the dissolution of C_3S clinker phase and at 876 cm^{-1} due to the dissolution of C_2S clinker phase [6, 17-19]. At 1119 cm^{-1}, the band due to the υ_3 vibration of the SO_4^{2-} group in sulphates (gypsum) [6, 20] was observed in the control sample (Figure 6.8a). As hydration progresses, this region is expected to be absorped by the υ_3 vibration of SiO_4^{2-}, therefore, leaving υ_3 vibration of the SO_4^{2-} to be obscured [17, 20-21]. The peak at 1416 cm^{-1} and overtone at 2945 cm^{-1} correspond to the CO_3 from calcium carbonate [6, 20] and they also coincide with one of the υ_3 vibration of SiO_4^{2-} [18]. As hydration progresses, the CO_3 band peak is expected to decrease [20] while υ_3 vibration of SiO_4^{2-} increases, therefore, any peak at the region 1420 cm^{-1} – 1490 cm^{-1}, at further hydration period will be assigned to υ_3 vibration of SiO_4^{2-}. The expected prominent peaks upon hydration and setting are the strong band due to CO_3/ SiO_4^{2-} and small sharp OH stretching band [17]. In pozzolanic reaction, the small sharp OH stretching band will be consumed.

The peak at 2174 cm^{-1} of control sample is attributed to asymmetric stretching of Si–O–Si in the silicate framework structures [22]. The peaks observed for control sample are similar to what had been reported previously by other researchers [6, 17-20]. The XRD results at this hydration period reported in this study revealed prominent peaks of C_3S and C_2S (Figure 6.1a) and confirmed the FT-IR result for the control sample. It has been reported that the shift of the Si–O asymmetric stretching vibration to higher wavenumbers due to the polymerisation of the SiO_4^{2-} units during C–S–H formation is an indication of improved hydration reaction [17, 21, 23, 24]. Delayed hydration reaction at the 24 hour hydration period was evident in all samples with FA, *β*-CD and FA-*β*-CD composite (Figure 6.8b - l) due to the shift of the Si–O asymmetric stretching vibration to lower wavenumbers. Broader and greater

intensities of Si-O asymmetric stretching bands (ν_3) were observed for C30FA and C50FA samples (Figure 6.8b, c) at lower wavenumbers compared to the control sample. This might be attributed to the dissolution of C_3S and contribution of the higher content of SiO_2 in FA. The higher the content of FA, the broader the Si-O asymmetric stretching band observed. Greater shift to lower wavenumbers of υ_3 vibration of the SO_4^{2-} group at 1116 cm^{-1} and 1100 cm^{-1} for C30FA and C50FA samples, respectively, also confirmed delayed hydration/pozzolanic reaction effect of FA. As expected, the intensity of the CO_3 peak at 1446 cm^{-1} and 1439 cm^{-1} for C30FA and C50FA samples respectively were reduced due to the reduced quantity of cement used for these samples.

β-CD aided the dissolution of C_3S clinker phase resulting in the greater and sharper intensity of Si-O asymmetric stretching band (ν_3) of samples containing *β*-CD (Figure 6.8d, e, f) compared to the control sample. The higher the content of *β*-CD, the greater the Si-O asymmetric stretching band (ν_3) intensity observed. The shift to lower wavelength of Si-O asymmetric stretching band of samples containing *β*-CD showed that the dissolved C_3S was not yet ready for hydration reaction at this hydration period, resulting in delayed hydration as revealed in XRD results (Figure 6.1d, e, f). Greater intensity of υ_3 vibration of the SO_4^{2-} group for samples containing *β*-CD (Figure 6.8d, e, f) also confirmed delayed hydration reaction for these samples at the 24 hour hydration period. The higher the *β*-CD content, the greater the intensity of υ_3 vibration of the SO_4^{2-} group and the greater the delay in hydration reaction envisaged.

The FA-*β*-CD composite samples (Figure 6.8g, h, i, j, k, l), revealed sharpness of Si-O asymmetric stretching band as compared to their respective original C30FA and C50FA samples (Figure 6.8b, c). This observation is in agreement with the XRD results. It was observed from the XRD results that FA-*β*-CD composite samples exhibited higher contents of C_3S and C_2S at the 24 hour hydration period than the C30FA and C50FA samples (Figure 6.1g, h, i, j, k, l). This indicated that a further

delay of the hydration reaction at this hydration period might be experienced for FA-*β*-CD composite samples when compared to their respective original C30FA and C50FA samples. Further evidence of delayed hydration at the 24 hour hydration period is the sharpness of the υ_3 vibration of the SO_4^{2-} group for FA-*β*-CD composite samples (Figure 6.8g, h, i, j, k, l) when compared to their respective original C30FA and C50FA samples (Figure 6.8b, c).

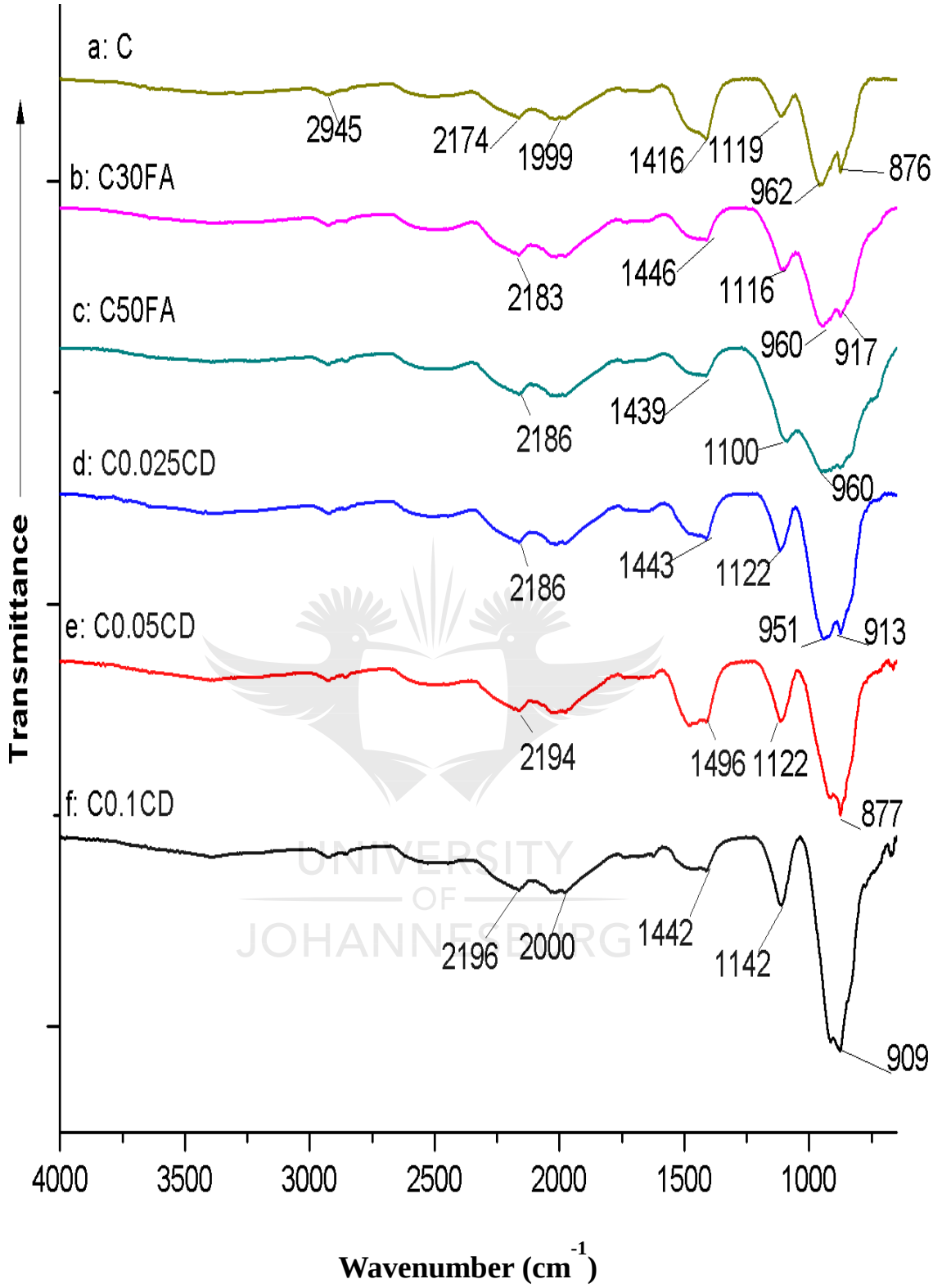

*Binary samples (24 hours hydration)

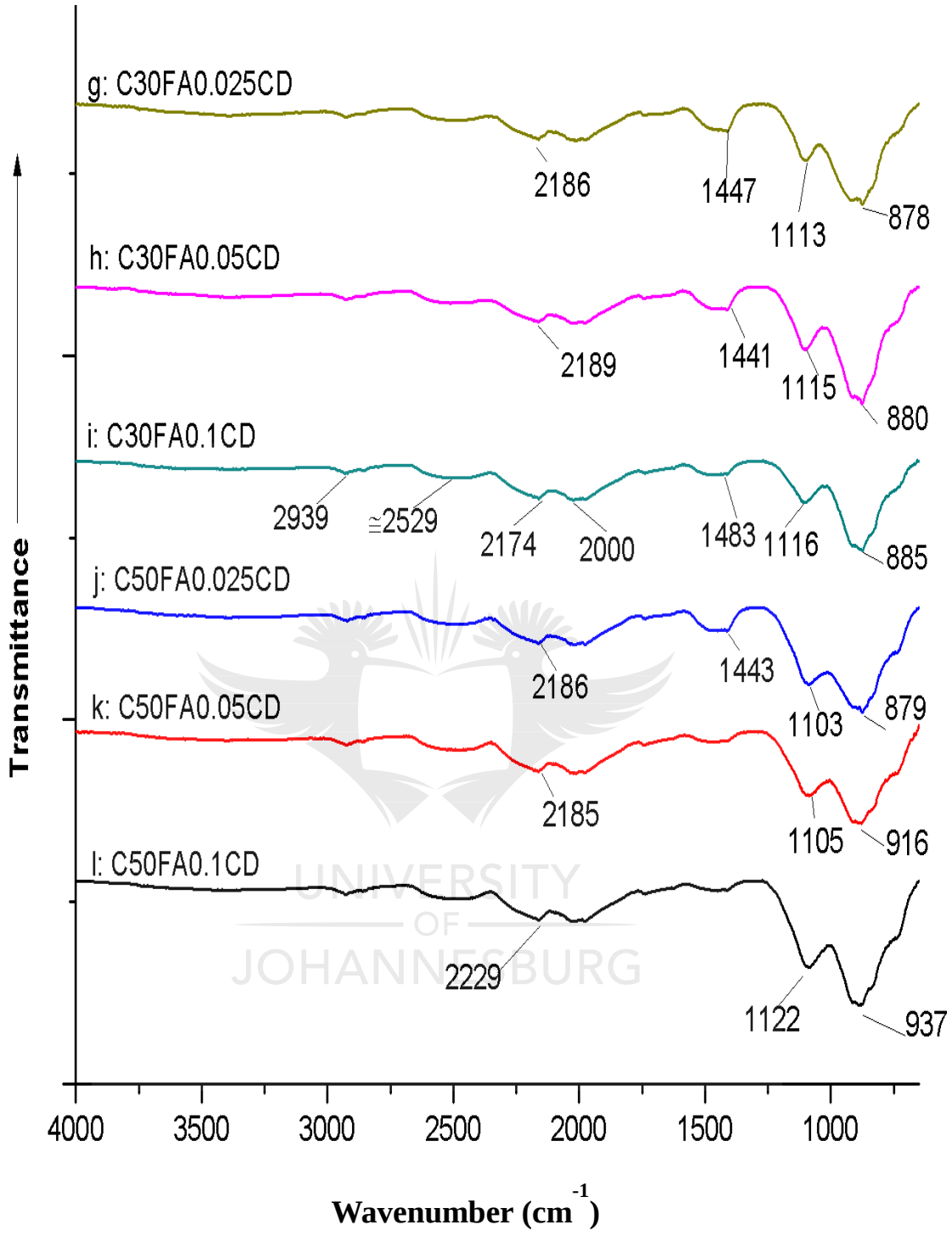

*****Ternary samples (24 hours hydration)

Figure 6.8: FT-IR spectra of cement paste of binary and ternary samples hydrated for 24 hours

6.4.3.2 FT-IR analysis after 7 days hydration period

A degree of hydration reaction and pozzolanic reaction was revealed in all the samples hydrated for 7 days (Figure 6.9a-l). Reduced intensity and shift to higher wavelength of υ_3 vibration of the SO_4^{2-} group at 1132 cm^{-1} is evidence that, at this hydration period, the hydration reaction had started for the control sample (Figure 6.9a). The peak at 3644 cm^{-1}, attributed to the OH-stretch from $Ca(OH)_2$ also confirmed the hydration reaction for the control sample at the 7 days hydration period. This result confirmed the XRD result, where at the 7 days hydration period, reduced intensity of C_3S and C_2S peaks (Figure 6.2a), showing dissolution of these phases during hydration reaction was observed for the control sample compared to the 24 hours hydrated sample. It would be inconclusive to assign the peak at approximately 1424 cm^{-1} to either the CO_3 band or υ_3 vibration of SiO_4^{2-} at this hydration period, because both will have an influence at this age and it will be difficult to distinguish the effect of each of them. As hydration continues (28 days), the peak at this region will be assigned to the υ_3 vibration of SiO_4^{2-}.

Greater intensity of Si-O asymmetric stretching bands (υ_3) was observed for C30FA and C50FA samples (Figure 6.9b, c) than the control sample. The SiO_2 from FA, which had not reacted to form hydration product (C-S-H) at this hydration period might have contributed to the increased intensity of Si-O asymmetric stretching band revealing a delayed in pozzolanic reaction for the C30FA and C50FA samples (Figure 6.9b, c). The higher the FA content, the greater the intensity of Si-O asymmetric stretching band observed. This is in agreement with the XRD result where a higher content of quartz was observed in samples containing 50% FA, than samples with 30% FA at this hydration period (Figure 6.2c, j, k, l). The peak of υ_3 vibration of the SO_4^{2-} group has been obscured in C30FA and C50FA samples (Figure 6.9b, c). An upcoming peak at 3645 cm^{-1} of OH-stretch from $Ca(OH)_2$, which has not being combined in pozzolanic reaction, was observed in C30FA sample (Figure 6.9b).

Sharper intensity of Si-O asymmetric stretching band (ν_3) and the shift of the Si–O asymmetric stretching vibration to higher wavenumbers as a result of the polymerisation of the SiO_4^{2-} units during C–S–H formation are revealed in samples containing *β*-CD (Figure 6.9d, e, f). This is an indication of improved hydration reaction compared to *β*-CD samples hydrated for 24 hours and control sample hydrated for 7 days. Reduced intensity of υ_3 vibration of the SO_4^{2-} group and upcoming O-H stretching band from $Ca(OH)_2$ (Figure 6.9d, e, f) also confirmed hydration reaction. These results correspond to the XRD results, which showed that at the 7 days hydration period, *β*-CD increased the dissolution of C_3S and C_2S and aided the formation of CH, a product of hydration reaction (Figure 6.2). The early formation of C-S-H and Portlandite (CH) at the 7 days hydration period for samples containing *β*-CD was also revealed in the SEM results (Figure 6.5d, e).

The transferred effect of *β*-CD in boosting hydration reaction at this hydration period, is revealed in the FA-*β*-CD composite samples (Figure 6.9g, h, i, j, k, l) showing sharpness of Si-O asymmetric stretching vibration band (ν_3) compared to the C30FA and C50FA samples. When compared to FA-*β*-CD composite samples hydrated for 24 hours (Figure 6.8), the shift of the Si–O asymmetric stretching vibration to higher wavenumbers, sharper intensity of Si-O asymmetric stretching vibration band (ν_3) and reduced intensity of υ_3 vibration of the SO_4^{2-} group were observed, revealing an improved hydration reaction.

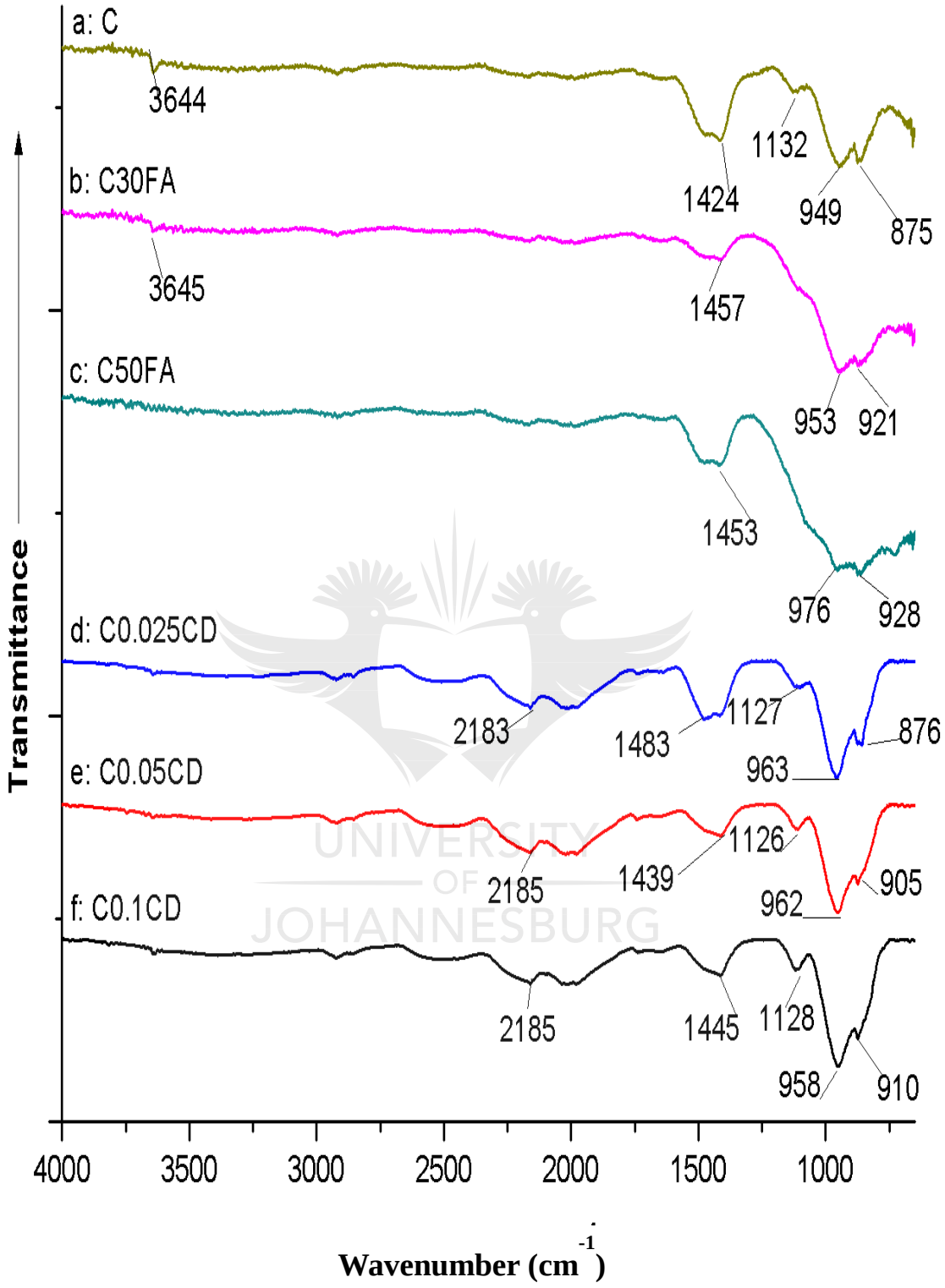

*Binary samples (7 days hydration)

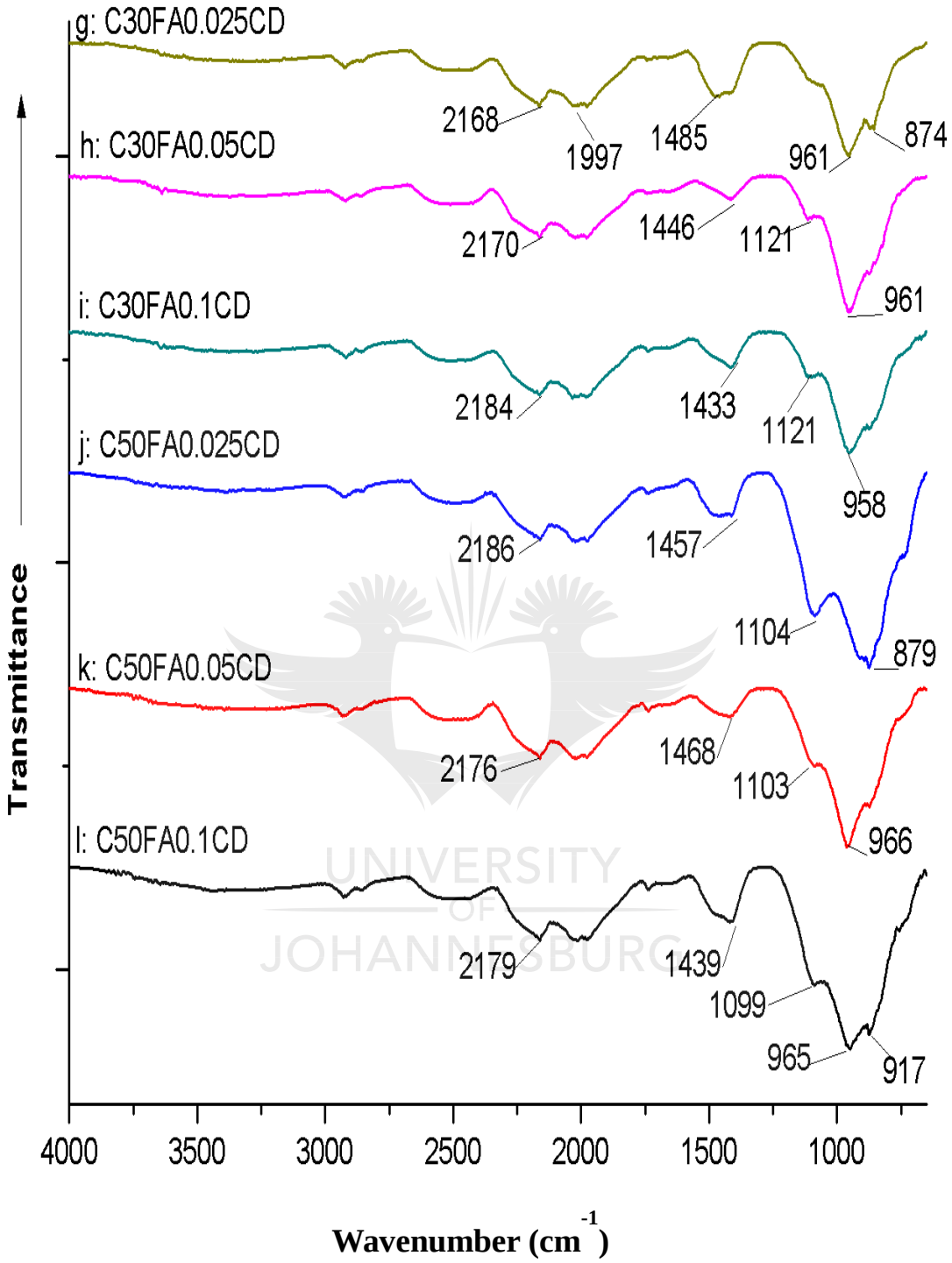

*Ternary samples (7 days hydration)

Figure 6.9: FT-IR spectra of cement paste of binary and ternary samples hydrated for 7 days

6.4.3.3 FT-IR analysis after 28 days hydration period

Due to improved hydration and pozzolanic reactions at this hydration age, an increased intensity and sharpness of Si-O asymmetric stretching band was observed for all the samples due to the polymerisation of the SiO_4^{2-} units during C–S–H formation (Figure 6.10a - l). The sharper intensity of υ_3 vibration of SiO_4^{2-} at the ranges 1435 to 1461 cm^{-1}, showing improved hydration reaction was also observed for all the samples (Figure 6.10a - l). The reduced intensity of υ_3 vibration of the SO_4^{2-} group at 1126 cm^{-1} of control sample (Figure 6.10a) and shift of Si-O asymmetric stretching band to the higher wavenumber at this hydration period compared to the 7 days hydrated control sample, further showed improved hydration reaction. The reduction in the OH-stretch from $Ca(OH)_2$ at this hydration period compared to 7 days might be as a result of $Ca(OH)_2$ being combined with CO_2 in the atmosphere to form more $CaCO_3$ [17, 21]. This is also in agreement with Mollah et al [21] and Bjornstrom et al [23], who reported that the O-H stretching band decreases with the progress of hydration and with the formation of the C–S–H binding phase.

More defined and sharper Si-O asymmetric stretching bands were observed for C30FA and C50FA samples (Figure 6.10b, c) at this hydration period than the 7 days hydration period. This is an evidence of improved pozzolanic reaction. The higher the FA content, the greater the intensity observed. There is no sign of an upcoming peak of OH-stretch from $Ca(OH)_2$ for the C30FA and C50FA samples (Figure 6.10b, c) due to the consumption of $Ca(OH)_2$ during pozzolanic reaction, in addition to other reasons given earlier. This is also in agreement with the XRD results, which revealed a reduction of the CH peak in all the FA samples at the 28 days hydration period (Figure 6.3b, c, g, h, i, j, k, l).

The samples containing β-CD (Figure 6.10d, e, f) showed a similar trend to the control sample at this hydration period, with a greater intensity of Si-O asymmetric stretching bands. A sharpness of Si-O asymmetric stretching bands was observed for the β-CD samples (Figure 6.10d, e, f) at this hydration period compared to the 7 days

hydration period, confirming an improved hydration reaction. No evidence of υ_3 vibration of the SO_4^{2-} group was observed in the samples containing FA-*β*-CD composites (Figure 6.10g, h, i, j, k, l) compared to 7 days hydration samples, showing an improved pozzolanic reaction. No major distinction was observed between the FA samples (Figure 6.10b, c) and the FA-*β*-CD composites samples (Figure 6.10g, h, i, j, k, l).

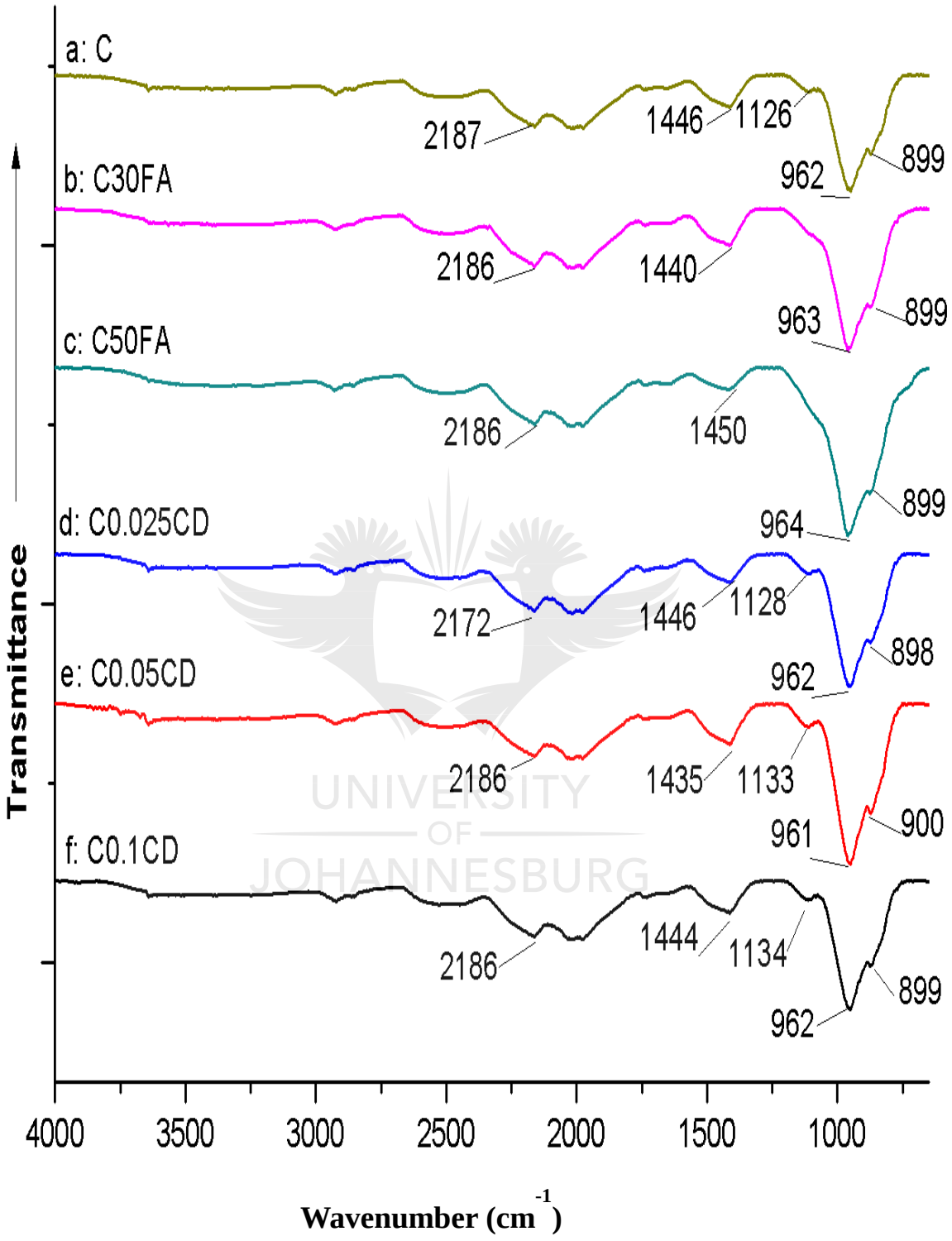

*Binary samples (28 days hydration)

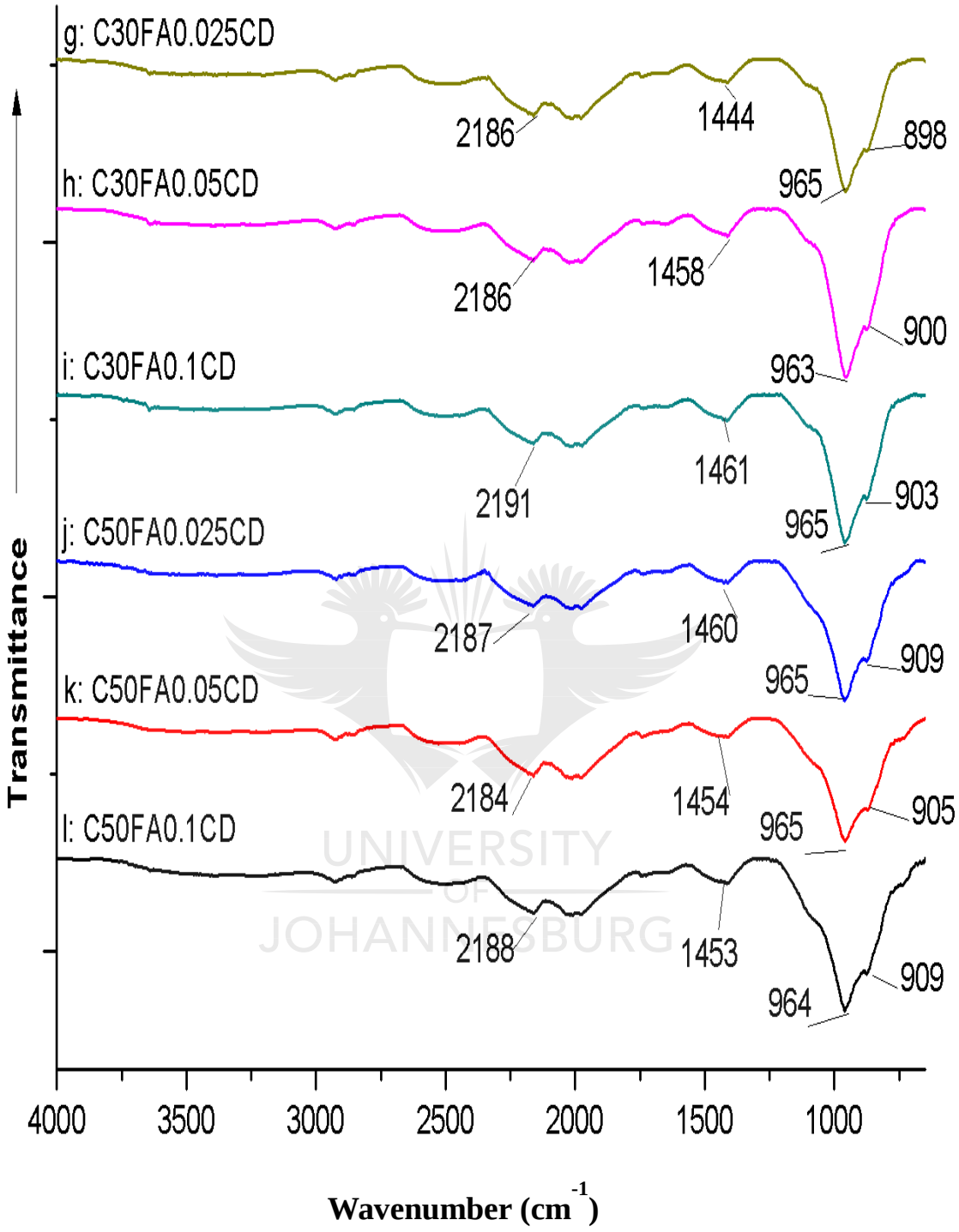

*Ternary samples (28 days hydration)

Figure 6.10: FT-IR spectra of cement paste of binary and ternary samples hydrated for 28 days

6.4.3.4 FT-IR analysis after 90 days hydration period

A well advanced hydrated control sample after 90 days hydration period was revealed in Figure 6.11a. The sharpness of the Si-O asymmetric stretching band and its shift to a higher wavenumber together with a reduced intensity of υ_3 vibration of the SO_4^{2-} group are evidence of an improved hydration reaction of control sample compared to the 28 days hydrated sample. Evidence of an improved pozzolanic reaction was revealed in the C30FA and C50FA samples (Figure 6.11b, c) through the sharpness of the Si-O asymmetric stretching band and its shift to a higher wavenumber compared to samples hydrated for 28 days. The spectra of the control sample are closely related to the spectra of FA samples, showing that at this hydration period, pozzolanic reaction has caught up with hydration reaction.

Improved hydration reaction was observed in the *β*-CD samples (Figure 6.11d, e, f) compared to the 28 days hydrated *β*-CD samples, revealing greater sharpness of the Si-O asymmetric stretching band, shift of the Si-O asymmetric stretching band to higher wavenumber and reduced intensity of υ_3 vibration of the SO_4^{2-}. Greater sharpness of the Si-O asymmetric stretching band was observed for the samples containing 0.025% and 0.1% *β*-CD replacements (Figure 6.11d, f) compared to control sample. More $Ca(OH)_2$ was formed in the control (Figure 6.11a) and *β*-CD samples (Figure 6.11d, e, f) at approximately 3650 cm^{-1}, showing an upcoming OH-stretch peak, as also revealed in the XRD results (Figure 6.4a, d, e, f). The OH-stretch peak from $Ca(OH)_2$ was consumed in all FA (Figure 6.11b, c) and FA-*β*-CD composites (Figure 6.11g, h, i, j, k, l) samples due to pozzolanic reaction. A major distinction cannot be traced in the spectra of the FA and the FA-*β*-CD composites samples. The XRD results revealed improved hydration and pozzolanic reactions at 90 days hydration period for samples containing 0.05% and 0.1% *β*-CD replacements (Figure 6.4 e, f, h, i, k, l).

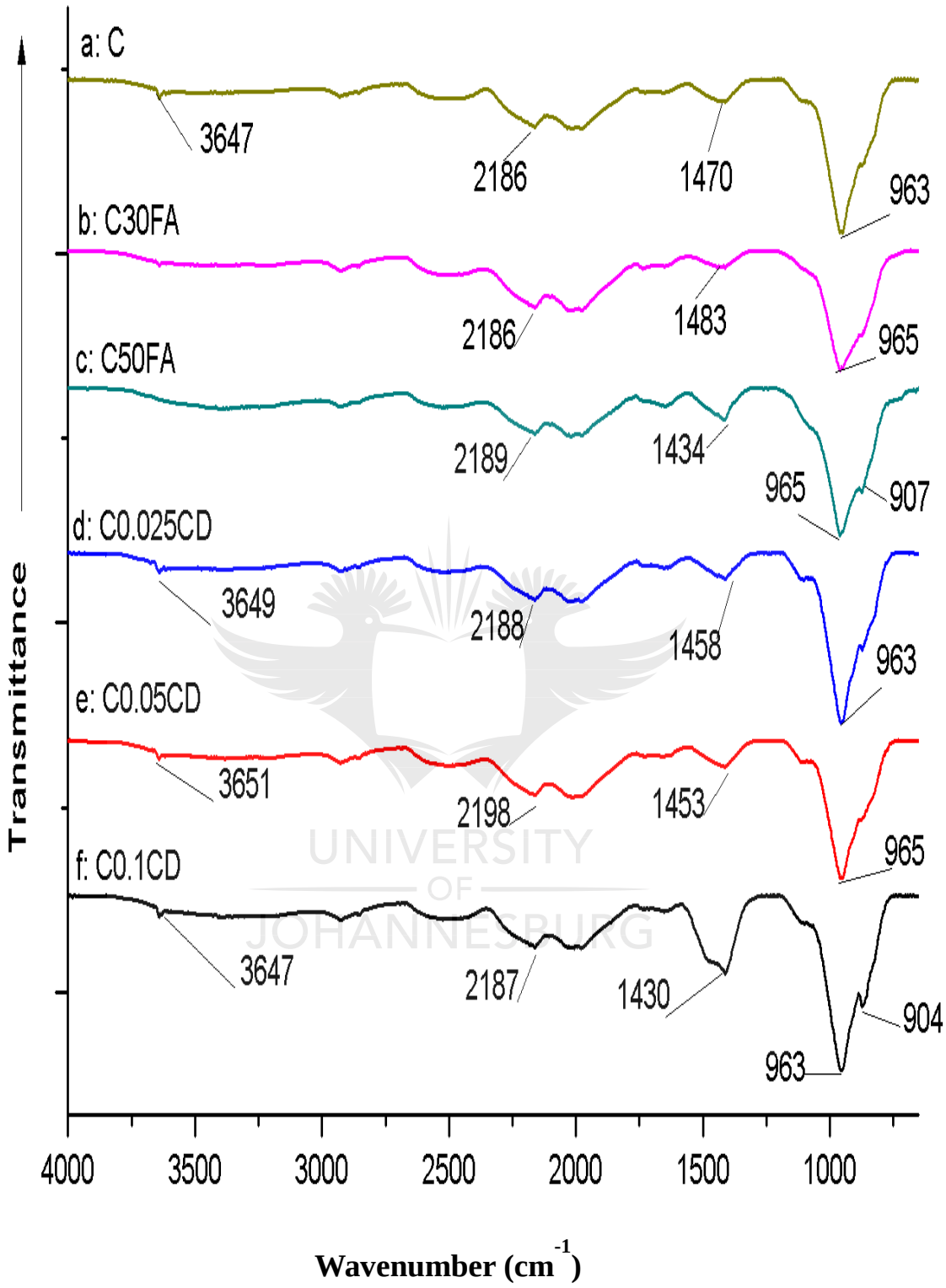

*Binary samples (90 days hydration)

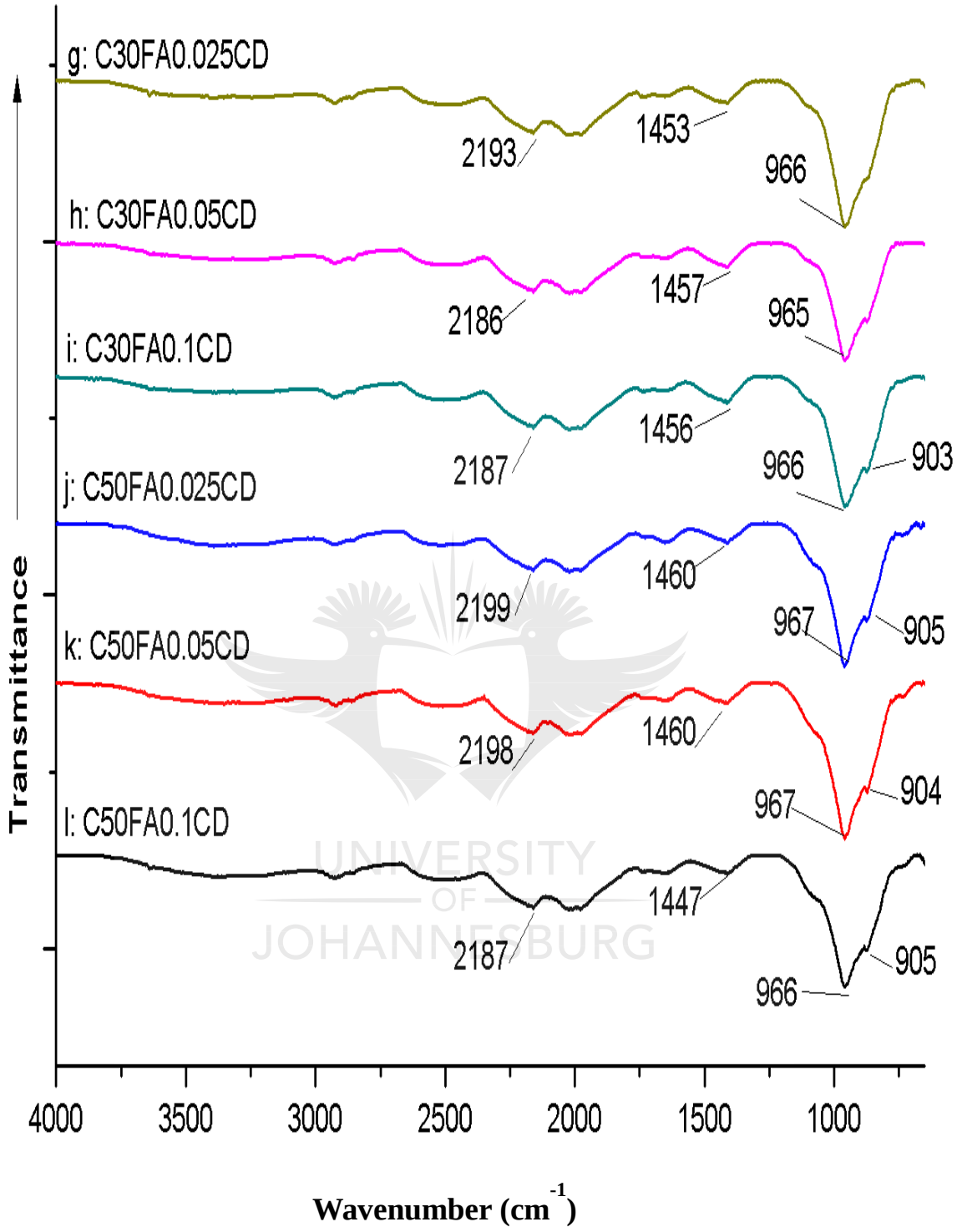

*Ternary samples (90 days hydration)

Figure 6.11: FT-IR spectra of cement paste of binary and ternary samples hydrated for 90 days

6.5 CONCLUSIONS

Studies on the structural and microstructural changes of FA, *β*-CD and FA-*β*-CD composite cement paste samples as hydration progressed were done using XRD, SEM and FT-IR. It was evident from all the analyses that at the 7 days hydration period, the control sample had shown hydration products while the effect of pozzolanic reaction was evident from the 28 days hydration period onwards. The *β*-CD samples aided both early (from 7 days) and late hydration processes compared to control samples with evidence of increased dissolution of the C_3S and C_2S at 7 days hydration period and higher formation of CH at the 90 days hydration period. The effect of *β*-CD on pozzolanic reaction was revealed from the 28 days hydration period in the XRD results.

The morphology of the *β*-CD samples studied by SEM revealed the crystalline structure of Portlandite (CH) at the 7 days hydration period for the C0.025CD sample compared to the control sample. The higher the *β*-CD content, the more the dissolution of anhydrous phase of the cement paste was observed in the SEM morphology at 7 days hydration period; as was also confirmed by the XRD results. At the 90 days hydration period, the *β*-CD and FA-*β*-CD composite samples showed an improved denser surface and reduced continuous capillary pores compared to the control, C30FA and C50FA samples. The FT-IR results showed that *β*-CD aided the dissolution of C_3S clinker phase resulting in the greater and sharper intensity of the Si-O asymmetric stretching band (ν_3) of samples containing *β*-CD compared to control sample at the 24 hour and 7 days hydration periods. At 90 days, the FT-IR spectra of control, FA, *β*-CD and FA-*β*-CD composites samples were closely related, revealing that at this hydration period, pozzolanic reaction has caught up with hydration reaction.

6.6 REFERENCES

[1] Diamond S.: The microstructure of cement paste and concrete a visual primer. Cement and Concrete Composites **26**, 919–933 (2004).

[2] Damme H.V., Gmira A. : Chapter 13.3 Cement hydrates, Handbook of Clay Science Edited by F. Bergaya, B.K.G. Theng and G. Lagaly Developments in Clay Science, Vol. 1, Elsevier Limited, 1113- 1127 (2006).

[3] Girão A.V., Richardson I.G., Porteneuve C.B., Brydson R.M.D.: Composition, morphology and nanostructure of C–S–H in white Portland cement pastes hydrated at 55 °C. Cement and Concrete Research **37,** 1571–1582 (2007).

[4] Moir G.: Cement, Advanced Concrete Technology Set, 3–45 (2003).

[5] Aimin X., Sarkar S.L: Microstructural study of gypsum activated fly ash hydration in cement paste. Cement and Concrete Research, 1137-1147 (1991).

[6] Hughes T.L., Methven C.M., Jones T.G.J., Pelham S.E., Fletcher P., Hall C.: Determining Cement Composition by Fourier Transform Infrared Spectoscopy. Advanced Cement Based Material **2**, 91-104 (1995).

[7] SANS 5861-3: 2006: South African national standard. Concrete tests, Part 3: Making and curing of test specimens, ISBN 978-0-626-27130-5. Edition 2.1.

[8] Jain N.: Effect of nonpozzolanic and pozzolanic mineral admixtures on the hydration character of ordinary Portland cement. Construction and Building Materials **27**, 39–44 (2012).

[9] Ali A.H., Kandeel A. M., Ouda A. S.: Hydration Characteristics of Limestone Filled Cement Pastes. Chemistry and Materials Research **5**, 68-73. (2013).

[10] Burgos-Montes O., Alonso M.M., Puertas F.: Viscosity and water demand of limestone- and fly ash-blended cement pastes in the presence of superplasticisers. Construction and Building Materials **48,** 417–423 (2013).

[11] Deschner F., Lothenbach B., Winnefeld F., Neubauer J.: Effect of temperature on the hydration of Portland cement blended with siliceous fly ash, Cement and Concrete Research **52**, 169–181 (2013).

[12] Khater H.M: Effect of silica fume on the characterization of the geopolymer materials. International Journal of Advanced Structural Engineering **5(12)**, 2-10. (2013).

[13] Pandya S.J., Mansuri J.S., Patel P.: Compatible Polymer used as complexes in various drug delivery systems : β-Cyclodextrin. Pharmaceutical Reviews **6**(2) (2008).

[14] Roncero J., Valls S., Gettu R.: Study of the influence of superplasticizers on the hydration of cement paste using nuclear magnetic resonance and X-ray diffraction techniques. Cement and Concrete Research **32,** 103–108 (2002).

[15] Snellings R., Salze A., Scrivener K.L.: Use of X-ray diffraction to quantify amorphous supplementary cementitious materials in anhydrous and hydrated blended cements. Cement and Concrete Research **64**, 89–98 (2014).

[16] Tang S.W., Li Z.J., Shao H.Y., Chen E.: Characterization of early-age hydration process of cement pastes based on impedance measurement. Construction and Building Materials **68,** 491–500 (2014).

[17] Mollah Y.A., Hess T.R., Tsai Y., Cocke D.L.: An FT-IR and XPS Investigations of the effects of carbonation on the solidification/stabilization of cement based

systems-Portland type V with zinc. Cement and concrete research **23,** 773-784 (1993).

[18] Omotoso O.E., Ivey D.G., Mikula R.: Characterization of chromium doped tricalcium silicate using SEM/EDS, XRD and FT-IR. Journal of Hazardous Materials **42**, 87-102 (1995).

[19] Mollah M.Y.A, Lu F., Cocke D.L.: An X-ray diffraction (XRD) and Fourier transform infrared spectroscopic (FT-IR) characterization of the speciation of arsenic (V) in Portland cement type-V. The Science of the Total Environment **224,** 57-68 (1998).

[20] Ylmén R., Jäglid U., Steenari B., Panas I.: Early hydration and setting of Portland cement monitored by IR, SEM and Vicat techniques. Cement and Concrete Research **39** 433–439 (2009).

[21] Mollah M.Y.A., Yu W., Schennach R., Cocke D.L.: A Fourier transform infrared spectroscopic investigation of the early hydration of Portland cement and the influence of sodium lignosulfonate. Cement and Concrete Research **30,** 267–273 (2000).

[22] Zhang Z., Wang H., Provis J.L.: Quantitative study of the reactivity of fly ash in geopolymerization by FT-IR. Journal of Sustainable Cement-Based Materials **1(4)**, 154–166 (2012).

[23] Bjornstrom J., Martinelli A., Matic A., Borjesson L., Panas I.: Accelerating effects of colloidal nano-silica for beneficial calcium–silicate–hydrate formation in cement. Chemical Physics Letters **392,** 242–248 (2004).

[24] Knapen E., Gemert D. V.: Cement hydration and microstructure formation in the presence of water-soluble polymers. Cement and Concrete Research **39**, 6–13 (2009).

CHAPTER SEVEN

THE EFFECT OF FLY ASH, *β*-CYCLODEXTRIN AND FLY ASH-*β*-CYCLODEXTRIN COMPOSITES ON CEMENT PASTE VISCOSITY AND SETTING TIMES

7.1 INTRODUCTION

The rheological properties of cement paste influence concrete workability, placement and eventually affect the mechanical and durability properties of concrete. According to Bingham's model [1-4], fresh concrete, mortar and cement paste are regarded as viscoplastic materials; whereby they have to overcome a certain yield stress (τ_0) in order to initialize flow. In addition, there is a linear relation between the shear stress (τ) and the shear rate ($\dot{\gamma}$), named plastic viscosity (μ) after the flow initialization [4]. The model is governed by Equation (7.1) and illustrated in Figure 7.1. The initial resistance to flow is quantitatively measured by yield stress (τ_0) while the flow after initiation is governed by plastic viscosity (μ) [5].

$$\tau = \tau_0 + \mu\,\dot{\gamma};\ \tau \geq \tau_0: \qquad (7.1)$$

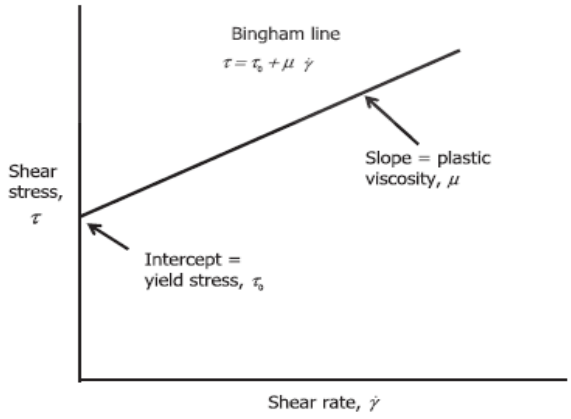

Figure 7.1: The Bingham model [3]

The addition of pozzolans in concrete will, in most cases lower the yield stress that needs to be overcome and cause early flow initialization. Laskar and Talukdar [5] accounted the reduction of the frictional forces responsible for the lower yield stress of FA to the spherical shape, which causes a ball bearing effect. The lowered yield stress would result in a lower viscosity and in principle retard setting. FA has been reported previously to have a retarding effect on the setting time of concrete [6-8], this was attributed to the adsorption of FA particles to the surface of the cement. *β*-cyclodextrin (*β*-CD) based superplasticizer was also reported to have retarded the setting time of concrete [9-10]. Li et al [10] attributed the retarding effect of the *β*-CD based superplasticizer to the active hydroxyl adsorption groups that were adsorbed on the surface of cement during the hydration process by hydrogen bonds, which prevent and retard further hydration of cement. Hua et al [11] studied the influence of cellulose ethers (CE) molecular parameters on hydration kinetics of Portland cement at early ages and reported that the lower the viscosity or molecular weight of the CE, the stronger the retardation ability is. Retardation is not totally disadvantageous in concrete production, especially when an increase in concrete strength and durability properties is envisaged. The retarding effect of some additives in concrete favors the increase of operating time and the decrease of the consistency or slump loss of freshly mixed materials [11].

Cement paste will be more appropriate to use in investigating the viscosity of FA, *β*-CD and FA-*β*-CD composites in a cementitious environment than concrete, following the observation of Wallevik and Wallevik [4]. They [4] reported that the plastic viscosity will remain relatively unaffected when a superplasticizer (SP) is added to concrete while in the case of cement paste, a SP could reduce the plastic viscosity in a similar way as when water is added as illustrated in Figure 7.2. Banfill [3] observed a similar behaviour for concrete, he stated that the addition of a superplasticiser to concrete reduces the yield stress (increases slump or flow) but does not change the plastic viscosity. *β*-CD might have a similar effect because the few documented works on *β*-CD in concrete technology dealt with *β*-CD as a superplasticiser [9-10].

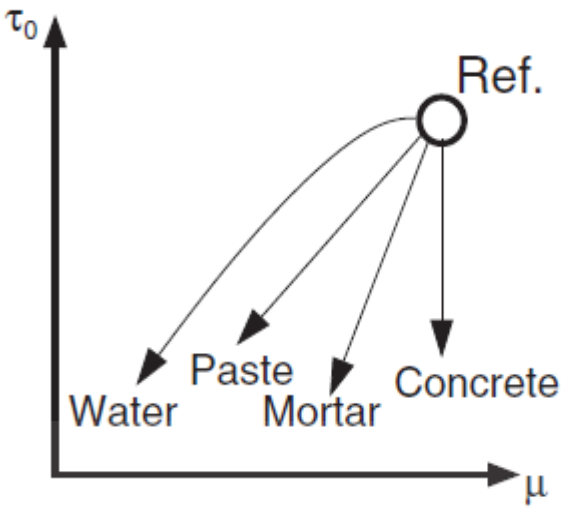

Figure 7.2: Rheology behaviour of cement paste, mortar and concrete with increased addition of SP [4]

A correlation between yield stress and setting time was reported by Kovler and Roussel [12]; the initial setting time corresponds to a yield stress of the order of a couple hundred kPa compared to a few Pa or tens of Pa of a freshly mixed cement paste. This chapter presents the effect of FA, *β*-CD and FA- *β*-CD composites on cement paste viscosity and setting time.

7.2 MATERIALS AND MIXES

Cement (CEM 1 52.5N), FA and *β*-CD used were the same as explained in Section 5.2. Twelve cement paste samples were prepared for the viscosity tests for each of the three different water/binder ratios (W/B) (0.4, 0.5 and 0.6) used. Thirty six samples were tested in all. FA-*β*-CD composites mixtures were made based on physical mixtures as explained in Section 6.2 and described in Table 6.2. The setting time test was also performed using the mixtures described in Table 6.2. The quantity of water used for the setting time test depends on the amount of water that produced a consistent mix for each sample as described in SANS50196-3 [13].

7.3 EXPERIMENTAL PROCEDURE

7.3.1 Viscosity

The viscosity of the cement paste samples was determined by a VT-04F portable viscotester manufactured by the Rion Co. Ltd as shown in Figure 7.3. The viscosity of the pastes was determined by the instrument through the rotation of a rotor in the sample which causes viscous resistance. Samples were prepared to fill the viscometer cup up till the center of the fluid mark on the rotor. Samples with a mass of 150 g were used for mixtures with 0.5 and 0.6-W/B with No. 3 rotor and No. 3 viscometer cup (as specified in the manual) due to the lower viscosity expected for these mixtures in comparison with the mixtures with 0.4-W/B. Samples with a mass of 300 g were used for the 0.4-W/B mixes, with a No. 1 rotor and 300 ml beaker. The calibration unit was attached to the clamp horizontally and the rotor was fixed to the calibration unit. Samples were mixed in the cup/beaker for 10 s and the rotor was placed in the center of the sample in the cup/beaker. The power switch was then set to ON. As the rotor started to turn, the viscosity indicator needle temporarily deflected to the right and then balanced out at the position that corresponded to the viscosity of the sample. The viscosity at this point was recorded as the initial viscosity reading. Thereafter, the viscosity was recorded at 1, 2, 3, 4, 5, 10, 15 and 20 mins or until a constant viscosity value was recorded. The results are expressed in deci Pascal second (d Pa s), which is equivalent to a kilogram per metre second (kg/ m s).

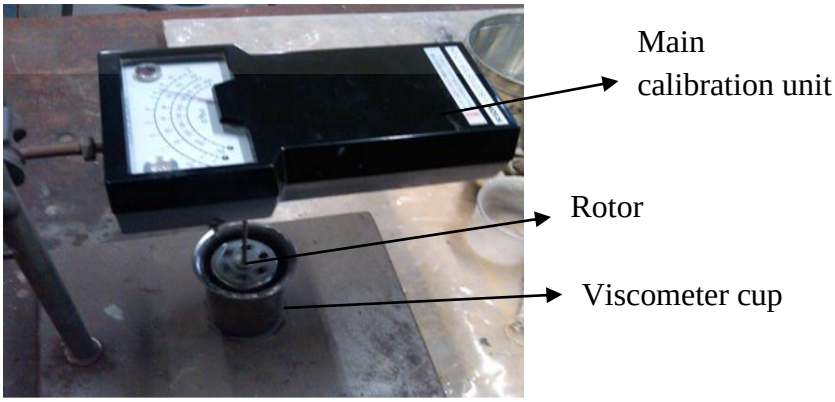

Figure 7.3: Viscometer

7.3.2 Setting time

The setting time test was done based on the procedure described in SANS 50196-3 [13] standard at the AFRISAM materials laboratory. An automatic, ToniSET Vicat apparatus, conforming to the requirements of the reference method, consisting of twelve Vicat moulds and connected to the computer for capturing setting time results was used. A mass of 500 g of cement/combined materials was measured. A mass of 170 g of water was measured; part of the water was added to the samples over 10 s, in a HOBART mixer, conforming to SANS 50196-1 [14]. The mixer was started at a low speed and zero time was recorded. The total mixing time was 3 mins according to SANS 50196-3 [13]. The paste was transferred to the already oiled mould placed on a lightly oiled base-plate. The mould was filled to have a smooth upper surface without undue compaction or vibration. The water for the standard consistence was determined by lowering the plunger into the filled mould within 4 min ±10 s after zero time. The scale was read at least 5 s after penetration had ceased. The scale reading indicates the distance between the bottom face of the plunger and the base-plate. The test was repeated by adding more water or reducing water, as the case may be, until the distance between plunger and base-plate was (6 ± 2) mm. The water content at this point was taken as the water for the standard consistence of the sample. The mould containing the consistence sample was then placed in a water bath such that the surface of the paste was submerged to a depth of at least 5 mm. The automatic Vicat apparatus used had been calibrated and programmed such that the needle was gently lowered into the paste at the required time. The initial and final setting times were recorded by the automatic Vicat apparatus. The setup is shown in Figure 7.4.

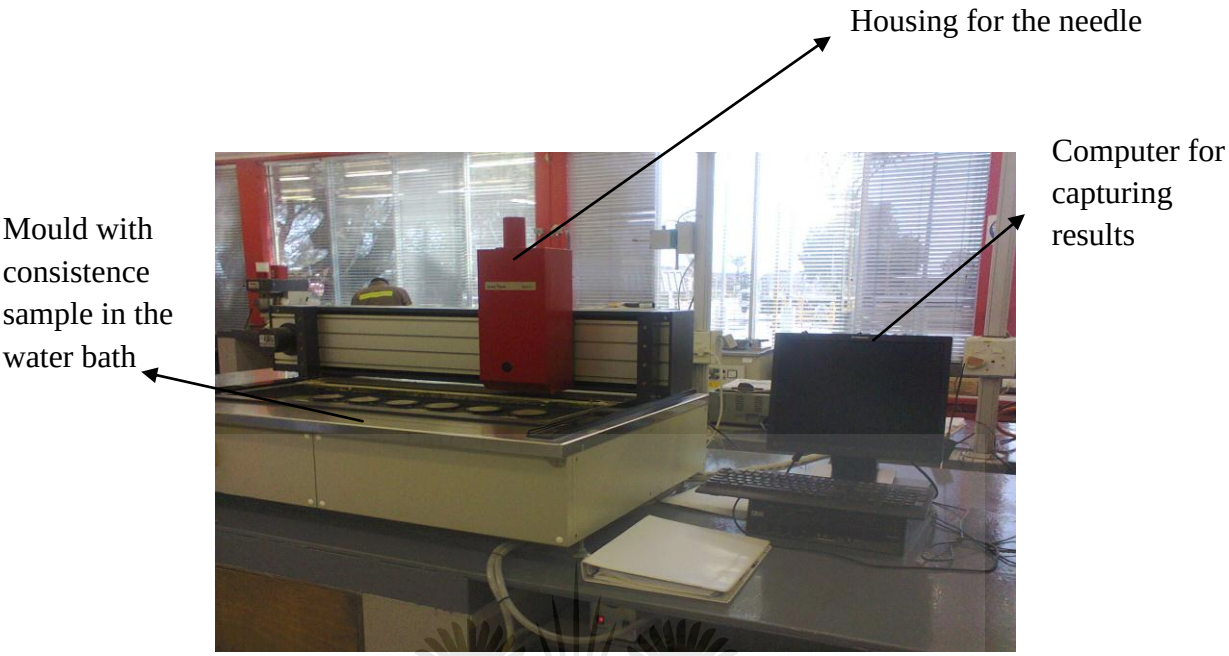

Figure 7.4: Setting time apparatus setup

7.4 RESULTS AND DISCUSSIONS

7.4.1 The effect of FA, *β*-CD and FA- *β*-CD composites on cement paste viscosity

The results are divided into binary samples (comprising two dry materials) and ternary samples (comprising three dry materials), for better graph visibility and interpretation. Figure 7.5 shows the viscosity results of the binary cement paste samples with a 0.6-W/B. It is evident from the graph that FA reduced the viscosity of the cement paste. With higher content of FA (50%), a higher reduction in viscosity was observed, which is in agreement with Laskar and Talukdar [5]. A reduction in viscosity was also observed for *β*-CD samples. The higher the *β*-CD content, the lower the viscosity observed. The *β*-CD samples generally showed a higher viscosity when compared to FA samples, but the sample with 0.1% *β*-CD exhibited a lower viscosity than the sample with 30% FA from 10 mins upward. The results of ternary samples with 0.6-W/B, shown in Figure 7.6, revealed a further reduction of viscosity with FA-*β*-CD composite samples. The lowest viscosity was observed for sample

with the combination of 50% FA and 0.1% β-CD due to the higher contents of FA and β-CD in this sample compared to the other samples.

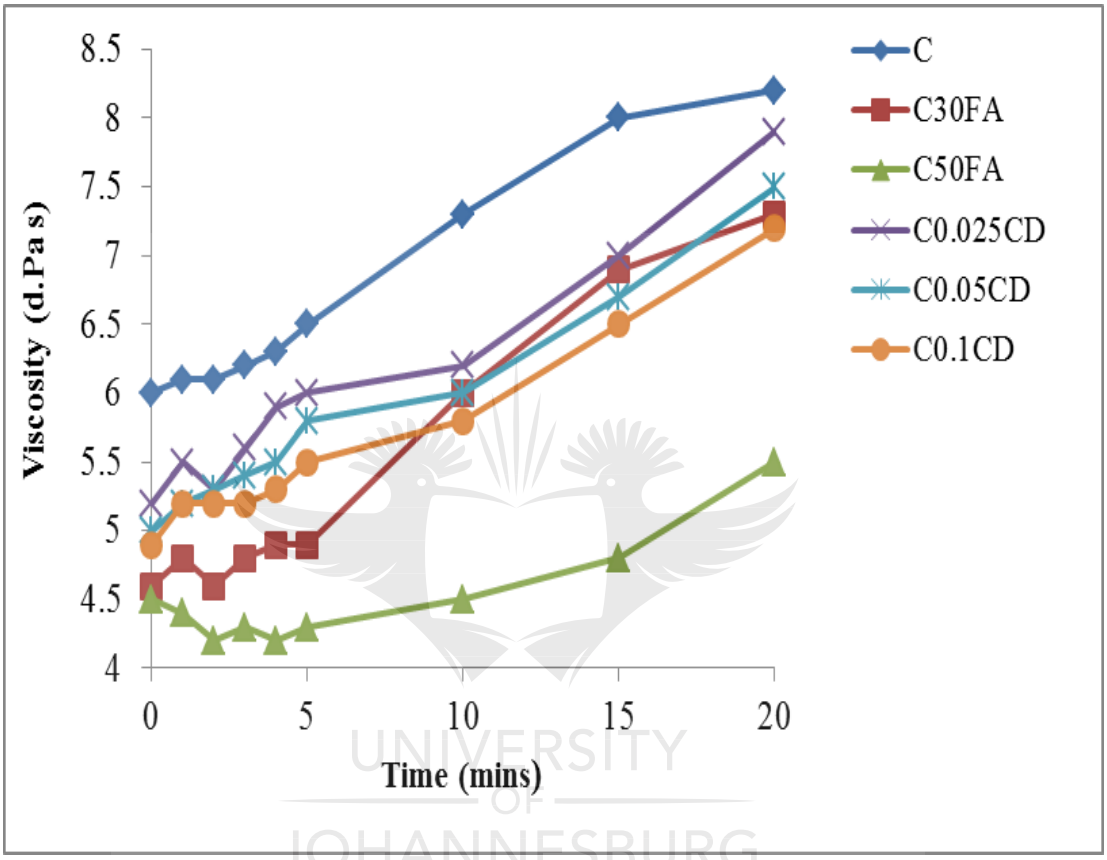

Figure 7.5: Viscosity of binary cement paste samples with 0.6-W/B

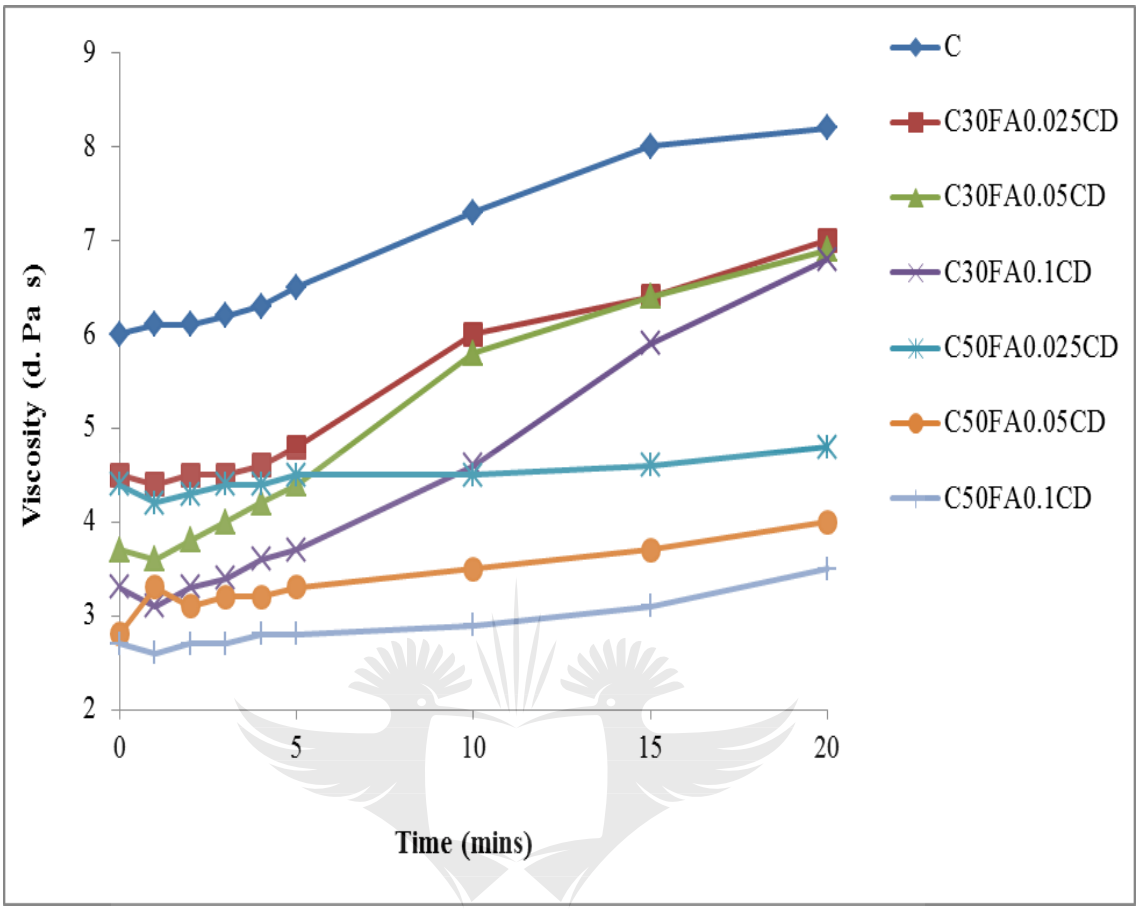

Figure 7.6: Viscosity of ternary cement paste samples with 0.6-W/B

As expected, the viscosity increased with a decrease in W/B (to 0.5) as shown in Figures 7.7 and 7.8 for the binary and ternary samples, respectively. For all samples (binary and ternary) with a 0.5-W/B, the rate of increase in viscosity with time decreased as compared to the samples with 0.6-W/B. In Figure 7.7, the β-CD showed a greater effect in reducing viscosity compared to FA. The higher the β-CD content, the higher the viscosity reduction effect as stated also for 0.6-W/B samples. The ternary samples (Figure 7.8) also revealed the same trend. The viscosity of the ternary samples was lower than the binary samples.

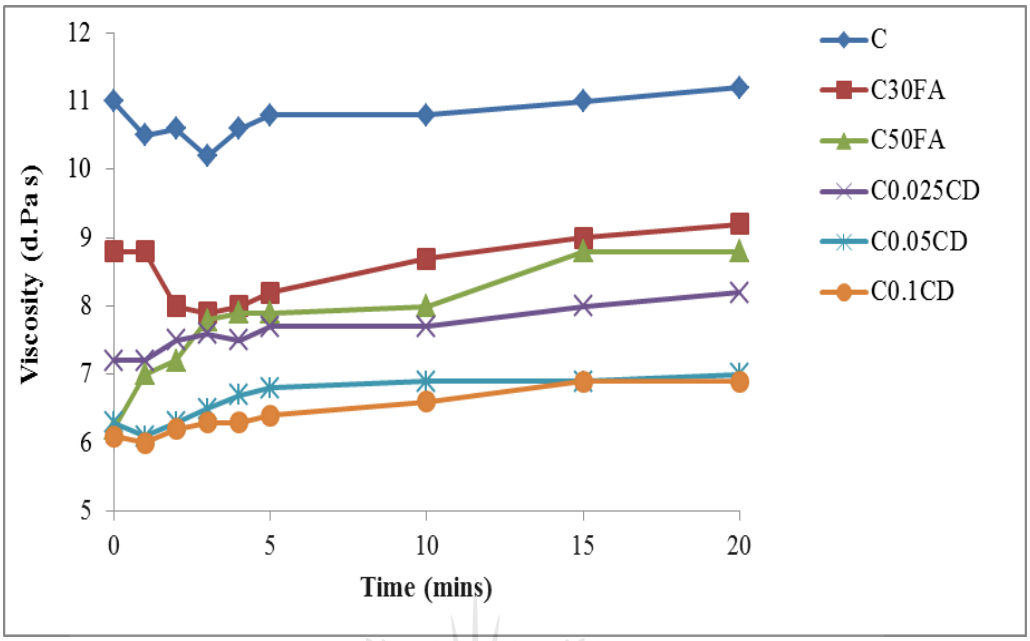

Figure 7.7: Viscosity of binary cement paste samples with 0.5-W/B

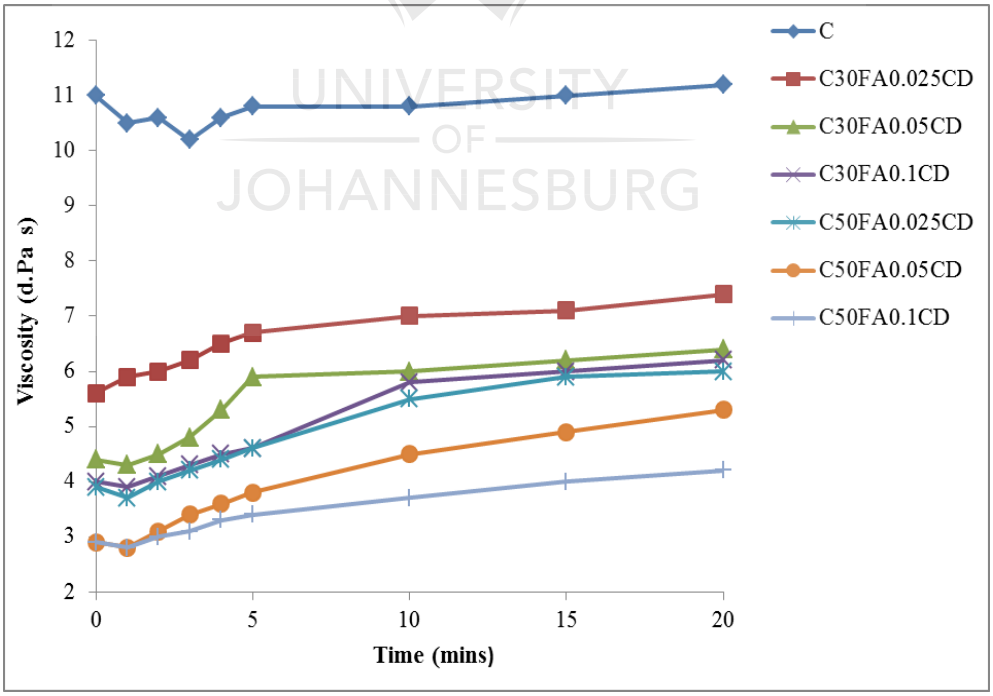

Figure 7.8: Viscosity of ternary cement paste samples with 0.5-W/B

The effect of yield stress to be overcome before initiation of flow was evident in the 0.4-W/B samples. This led to the drastic drop in viscosity at the initial minutes (0 to 15 mins) for all the binary samples shown in Figure 7.9 with the largest drop for FA samples (approximately 65% for the C30FA and 46% for the C50FA). In the case of 0.6-W/B and 0.5-W/B samples, small yield stress was required to be overcome because of the fluidity of the samples. Little or no drop was observed for these samples at the initial minutes (Figures 7.5-7.8). In the case of the ternary samples with 0.4-W/B (Figure 7.10), the samples exhibited an insignificant yield stress to be overcome because of the effect of FA-β-CD composite in the samples, which caused more fluidity of the samples. As shown in Figure 7.9, the viscosities of the FA samples picked up after 20 mins while the viscosities of β-CD samples were approximately maintained. A further reduction in viscosity was observed for all the ternary samples compared to binary samples. The reduction of viscosity with time of the ternary samples (relative to the binary samples of each W/B) decreased with decreasing W/B.

The results (Figures 7.5–7.10) also showed that the fluidity of the cement paste increased with an increase in the FA and β-CD contents. According to Burgos-Montes [15], the increase fluidity of cement paste with FA may be due to the spherical morphology of the FA particles, which would reduce inter-particulate friction and therefore raise paste fluidity. The viscosity results also confirmed the XRD results reported in Chapter Six (Figure 6.1). The XRD results showed a higher dissolution of anhydrous phases of cement paste samples with lower formation of CH at higher contents of FA and β-CD at the early period of hydration (24 hours). The lower formation of CH was also attributed to the dilution effect, which resulted from the addition of FA and reduced content of clinker.

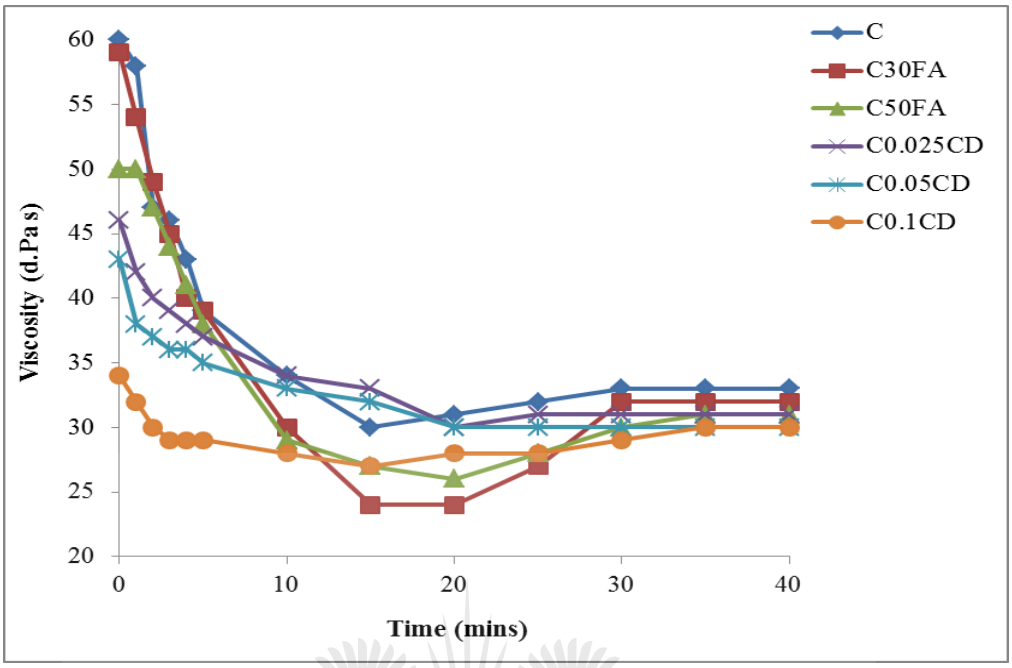

Figure 7.9: Viscosity of binary cement paste samples with 0.4-W/B

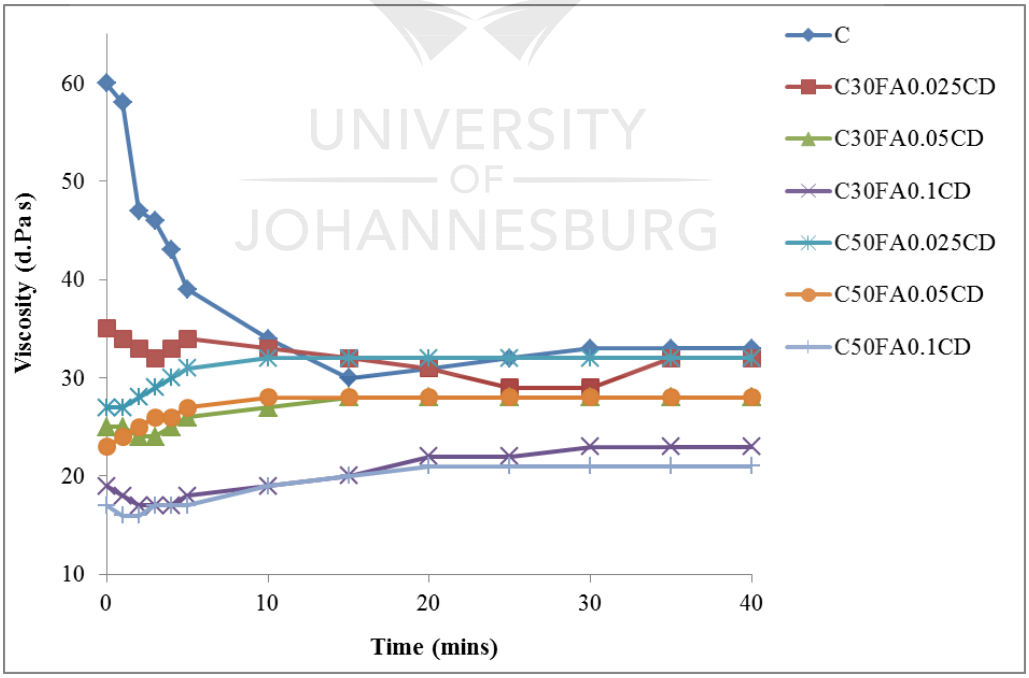

Figure 7.10: Viscosity of ternary cement paste samples with 0.4-W/B

7.4.2 The effect of FA, *β*-CD and FA- *β*-CD composites on cement paste setting times

Figure 7.11 shows the water content needed to maintain the cement paste consistency of the samples. It was observed that decreased water content was needed for samples containing FA and *β*-CD when compared to the control sample. A further decrease in water content was also observed for the samples with FA-*β*-CD composites (ternary samples). Similar observations were recorded by some researchers for FA and *β*-CD based superplasticisers [9, 15, 16]. The higher the FA and *β*-CD contents, the lesser the water required for consistency. The lower water content required for cement paste consistency for FA-*β*-CD composite samples will help the samples to have adequate workability at reduced W/B.

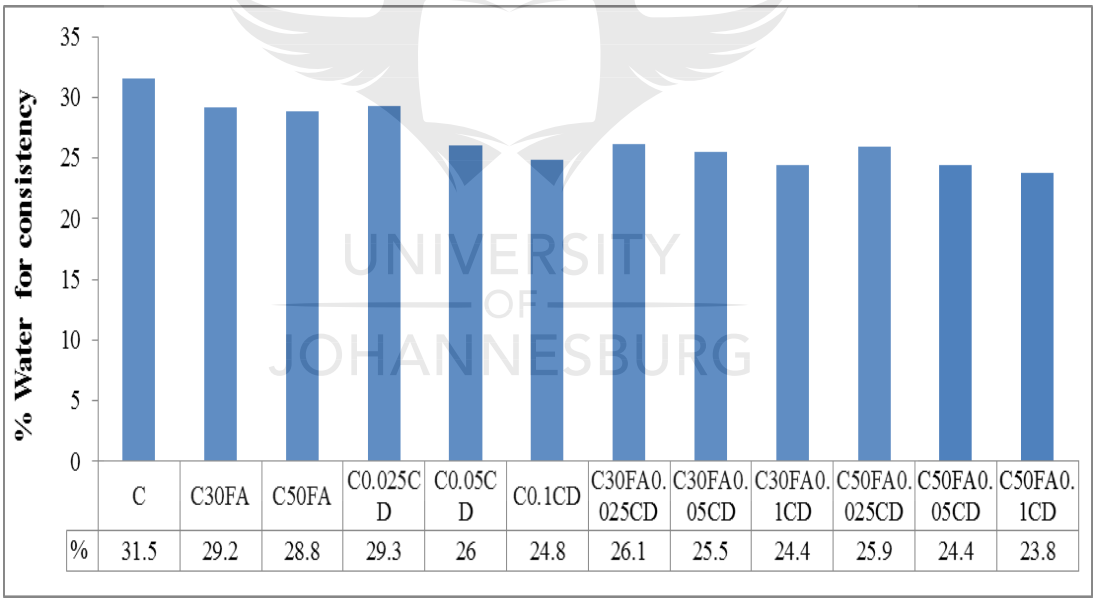

Figure 7.11: Percentage of water for the consistency of cement paste samples

The initial and final setting times of the cement pastes were affected by FA, *β*-CD and FA-*β*-CD composites. Figure 7.12 shows the initial and final setting times of the samples. An increase in both the initial and final setting times was observed in binary

samples while a further increase in both initial and final setting times was observed in ternary samples. The β-CD showed a higher effect in increasing setting time than FA, which can be attributed to the β-CD effect in increasing the fluidity of cement paste than FA as shown in the viscosities results (Figures 7.5–7.10). The greater fluidity of sample retarded the hydration process and thereby increased the setting time. Li et al [10] attributed the retarding effect of a β-CD based superplasticiser on the setting time to the large amount of hydroxyl groups in the β-CD based superplasticiser that prevented the hydration process.

According to Brooks et al [7], retardation in the setting times could be as a result of the dispersion effects of mineral admixtures (FA) and superplasticiser on the cement particles. They also reported that the setting of cement paste has been postulated to result from two fundamental steps: establishing contacts between particles (coagulation) and the formation of hydrates in the contact zones making rigid the coagulation structure. This postulation was also confirmed by Lv et al [9] and Li et al [10], they stated that the retardation in cement paste depends on the connectivity of particles. Due to increase in the fluidity effect of FA and β-CD on cement paste, the inter-particle contact could be reduced leading to the retardation of setting times.

The XRD results (Figure 6.1) showed that at an early hydration period (24 hours), β-CD aided the dissolution of anhydrous phases of cement paste samples with a lower formation of CH. The lower formation of CH will therefore reduce the rigidity of the coagulation structure as explained by Brooks et al [7], resulting in setting retardation at this hydration period. The FT-IR results reported in Chapter Six (Figure 6.8) also revealed that samples with FA, β-CD and FA-β-CD composites exhibited IR shift of the Si–O asymmetric stretching vibration to lower wavenumbers compared to control sample at a 24 hour hydration period, which confirmed the potential retardation effect of FA, β-CD and FA-β-CD composites. The higher the FA and β-CD contents, the greater the setting times observed (Figure 7.12), with the highest of 696 mins and

1420 mins initial and final setting times, respectively, observed for C50FA0.1CD sample.

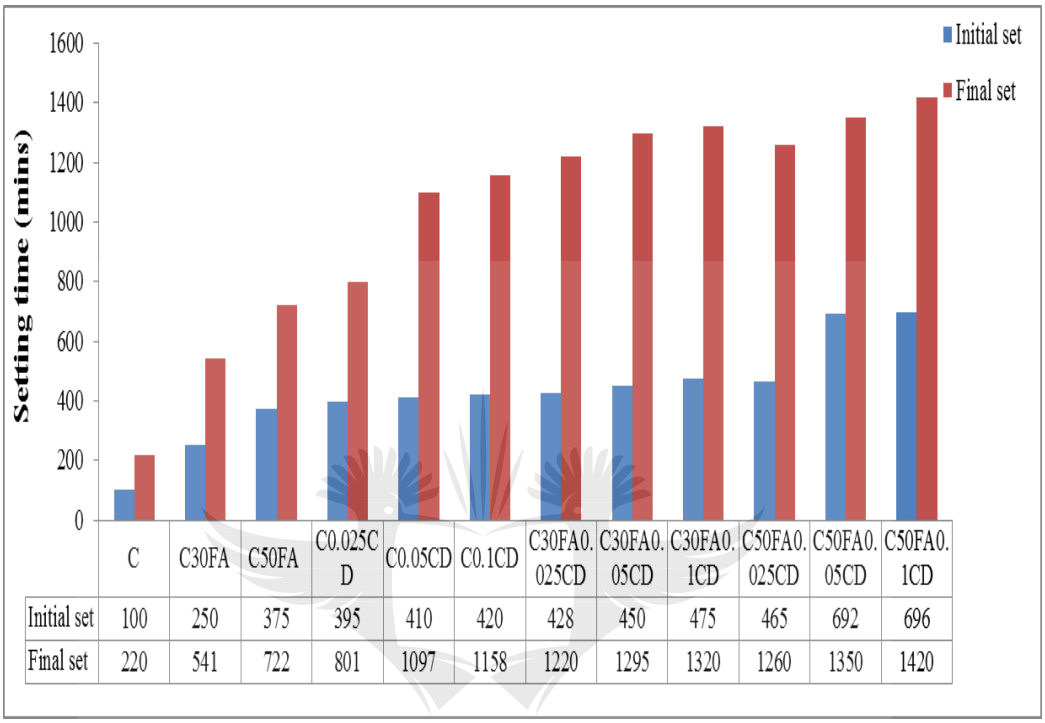

	C	C30FA	C50FA	C0.025CD	C0.05CD	C0.1CD	C30FA0.025CD	C30FA0.05CD	C30FA0.1CD	C50FA0.025CD	C50FA0.05CD	C50FA0.1CD
Initial set	100	250	375	395	410	420	428	450	475	465	692	696
Final set	220	541	722	801	1097	1158	1220	1295	1320	1260	1350	1420

Figure 7.12: Setting times of cement paste samples

7.5 CONCLUSIONS

The viscosity results showed that W/B had an inverse effect on the viscosity of cement paste. The higher the W/B, the lower the viscosity observed for all the samples. The FA, *β*-CD and FA-*β*-CD composites reduced the viscosity of the cement paste, with the *β*-CD having a higher effect in reducing the viscosity compared to the FA. The lowest viscosity was observed with the FA-*β*-CD composites samples for all the W/B. The higher the FA and *β*-CD contents, the lower the viscosity observed. These observations revealed an indication of the effect of FA, *β*-CD and FA-*β*-CD composites on the amount of water required for consistency and setting time. The trend observed with the viscosity results was also observed in setting times results.

The higher the FA and β-CD contents, the lower the water required for consistency and the longer the setting times observed, with FA-β-CD composites samples exhibiting the longest setting times. The XRD and FT-IR results presented in Chapter Six also confirmed these observations.

7.6 REFERENCES

[1] Banfill P. F. G.: Rheology of fresh cement and concrete. Rheology Reviews, 61 – 130 (2006).

[2] Zhang M., Sisomphon K., Ng T.S., Sun D.J.: Effect of superplasticizers on workability retention and initial setting time of cement pastes. Construction and Building Materials **24**, 1700–1707 (2010).

[3] Banfill P.F.G.: Additivity effects in the rheology of fresh concrete containing water-reducing admixtures. Construction and Building Materials **25,** 2955–2960 (2011).

[4] Wallevik O.H., Wallevik J.E.: Rheology as a tool in concrete science: The use of rheographs and workability boxes. Cement and Concrete Research **41,** 1279–1288 (2011).

[5] Laskar A.I., Talukdar S.: Rheological behavior of high performance concrete with mineral admixtures and their blending. Construction and Building Materials **22,** 2345–2354 (2008).

[6] Ravina D., Mehta P.K.: Properties of fresh concrete containing large amounts of fly ash. Cement and concrete research **16,** 227-238 (1986).

[7] Brooks J.J., Johari M.A.M., Mazloom M.: Effect of admixtures on the setting times of high-strength concrete. Cement and Concrete Composites **22,** 293-301 (2000).

[8] Durán-Herrera A., Juárez C.A., Valdez P., Bentz D.P.: Evaluation of sustainable high-volume fly ash concretes. Cement and Concrete Composites **33,** 39-45 (2011).

[9] Lv S., Gao R., Cao Q., Li D., Duan J.: Preparation and characterization of poly-carboxymethyl-β-cyclodextrin superplasticizer. Cement and Concrete Research **42,** 1356–1361 (2012).

[10] Li Y., Guo H., Zhang Y., Zheng J., Li Z., Yang C., Lu M.: Synthesis of copolymers with cyclodextrin as pendants and its end group effect as superplasticizer. Carbohydrate Polymers **102**, 278– 287 (2014).

[11] Hua O.Z., Guo M.B., Wei J.S.: Influence of cellulose ethers molecular parameters on hydration kinetics of Portland cement at early ages. Construction and Building Materials **33**, 78–83 (2012).

[12] Kovler K., Roussel N.: Properties of fresh and hardened concrete. Cement and Concrete Research **41,** 775–792 (2011).

[13] SANS50196-3:2006: South African national standard. Methods of testing cement Part 3: Determination of setting times and soundness, ISBN 0-626-17598-4. Edition 2.

[14] SANS 50196-1:2006: South African national standard. Methods of testing cement Part 1: Determination of strength, ISBN 0-626-17596-8. Edition 2.

[15] Burgos-Montes O., Alonso M.M., Puertas F.: Viscosity and water demand of limestone- and fly ash-blended cement pastes in the presence of superplasticisers. Construction and Building Materials **48**, 417–423 (2013).

[16] Tkaczewska E.: Effect of the superplasticizer type on the properties of the fly ash blended cement. Construction and Building Materials **70,** 388–393 (2014).

CHAPTER EIGHT

THE EFFECT OF FLY ASH, *β*-CYCLODEXTRIN AND FLY ASH-*β*-CYCLODEXTRIN COMPOSITES ON CONCRETE WORKABILITY AND STRENGTH

8.1 INTRODUCTION

As discussed in Chapter Five, strength is one of the main properties of concrete that is being used to indicate the overall behaviour of the concrete. The strength of the concrete can be influenced by several factors like the cement type, aggregate type, curing ages, curing type, admixtures and so on [1-8]. Based on the indicative tests (reported in Chapter Five) and the behaviour of fly ash (FA), *β*-cyclodextrin (*β*-CD) and fly ash-*β*-cyclodextrin (FA-*β*-CD) composites on hydration, viscosity and setting time (reported in Chapter Six and Seven), further investigation was done to study the effect of FA, *β*-CD and FA-*β*-CD composites on concrete workability and strength. The results of this study are presented and discussed in this chapter.

8.2 MATERIALS AND MIXES

The cement (CEM 1 52.5N), FA, *β*-CD, granite crusher sand and coarse aggregate used were the same as in Section 5.2. A physical mixture of a pre-weighed amount of *β*-CD and FA was used for the composite preparation. Proportions of 30% FA and 50% FA (by mass of cement) were incorporated in the mix. *β*-CD proportions of 0.025%, 0.05% and 0.1% *β*-CD (by mass of cement) were used. Two different water/binder ratio (W/Bs) of 0.5 and 0.4-Were used for the mixtures. A total of twelve mixtures were produced for each W/B, resulting in twenty four mixtures in total. A quantity of 0.08 m^3 of concrete was batched for each of the twenty four mixtures produced, according to the mixture proportions presented in Tables 8.1 and 8.2 for 0.5-W/B and 0.4-W/B, respectively. Total of 360 cubes and 288 cylinders were produced for the strength tests. The mixing and casting procedures were the same as explained in Section 5.2.1. Samples with *β*-CD were kept covered with

polythene sheets for two days rather than three days, as was done for the indicative tests, before demoulding because of the lower content of β-CD in the mixtures compared to the indicative samples. The samples descriptions were the same as presented in Table 6.2.

Table 8.1: Mixture proportions for 1 m^3 of concrete samples for 0.5-W/B

Samples	Cement	Crusher sand (kg)	Coarse aggregate (kg)	FA (kg)	β-CD (kg)	Water (kg)	W/B	Slump (mm)
C	450.00	720	1076	0.00	0.00	225	0.5	35
C30FA	315.00	720	1076	135	0.00	225	0.5	45
C50FA	225.00	720	1076	225	0.00	225	0.5	65
C0.025CD	449.89	720	1076	0.00	0.1125	225	0.5	95
C0.05CD	449.78	720	1076	0.00	0.225	225	0.5	110
C0.1CD	449.55	720	1076	0.00	0.450	225	0.5	180
C30FA0.025CD	315.00	720	1076	134.89	0.1125	225	0.5	100
C30FA0.05CD	315.00	720	1076	134.78	0.225	225	0.5	160
C30FA0.1CD	315.00	720	1076	134.55	0.450	211.5	0.47	145
C50FA0.025CD	225.00	720	1076	224.89	0.1125	211.5	0.47	100
C50FA0.05CD	225.00	720	1076	224.78	0.225	202.5	0.45	105
C50FA0.1CD	225.00	720	1076	224.55	0.450	202.5	0.45	160

Table 8.2: Mixture proportions for 1 m^3 of concrete samples for 0.4-W/B

Samples	Cement	Crusher sand (kg)	Coarse aggregate (kg)	FA (kg)	β-CD (kg)	Water (kg)	W/B	Slump (mm)
C	520.00	650	1000	0.00	0.00	208	0.4	30
C30FA	364.00	650	1000	156.00	0.00	208	0.4	40
C50FA	260.00	650	1000	260.00	0.00	208	0.4	55
C0.025CD	519.87	650	1000	0.00	0.13	208	0.4	40
C0.05CD	519.74	650	1000	0.00	0.26	208	0.4	55
C0.1CD	519.48	650	1000	0.00	0.52	208	0.4	135
C30FA0.025CD	364.00	650	1000	155.87	0.13	208	0.4	55
C30FA0.05CD	364.00	650	1000	155.74	0.26	208	0.4	70
C30FA0.1CD	364.00	650	1000	155.48	0.52	208	0.4	180
C50FA0.025CD	260.00	650	1000	259.87	0.13	208	0.4	80
C50FA0.05CD	260.00	650	1000	259.74	0.26	208	0.4	115
C50FA0.1CD	260.00	650	1000	259.48	0.52	208	0.4	200

8.3 EXPERIMENTAL PROCEDURE

8.3.1 Workability test

Workability was measured by slump test according to SANS 5862-1:2006 [9].

8.3.2 Compressive strength test

The compressive strength test was performed according to SANS 5863: 2006 [10] and calculated as explained in Section 5.3.1. Samples were tested after being cured for 7, 14, 28, 90 and 180 curing days.

8.3.3 Split tensile strength test

The split tensile test was performed on the cylinders, according to SANS 6253: 2006 [11] and calculated as explained in Section 5.3.2. Samples were tested after being

cured for 14, 28, 90 and 180 days respectively. The percentage decrease or increase in compressive strength or split tensile strength was calculated using Equations (5.3) and (8.1). A positive value indicates an increase in the compressive strength or split tensile strength (CSt), while a negative value indicates a decrease in the compressive strength or split tensile strength (CSt).

$$\%increase/decrease\ (ref.\ FA\ pozzolanic) = \frac{FA-\beta CD\ composite\ CSt - FA\ pozzolanic\ CSt}{FA\ pozzolanic\ CSt} x\,100 \tag{5.3}$$

$$\%increase/decrease\ (ref.\ control) = \frac{other\ samples\ CSt - control\ CSt}{control\ CSt} x\,100 \tag{8.1}$$

8.4 RESULTS AND DISCUSSION

The workability and the strength results are discussed under the sub-headings below. The strength results are further drawn into comparative graphs for easy interpretation. The comparative graphs revealed the percentage increase/decrease of concrete strength at each curing age based on the effect of FA, β-CD and FA-β-CD composites.

8.4.1 Workability

The slump test results for the 0.5-W/B and 0.4-W/B samples are presented in Tables 8.1 and 8.2, respectively. It was difficult to maintain a 0.5-W/B for FA-β-CD composites samples because non-cohesive mixtures were observed at 0.5-W/B. The results (for both 0.4 and 0.5-W/B) showed an increase in slump with an increase in FA and β-CD contents. When compared with the viscosity results (Figures 7.5-7.10) presented in Chapter Seven, the trend showed that the higher the viscosity, the lower the flow ability and the lower the slump. This is in agreement with the observation of Lachemi et al [12], when the rheological properties of cement paste using new

viscosity modifying admixtures were studied, that an increase in the viscosity of the paste reduces the flow ability.

8.4.2 Compressive strength results for 0.5-W/B samples

Figure 8.1 presents the compressive strength results of the samples with 0.5-W/B. A progressive increase in compressive strength was observed for all the samples as curing age increased. This is an evidence of improved hydration reaction as curing age increased, resulting in an increase in strength. When compared with the control sample, the incorporation of β-CD resulted in an increase in compressive strength, with an increase in β-CD, for contents up to 0.05%. The samples containing 0.1% β-CD yielded slightly lower strengths than those containing 0.05% β-CD. Furthermore, in the case of the samples containing FA, the samples with 50% FA exhibited lower compressive strengths, at all curing ages, compared to to those containing 30% FA.

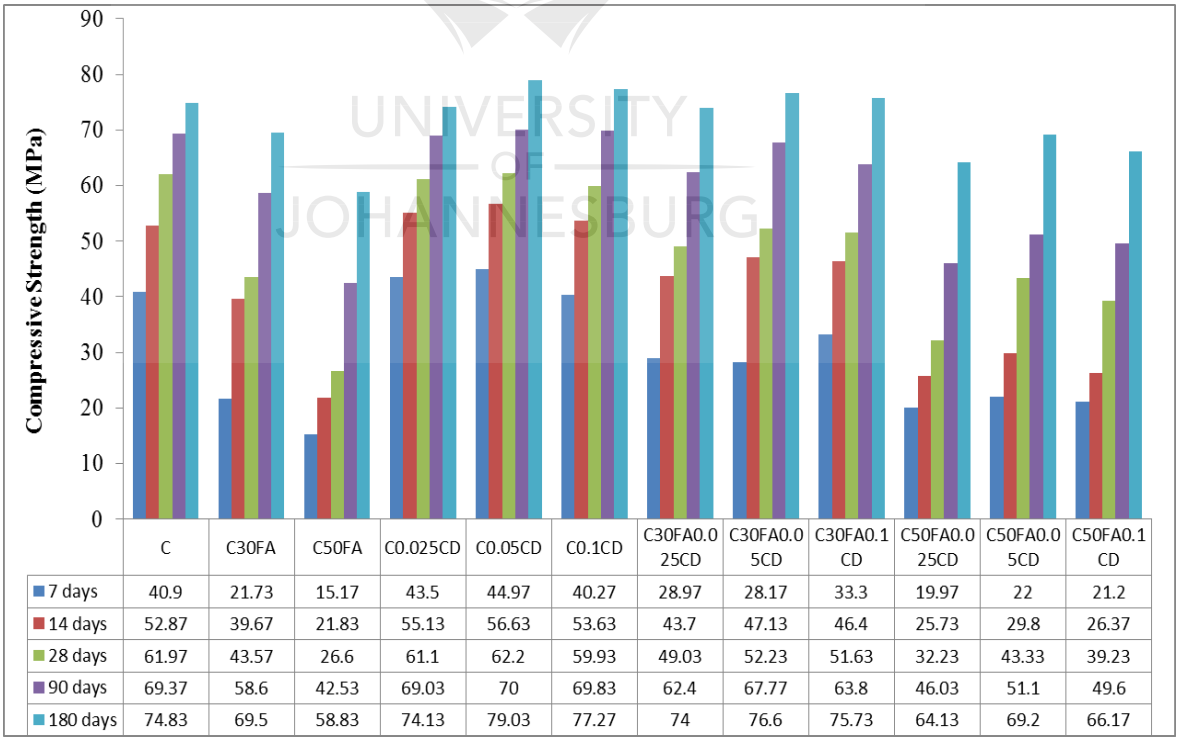

	C	C30FA	C50FA	C0.025CD	C0.05CD	C0.1CD	C30FA0.025CD	C30FA0.05CD	C30FA0.1CD	C50FA0.025CD	C50FA0.05CD	C50FA0.1CD
7 days	40.9	21.73	15.17	43.5	44.97	40.27	28.97	28.17	33.3	19.97	22	21.2
14 days	52.87	39.67	21.83	55.13	56.63	53.63	43.7	47.13	46.4	25.73	29.8	26.37
28 days	61.97	43.57	26.6	61.1	62.2	59.93	49.03	52.23	51.63	32.23	43.33	39.23
90 days	69.37	58.6	42.53	69.03	70	69.83	62.4	67.77	63.8	46.03	51.1	49.6
180 days	74.83	69.5	58.83	74.13	79.03	77.27	74	76.6	75.73	64.13	69.2	66.17

Figure 8.1: Compressive strength of concrete samples with 0.5-W/B

The percentage increase/decrease in C30FA, C50FA and *β*-CD samples compressive strengths, compared to the control sample (C) for a W/B of 0.5, is shown in Figure 8.2. A decrease in compressive strength was observed for samples with C30FA and C50FA, compared to the control sample. The compressive strength was further decreased for the C50FA sample than in the case of the C30FA sample. As curing increased, the compressive strength got closer to the control sample value, showing the effect of slower pozzolanic reaction at early hydration periods. The *β*-CD samples revealed an increase in early compressive strength compared to the control sample for the C0.025CD and C0.05CD samples. The C0.05CD sample showed an increased compressive strength compared to the control sample at all curing ages. Less than 3.5% decrease in compressive strength at 28 days curing period was observed for the C0.1CD sample, compared to the control sample.

The observed results (Figure 8.2) correspond to the earlier discussions in Chapter Six and Seven. The XRD results reported in Chapter Six (Figures 6.2 – 6.4) showed that at early hydration periods (7 and 28 days) evidence of SiO_2 is observed for C30FA and C50FA samples showing delay pozzolanic reaction, resulting in a reduced compressive strength compared to the control sample. The C0.025CD and C0.05CD samples showed early formation of amorphous C-S-H at the 7 and 28 days hydration periods, resulting in a higher compressive strength than the control samples at these early hydration periods. The early formation of C-S-H and Portlandite (CH) at 7 days hydration period for *β*-CD samples shown in the FT-IR results (Figure 6.9) also confirmed this observation. The lower viscosity of samples with FA and *β*-CD compared to control samples, leading to delayed setting times, as explained in Chapter Seven would have also contributed to the observed results. The higher the FA and *β*-CD contents, the lower the viscosity, the longer the setting times and the lower the compressive strength observed compared to the control sample.

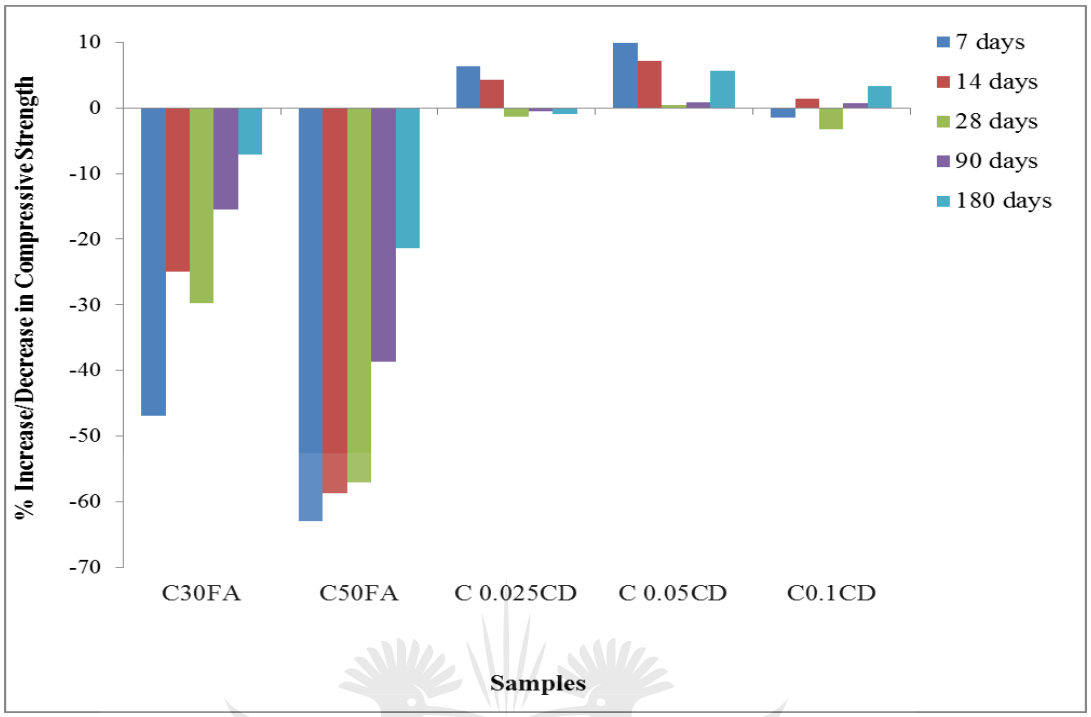

Figure 8.2: Percentage increase/decrease in the compressive strength of C30FA, C50FA and *β*-CD samples compared to control sample (C) for 0.5-W/B

Figure 8.3 shows the percentage increase/decrease in FA-*β*-CD composite samples compressive strengths compared to the control sample (C) for a W/B of 0.5. A relatively lower reduction in compressive strengths of the FA-*β*-CD composite samples was observed than in the C30FA and C50FA samples, when compared to the control sample. At 180 days curing period, an increase in compressive strength was observed for the C30FA0.05CD and C30FA0.1CD samples compared to the control sample. These results prove the positive effect of these composite samples on concrete compressive strength compared to the C30FA sample. This can be attributed to the improved hydration reaction at early curing age and improved pozzolanic reaction at from 28 days hydration periods caused by *β*-CD as revealed in the XRD and FT-IR results discussed in Chapter Six.

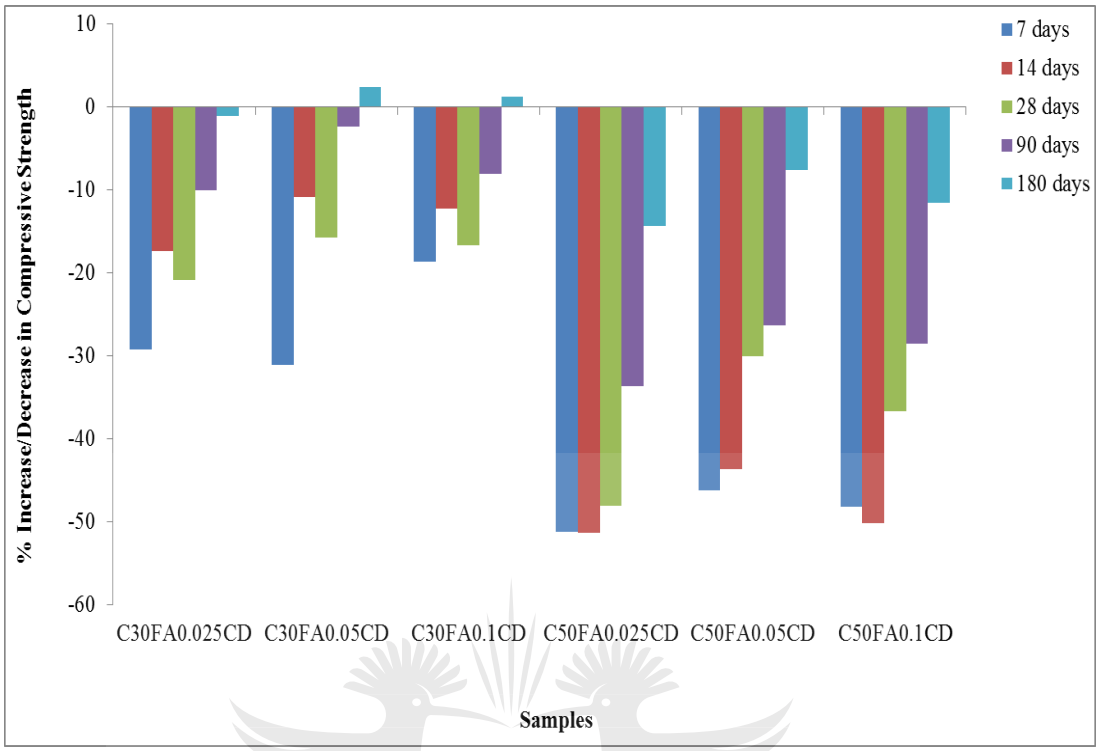

Figure 8.3: Percentage increase/decrease in FA-*β*-CD composites samples compressive strength compared to control sample (C) for 0.5-W/B

The effects of the FA-*β*-CD composite samples on the pozzolanic behaviour of their original C30FA and C50FA samples, as reflected in their compressive strengths, are presented in Figures 8.4 and 8.5, respectively. For all FA-*β*-CD composite samples, the compressive strengths were increased compared to their original C30FA and C50FA samples, at all curing ages. The trend showed the effect of *β*-CD on early increase in hydration reaction from 7 days, revealing a greater compressive strength at 7 days for all composite samples than the corresponding C30FA and C50FA samples. Also, the effect of *β*-CD on an increase in pozzolanic reaction from 28 days onwards was revealed for all the samples. These observations can also be attributed to the early dissolution of C_3S and C_2S by *β*-CD, which aided the formation of CH and amorphous C-S-H in the XRD results (Figure 6.2) and the sharpness of Si-O asymmetric stretching vibration band (ν_3) compared to C30FA and C50FA samples in

the FT-IR results (Figure 6.9), discussed in Chapter Six. The early dissolution of C_3S and C_2S will lead to the release of more active silica that probably will get used in the reaction. This is in agreement with Papadakis [13], who observed, during the study of the effect of FA on Portland cement systems, that the final concrete strength is proportional to the content of the active silica in the concrete volume. A greater effect of *β*-CD on pozzolanic reaction was observed for samples containing 50% FA (Figure 8.5) than for the samples with 30% FA (Figure 8.4). The samples with 0.05% *β*-CD increased more, the compressive strength of the original C30FA and C50FA samples in comparison with the samples with 0.025% and 0.1% *β*-CD, from the 28 days hydration period.

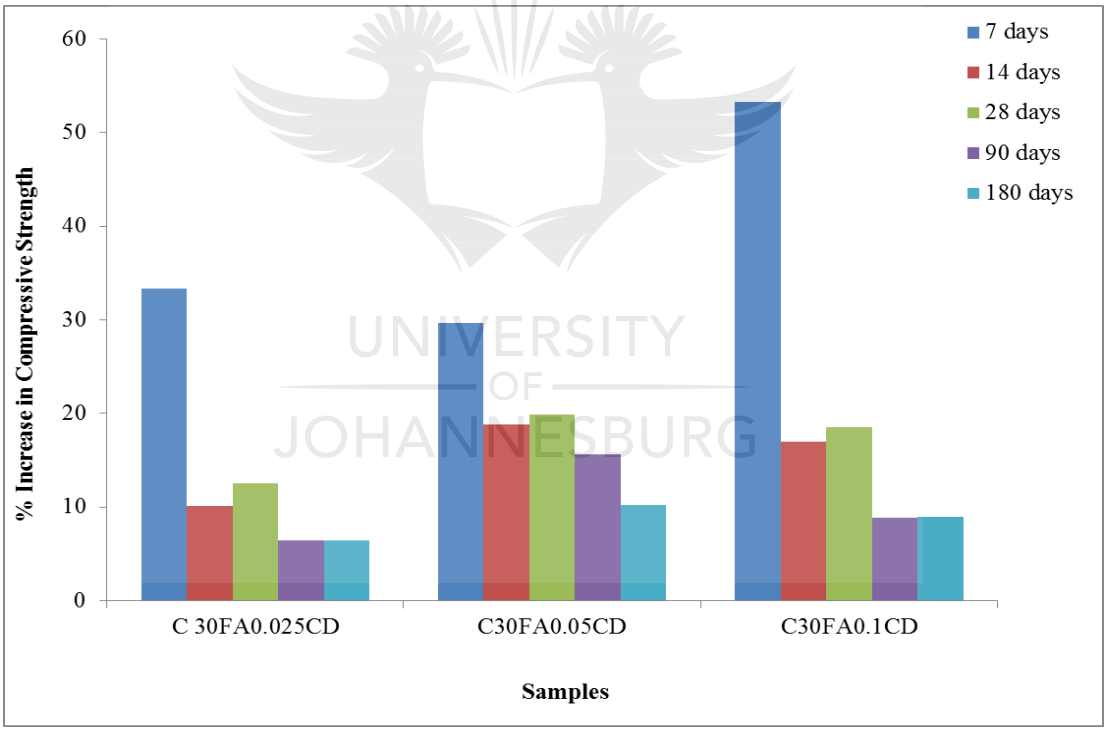

Figure 8.4: Percentage increase in the compressive strength of FA-*β*-CD-composite samples compared to C30FA pozzolanic sample for 0.5-W/B

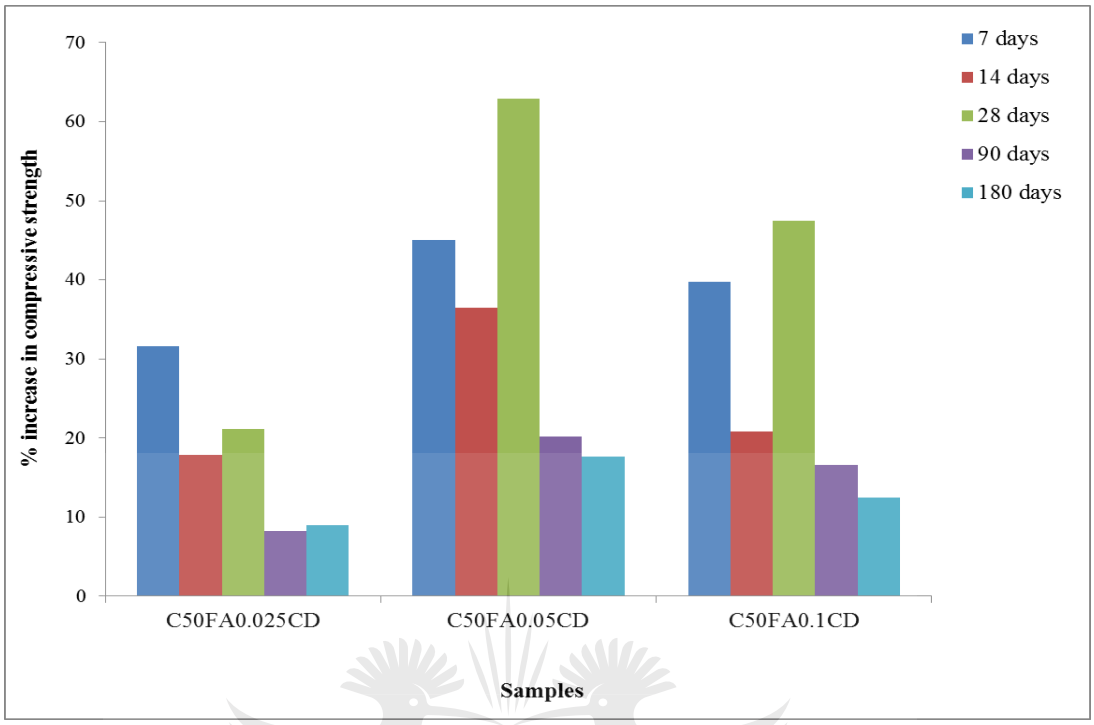

Figure 8.5: Percentage increase in the compressive strength of FA-*β*-CD-composite samples compared to C50FA pozzolanic sample for 0.5-W/B

8.4.3 Compressive strength results for 0.4-W/B samples

General observations reported by other researchers [14-18] on the effect of W/B on compressive strength showed that the lower the W/B, the higher the compressive strength. This observation was revealed in the results of the compressive strength for the 0.4-W/B samples presented in Figure 8.6. With 0.4-W/B, an increase in compressive strength was observed for all samples when compared with the compressive strength results of 0.5-W/B samples (Figure 8.1). As observed for the 0.5-W/B samples, compressive strength increased with an increase in curing age. The samples with 50% FA exhibited lower compressive strengths than other samples.

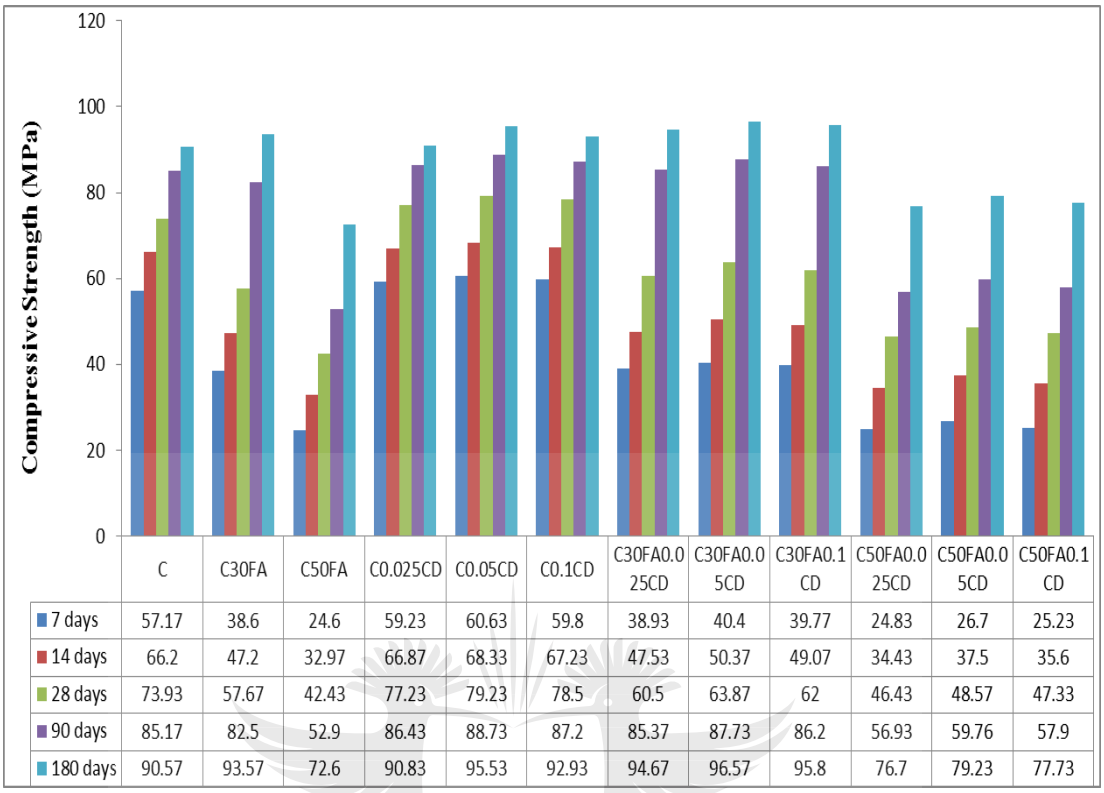

	C	C30FA	C50FA	C0.025CD	C0.05CD	C0.1CD	C30FA0.025CD	C30FA0.05CD	C30FA0.1CD	C50FA0.025CD	C50FA0.05CD	C50FA0.1CD
7 days	57.17	38.6	24.6	59.23	60.63	59.8	38.93	40.4	39.77	24.83	26.7	25.23
14 days	66.2	47.2	32.97	66.87	68.33	67.23	47.53	50.37	49.07	34.43	37.5	35.6
28 days	73.93	57.67	42.43	77.23	79.23	78.5	60.5	63.87	62	46.43	48.57	47.33
90 days	85.17	82.5	52.9	86.43	88.73	87.2	85.37	87.73	86.2	56.93	59.76	57.9
180 days	90.57	93.57	72.6	90.83	95.53	92.93	94.67	96.57	95.8	76.7	79.23	77.73

Figure 8.6: Compressive strength of concrete samples with 0.4-W/B

The percentage increase/decrease in the compressive strength of the C30FA, C50FA and β-CD samples compared to the control sample, for 0.4-W/B, is shown in Figure 8.7. The results showed that the FA and β-CD influenced the compressive strength of the control sample more favourably than in the case of the 0.5-W/B (Figure 8.2). The C30FA sample showed increased compressive strength compared to the control sample at the 180 days curing period. A reduced compressive strength was observed for C50FA samples at all curing ages compared to the control sample but to a lesser degree than was the case in the 0.5-W/B samples (Figure 8.2). The β-CD samples (C0.025CD, C0.05CD and C0.1CD) showed an increase in concrete compressive strength at all ages of curing, compared to the control sample. A higher increase in compressive strength was observed with the C0.05CD sample than for the C0.025CD and C0.1CD samples. The effect of β-CD in increasing hydration reaction from as early as the 7 days hydration period, as reported in Chapter Seven, was evident in

Figure 8.7. As observed, the lower the W/B, the more obvious the improved effect of *β*-CD on hydration reaction, leading to an increase in concrete compressive.

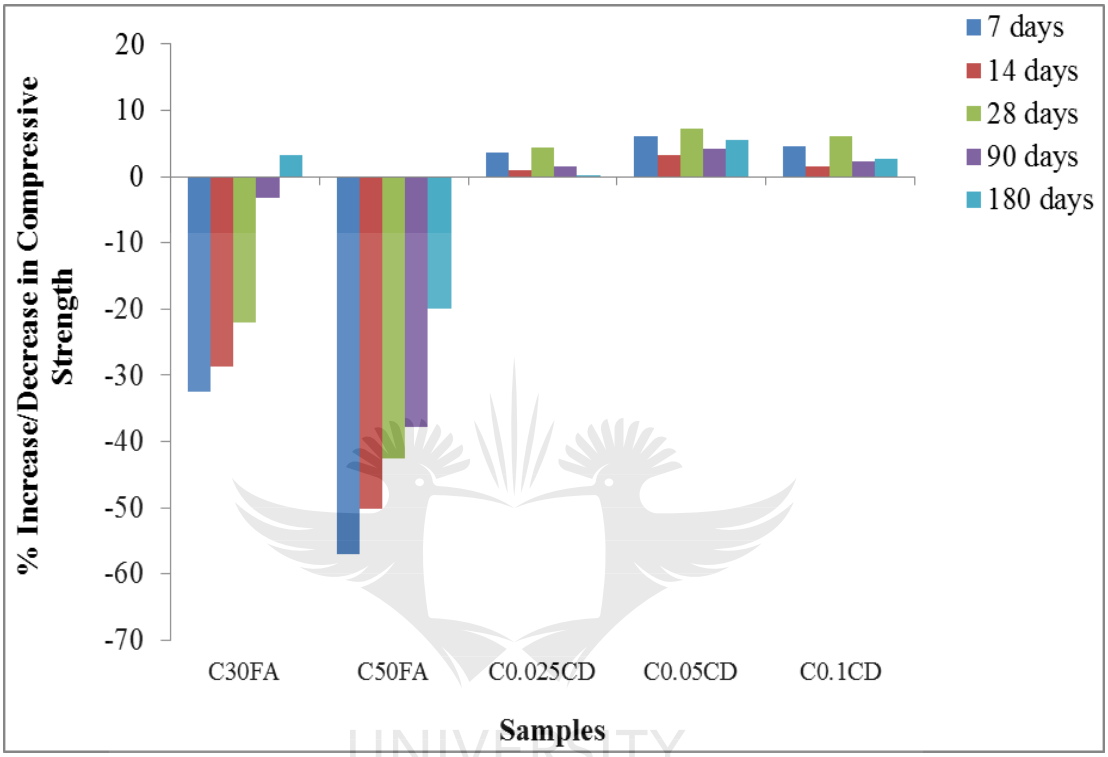

Figure 8.7: Percentage increase in C30FA, C50FA and *β*-CD samples compressive strength compared to control sample (C) for 0.4-W/B

The increase/decrease in compressive strength was observed for the FA-*β*-CD composite samples containing 30% FA compared to the control sample for 0.4-W/B from 90 days curing age as seen in Figure 8.8. These results prove that with lower W/B (0.4), FA and *β*-CD have a better effect on hydration and pozzolanic reactions than with higher W/B (0.5). However, since the control samples with 0.4-W/B were denser than the samples with 0.5-W/B, at early curing ages (7 and 14 days) a greater decrease in compressive strength was observed for the 0.4-W/B samples with 30% FA than in their corresponding 0.5-W/B samples. Notwithstanding, a greater increase

in compressive strength with time was observed for 0.4-W/B composites samples containing 30% FA than in their corresponding 0.5-W/B samples resulting in a greater compressive strength than the control sample at later curing ages (90 and 180 days). The composite samples containing 50 % FA showed a different trend; a greater decrease in compressive strength was observed with these samples than their corresponding 0.5-W/B samples (Figure 8.3), when compared with the control samples. However, all the FA-*β*-CD composite samples improved in compressive strength, compared to the C30FA and C50FA samples at 0.4-W/B (Figure 8.7), when compared with the control sample.

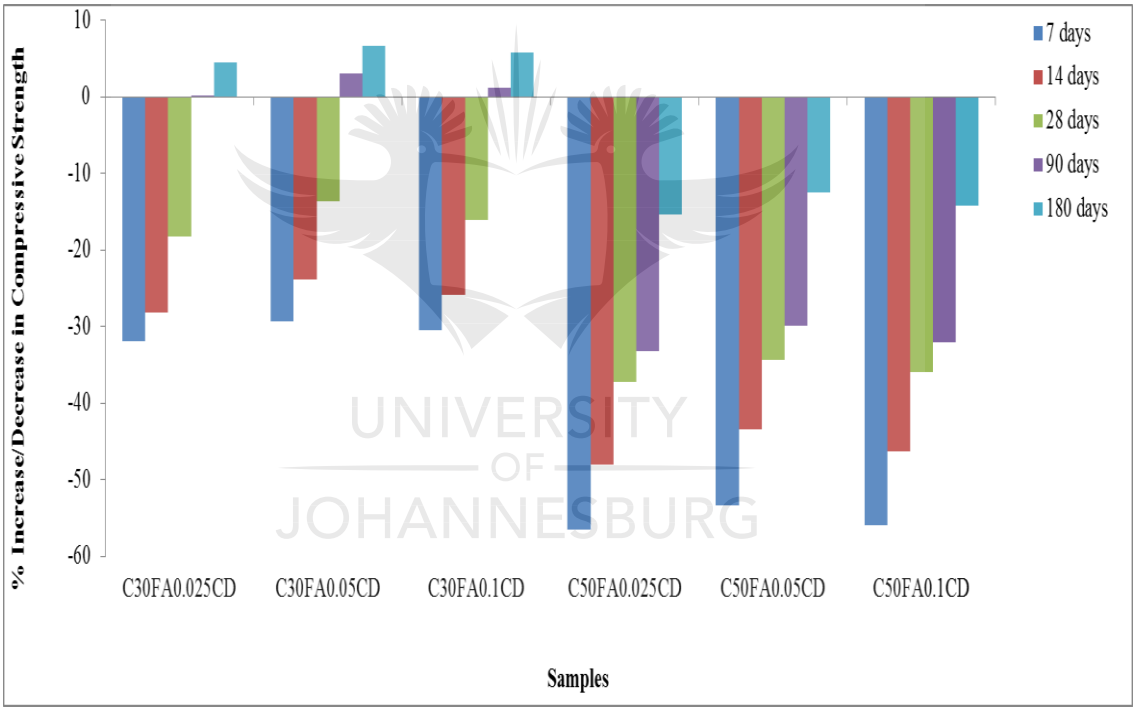

Figure 8.8: Percentage increase/decrease in the compressive strength of FA-*β*-CD-composites samples compared to control sample (C) for 0.4-W/B

It is obvious from Figures 8.9 and 8.10 that *β*-CD improved hydration/pozzolanic reactions from the 7 days hydration period. An increase in compressive strength was observed for all composite samples compared to their original C30FA and C50FA samples. The increase in compressive strength observed reached its peak at 28 days

curing age for all the samples. The trend observed with 0.5-W/B samples was also observed. Samples containing 50% FA (Figure 8.10) exhibited a greater influence of β-CD in improving compressive strength compared to the samples with 30% FA (Figure 8.9). Also, samples with 0.05% β-CD showed the best performance in increasing compressive strengths of the C30FA and C50FA samples from the 28 days hydration period, in comparison with the samples with 0.025% and 0.1% β-CD.

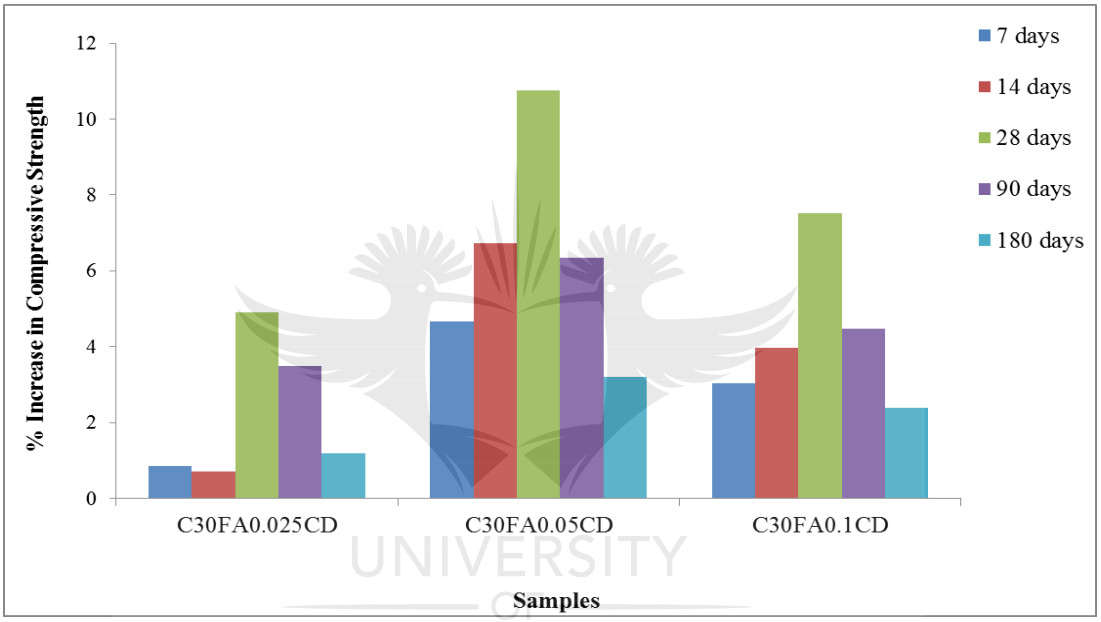

Figure 8.9: Percentage increase in the compressive strength of FA-β-CD-composite samples compared to C30FA pozzolanic sample for 0.4-W/B

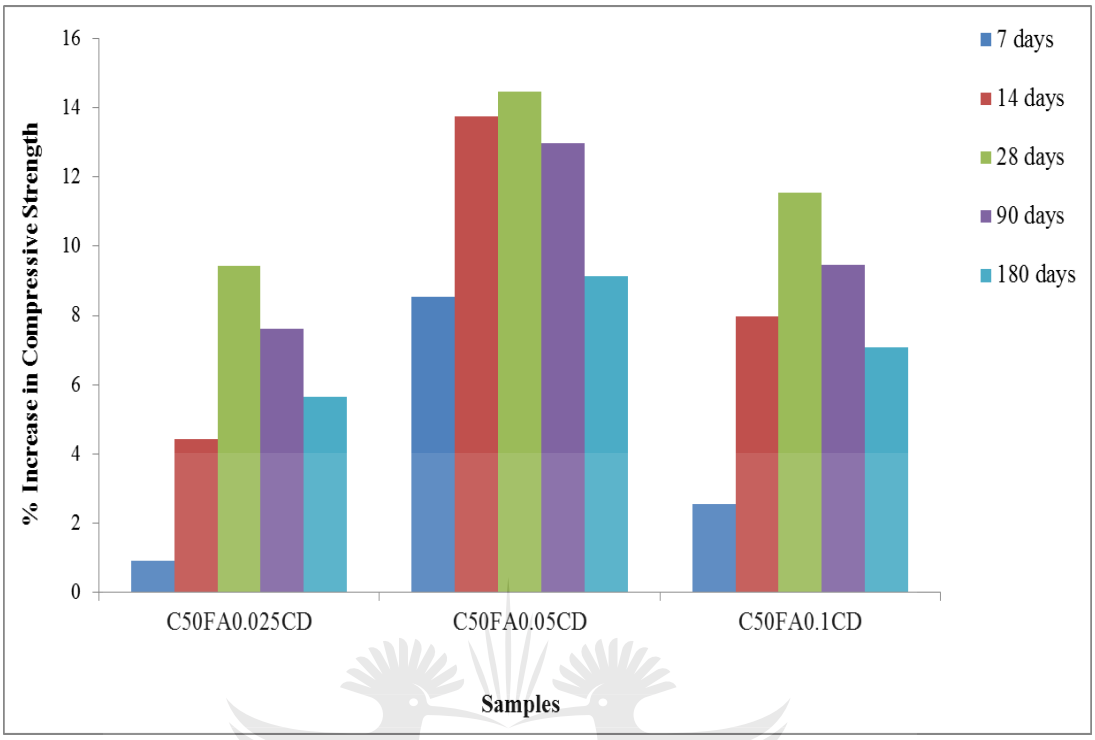

Figure 8.10: Percentage increase in the compressive strength of FA-*β*-CD-composite samples compared to C50FA pozzolanic sample for 0.4-W/B

8.4.4 Split tensile strength results for 0.5-W/B samples

Figure 8.11 shows the split tensile strength of all samples with 0.5-W/B. Concrete is known to be strong in compression and weak in tension, therefore generally, all samples decreased in split tensile strength in comparison to their compressive strength. A progressive increase in split tensile strength was observed as curing age increased, for all the samples. A higher rate of increase in split tensile strength with time was observed for samples with 50% FA than for the other samples. The samples with 0.1% *β*-CD generally exhibited an improved split tensile strength, at all curing ages, relative to the corresponding mixture samples containing lesser amounts of *β*-CD.

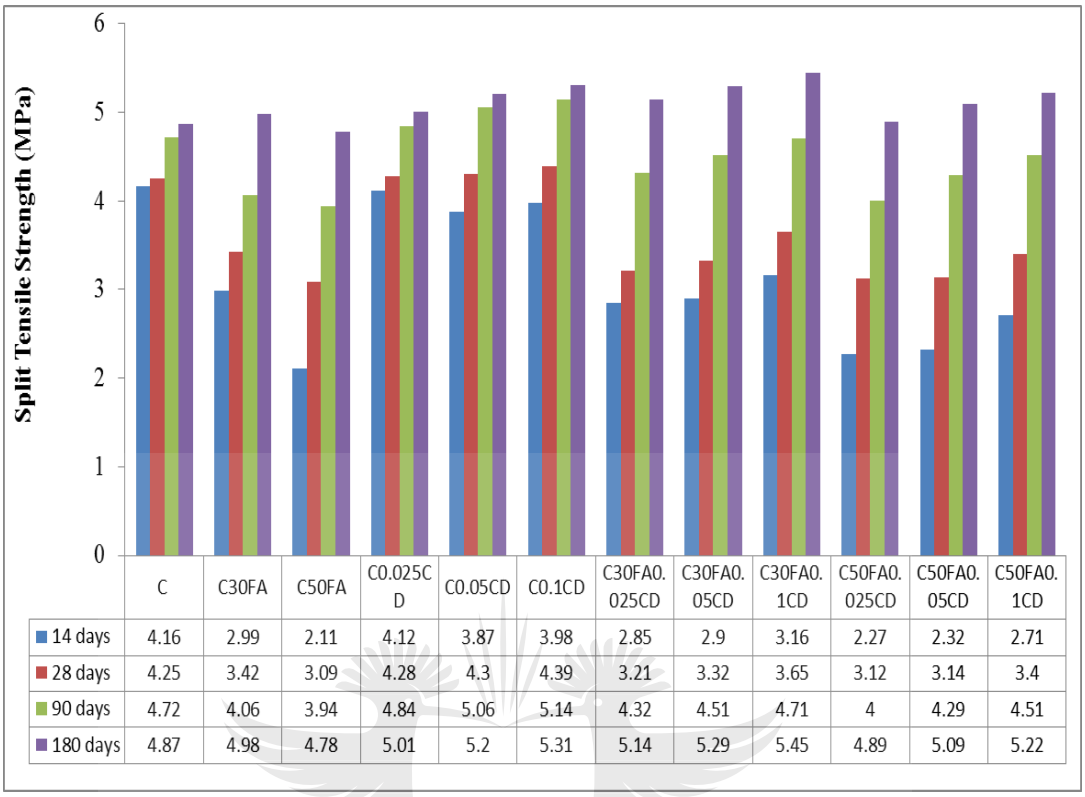

	C	C30FA	C50FA	C0.025CD	C0.05CD	C0.1CD	C30FA0.025CD	C30FA0.05CD	C30FA0.1CD	C50FA0.025CD	C50FA0.05CD	C50FA0.1CD
14 days	4.16	2.99	2.11	4.12	3.87	3.98	2.85	2.9	3.16	2.27	2.32	2.71
28 days	4.25	3.42	3.09	4.28	4.3	4.39	3.21	3.32	3.65	3.12	3.14	3.4
90 days	4.72	4.06	3.94	4.84	5.06	5.14	4.32	4.51	4.71	4	4.29	4.51
180 days	4.87	4.98	4.78	5.01	5.2	5.31	5.14	5.29	5.45	4.89	5.09	5.22

Figure 8.11: Split tensile strength of concrete samples with 0.5-W/B

Figure 8.12 revealed that FA and *β*-CD had a greater effect in improving the split tensile strength of the 0.5-W/B samples than in the case of their compressive strengths (Figure 8.2), from 28 days curing period, when compared to control samples. The greatest increase in split tensile strength for the 0.5-W/B samples was observed for C0.1CD sample from the 28 days curing age. The results showed that the retarding effect of a higher content of FA and *β*-CD probably favoured the split tensile strengths. If the setting time results from Chapter Seven (Section 7.4.2) are compared with these results, it can be deduced that the higher the FA and *β*-CD contents, the longer the setting time and the better their influence on the split tensile strength.

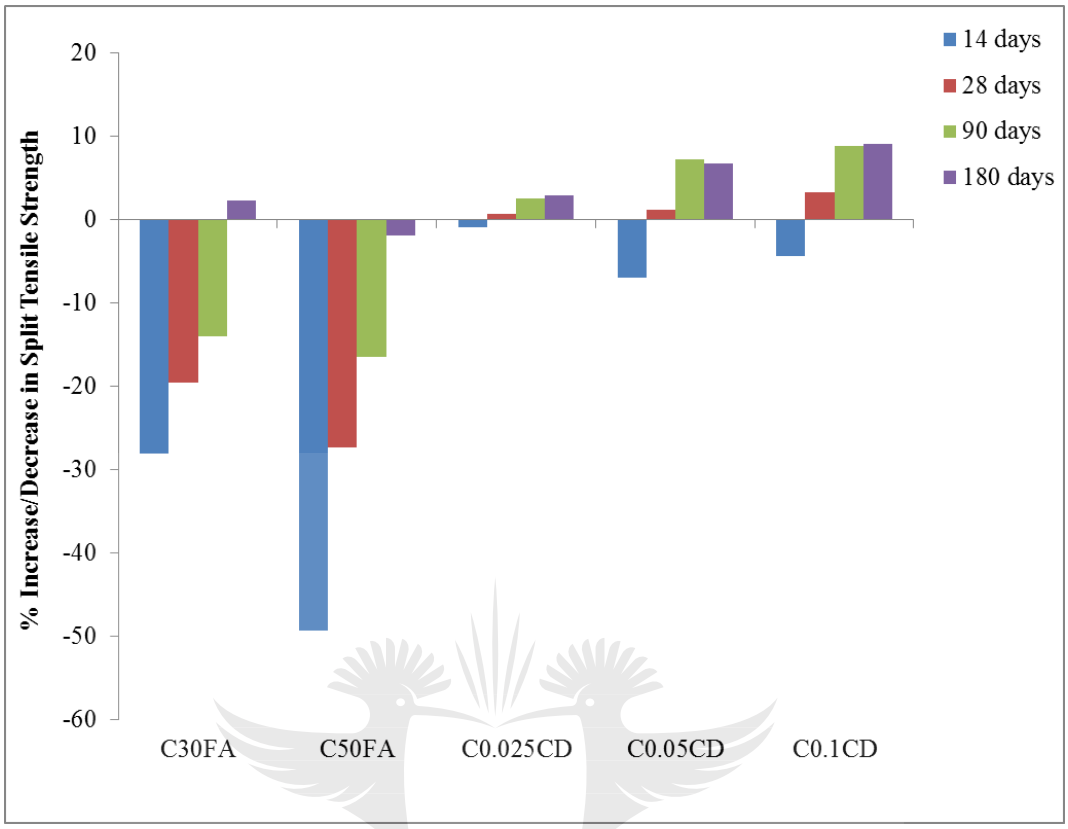

Figure 8.12: Percentage increase/decrease in C30FA, C50FA and *β*-CD samples split tensile strength compared to control sample (C) for 0.5-W/B

The percentage increase/decrease in split tensile strength of the FA-*β*-CD composites samples compared to the control sample with 0.5-W/B, presented in Figure 8.13, prove that FA-*β*-CD composites generally improve split tensile strength more than they improve compressive strength (Figure 8.3). The better effect the FA-*β*-CD on the split tensile strength, compared to compressive strength, was revealed from the 90 days curing period in most composite samples, resulting in all the samples having a higher split tensile strength at the 180 days curing period compared to the control sample, which was not the case for compressive strength (Figure 8.3). Figure 8.13 also showed that 0.1% *β*-CD had a better effect on the split tensile strength than the inclusion of smaller quantities of *β*-CD. The FA-*β*-CD composites samples also showed an improved split tensile strength in comparison with the C30FA and C50FA

samples (Figure 8.12), when compared to control sample. The same trend was identified in the compressive strength test results.

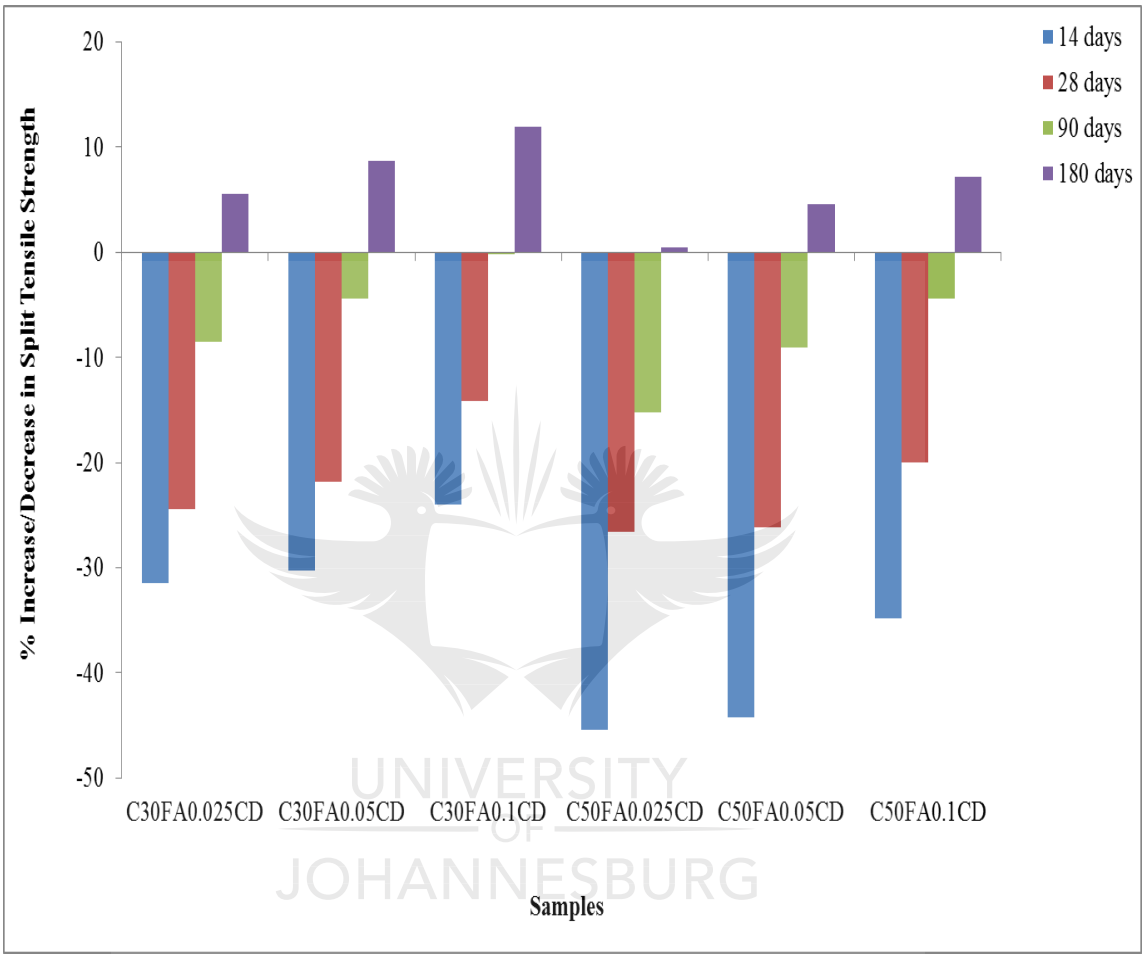

Figure 8.13: Percentage increase/decrease in FA-*β*-CD composites samples split tensile strength compared to control sample for 0.5-W/B

Figures 8.14 and 8.15 show the effect of FA-*β*-CD composites on the pozzolanic split tensile strength of their original C30FA and C50FA samples, respectively. A higher increase in split tensile strength was observed for C30FA0.1CD samples at all curing ages compared to their original C30FA sample. While for C30FA0.025CD and C30FA0.05CD samples, an increase in split tensile strength was observed from the 90 days curing period compared to their original C30FA sample (Figure 8.14). These

observations also confirmed that the higher contents of *β*-CD improved split tensile strength. Figure 8.15 showed a higher increase in split tensile strength for all FA-*β*-CD composites compared to their original C50FA samples, than in the case of the C30FA samples. An increase in split tensile strength was observed for all FA-*β*-CD composites samples compared to the C50FA samples, at all curing ages. The highest increase in split tensile strength was exhibited in C50FA0.1CD. The general trend observed confirmed the compressive strength results that a greater effect of *β*-CD on pozzolanic reaction was observed for samples containing 50% FA (Figure 8.5) than for samples with 30% FA (Figure 8.4).

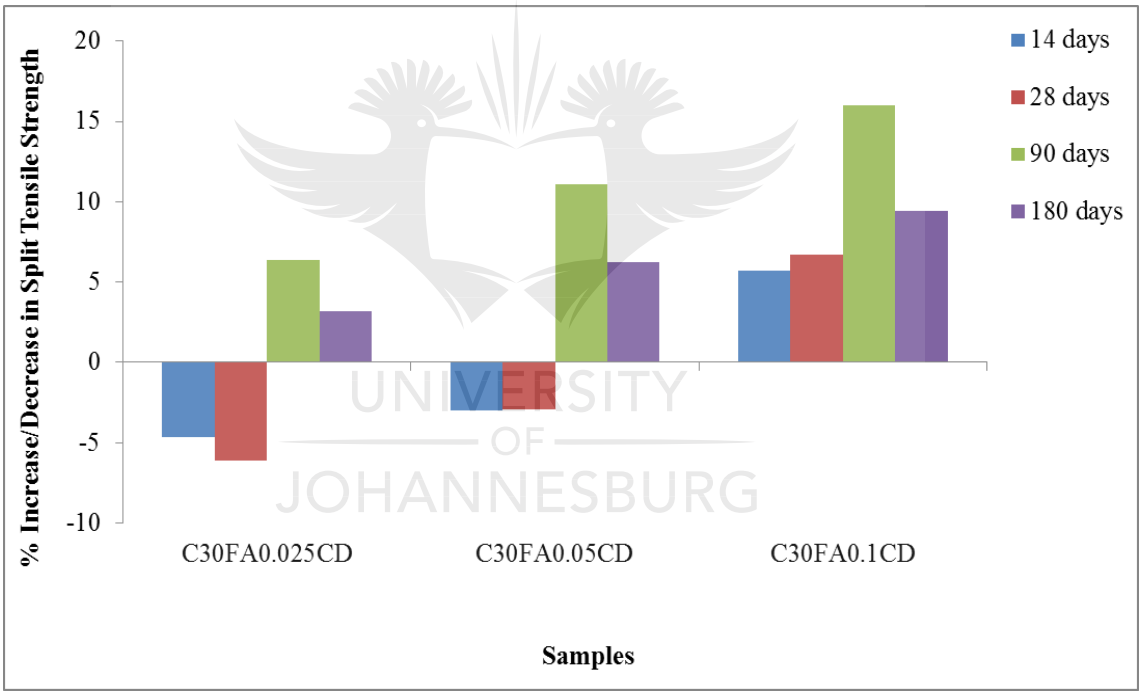

Figure 8.14: Percentage increase/decrease in the split tensile strength of FA-*β*-CD-composite samples compared to C30FA pozzolanic sample for 0.5-W/B

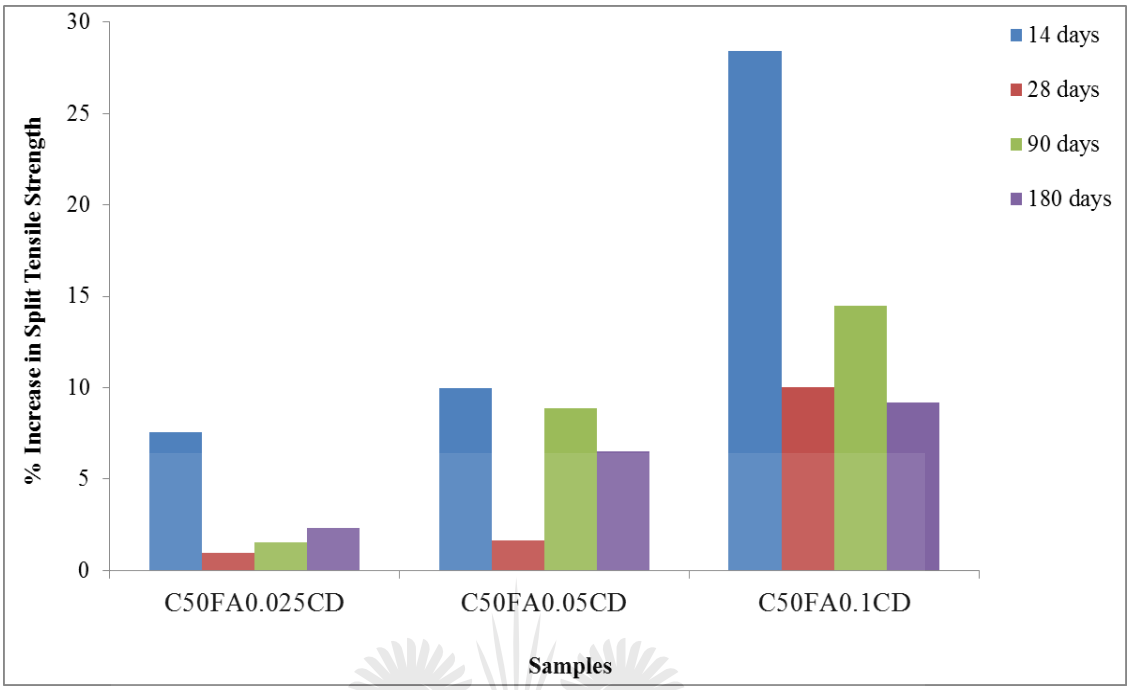

Figure 8.15: Percentage increase in the split tensile strength of FA-β-CD-composite samples compared to C50FA pozzolanic sample for 0.5-W/B

8.4.5 Split tensile strength results for 0.4-W/B samples

The split tensile strength results of 0.4-W/B samples are presented in Figure 8.16. As observed for 0.5-W/B samples, Figure 8.16 shows that the 0.4-W/B samples have a reduced split tensile strengths compared to their compressive strengths (Figure 8.6). However, the split tensile strengths of all the 0.4-W/B samples were slightly higher than the split tensile strength of all the 0.5-W/B samples at all curing ages. Comparing the compressive strength results (Figures 8.1 and 8.6), it can be deduced that the lower the W/B, the higher the compressive and split tensile strengths of the samples. As curing ages increased, an increase in split tensile strengths was observed for all the samples.

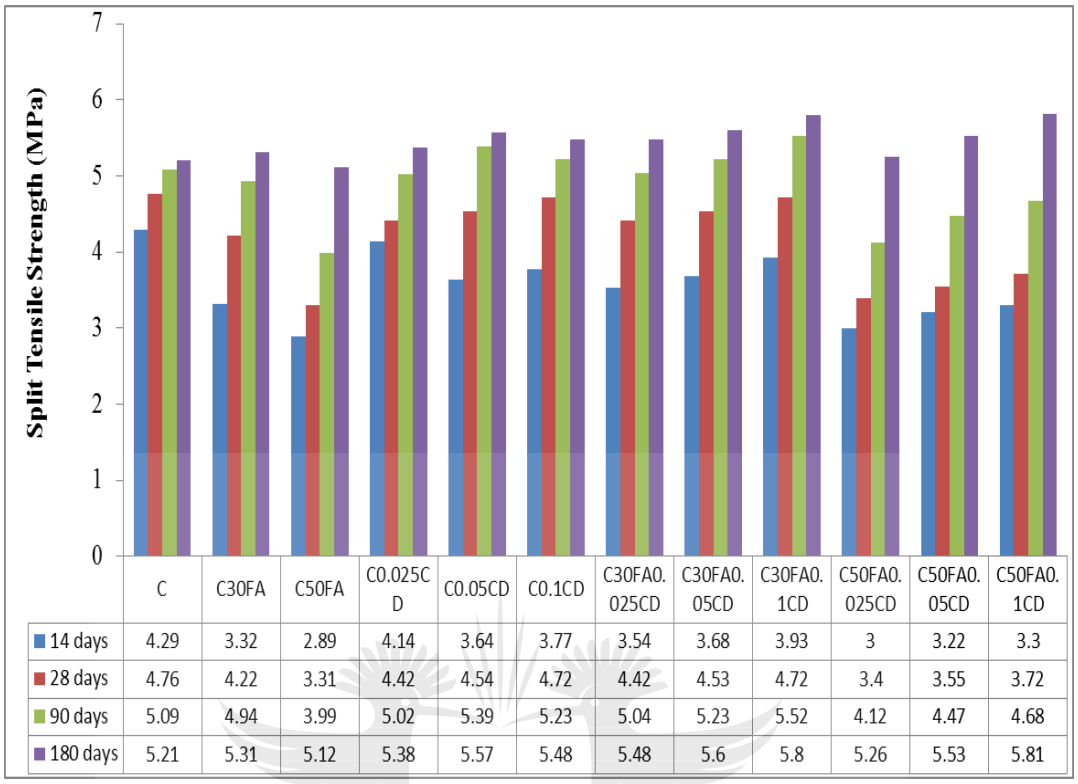

	C	C30FA	C50FA	C0.025CD	C0.05CD	C0.1CD	C30FA0.025CD	C30FA0.05CD	C30FA0.1CD	C50FA0.025CD	C50FA0.05CD	C50FA0.1CD
14 days	4.29	3.32	2.89	4.14	3.64	3.77	3.54	3.68	3.93	3	3.22	3.3
28 days	4.76	4.22	3.31	4.42	4.54	4.72	4.42	4.53	4.72	3.4	3.55	3.72
90 days	5.09	4.94	3.99	5.02	5.39	5.23	5.04	5.23	5.52	4.12	4.47	4.68
180 days	5.21	5.31	5.12	5.38	5.57	5.48	5.48	5.6	5.8	5.26	5.53	5.81

Figure 8.16: Split tensile strength of concrete samples with 0.4-W/B

The effect of FA and *β*-CD in improving split tensile strength on samples with a 0.4-W/B showed a different trend from samples with 0.5-W/B. Figure 8.17 revealed the separate effect of FA and *β*-CD in increasing/decreasing the split tensile strength of 0.4-W/B samples when compared with the control sample. It was observed that the FA had a greater effect in improving split tensile strength of the 0.4-W/B samples than it had on their compressive strengths (Figure 8.7) from the 14 days curing age onwards, when compared with the control sample. However, the *β*-CD showed less improvement of the split tensile strengths (than on compressive strengths) up till 28 days and showed a higher improvement on the split tensile strength of the C0.05CD and C0.1CD samples, (in comparison to their compressive strengths) from the 90 days curing age, when compared with the control samples. In comparing the separate effect of FA and *β*-CD on the increase/decrease of the split tensile strength of the 0.4-W/B and 0.5-W/B, a trend could not be established. However, the C30FA sample

showed a better influence on split tensile strength when compared with the control sample (0.4-W/B) than the C50FA sample. For samples with β-CD, at 14 and 28 days curing ages, the C0.1CD sample showed a better influence on the split tensile strength than the C0.05CD sample, while at 90 and 180 days, the C0.05CD sample showed a better influence on split tensile strength than the C0.025CD and C0.1CD samples, when compared with the control sample (0.4-W/B).

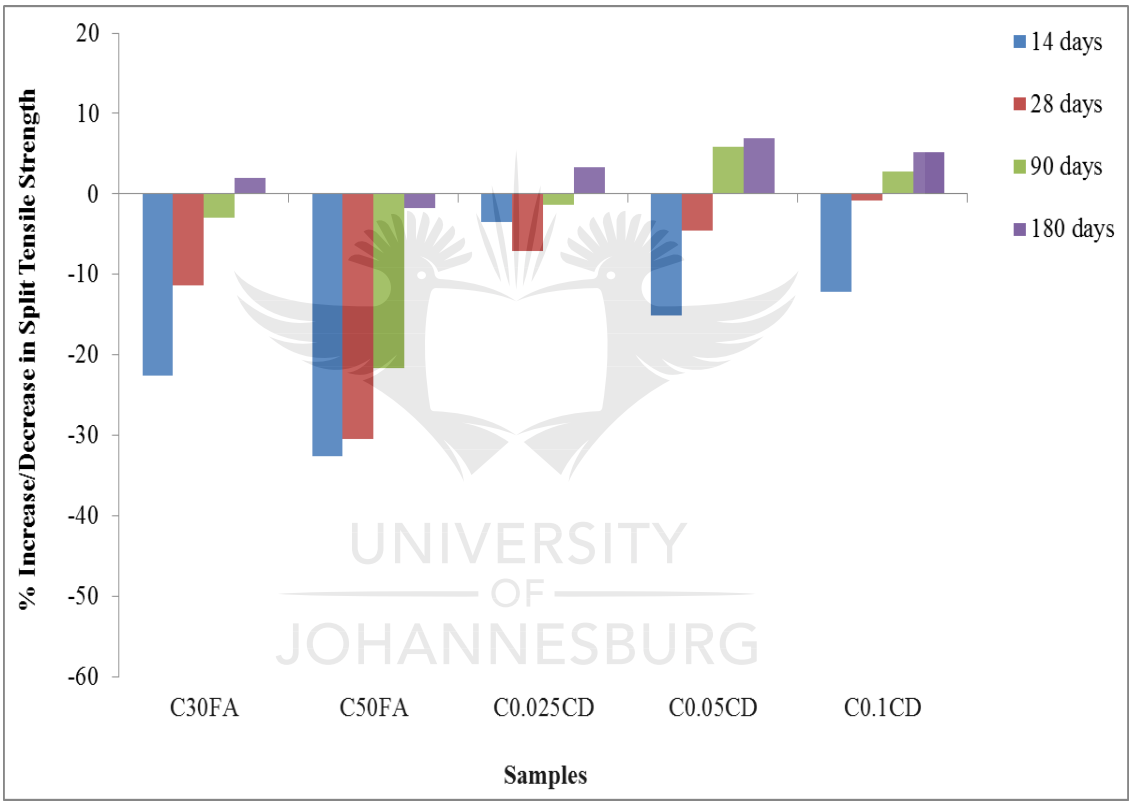

Figure 8.17: Percentage increase/decrease in the split tensile strength of C30FA, C50FA and β-CD samples compared to control sample (C) for 0.4-W/B

The effect of FA-β-CD composites on increasing/decreasing split tensile strength when compared to the 0.4-W/B control sample is presented in Figure 8.18. All the FA-β-CD composites samples with a 0.4-W/B showed a better influence on split tensile strength than on compressive strength (Figure 8.8), at all curing ages. A

similar trend was observed for the FA-β-CD composites samples with a 0.5-W/B (Figure 8.13). It was also revealed that all the FA-β-CD composites samples improved split tensile strength at all curing ages compared to the C30FA and C50FA samples (Figure 8.17) when compared with the 0.4-W/B control samples. The greater the β-CD content used, the better the influence on split tensile strength for all the composite samples. This trend of increased split tensile strength with a concomitant increase in β-CD was also observed for 0.5-W/B composites samples (Figures 8.14 and 8.15). As shown in Figures 8.14 and 8.18 for the 0.5-W/B and 0.4-W/B composite samples, respectively, composites with 30% FA exhibited greater positive influence on split tensile strength than composites with 50% FA for all curing ages, when compared with the control sample. For the 0.4-W/B samples, the C30FA0.05CD and C30FA0.1CD samples showed higher split tensile strength than the control sample from 90 days curing age, while all composites with 50% FA, showed higher split tensile strength than the control sample at 180 days curing age. These observations are in line with the assumption made earlier that the retarding effect of a higher content of β-CD might have favoured the split tensile strengths.

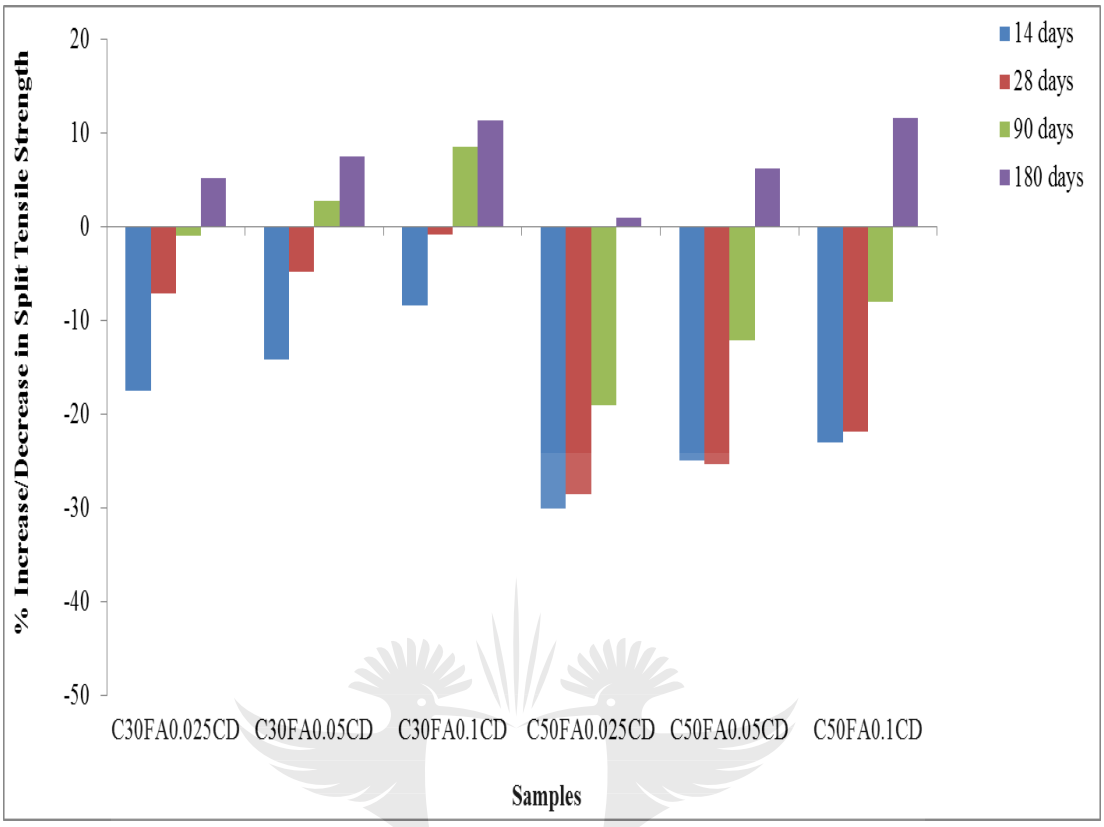

Figure 8.18: Percentage increase/decrease in the split tensile strength of FA-*β*-CD composites samples compared to control sample for 0.4-W/B

The FA-*β*-CD composites showed an increase in split tensile strength (Figures 8.19 and 8.20) of the C30FA and C50FA samples, at all curing ages, with an increase in *β*-CD. The composite samples with 0.4-W/B generally exhibited a better improvement in split tensile strength of their respective C30FA and C50FA samples than the samples with 0.5-W/B (Figures 8.14 and 8.15). The improvement trend shown in Figures 8.19 and 8.20 reveals that the higher the content of *β*-CD, the better the influence it has in improving the pozzolanic split tensile strength of C30FA and C50FA. Samples with 0.1% *β*-CD have a greater improved split tensile strength than samples with 0.025% and 0.05% *β*-CD when compared to both original C30FA and C50FA samples (Figure 8.19 and 8.20). A similar trend was also observed for the

composite samples with 0.5-W/B (Figures 8.14 and 8.15). Composite samples with 0.05% β-CD of both 0.4-W/B and 0.5-W/B showed a better improvement in the pozzolanic compressive strength generally from 28 days curing age onwards than composite samples with 0.025% and 0.1% β-CD (Figures 8.1 and 8.6). A greater influence of the composite samples on split tensile strength was observed with samples with 50% FA (Figure 8.20) than samples with 30% FA (Figure 8.19). This confirms the previous observations for 0.5-W/B and 0.4-W/B samples compressive strengths (Figures 8.4, 8.5, 8.9 and 8.10) and 0.5-W/B samples split tensile strengths (Figure 8.14 and 8.15) that β-CD has greater effect on pozzolanic reaction for samples containing 50% FA than samples with 30% FA.

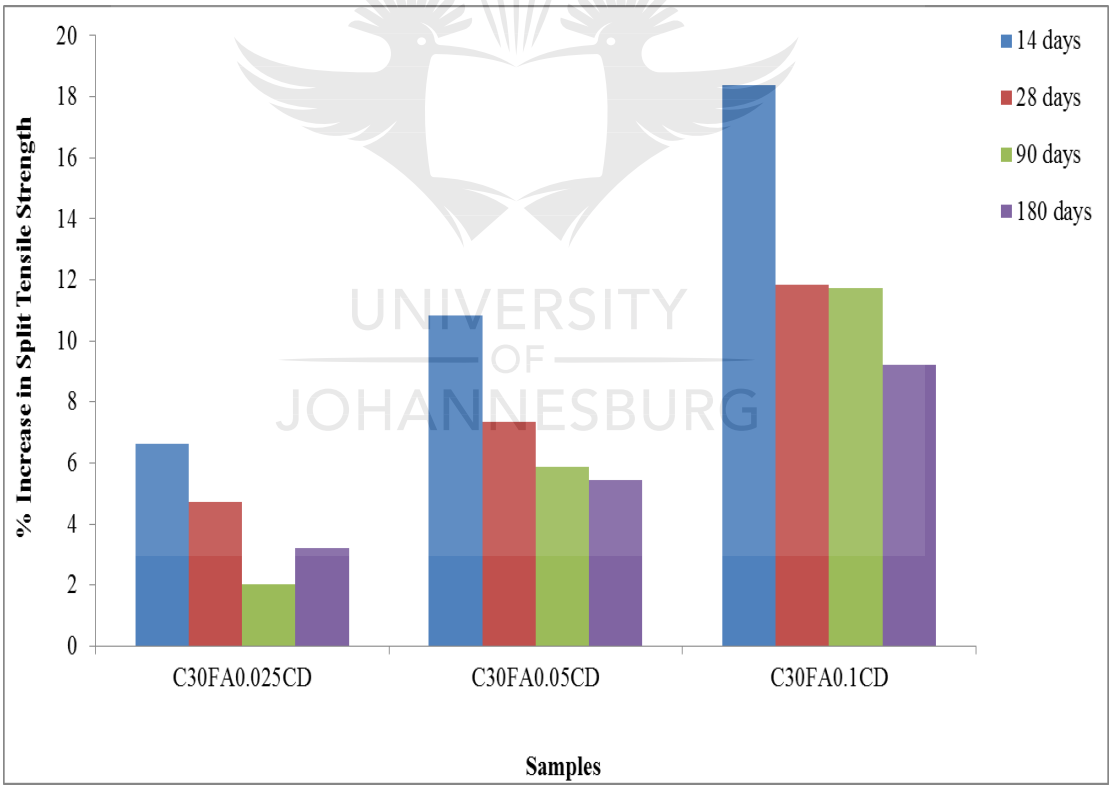

Figure 8.19: Percentage increase in the split tensile strength of FA-β-CD composite samples compared to C30FA pozzolanic sample for 0.4-W/B

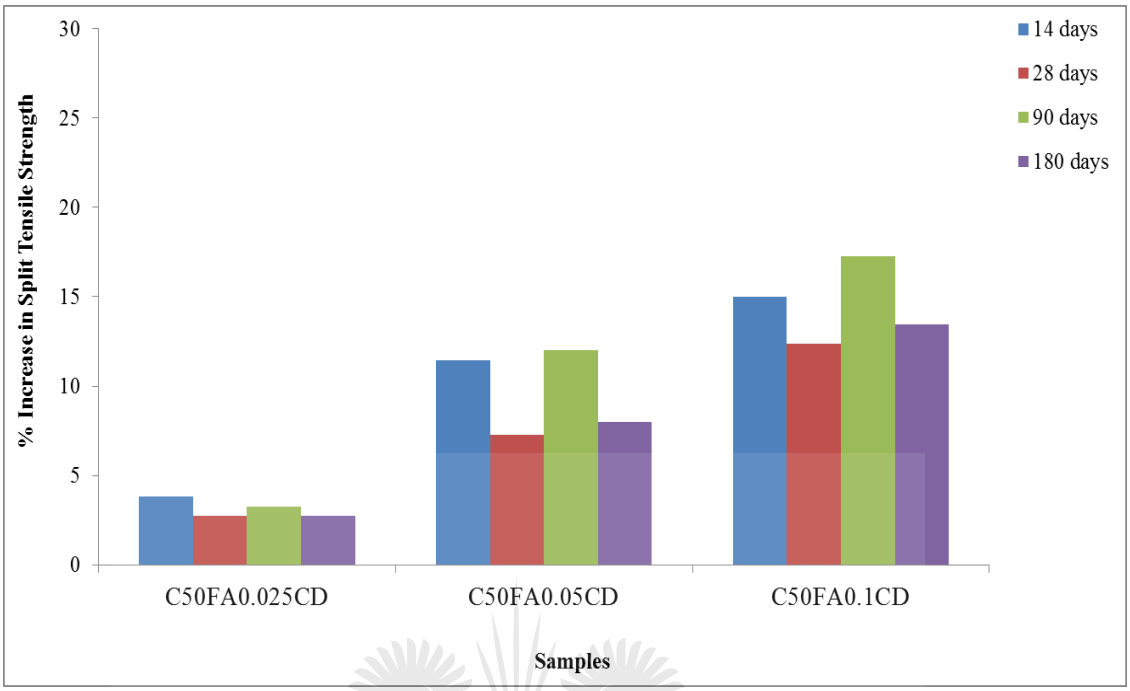

Figure 8.20: Percentage increase in the split tensile strength of FA-β-CD composite samples compared to C50FA pozzolanic sample for 0.4-W/B

8.5 SUMMARY OF INCREASE/DECREASE IN COMPRESSIVE AND SPLIT TENSILE STRENGTHS OF VARIOUS MIXTURES RELATIVE TO THE CONTROL MIXTURE

Table 8.3 summarises the increase/decrease in compressive and split tensile strengths of various mixtures relative to the control mixture. The negative values represent relative decrease while positive values represent relative increase. The best results of the mixtures in columns are highlighted in grey, while the worst result of the mixtures in columns are highlighted in yellow.

Table 8.3: Summary of increase/decrease in compressive and split tensile strengths of various mixtures relative to the control mixture

Mixtures	Compressive Strength										Split Tensile Strength							
	0.5-W/B					0.4-W/B					0.5-W/B				0.4-W/B			
	7 d	14 d	28 d	90 d	180 d	7 d	14 d	28 d	90 d	180 d	14 d	28 d	90 d	180 d	14 d	28 d	90 d	180 d
C30FA	- 46.9	- 24.97	- 29.69	- 15.53	- 7.12	- 32.48	- 28.70	- 21.99	- 3.13	+ 3.31	- 28.13	- 19.53	- 13.98	+ 2.26	- 22.61	- 11.34	- 2.95	+ 1.92
C50FA	- 62.9	- 58.71	- 57.08	- 38.69	- 21.38	- 56.97	- 50.20	- 42.61	- 37.89	- 19.84	- 49.28	- 27.29	- 16.53	- 1.85	- 32.63	- 30.46	- 21.61	- 1.73
C0.025CD	+ 6.36	+ 4.27	- 1.40	- 0.49	- 0.94	+ 3.60	+ 1.01	+ 4.46	+ 1.48	+ 0.29	- 0.96	+ 0.71	+ 2.54	+ 2.87	- 3.50	- 7.14	- 1.38	+ 3.26
C0.05CD	+ 9.95	+ 7.11	+ 0.37	+ 0.91	+ 5.61	+ 6.05	+ 3.22	+ 7.17	+ 4.18	+ 5.48	- 6.97	+ 1.18	+ 7.20	+ 6.78	- 15.15	- 4.62	+ 5.89	+ 6.91
C0.1CD	- 1.54	+ 1.44	- 3.29	+ 0.66	+ 3.26	+ 4.60	+ 1.56	+ 6.18	+ 2.38	+ 2.61	- 4.33	+ 3.29	+ 8.90	+ 9.03	- 12.12	- 0.84	+ 2.75	+ 5.18
C30FA0.025 CD	- 29.17	- 17.34	- 20.88	- 10.05	- 1.11	- 31.90	- 28.20	- 18.17	+ 0.23	+ 4.53	- 31.49	- 24.47	- 8.47	+ 5.54	- 17.48	- 7.14	- 0.98	+ 5.18
C30FA0.05C D	- 31.13	- 10.86	- 15.72	- 2.31	+ 2.37	- 29.33	- 23.91	- 13.61	+ 3.01	+ 6.62	- 30.29	- 21.88	- 4.45	+ 8.62	- 14.22	- 4.83	+ 2.75	+ 7.49
C30FA0.1CD	- 18.58	- 12.24	- 16.69	- 8.03	+ 1.20	- 30.44	- 25.88	- 16.14	+ 1.21	+ 5.77	- 24.04	- 14.12	- 0.21	+ 11.91	- 8.39	- 0.84	+ 8.45	+ 11.32
C50FA0.025 CD	- 51.17	- 51.33	- 47.99	- 33.65	- 14.30	- 56.57	- 47.99	- 37.20	- 33.16	- 15.31	- 45.43	- 26.59	- 15.25	+ 0.41	- 30.07	- 28.57	- 19.06	+ 0.96
C50FA0.05C D	- 46.21	- 43.64	- 30.08	- 26.33	- 7.52	- 53.30	- 43.35	- 34.30	- 29.83	- 12.52	- 44.23	- 26.12	- 9.11	+ 4.51	- 24.94	- 25.42	- 12.18	+ 6.14
C50FA0.1CD	- 48.17	- 50.12	- 36.70	- 28.50	- 11.57	- 55.87	- 46.22	- 35.98	- 32.02	- 14.18	- 34.86	- 20.00	- 4.45	+ 7.19	- 23.08	- 21.85	- 8.06	+ 11.52

8.6 CONCLUSIONS

The effect of FA, β-CD and FA- β-CD composites on concrete workability and strength was studied in this chapter. The results showed that the higher the contents of FA and β-CD, as used in this study, the greater the workability of the concrete for both 0.5-W/B and 0.4-W/B mixtures. The influence of FA, β-CD and FA-β-CD composites on hydration and pozzolanic reactions as reported in Chapter Six contributed to the observed results in this chapter. A progressive increase in both compressive strength and split tensile strength was observed for all the samples as curing ages increased. The 0.4-W/B samples had higher compressive and split tensile strengths compared to the samples with a 0.5-W/B, at all curing ages. The C30FA sample, showed a 3.31% increase in the case of the 0.4-W/B when compared with the compressive strength of the control sample at the 180 days curing age. However, C50FA sample with 0.4-W/B had a lower compressive strength at all curing ages with 19.84% decrease at 180 days curing age than the control sample. The β-CD increased both compressive and split tensile strengths of the control, C30FA and C50FA samples for both 0.5-W/B and 0.4-W/B. The presence of β-CD substantially increased the compressive strength for samples with 0.05% β-CD and, split tensile strength for samples with 0.1% β-CD.

8.7 REFERENCES

[1] Ravina D., Mehta P.K.: Compressive strength of low cement/high fly ash concrete. Cement and concrete research **18**, 571-583 (1988).

[2] Siddique R.: Performance characteristics of high-volume Class F fly ash concrete. Cement and Concrete Research **34,** 487–493 (2004).

[3] Yasar E., Erdogan Y., Kılıc A.: Effect of limestone aggregate type and water–cement ratio on concrete strength. Materials Letters **58,** 772– 777 (2004).

[4] Yılmaz M., Tugrul A.: The effects of different sandstone aggregates on concrete strength. Construction and Building Materials **35**, 294–303 (2012).

[5] Gayarre F.L., Pérez C.L., López M.A.S., Cabo A.D.: The effect of curing conditions on the compressive strength of recycled aggregate concrete. Construction and Building Materials **53,** 260–266 (2014).

[6] Kaikea A., Achoura D., Duplan F., Rizzuti L.: Effect of mineral admixtures and steel fiber volume contents on the behavior of high performance fiber reinforced concrete. Materials and Design **63** 493–499 (2014).

[7] Prommas R., Rungsakthaweekul T.: Effect of Microwave Curing Conditions on High Strength Concrete Properties. Energy Procedia **56**, 26 – 34 (2014).

[8] Beushausen H., Dittmer T.: The influence of aggregate type on the strength and elastic modulus of high strength concrete. Construction and Building Materials **74** 132–139 (2015).

[9] SANS 5862-1:2006, Concrete tests-consistence of freshly mixed concrete – slump test, Pretoria: South Africa Bureau of Standards.

[10] SANS 5863:2006 Concrete tests-compressive strength of hardened concrete, Pretoria: South Africa Bureau of Standards.

[11] SANS 6253:2006 Concrete tests-tensile splitting strength of concrete. Pretoria: South Africa Bureau of Standards.

[12] Lachemi M., Hossain K.M.A., Lambros V., Nkinamubanzi P.-C., Bouzoubaa N.: Performance of new viscosity modifying admixtures in enhancing the rheological properties of cement paste. Cement and Concrete Research **34** 185–193 (2004).

[13] Papadakis V.G.: Effect of fly ash on Portland cement systems Part I. Low-calcium fly ash. Cement and Concrete Research **29,** 1727–1736 (1999).

[14] Fu X., Chung D.D.L.: Improving the bond strength between steel rebar and concrete by increasing the water/cement ratio. Cement and Concrete Research. **27**(12), 1805-1809 (1997).

[15] Kharita M.H., Yousef S., AlNassar M.: The effect of the initial water to cement ratio on shielding properties of ordinary concrete. Progress in Nuclear Energy **52,** 491–493 (2010).

[16] Rahmani K., Shamsai A., Saghafian B., Peroti S.: Effect of Water and Cement Ratio on Compressive Strength and Abrasion of Microsilica Concrete. Middle-East Journal of Scientific Research **12** (8): 1056-1061 (2012).

[17] Sata V., Tangpagasit J., Jaturapitakkul C., Chindaprasirt P.: Effect of W/B ratios on pozzolanic reaction of biomass ashes in Portland cement matrix. Cement and Concrete Composites **34**. 94–100 (2012).

[18] Wang G., Kong Y., Sun T., Shui Z.: Effect of water–binder ratio and fly ash on the homogeneity of concrete. Construction and Building Materials **38**, 1129–1134 (2013).

CHAPTER NINE

THE EFFECT OF FLY ASH, *β*-CYCLODEXTRIN AND FLY ASH-*β*-CYCLODEXTRIN COMPOSITES ON CONCRETE DURABILITY

9.1 INTRODUCTION

Durability is an important property that determines the serviceability of a concrete structure. A durable concrete should be dense enough to limit the ingress of water or chemicals which could enter the concrete through permeation, absorption and diffusion. According to Heede et al [1], the best way to study concrete durability is to study the parameters that influence the deterioration process. These parameters are the ones related to the transportation mechanisms. The durability index tests used in this study are based on three transportation mechanisms; permeation for oxygen permeability, absorption for water sorptivity, and diffusion for chloride conductivity. These three durability index tests were developed by Alexander and co-researchers [2-4]. The study of the effect of fly ash (FA), *β*-cyclodextrin (*β*-CD) and fly ash-*β*-cyclodextrin (FA-*β*-CD) composites on concrete durability, which is presented and discussed in this chapter is based on the indicative tests reported in Chapter Five and subsequent behaviour of FA, *β*-CD and FA-*β*-CD composites on microstructure reported in Chapter Six.

9.2 MATERIALS AND MIXES

Cement (CEM 1 52.5N), FA, *β*-CD, granite crusher sand and coarse aggregate as explained in Section 5.2 were used. The composite preparation explained in Section 8.2 and the sample descriptions presented in Table 6.2 were followed. The mixing and casting procedures were the same as explained in Section 5.2.1. A total of 24 mixtures were produced, 12 mixtures for each of the 0.4 and 0.5-W/Bs. The mixture proportions presented in Tables 8.1 and 8.2 were used. Eight cubes (100 x 100 mm)

were produced for each mixture resulting to the total of 192 cubes for the durability index tests. A total of 16 discs, each having a diameter of 68 mm and thickness of 30 ± 2 mm, were core drilled from the eight cubes for each mixture after being cured for 28 and 90 days. Eight discs were used for permeability and sorptivity tests while eight discs were used for chloride conductivity test (per mixture). Four discs for permeability/sorptivity and four discs for chloride conductivity were tested at each curing age per mixture; the disc samples were preconditioned in an oven at 50 ^{0}C for 7 days before testing.

9.3 EXPERIMENTAL PROCEDURE

9.3.1 Permeability

The permeability test was performed as explained in Section 5.3.3.1.

9.3.2 Sorptivity and porosity tests

The sorptivity and porosity tests were performed as explained in Section 5.3.3.2.

9.3.3 Chloride conductivity Index test (CCI)

The discs samples were preconditioned in an oven at 50 ^{0}C for 7 days, as for permeability and sorptivity tests. The preconditioned samples were allowed to cool for two hours. The samples were then subjected to a vacuum saturation in a 5M NaCl solution for four hours and allowed to soak for another 18 hours. Each sample was then placed in a rubber collar contained within a rigid plastic ring. The anode and the cathode chambers were filled with salt solution; these chambers were then screwed to the rigid plastic ring such that no solution leaked from the conduction cell. The conduction cell was then connected to the ammeter and voltmeter after being placed horizontally. To accelerate the movement of chloride ions, a 10 Volt (V) potential difference was applied across the sample and at the same time, the current flowing through the concrete sample was measured. The test setup is shown in Figure 9.1.

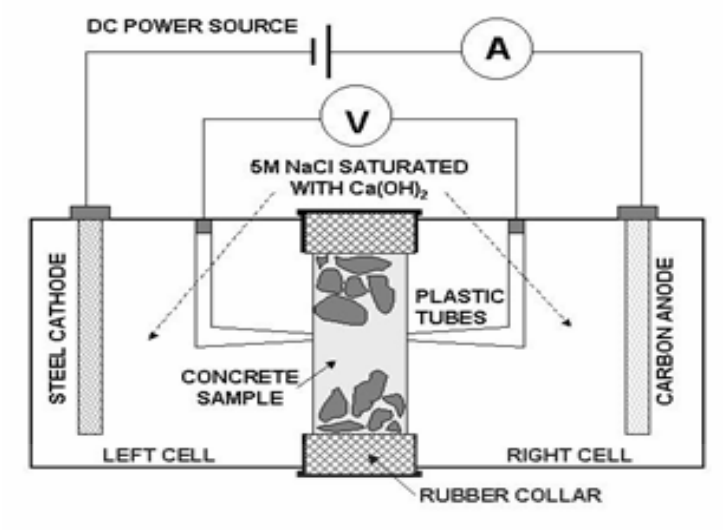

Figure 9.1: Chloride conductivity test apparatus [3]

The chloride conductivity, σ (mS/cm) was calculated from Equation (9.1).

$$\sigma = \frac{it}{VA} \tag{9.1}$$

where:

i = electric current (mA)

t = sample thickness (cm)

V = voltage difference (V)

A = cross section area of sample (cm^2)

The results recorded were the average of four discs.

Equations (9.2) and (9.3) were used in calculating the percentage decrease or increase in the permeability, sorptivity, porosity or chloride conductivity (PSPC). A positive value indicates an increase in the permeability, sorptivity, porosity or chloride

conductivity (PSPC), while a negative value indicates a decrease in the permeability, sorptivity, porosity or chloride conductivity (PSPC).

$$\%increase/decrease\ (ref.control) = \frac{other\ samples\ PSPC - control\ PSPC}{control\ PSPC} x\,100 \tag{9.2}$$

$$\%increase/decrease\ (ref.FA\ pozzolanic) = \frac{FA - \beta CD\ composite\ PSPC - FA\ pozzolanic\ PSPC}{FA\ pozzolanic\ PSPC} x\,100 \tag{9.3}$$

9.4 RESULTS AND DISCUSSION

9.4.1 Permeability results for 0.5-W/B samples

The permeability behaviour of concrete samples is related to the pore connectivity of the samples [5]. The oxygen permeability index (OPI) values of the 0.5-W/B samples are presented in Table 9.1. It is evident that the samples had a good to excellent permeability at both curing ages except in the case of the samples with 0.1% β-CD. The samples (with 0.1% β-CD) OPI and coefficient of permeability showed invalid, meaning that some of the discs did not give interpretable results, therefore the average results could not be recorded rendering the overall results invalid. The samples with 0.1% β-CD will further be excluded in the permeability discussion. This behaviour was also observed while indicative tests were performed with concrete samples having 0.1% and 0.2% β-CD, which was reported in Chapter Five (Section 5.4.4). Permeability results of these indicative concrete samples could not be discussed for the same reason. The SEM results on cement pastes discussed in Chapter Six revealed that the samples with 0.1% β-CD had a less compacted surface than their respective samples at both 28 and 90 days hydration periods (Figures 6.6 and 6.7). These morphology observations might have also contributed to poor permeability of these samples leading to invalid results. In Table 9.1, the samples with FA showed a better

permeability indication than the control sample. An increased better permeability indication, compared to the samples with FA, was observed for composite samples with 0.025% β-CD.

Table 9.1: Oxygen permeability index (OPI) values for 0.5-W/B samples

	28 days	**Variability check**	**90 days**	**Variability check**
C	9.84	Good	9.95	Good
C30FA	9.95	Good	10.16	Excellent
C50FA	9.85	Good	10.26	Excellent
C0.025CD	9.73	Good	9.96	Good
C0.05CD	9.84	Good	9.90	Good
C0.1CD	Invalid	Invalid	Invalid	Invalid
C30FA0.025CD	10.21	Excellent	10.24	Excellent
C30FA0.05CD	9.99	Good	9.99	Good
C30FA0.1CD	Invalid	Invalid	Invalid	Invalid
C50FA0.025CD	10.07	Excellent	10.40	Excellent
C50FA0.05CD	10.25	Excellent	10.53	Excellent
C50FA0.1CD	9.10	Poor	Invalid	Invalid

The coefficient of permeability results of the 0.5-W/B samples, as shown in Figure 9.2, revealed a decrease in permeability with increased curing age for all the samples. This is an indication that as hydration progressed the concrete became denser and reduce the amount of continuous pores where most of the flow would pass. As indicated in the OPI results, FA and FA-β-CD composite samples showed decreased permeability at both curing ages compared to the control sample. However, the presence of β-CD in plain concrete increased the permeability compared to the control sample.

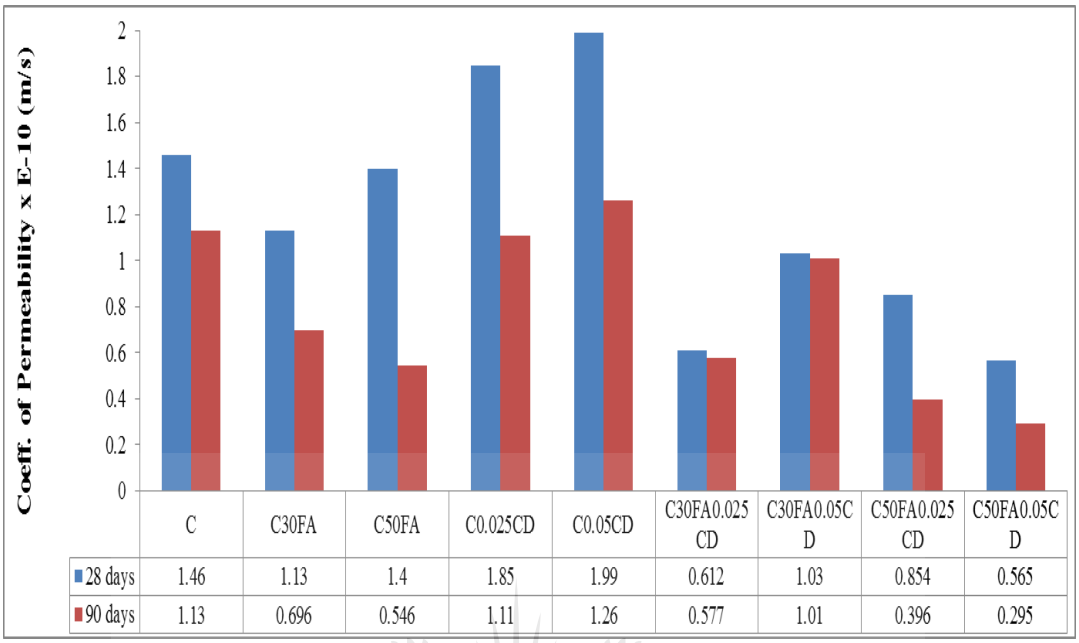

	C	C30FA	C50FA	C0.025CD	C0.05CD	C30FA0.025 CD	C30FA0.05C D	C50FA0.025 CD	C50FA0.05C D
28 days	1.46	1.13	1.4	1.85	1.99	0.612	1.03	0.854	0.565
90 days	1.13	0.696	0.546	1.11	1.26	0.577	1.01	0.396	0.295

Figure 9.2: Coefficient of permeability of 0.5-W/B samples

Figure 9.3 shows the percentage increase/decrease in C30FA, C50FA, *β*-CD and FA-*β*-CD composite samples permeabilities compared to the control sample (C) for 0.5-W/B. It was observed that at the 28 days curing period, the C30FA sample had a greater decrease in permeability compared to the C50FA sample (when compared to the control sample), but at the 90 days curing period, the C50FA decreased permeability better than the C30FA, when compared with the control sample. An increased permeability was observed for the samples with *β*-CD with a lower increase in sample with 0.025% *β*-CD than in the sample with 0.05% *β*-CD, when compared with the control sample. The FA-*β*-CD composite samples containing 30% FA showed a decreased permeability at both curing ages with the 0.025% *β*-CD, while with 0.05% *β*-CD, it exhibited a decreased permeability compared to the comparative C30FA sample at the 28 days curing age (when compared with the control sample). The FA-*β*-CD composite samples containing 50% FA revealed a decrease in permeability at both curing ages in comparison with the C50FA sample, when compared with the control sample. However, the C50FA0.05CD showed a greater

decrease in permeability at both curing ages than the C50FA0.025CD sample. The better influence of FA on the permeability at 90 days curing age, compared to the 28 days curing age, can be linked to the slower pozzolanic reaction, which only had a visible effect on the concrete properties after 28 days curing age as revealed in the XRD, FTIR and SEM results discussed in Chapter Six.

The results observed can also be related to the morphologies of the sample pastes as shown by the SEM results discussed in Chapter Six. Evidence of pozzolanic reaction was observed from the 28 days hydration period, the SEM results (Figure 6.6) revealed breaking of FA particles, resulting in smaller particle sizes and a denser surface at the 28 days hydration period. Further reduced capillary pores were evident in C30FA sample compared to the control sample at the 90 days hydration period (Figure 6.7). The denser surface, reduction in particle sizes and capillary pores, which was evident in the SEM results for the FA samples from the 28 and 90 days hydration periods, respectively, could have resulted in the decrease in permeability observed for the FA samples compared to the control sample (shown in Figures 9.2 and 9.3).

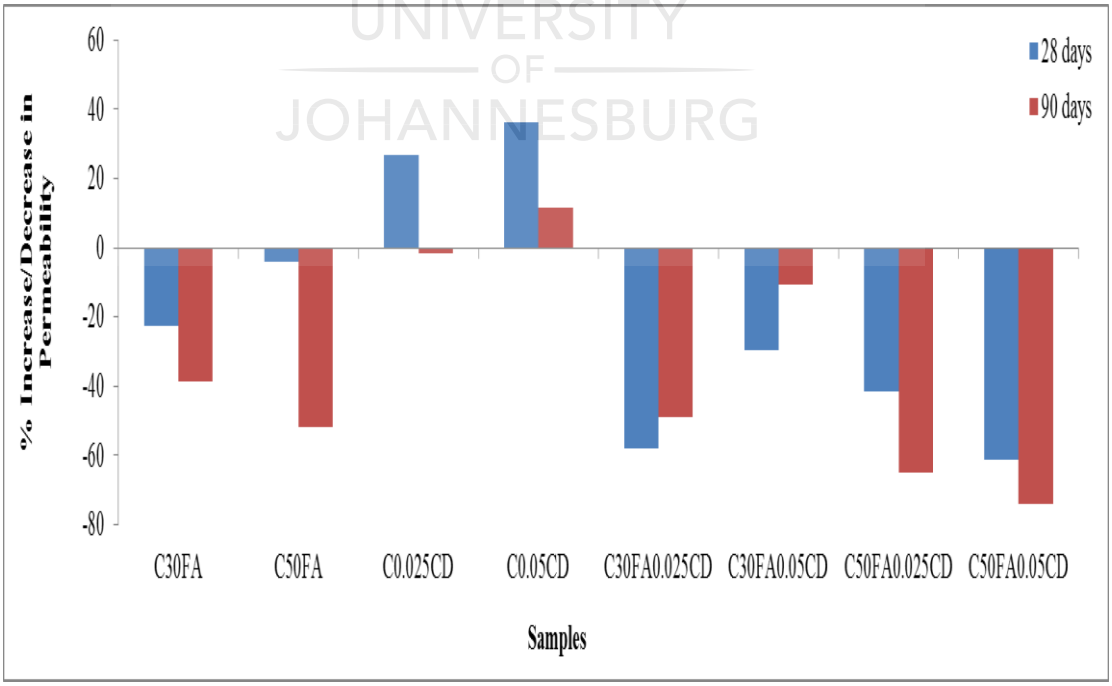

Figure 9.3: Percentage increase/decrease in the permeability of C30FA, C50FA, *β*-CD and FA-*β*-CD-composite samples compared to control sample (C) for 0.5-W/B

The effects of the FA-*β*-CD composite samples on the permeability of their comparative C30FA and C50FA samples (0.5-W/B) are presented in Figures 9.4 and 9.5, respectively. The FA-*β*-CD composite samples improved the permeability of their comparative C30FA and C50FA samples by decreasing the coefficient of their permeabilities at both curing ages, except for C30FA0.05CD sample, where an increase in permeability was observed at the 90 days curing age, when compared with the comparative C30FA sample. This positive effect of the FA-*β*-CD composite samples on the permeability of their comparative C30FA and C50FA samples can be attributed to the improved denser morphology observed for FA-*β*-CD composite samples from 28 days hydration period (Figure 6.6).

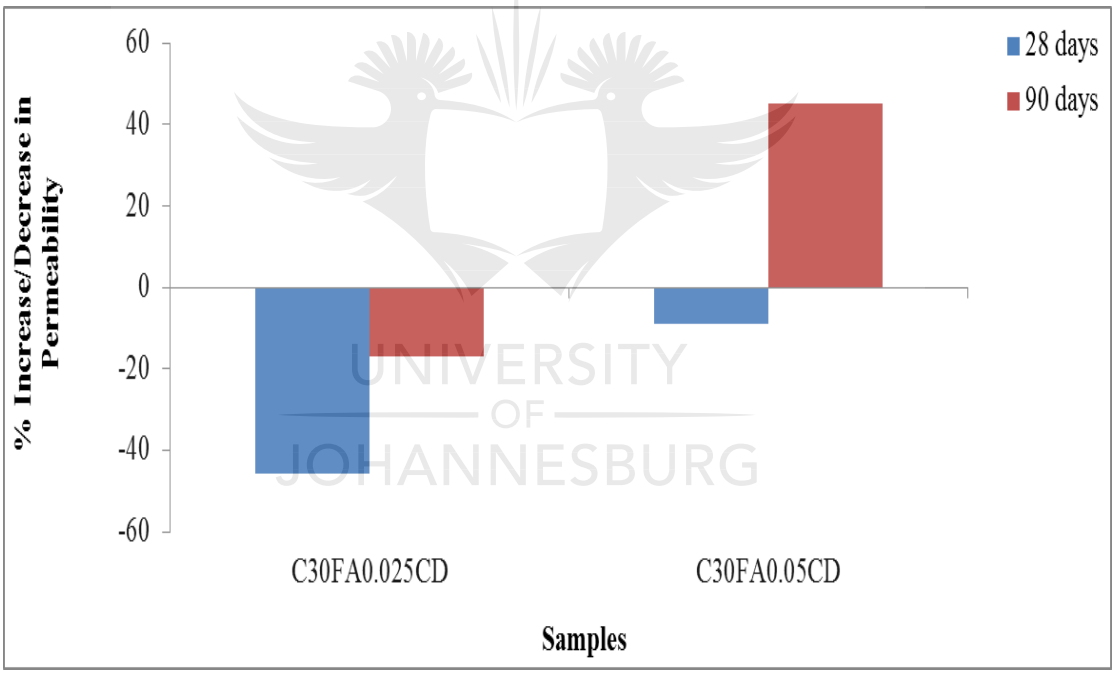

Figure 9.4: Percentage increase/decrease in the permeability of FA-*β*-CD-composite samples compared to C30FA pozzolanic sample for (0.5-W/B)

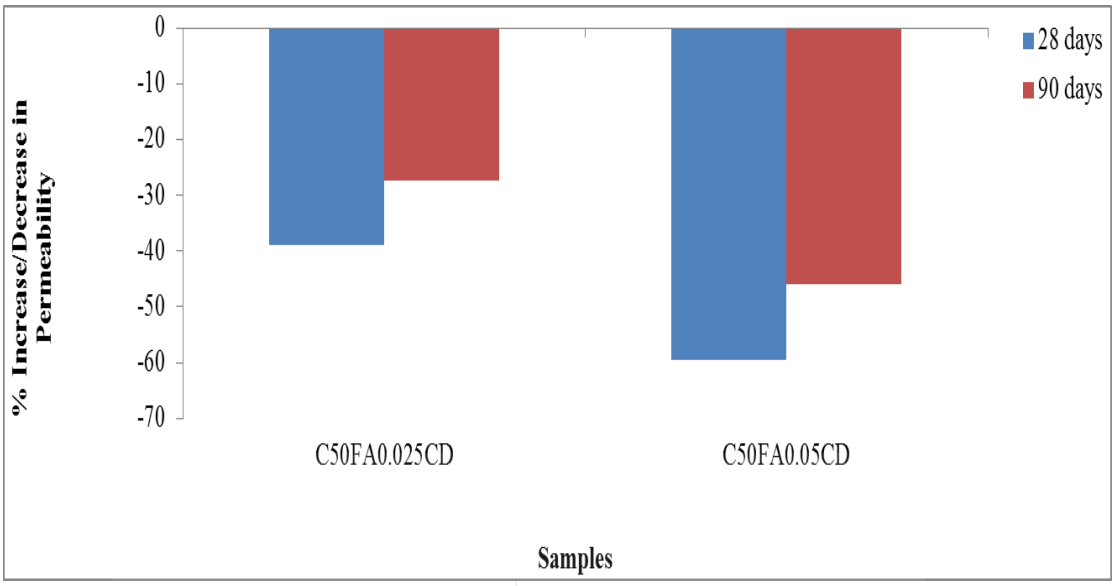

Figure 9.5: Percentage increase/decrease in the permeability of FA-β-CD-composite samples compared to C50FA pozzolanic sample (0.5-W/B)

9.4.2 Permeability results for 0.4-W/B samples

Table 9.2 presents the OPI values of 0.4-W/B samples. The trend observed for 0.5-W/B samples was also observed for 0.4-W/B samples. The durability indication of all the samples range between good and excellent except in the case of the samples with 0.1% β-CD, which revealed invalid OPI values, as seen in 0.5-W/B samples. The possible explanation for this has been discussed in Section 9.4.1. As stated for 0.5-W/B samples, the samples with 0.1% β-CD will further be excluded in the permeability discussion because of these invalid results. The samples with FA and 0.025% β-CD revealed a better permeability indication than the control samples. Generally, the 0.4-W/B samples showed a better permeability than the 0.5-W/B samples except for few exceptions. The FA-β-CD composite samples containing 50% FA for 0.4-W/B revealed a lower permeability than the samples with the 0.5-W/B at both curing ages; also, the control sample and the C0.05CD sample for 0.4-W/B had a lower permeability than their corresponding samples with 0.5-W/B at 90 days curing age.

Table 9.2: Oxygen permeability index (OPI) values for 0.4-W/B samples

	28 days	**Variability check**	**90 days**	**Variability check**
C	9.88	Good	9.89	Good
C30FA	9.99	Good	10.43	Excellent
C50FA	10.51	Excellent	10.76	Excellent
C0.025CD	9.77	Good	10.03	Excellent
C0.05CD	9.73	Good	9.85	Good
C0.1CD	Invalid	Invalid	Invalid	Invalid
C30FA0.025CD	10.28	Excellent	10.42	Excellent
C30FA0.05CD	9.95	Good	10.06	Excellent
C30FA0.1CD	Invalid	Invalid	Invalid	Invalid
C50FA0.025CD	9.96	Good	10.08	Excellent
C50FA0.05CD	10.15	Excellent	10.23	Excellent
C50FA0.1CD	Invalid	Invalid	Invalid	Invalid

A decrease in permeability at increased curing age was observed for all the 0.4-W/B samples as shown in Figure 9.6. The FA and FA-β-CD composite samples had a positive effect on permeability; decreased permeability was observed for these samples at both curing ages, when compared with the control sample. The C50FA sample showed a greater decrease in permeability than C30FA sample. As observed for the 0.5-W/B samples, increased permeability was observed for sample containing 0.05 % β-CD in plain concrete at both curing ages. The sample with 0.025% β-CD in plain concrete showed an increase in permeability at the 28 days curing age and lower permeability at 90 days curing age when compared with the control sample.

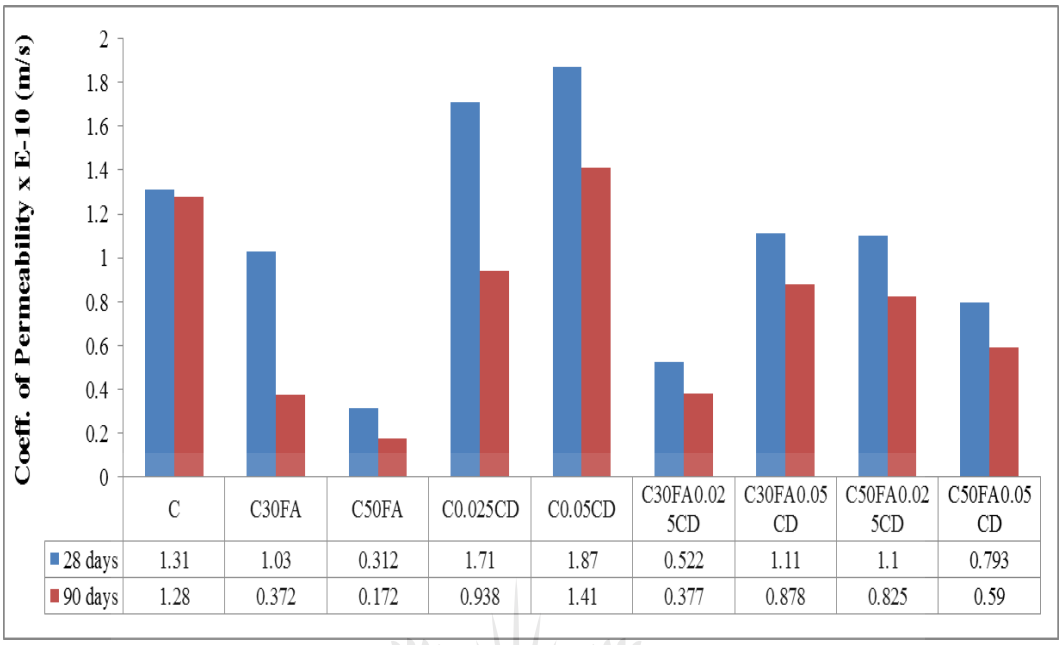

Figure 9.6: Coefficient of permeability of 0.4-W/B samples

The FA and FA-*β*-CD composite samples decreased permeability at both curing ages, when compared with the control sample (C) for 0.4-W/B, as revealed in Figure 9.7. This trend was also observed for 0.5-W/B (Figure 9.3). However, the FA and FA-*β*-CD composite samples (with 30% FA) had a greater influence in decreasing the permeability of the 0.4-W/B control sample than the 0.5-W/B control sample. The C50FA sample showed a greater decrease in permeability at both curing ages than the C30FA sample, when compared with the control sample (for 0.4-W/B). The FA-*β*-CD composite samples with 50% FA showed a decrease in permeability at both curing ages when compared with the control sample but a greater decrease was observed for C50FA sample. A greater decrease in permeability was observed for C30FA0.025CD sample at 28 days curing age than in the C30FA sample when compared with the control sample (for 0.4-W/B). The influence of 0.025CD on permeability was better for the 0.4-W/B than for 0.5-W/B, as decreased permeability was observed for C0.025CD sample at the 90 days curing age when compared with the control sample (for 0.4-W/B), and this was not the case for 0.5-W/B sample. Generally, the FA and

FA-β-CD composite samples had a better influence on concrete permeability at the 90 days curing age than at the 28 days curing age; this is attributed to slower pozzolanic reaction in these samples. The positive effect of FA and FA-β-CD composite samples on concrete permeability, as compared with the control sample, is also linked to their surface morphologies as revealed in the SEM results discussed in Chapter Six and elaborated in Section 9.4.1.

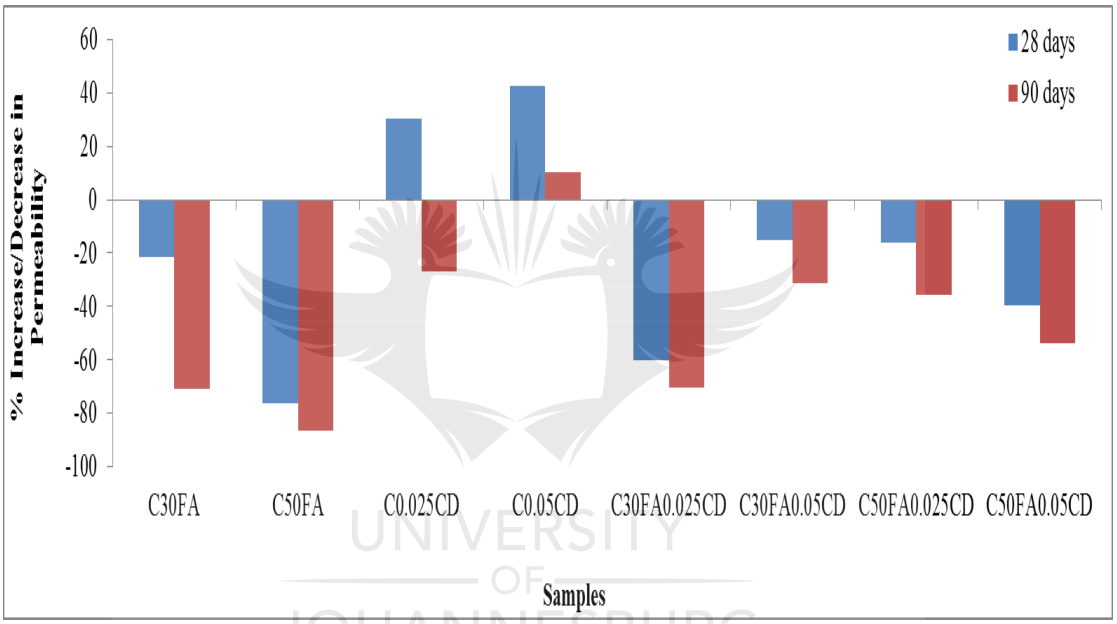

Figure 9.7: Percentage increase/decrease in the permeability of C30FA, C50FA, β-CD and FA-β-CD-composite samples permeability compared to control sample (C) for 0.4-W/B

Figures 9.8 and 9.9 show the effect of FA-β-CD composite samples on the permeability of their comparative C30FA and C50FA samples. It was observed that the FA-β-CD composite samples had a lower influence on the permeability in 0.4-W/B samples than in the 0.5-W/B samples (see Figures 9.4 and 9.5). For the composite samples containing 30% FA, for a 0.4-W/B, a decrease in permeability was only observed for C30FA0.025CD sample at the 28 days curing age when

compared to the comparative C30FA samples. A slight increase in permeability was observed for this sample (C30FA0.025CD) at the 90 days curing age and the C30FA0.05CD sample showed permeability increase at both 28 and 90 days curing ages. A greater increase in permeability was observed for the C30FA0.05CD sample at 90 days in the 0.4-W/B samples than in the 0.5-W/B samples, when compared to their respective comparative C30FA sample. The FA-*β*-CD composite samples containing 50% FA showed increased permeability at both curing ages compared to the C50FA samples (for 0.4-W/B). This is contrary to the observed trend for 0.5-W/B samples, where permeability reduced for the FA-*β*-CD composite samples containing 50% FA compared to the C50FA samples (Figure 9.5). This might be an indication of a better effect of C50FA on concrete permeability in the 0.4-W/B samples (Figure 9.7) than in the 0.5-W/B samples (Figure 9.3).

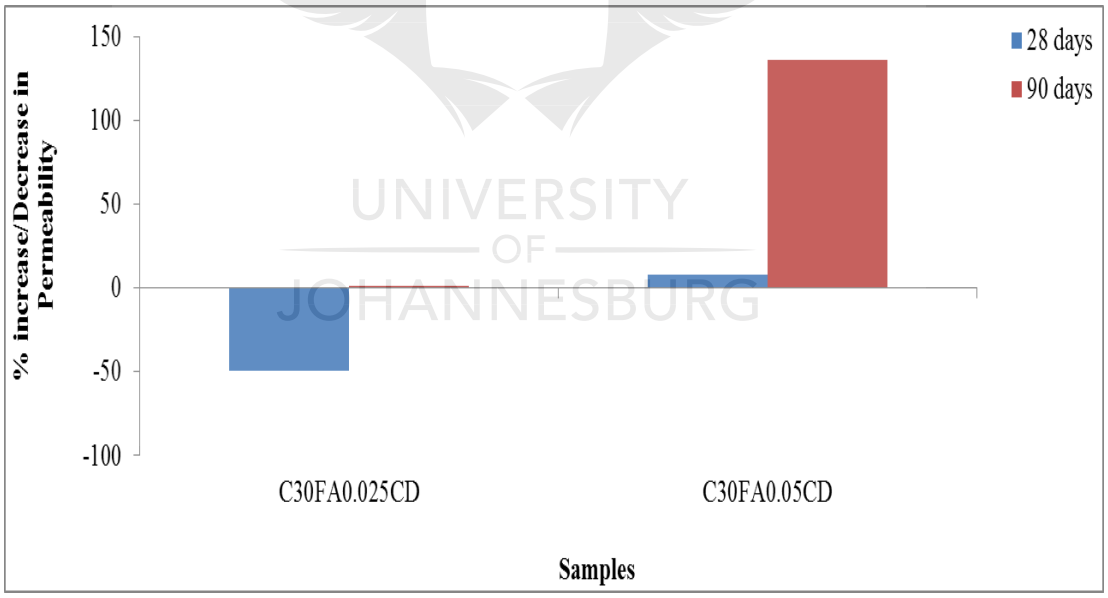

Figure 9.8: Percentage increase in the permeability of FA-*β*-CD-composite samples compared to C30FA pozzolanic sample for (0.4-W/B**)**

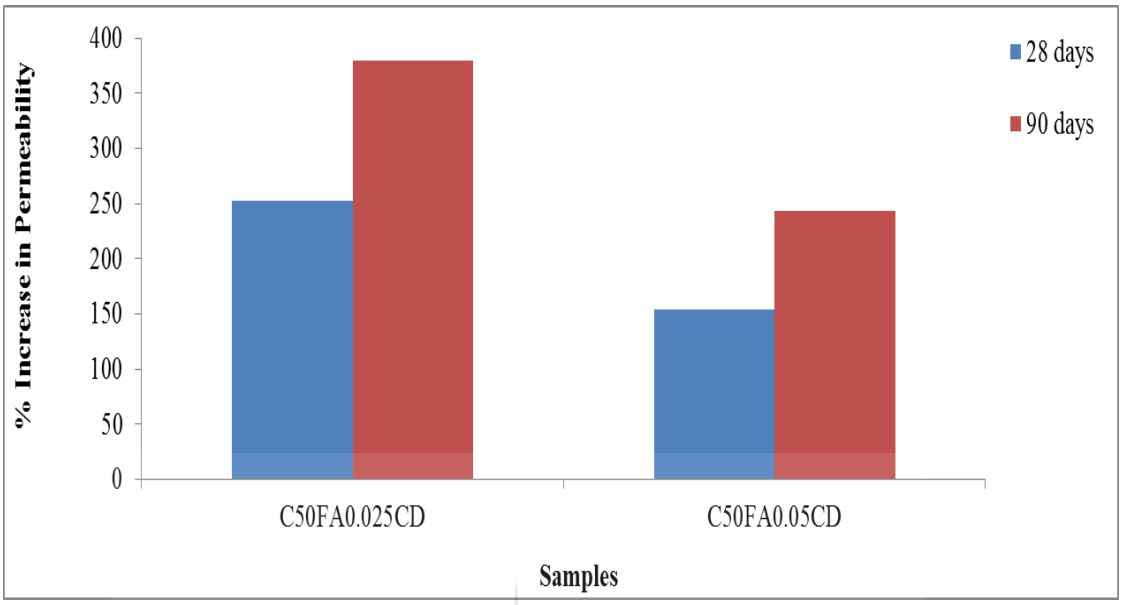

Figure 9.9: Percentage increase in the permeability of FA-*β*-CD-composite samples compared to C50FA pozzolanic sample for (0.4-W/B)

9.4.3 Sorptivity results for 0.5-W/B samples

Sorptivity measures the volume of pores that are accessible to water by capillary action [6]; it is not related to the pore connectivity as in the case with permeability. Figure 9.10 shows the sorptivity results of samples with a 0.5-W/B. As expected, a decrease in sorptivity was observed for all the samples as curing age increased. This is an indication of improved hydration and pozzolanic reactions resulting in denser concrete at higher curing age with reduced volume of capillary pores. The FA and FA-*β*-CD composite samples showed reduced sorptivity at both curing ages when compared with the control sample. The *β*-CD in plain concretes showed reduced sorptivity at a lower percentage (0.025%) compared to the control sample at both curing ages. Samples with 0.05% *β*-CD had approximately the same sorptivity as the control sample. However, an increase in sorptivity was observed for sample containing 0.1% *β*-CD at both curing ages, when compared to the control sample. The lower the *β*-CD content, the more favourable the sorptivity observed. The C50FA

samples showed a further reduced sorptivity than the C30FA sample at the 90 days curing age when, compared with the control sample (0.5-W/B).

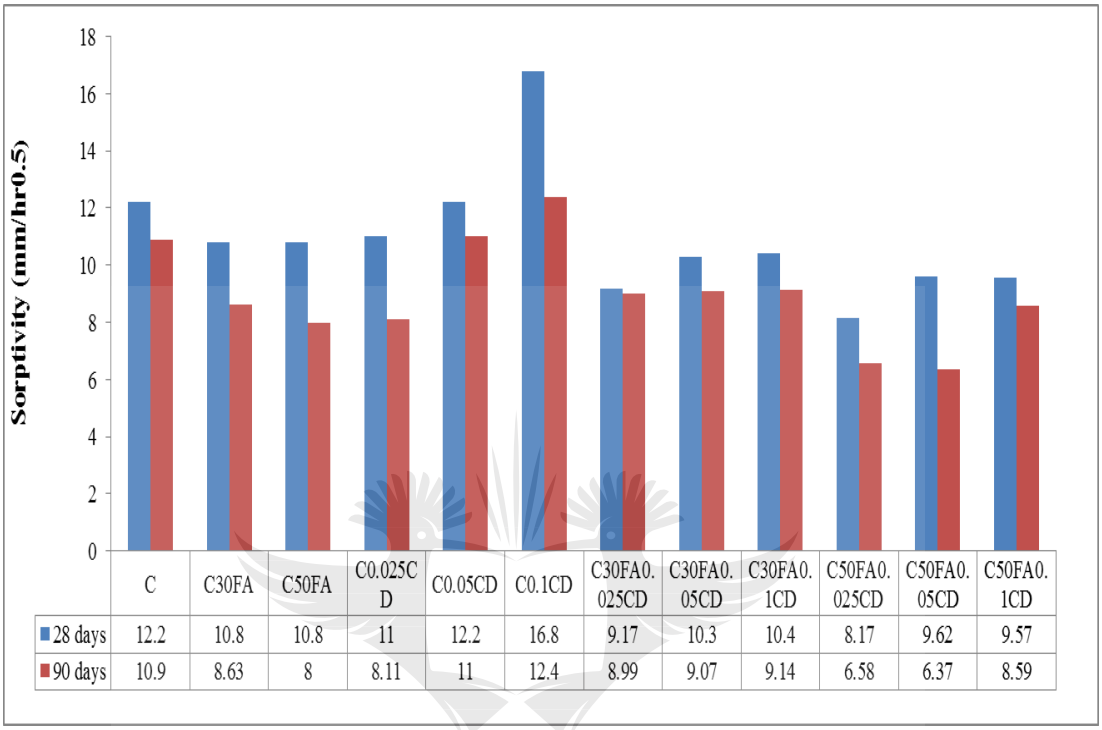

	C	C30FA	C50FA	C0.025CD	C0.05CD	C0.1CD	C30FA0.025CD	C30FA0.05CD	C30FA0.1CD	C50FA0.025CD	C50FA0.05CD	C50FA0.1CD
28 days	12.2	10.8	10.8	11	12.2	16.8	9.17	10.3	10.4	8.17	9.62	9.57
90 days	10.9	8.63	8	8.11	11	12.4	8.99	9.07	9.14	6.58	6.37	8.59

Figure 9.10: Sorptivity of 0.5-W/B samples

The percentage increase/decrease in the sorptivities of C30FA, C50FA, *β*-CD and FA-*β*-CD composite samples as compared to control sample (0.5-W/B) is shown in Figure 9.11. The results revealed the positive effect of FA and FA-*β*-CD composite samples in reducing concrete sorptivity. The FA-*β*-CD composite samples showed much lesser sorptivity than their comparative C30FA and C50FA samples at lower percentages of *β*-CD, when compared to the control sample. The FA-*β*-CD composite samples with 30% FA showed reduced sorptivity than their comparative C30FA sample at 28 days curing age when compared to the control sample. A reduction in sorptivity was observed for the C50FA0.025CD and C50FA0.05CD samples at both 28 and 90 days curing ages and for C50FA0.1CD sample at 28 days curing age than

their compartive C50FA samples when compared with the control sample. In general, the lower the amount of β-CD in plain and composite samples, the better influence on sorptivity was observed.

The effect of slower pozzolanic reaction was revealed for FA samples showing better influence on concrete sorptivity at 90 days curing age than 28 days curing age. The observed results also correlate with the SEM results, as explained for permeability. The denser surface of the FA samples from the 28 and 90 days hydration periods, revealed in the SEM results (Figures 6.6 and 6.7), as compared to the control sample resulted in reduced pores that are accessible to water by capillary action, leading to a lower sorptivity than the control samples at these curing ages.

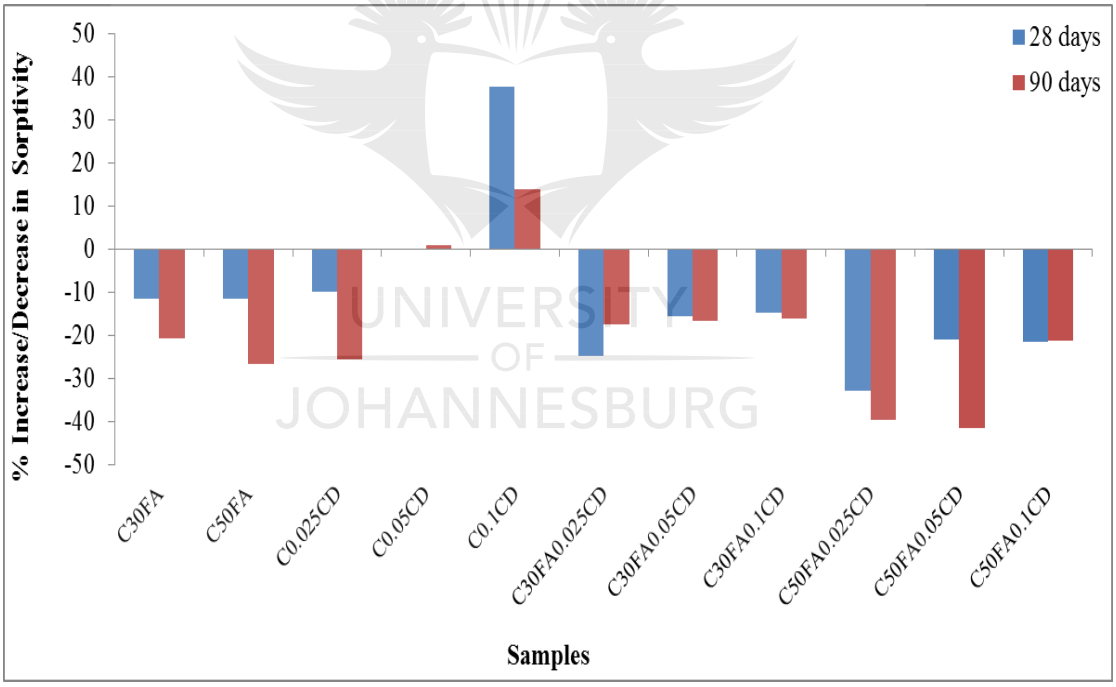

Figure 9.11: Percentage increase/decrease in the sorptivity of C30FA, C50FA, β-CD and FA-β-CD-composite samples compared to control sample (C) for 0.5-W/B

In studying the effect of FA-β-CD composite samples on the sorptivity of their comparative C30FA and C50FA samples, Figures 9.12 and 9.13 revealed their percentage increase/decrease in relation to the pozzolanic samples. The FA-β-CD composite samples decreased sorptivity of the comparative C30FA sample at 28 days curing age while an increase in sorptivity was observed at 90 days curing age (Figure 9.12). The composite sample with 0.025% β-CD showed a better influenced on sorptivity than the samples with 0.05% and 0.1% β-CD, when compared with their comparative C30FA sample. The FA-β-CD composite samples with 50 %FA showed decreased sorptivity at both curing ages for the C50FA0.025CD and C50FA0.05CD samples, also, decreased sorptivity was observed for C50FA0.1CD at 28 days curing age (Figure 9.13). This further showed better influence of 0.025% β-CD on sorptivity than the samples with 0.05% and 0.1% β-CD.

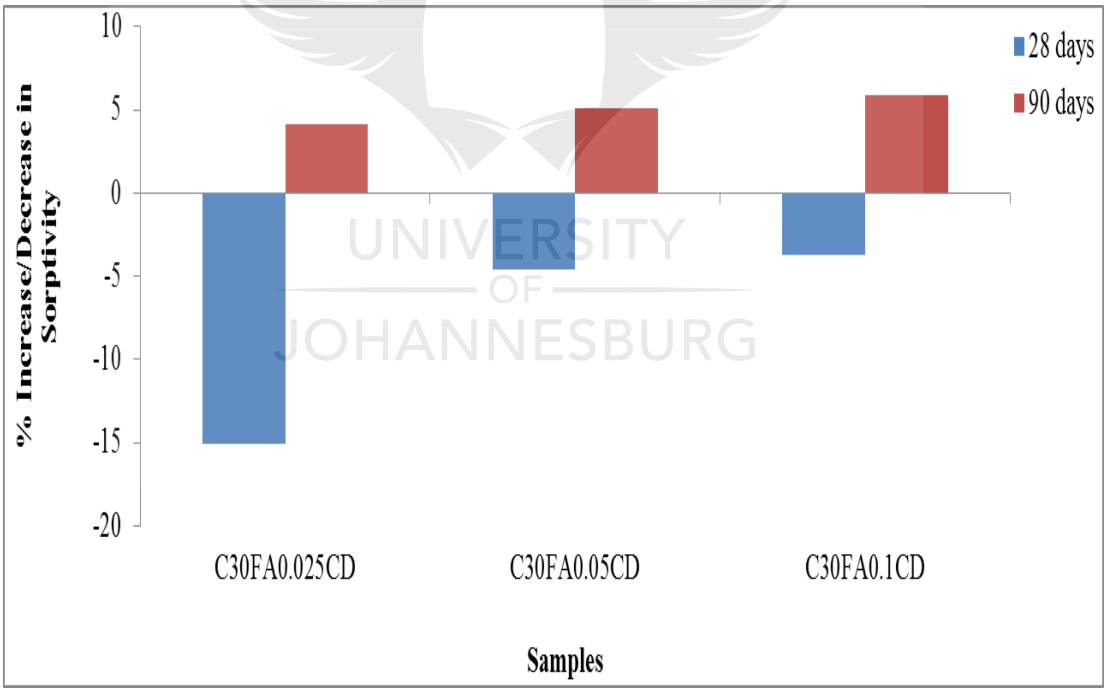

Figure 9.12: Percentage increase/decrease in the sorptivity of FA-β-CD-composite samples compared to C30FA pozzolanic sample for 0.5-W/B

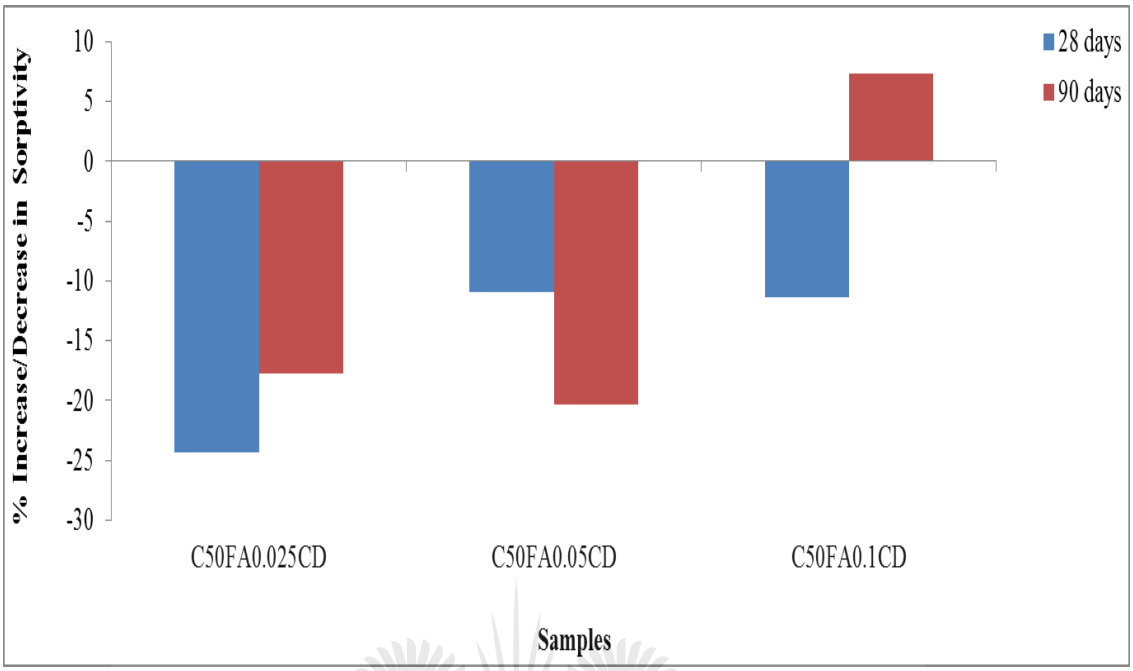

Figure 9.13: Percentage increase in the sorptivity of FA-β-CD-composite samples compared to C50FA pozzolanic sample for 0.5-W/B

9.4.4 Sorptivity results for 0.4-W/B samples

The sorptivity results of the 0.4-W/B samples are shown in Figure 9.14. The control, C30FA, C0.05CD, C0.1CD and C30FA0.05CD samples with 0.4-W/B have a reduced sorptivity when compared with their respective 0.5-W/B samples at both curing ages. The C0.025CD sample with 0.4-W/B showed a higher sorptivity at 90 days curing age than C0.025CD sample with 0.5-W/B (Figure 9.10), while C30FA0.025CD sample with 0.4-W/B showed higher sorptivity at 28 days than its comparative 0.5-W/B sample (Figure 9.10). The 0.4-W/B samples were expected to be denser than 0.5-W/B samples, therefore, exhibiting lower sorptivity, but on the contrary for all composite samples containing 50% FA, higher sorptivity at both curing ages was exhibited for 0.4-W/B samples than for the 0.5-W/B samples. Figure 9.14 revealed decreased sorptivity at higher curing age for all samples, as also shown for 0.5-W/B samples (Figure 9.10).

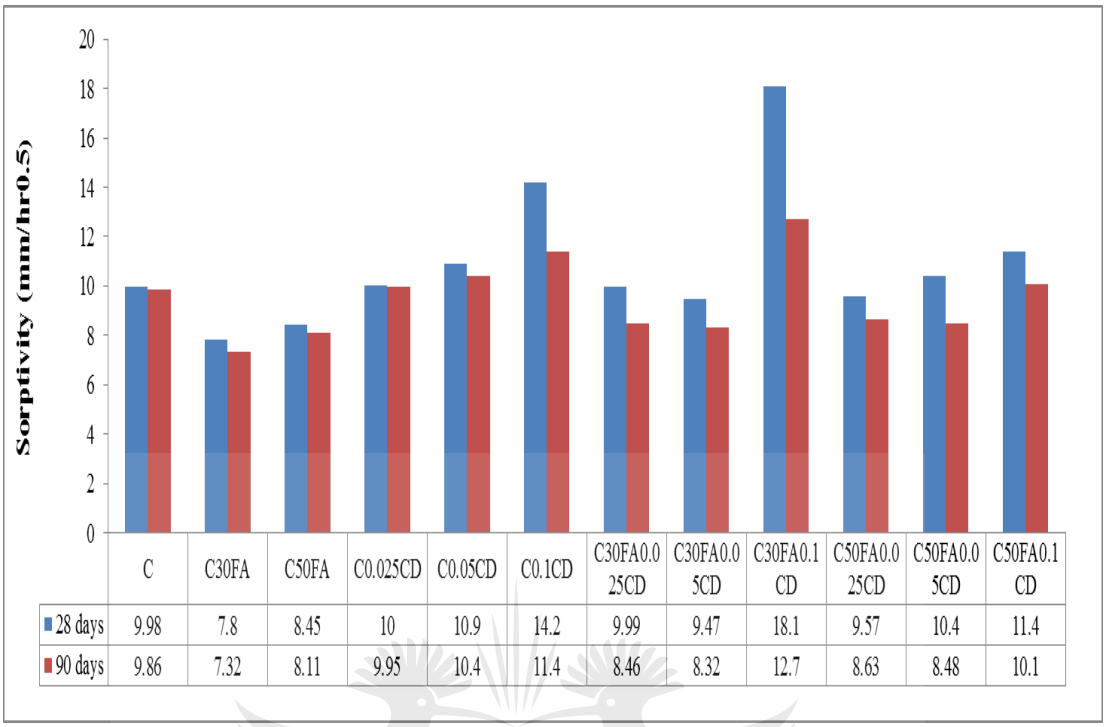

	C	C30FA	C50FA	C0.025CD	C0.05CD	C0.1CD	C30FA0.025CD	C30FA0.05CD	C30FA0.1CD	C50FA0.025CD	C50FA0.05CD	C50FA0.1CD
28 days	9.98	7.8	8.45	10	10.9	14.2	9.99	9.47	18.1	9.57	10.4	11.4
90 days	9.86	7.32	8.11	9.95	10.4	11.4	8.46	8.32	12.7	8.63	8.48	10.1

Figure 9.14: Sorptivity of 0.4-W/B samples

The percentage increase/decrease in the sorptivities of C30FA, C50FA, *β*-CD and FA-*β*-CD composite samples as compared to the control sample (for 0.4-W/B), presented in Figure 9.15, showed reduced sorptivity for the FA samples at both curing ages, when compared with the control sample. The C30FA sample revealed a greater reduction in sorptivity than C50FA sample, when compared with the control sample. The effect of the *β*-CD on the sorptivity of plain concrete with 0.4W/B was negligible at lower contents of *β*-CD, at 0.025% *β*-CD, a similar sorptivity was observed at both curing ages when compared with the control sample. For the C0.05CD sample, a slightly increased sorptivity was observed at both curing ages compared to the control sample, while for C0.1CD sample, increased sorptivity was observed at both curing ages, when compared with the control sample. Generally, the composite samples showed a decrease in sorptivity at lower contents of *β*-CD at 90 days curing age compared to the control sample, while composite samples with 0.1% *β*-CD increased

in sorptivity at both curing ages relative to the control sample. In general, the lower the β-CD content in both plain and composite samples, the better the influence it had on the sorptivity.

The observed results are a reflection of the SEM results, as explained in Section 9.4.3. In addition, the SEM results (Figure 6.6 and 6.7) revealed that the samples with 0.025% and 0.05% β-CD had a more improved surface than samples with 0.1% β-CD for both 28 and 90 days hydration periods.

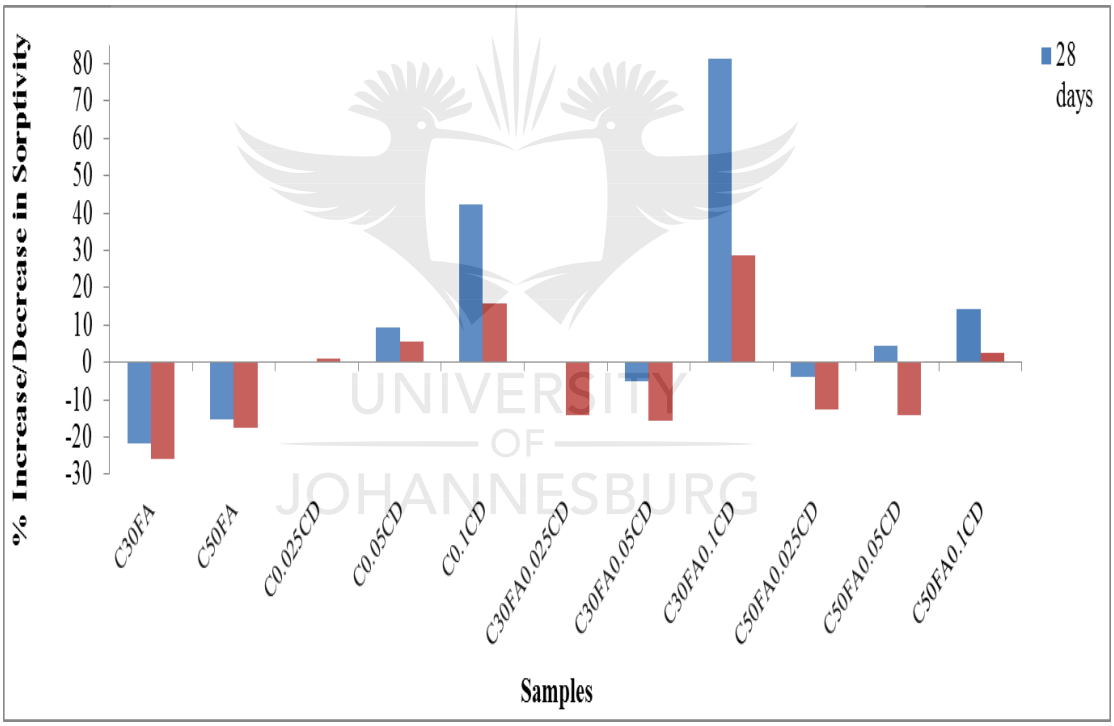

Figure 9.15: Percentage increase/decrease in the sorptivity of C30FA, C50FA, β-CD and FA-β-CD composite samples compared to control sample (C) for 0.4-W/B

The effect of the FA-β-CD composite samples on the sorptivity of their comparative C30FA and C50FA is shown in Figures 9.16 and 9.17, respectively. An adverse effect

(increased sorptivity) was observed for all the composite samples, when compared with their respective comparative C30FA and C50FA samples. The *β*-CD improved the sorptivity of their comparative pozzolanic concretes better in the 0.5-W/B samples than in 0.4-W/B samples. This trend was also observed for permeability, less effect of *β*-CD was revealed in the 0.4-W/B pozzolanic samples (Figures 9.8 and 9.9) than in the 0.5-W/B samples (Figures 9.4 and 9.5). The composite samples with 0.1 % *β*-CD showed a higher increased in sorptivity compared to the composite samples with 0.025% and 0.05% *β*-CD at both curing ages, when compared to their comparative C30FA and C50FA samples.

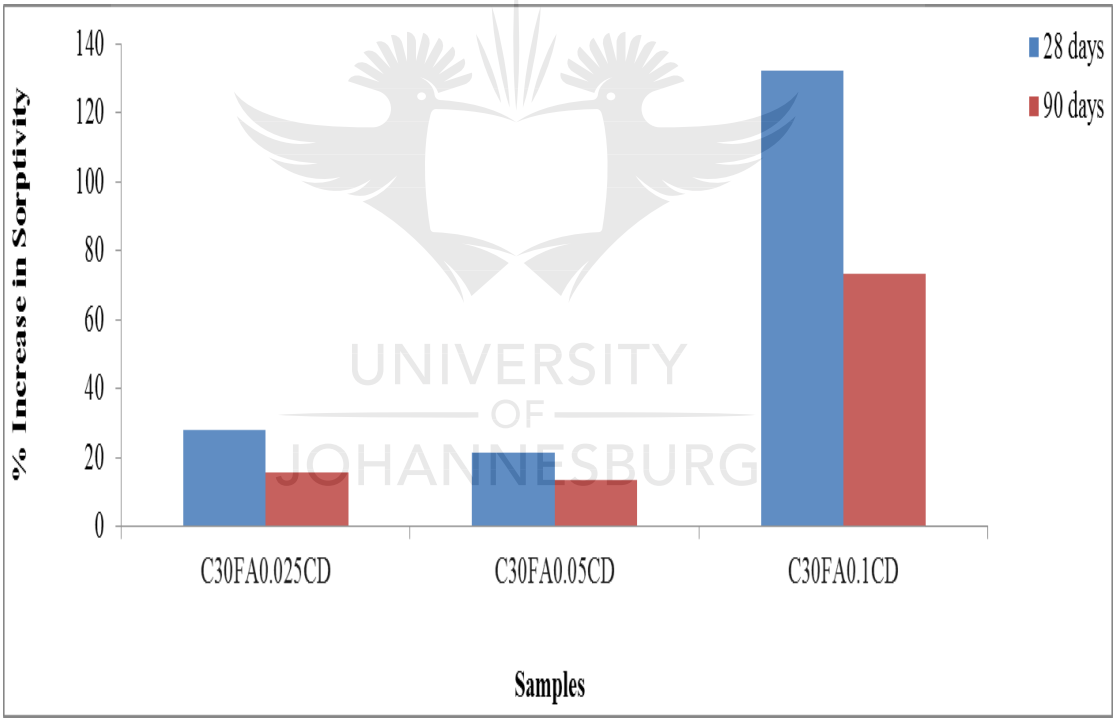

Figure 9.16: Percentage increase in the sorptivity of FA-*β*-CD-composite samples compared to C30FA pozzolanic sample for 0.4-W/B

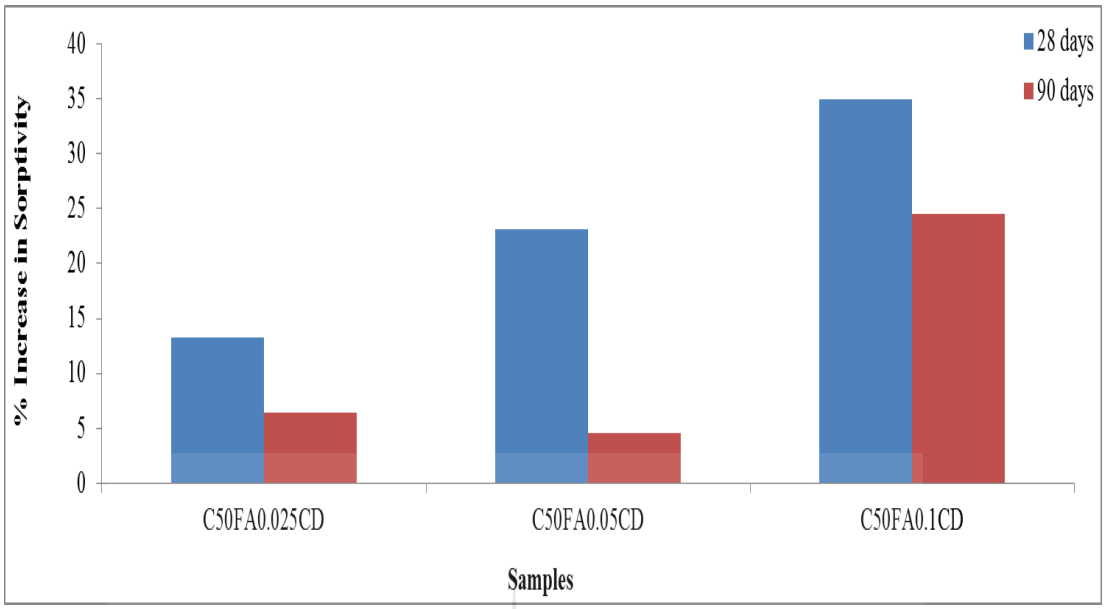

Figure 9.17: Percentage increase in the sorptivity of FA-β-CD composite samples compared to C50FA pozzolanic sample for 0.4-W/B

9.4.5 Porosity results for 0.5-W/B samples

The total porosity of the concrete affects the compressive strength of that concrete [5]. An increase in the total porosity of a concrete is an indication of reduced compressive strength. The porosity results of the 0.5-W/B samples are shown in Figure 9.18. For all the samples, a decrease in porosity was observed as the curing age increased. The samples with FA showed a higher porosity at both curing ages than the control sample, while a lower porosity was observed for the β-CD samples at both curing ages than the control sample.

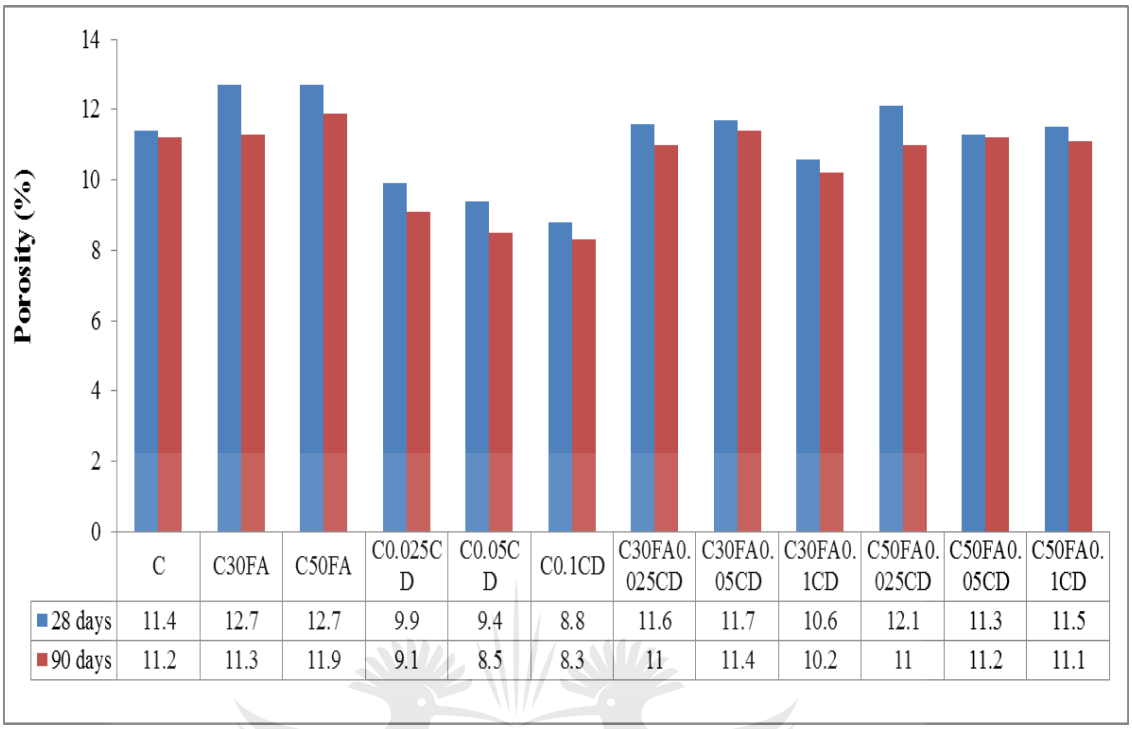

	C	C30FA	C50FA	C0.025CD	C0.05CD	C0.1CD	C30FA0.025CD	C30FA0.05CD	C30FA0.1CD	C50FA0.025CD	C50FA0.05CD	C50FA0.1CD
28 days	11.4	12.7	12.7	9.9	9.4	8.8	11.6	11.7	10.6	12.1	11.3	11.5
90 days	11.2	11.3	11.9	9.1	8.5	8.3	11	11.4	10.2	11	11.2	11.1

Figure 9.18: Porosity of 0.5-W/B samples

Figure 9.19 shows the percentage increase/decrease in in the porosity of the C30FA, C50FA, *β*-CD and FA-*β*-CD composite samples, compared to the control sample (0.5-W/B). It was deduced from the Figure that the C50FA sample showed an increased porosity compared to the C30FA sample at 90 days curing age when compared with the control sample. The total porosity of samples with 0.1% *β*-CD was reduced at both curing ages compared to the samples with 0.025% and 0.05% *β*-CD. This was also observed for the composite samples containing 30% FA, the C30FA0.1CD showed reduced porosity at both curing ages, when compared with the control sample, while a slightly reduced porosity was observed for C30FA0.025CD at 90 days curing age and an increase in porosity was observed for C30FA0.05CD at both curing ages when compared with the control samples. The composite samples with 50% FA showed a different trend; the C50FA0.025CD had a higher porosity at the 28 days curing age and reduced porosity at 90 days curing age, when compared

with the control sample, while the C50FA0.05CD and C50FA0.1CD samples had a relatively similar porosity at both curing ages, when compared with the control sample.

Comparing the observed results with the compressive strength results discussed in Chapter Eight, it is evident that porosity has effect on compressive strength. For the 0.5-W/B samples, samples with β-CD showed an improved compressive strength, generally from the 90 days curing age (Figure 8.2), while samples with FA showed lower compressive strength at both 28 days and 90 days curing ages when compared with the control sample (Figure 8.2).

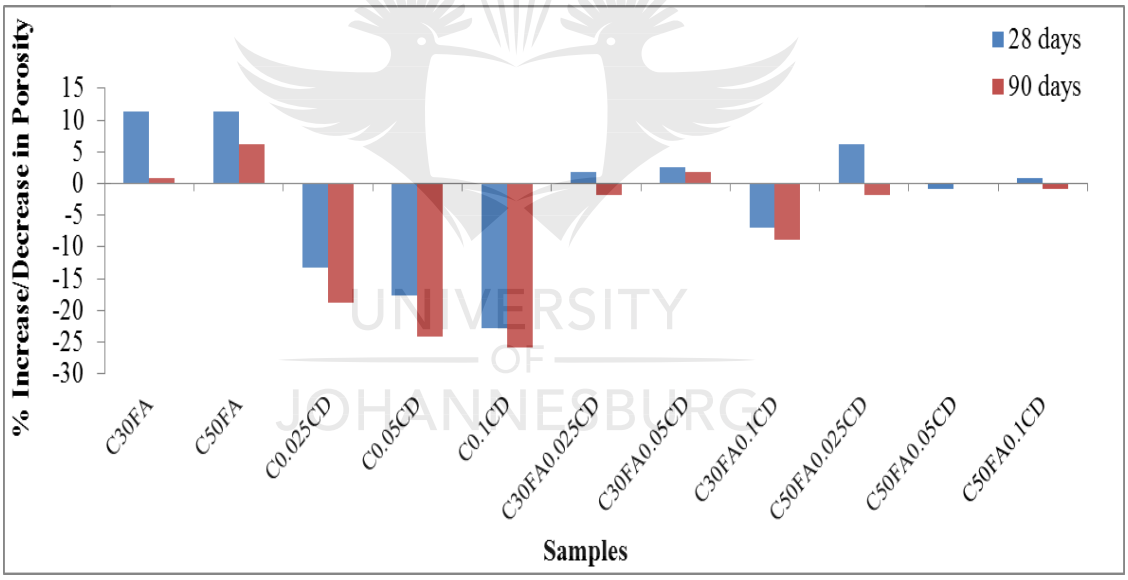

Figure 9.19: Percentage increase/decrease in the porosity of C30FA, C50FA, β-CD and FA-β-CD composite samples compared to control sample (C) for 0.5-W/B

The percentage increase/decrease in the porosity of the FA-β-CD composite samples, compared to C30FA and C50FA pozzolanic samples is shown in Figures 9.20 and 9.21, respectively. A reduced porosity was observed for all the samples at both curing ages when compared with their respective comparative C30FA and C50FA samples.

An exception was seen in C30FA0.05CD sample where a little increase in porosity was observed at the 90 days curing age, when compared with its comparative C30FA sample. This can also be related to the compressive strength results where for the 0.5-W/B samples, an increase in compressive strength was observed for all the composite samples at both 28 and 90 days curing ages when compared with their comparative C30FA and C50FA samples (Figures 8.4 and 8.5).

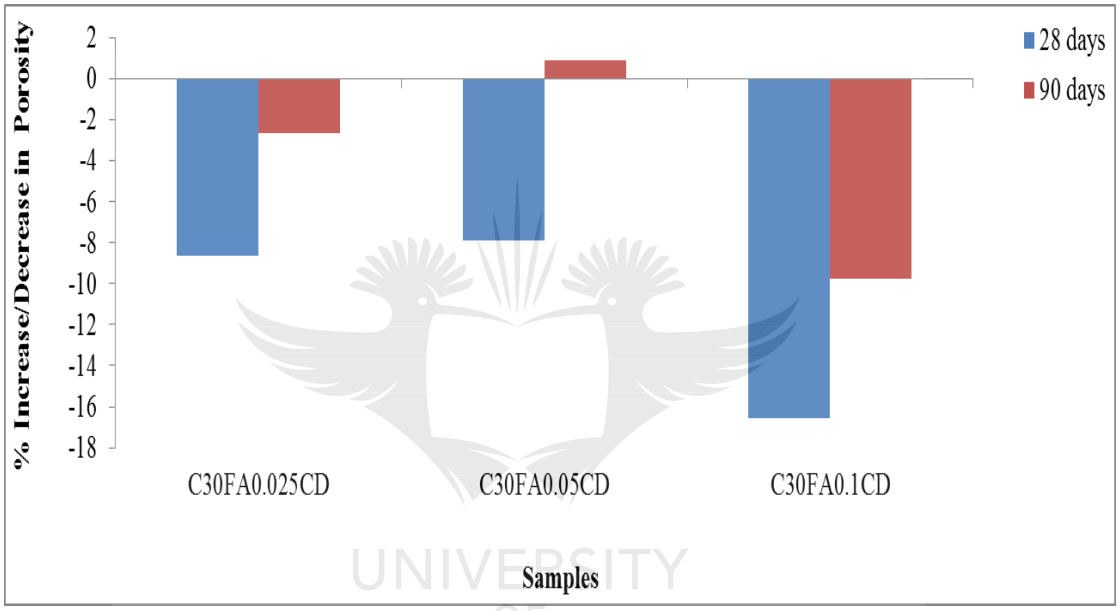

Figure 9.20: Percentage increase/decrease in FA-β-CD composite samples porosity compared to C30FA pozzolanic sample for 0.5-W/B

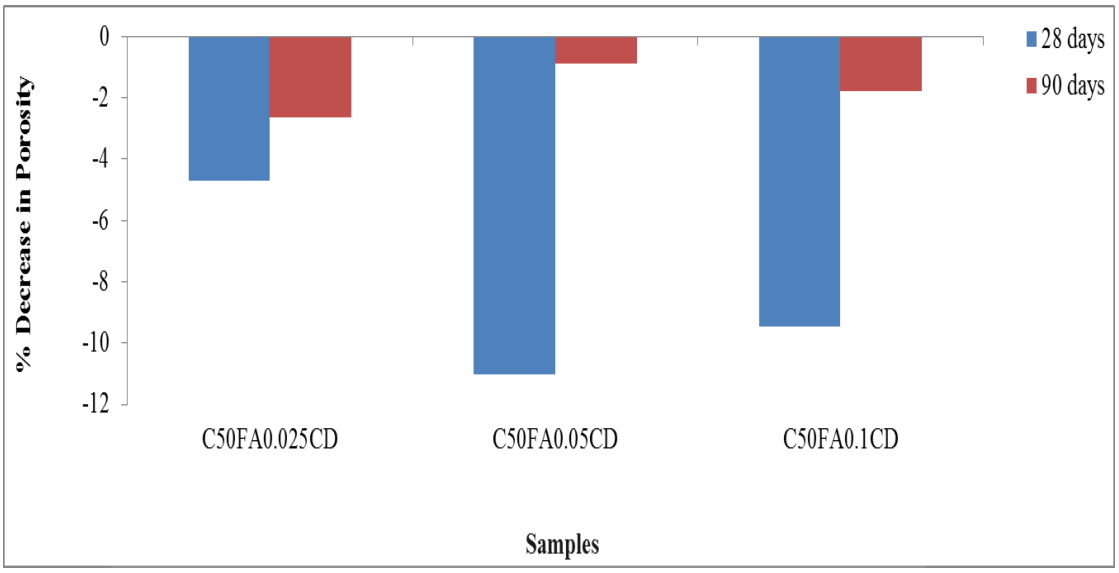

Figure 9.21: Percentage decrease in FA-β-CD composite samples porosity compared to C50FA pozzolanic sample for 0.5-W/B

9.4.6 Porosity results for 0.4-W/B samples

Figure 9.22 presents the porosity results of the 0.4-W/B samples. Evidence of improved hydration as curing age increased is shown with a reduced porosity for all the samples at the 90 days curing age compared to the 28 days curing age. A reduced porosity was observed for all FA, β-CD and FA-β-CD composite samples (with 30% FA) with 0.4-W/B when compared with 0.5-W/B samples (Figure 9.18) at both curing ages. In Figure 9.22, the FA samples showed a reduced porosity at 90 days curing age compared to the control sample (0.4-W/B), while a reduced porosity was observed at both 28 and 90 days curing ages for samples with β-CD compared to the control sample.

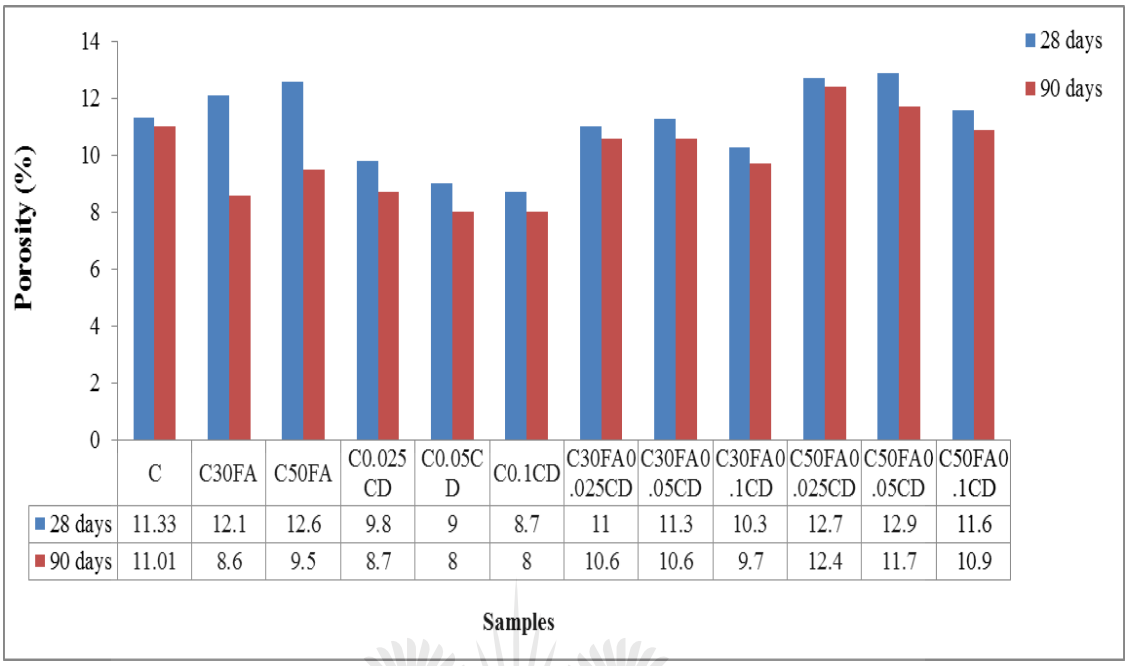

	C	C30FA	C50FA	C0.025CD	C0.05CD	C0.1CD	C30FA0.025CD	C30FA0.05CD	C30FA0.1CD	C50FA0.025CD	C50FA0.05CD	C50FA0.1CD
28 days	11.33	12.1	12.6	9.8	9	8.7	11	11.3	10.3	12.7	12.9	11.6
90 days	11.01	8.6	9.5	8.7	8	8	10.6	10.6	9.7	12.4	11.7	10.9

Figure 9.22: Porosity of 0.4-W/B samples

The percentage increase/decrease in porosity of the C30FA, C50FA, *β*-CD and FA-*β*-CD composite samples, compared to control sample (0.4-W/B) is shown in Figure 9.23. The C30FA sample revealed a greater reduction in porosity than the C50FA sample at the 90 days curing age, when compared with the control sample. As observed for the 0.5-W/B samples, the total porosity of samples with 0.1% *β*-CD reduced more at both curing ages than samples with 0.025% and 0.05% *β*-CD, when compared with the control sample (0.4-W/B). A Reduced porosity was also observed for all FA-*β*-CD composite samples containing 30% FA at both the 28 and 90 days curing ages, when compared with the control sample. The FA-*β*-CD composite samples containing 50% FA showed an increase in porosity especially for the C50FA0.025CD and C50FA0.05CD samples at both the 28 and 90 days curing ages, when compared with the control samples.

The compressive strength results of these samples showed a better compressive strength for the FA samples with 0.4-W/B (Figures 8.7) than with the 0.5-W/B

(Figure 8.2). An increase in compressive strength was observed for all samples with β-CD at both the 28 and 90 days curing ages (Figure 8.7), when compared with the control sample. The FA-β-CD composite samples containing 30% FA showed an improved compressive strength from the 90 days curing age (Figure 8.8) than the control sample, while FA-β-CD composite samples containing 50% FA showed decrease in compressive strength at both the 28 and 90 days curing ages (Figure 8.8) compared to the control sample. The observed results confirm that the compressive strength of concrete is affected by its total porosity.

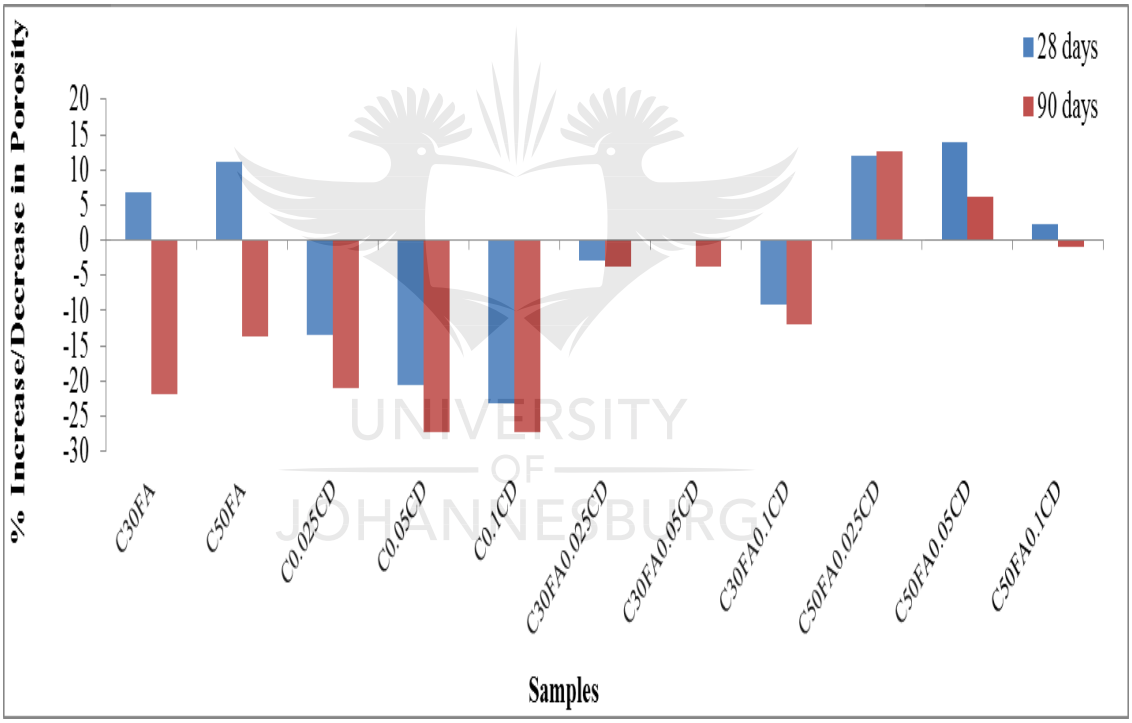

Figure 9.23: Percentage increase/decrease in C30FA, C50FA, β-CD and FA-β-CD composite samples porosity compared to control sample (C) for 0.4-W/B

Relative to C30FA, the FA-β-CD composite samples with 30% FA showed reduced porosity at 28 days curing age and higher porosity at 90 days curing age (Figure 9.24) than C30FA sample. A better influence of these composites on C30FA porosity was

observed for 0.5-W/B samples, where in general (except for 90 days porosity of C30FA0.05CD sample), a reduced porosity was observed for both the 28 and 90 days curing ages relative to C30FA sample (Figure 9.20). The FA-β-CD composite samples with 50% FA also revealed an increased porosity for the C50FA0.025CD and C50FA0.05CD samples at both curing ages, while the C50FA0.1CD sample had a reduced porosity at the 28 days curing age and higher porosity at the 90 days curing age when compared with their comparative C50FA sample (Figure 9.25).

A greater percentage increase in compressive strength was observed at the 28 days curing age for all composite samples than for the other curing ages, when compared with their respective C30FA and C50FA samples (Figures 8.9 and 8.10). This observation is also a reflection of the porosity results.

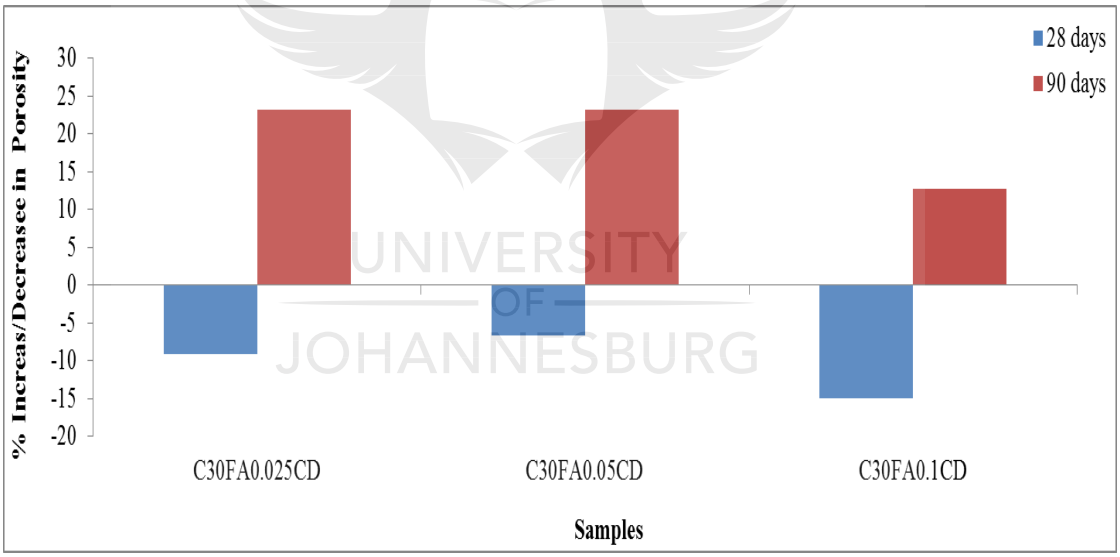

Figure 9.24: Percentage increase in FA-β-CD composite samples porosity compared to C30FA pozzolanic sample (0.4-W/B)

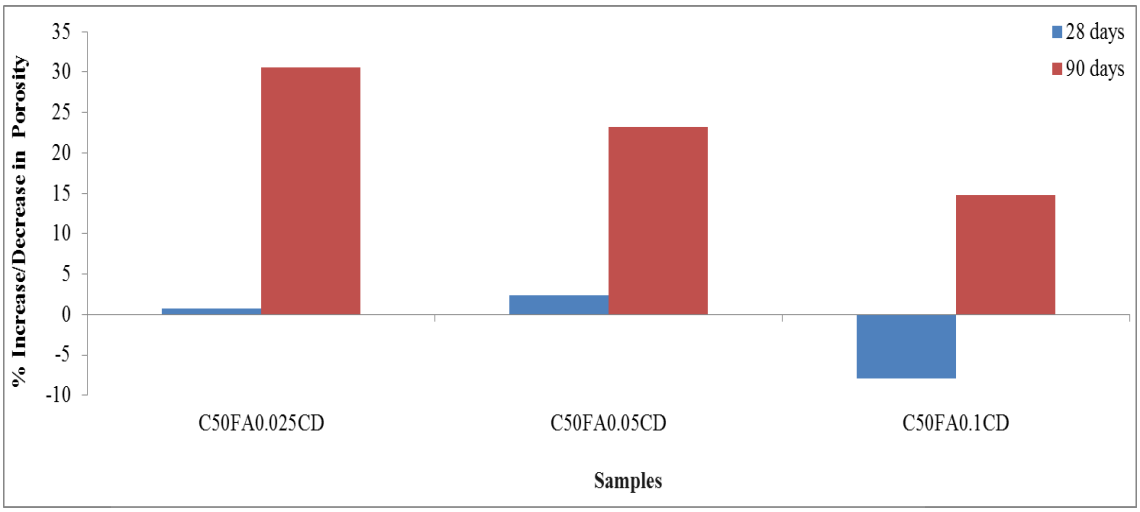

Figure 9.25: Percentage increase in FA-β-CD composite samples porosity compared to C50FA pozzolanic sample (0.4-W/B)

9.4.7 Chloride conductivity results for 0.5-W/B samples

The chloride conductivity index (CCI) is related to the chloride diffusion into the concrete. As revealed in Figure 9.26, the chloride conductivity results of all the samples (0.5-W/B) showed an excellent indication, being less than 0.75 mS/cm as stipulated by Alexander et al [3] at both curing ages. This might be as a result of the wet curing (water bath) method used. A reduced CCI was observed at higher curing age for all the samples. FA, β-CD and FA-β-CD composite samples showed a lower CCI at 28 days curing age compared to the control sample.

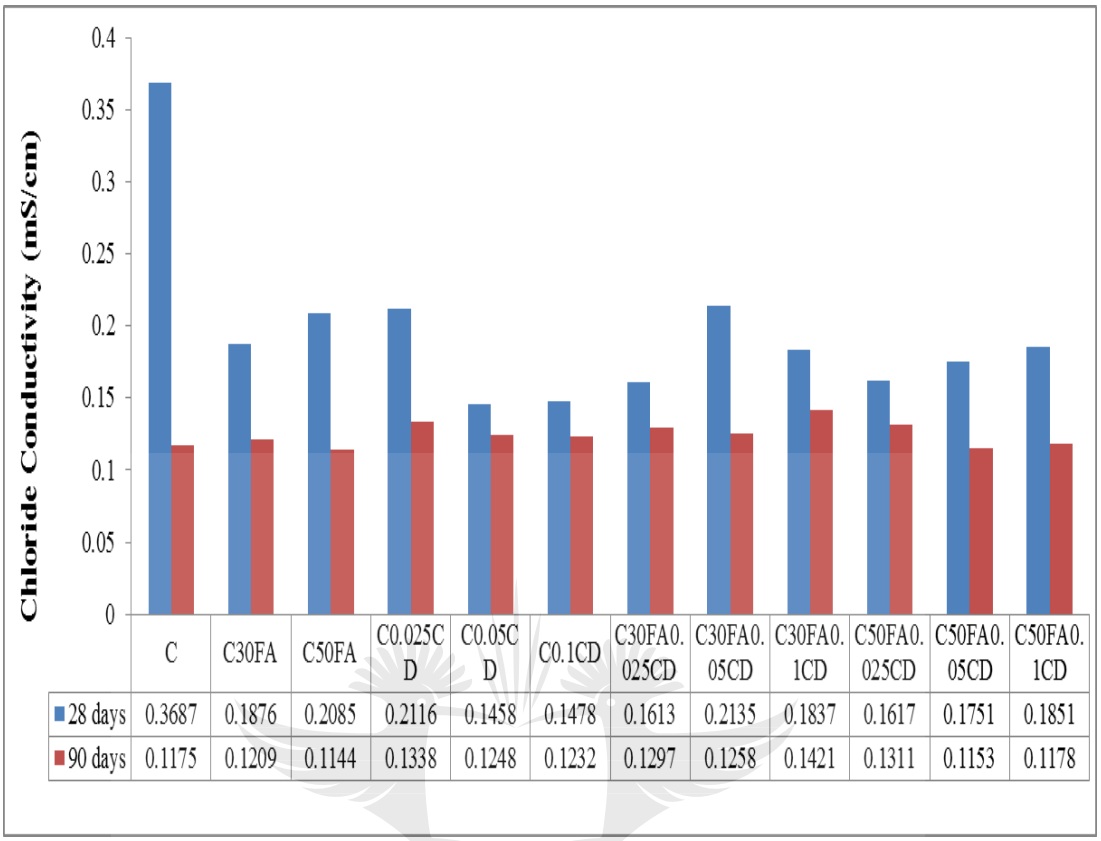

	C	C30FA	C50FA	C0.025CD	C0.05CD	C0.1CD	C30FA0.025CD	C30FA0.05CD	C30FA0.1CD	C50FA0.025CD	C50FA0.05CD	C50FA0.1CD
28 days	0.3687	0.1876	0.2085	0.2116	0.1458	0.1478	0.1613	0.2135	0.1837	0.1617	0.1751	0.1851
90 days	0.1175	0.1209	0.1144	0.1338	0.1248	0.1232	0.1297	0.1258	0.1421	0.1311	0.1153	0.1178

Figure 9.26: Chloride conductivity of 0.5-W/B samples

The percentage increase/decrease in the chloride conductivity of the C30FA, C50FA, *β*-CD and FA-*β*-CD composite samples compared to the control sample, shown in Figure 9.27, revealed that at 90 days curing age, the higher content of FA and *β*-CD had a better influenced on concrete CCI except for C30FA0.1CD sample where higher CCI was observed than for the C30FA0.025CD and C30FA0.05CD samples at the 90 days curing age. The *β*-CD and FA-*β*-CD composite samples (with 30% FA) showed an increased CCI at the 90 days curing age when compared to the control sample.

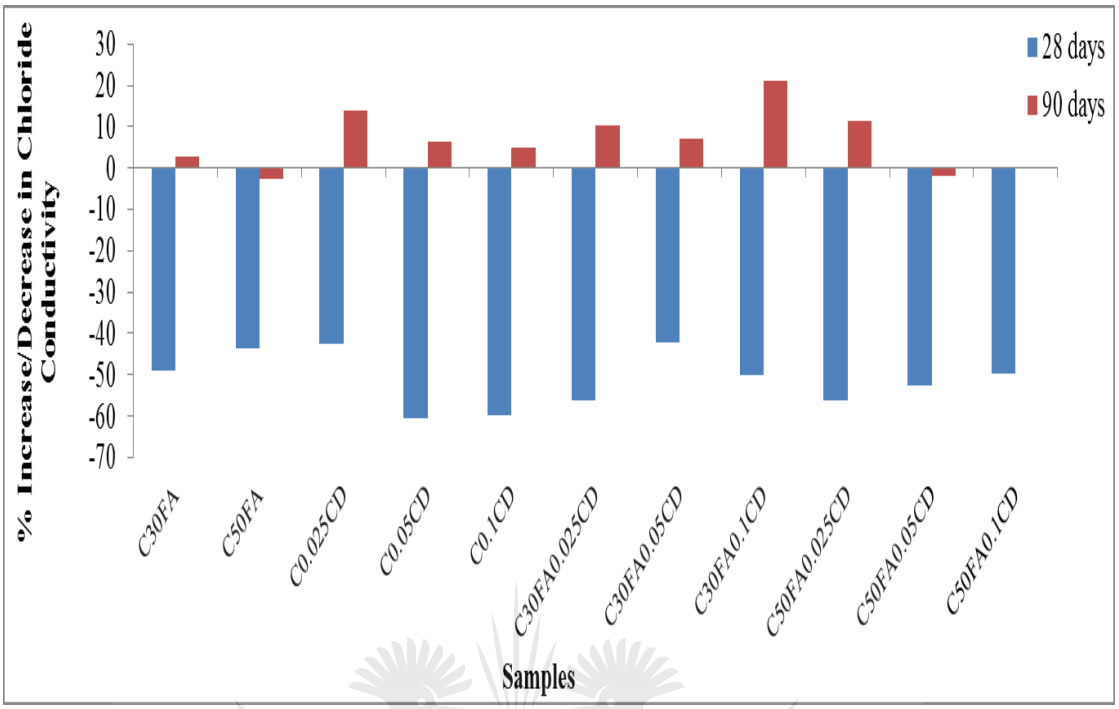

Figure 9.27: Percentage increase/decrease in the chloride conductivity of C30FA, C50FA, *β*-CD and FA-*β*-CD composite samples compared to control sample (C) for 0.5-W/B

Figures 9.28 and 9.29 present the percentage increase/decrease in the CCI of the FA-*β*-CD composite samples, compared to the respective comparative C30FA and C50FA pozzolanic samples (for 0.5-W/B). The observed results confirmed that FA-*β*-CD composite samples have a greater effect in reducing chloride conductivity of samples with 50% FA than samples with 30% FA. A reduced CCI was observed for all composite samples containing 50% FA at 28 days curing age and an increased CCI was observed at 90 days curing age when compared with their comparative C50FA samples (Figure 9.29). The FA-*β*-CD composite samples containing 30% FA had a reduced CCI for the C30FA0.025CD and C30FA0.1CD samples at the 28 days curing age and an increased CCI at 90 days curing age while an increase in CCI was observed for C30FA0.05CD sample at both the 28 and 90 days curing ages, when compared with their comparative C30FA.

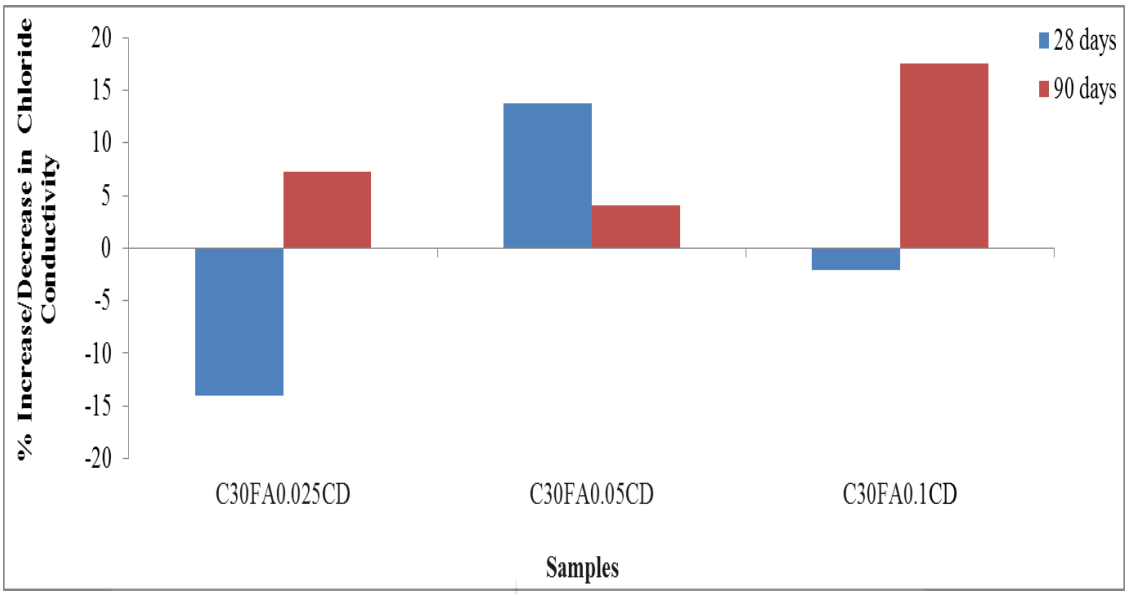

Figure 9.28: Percentage increase in the chloride conductivity of FA-*β*-CD composite samples compared to C30FA pozzolanic sample for 0.5-W/B

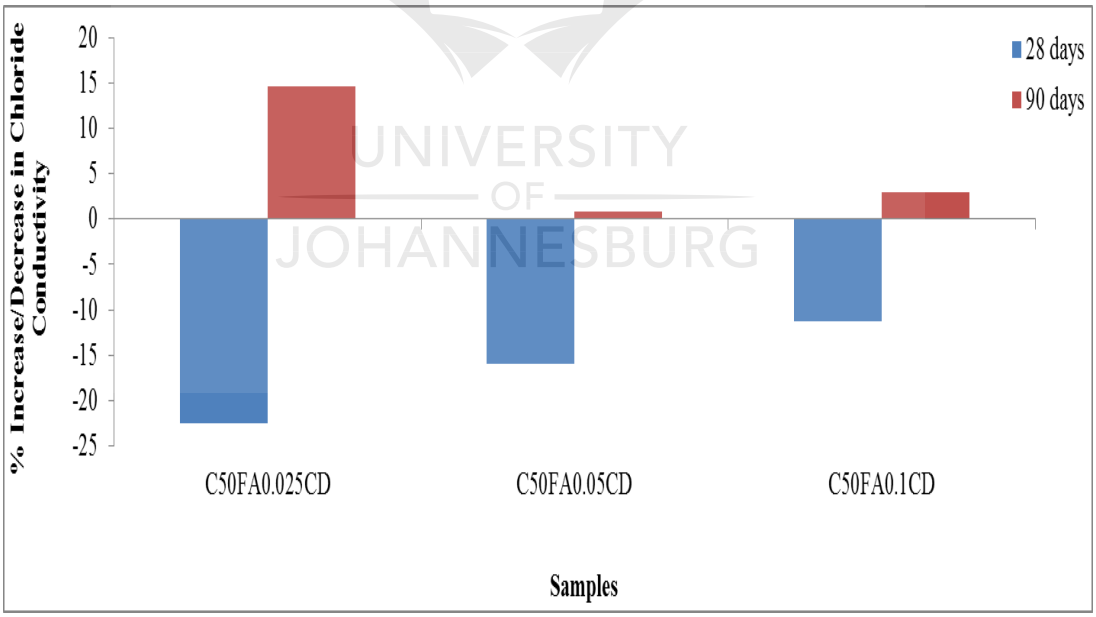

Figure 9.29: Percentage increase in the chloride conductivity of FA-*β*-CD composite samples compared to C50FA pozzolanic sample for 0.5-W/B

9.4.8 Chloride conductivity results for 0.4-W/B samples

The CCI results of all the 0.4-W/B samples also showed lower CCI values than 0.75 mS/cm [3] at both curing ages, as revealed in Figure 9.30. The general trend that was observed with these samples was a reduced CCI at 28 days curing age and increased CCI at 90 days curing age when compared with 0.5-W/B samples (Figure 9.26). A few exceptions were observed for the C0.05CD, C0.1CD and C30FA0.1CD samples. The C0.05CD and C0.1CD samples (0.4-W/B) showed an increased CCI at both curing ages compared to their 0.5-W/B samples (Figure 9.26), while the C30FA0.1CD sample showed a decrease in the CCI at both curing ages compared to its 0.5-W/B samples (Figure 9.26). A decrease in CCI was observed for all samples at increased curing age.

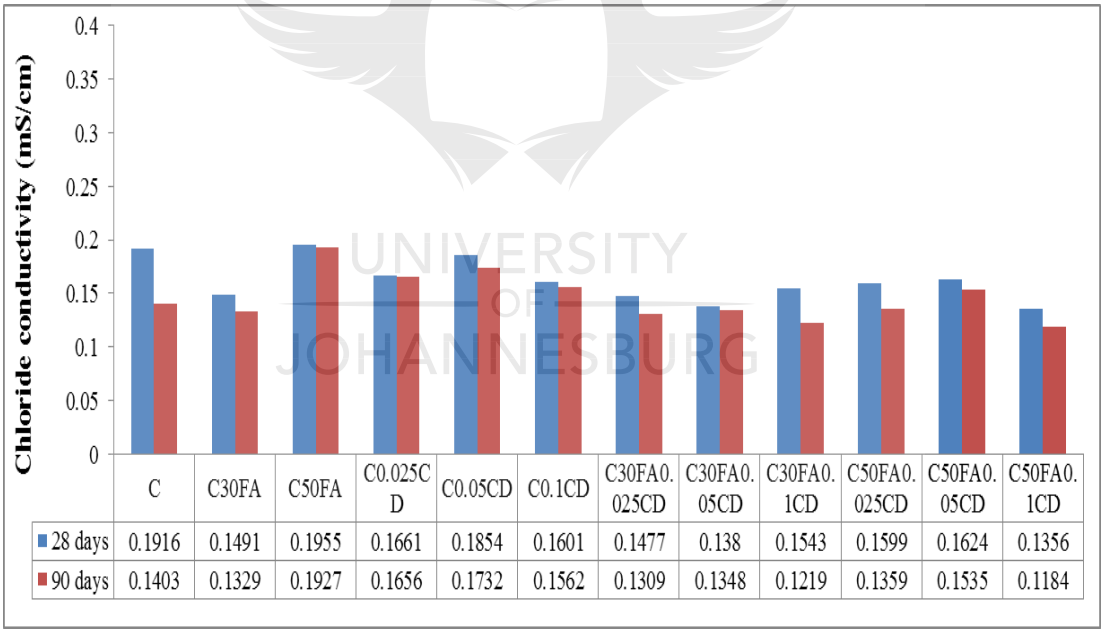

Figure 9.30: Chloride conductivity of 0.4-W/B samples

The percentage increase/decrease in the CCI of the C30FA, C50FA, *β*-CD and FA-*β*-CD composite samples compared to control sample (for 0.4-W/B) is shown in Figure

9.31. The C30FA showed a decrease in CCI at both curing ages while the C50FA showed an increase in the CCI at both curing ages (with only slight increase at the 28 days curing age), when compared with the control sample. A decrease in the CCI at the 28 days curing age and an increase of the CCI at the 90 days curing age was observed for all the β-CD and for the C50FA0.05CD samples, when compared with the control sample. The remaining composite samples, other than the C50FA0.05CD showed a reduction in the CCI at both curing ages, when compared with the control sample.

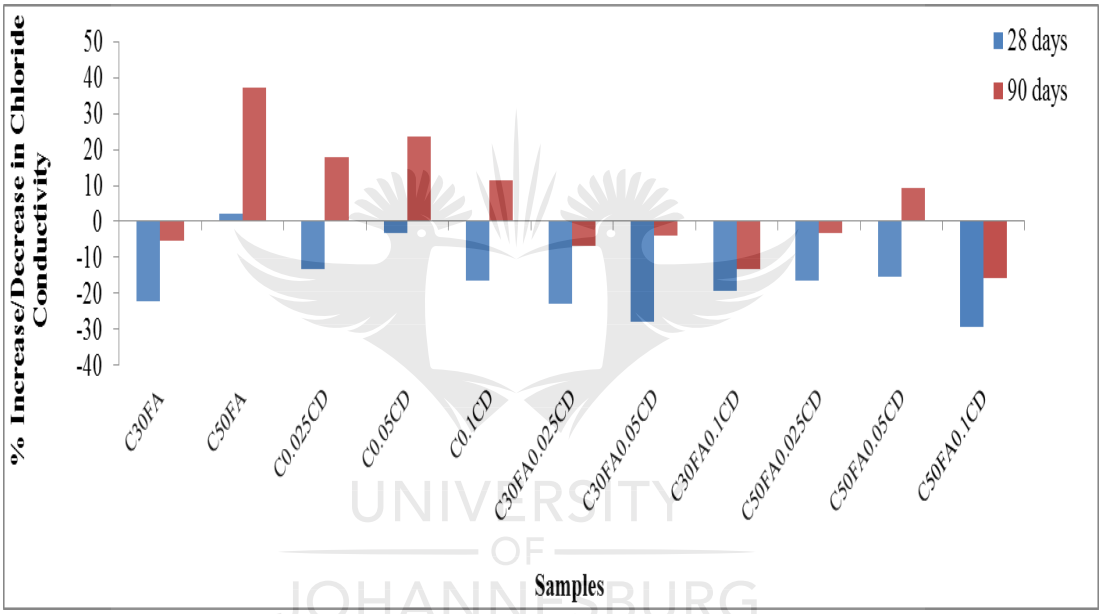

Figure 9.31: Percentage increase/decrease in the chloride conductivity of C30FA, C50FA, β-CD and FA-β-CD composite samples compared to control sample (C) for 0.4-W/B

The trend observed for CCI results was different from the permeability, sorptivity and porosity, where better effect of FA-β-CD composite samples on their respective comparative C30FA and C50FA was observed for 0.5-W/B pozzolanic concretes than for the 0.4-W/B pozzolanic concretes. A better influence of FA-β-CD composite samples on CCI values was observed for the 0.4-W/B samples compared to the 0.5-W/B samples (Figures 9.28 and 9.29) when compared with their respective comparative C30FA and C50FA as shown in Figures 9.32 and 9.33. The CCI values

of all the samples revealed are below 0.75 mS/cm; therefore the increasing/decreasing influence of the FA, β-CD and FA-β-CD composite samples on the CCI of the control samples appeared insignificant.

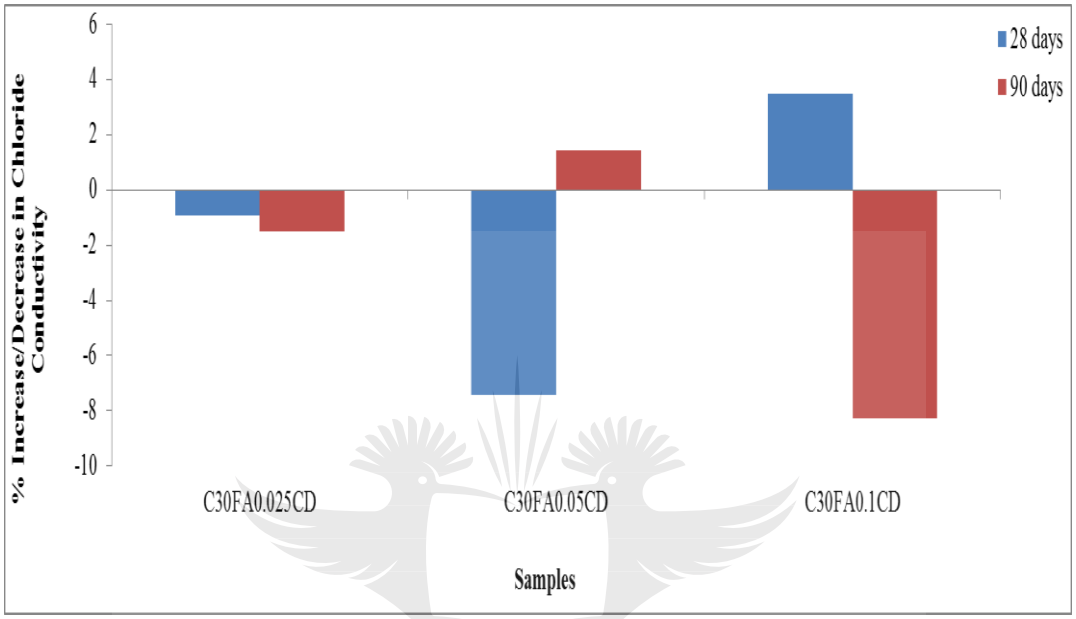

Figure 9.32: Percentage increase in the chloride conductivity of FA-β-CD composite samples compared to C30FA pozzolanic sample for 0.4-W/B

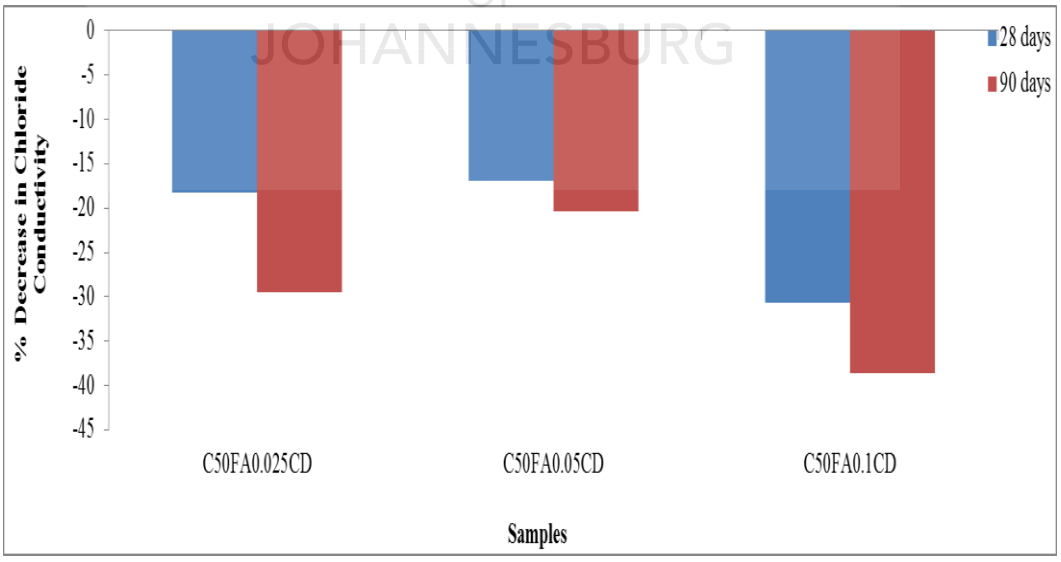

Figure 9.33: Percentage increase in the chloride conductivity of FA-β-CD composite samples compared to C50FA pozzolanic sample for 0.4-W/B

9.5 SUMMARY OF INCREASE/DECREASE IN DURABILITY PROPERTIES OF VARIOUS MIXTURES RELATIVE TO THE CONTROL MIXTURE

Table 9.3 summarises the increase/decrease in durability properties of various mixtures relative to the control mixture. The negative values represent relative decrease while positive values represent relative increase. The best results of the mixtures in column are highlighted in grey, while the worst result of the mixtures in column are highlighted in yellow.

Table 9.3: Summary of increase/decrease in durability properties of various mixtures relative to the control mixture

Mixture	Durability Properties															
	Permeability				Sorptivity				Porosity				CCI			
	0.5-W/B		0.4-W/B		0.5-W/B		0.4-W/B		0.5-W/B		0.4-W/B		0.5-W/B		0.4-W/B	
	28 d	90 d	28 d	90 d	28 d	90 d	28 d	90 d	28 d	90 d	28 d	90 d	28 d	90 d	28 d	90 d
C30FA	- 22.60	- 38.41	- 21.37	- 70.94	- 11.48	- 20.83	- 21.84	- 25.76	+ 11.40	+ 0.89	+ 6.80	- 21.89	- 49.12	+ 2.89	- 22.18	- 5.27
C50FA	- 4.11	- 51.68	- 76.18	- 86.56	- 11.48	- 26.61	- 15.33	- 17.75	+ 11.40	+ 6.25	+ 11.21	- 13.71	- 43.45	- 2.64	+ 2.04	+ 37.35
C0.025CD	+ 26.71	- 1.77	+ 30.53	- 26.71	- 9.84	- 25.60	+ 0.20	+ 0.91	- 13.16	- 18.75	- 13.50	- 20.98	- 42.61	+ 13.87	- 13.31	+ 18.03
C0.05CD	+ 36.30	- 11.50	+ 42.75	+ 10.16	0	+ 0.92	+ 9.22	+ 5.48	- 17.54	- 24.10	- 20.56	- 27.34	- 60.46	+ 6.21	- 3.24	+ 23.45
C0.1CD	-	-	-	-	+ 37.70	+ 13.76	+ 42.28	+ 15.62	- 22.80	- 25.89	- 23.21	- 27.34	- 59.91	+ 4.85	- 16.44	+ 11.33
C30FA0.025CD	- 58.08	- 48.94	- 60.15	- 70.55	- 24.84	- 17.52	+ 0.10	- 14.19	+ 1.75	- 1.79	- 2.91	- 3.72	- 56.25	+ 10.38	- 22.91	- 6.70
C30FA0.05CD	- 29.45	- 10.62	- 15.27	- 31.41	- 15.57	- 16.79	- 5.11	- 15.62	+ 2.63	+ 1.79	0	- 3.72	- 42.09	+ 7.06	- 27.97	- 3.92
C30FA0.1CD	-	-	- 16.03	- 35.55	- 14.75	- 16.15	+ 81.36	+ 28.80	- 7.02	- 8.93	- 9.09	- 11.90	- 50.18	+ 20.94	- 19.47	- 13.11
C50FA0.025CD	- 41.51	- 65.96	- 39.46	- 53.91	- 33.03	- 39.63	- 4.11	- 12.47	+ 6.14	- 1.79	+ 12.09	+ 12.62	- 56.14	+ 11.57	- 16.54	- 3.14
C50FA0.05CD	- 61.30	- 73.89	- 60.15	- 70.55	- 21.15	- 41.56	+ 4.21	- 14.00	- 0.88	0	+ 13.85	+ 6.27	- 52.51	- 1.87	- 15.24	+ 9.41
C50FA0.1CD	-	-	- 15.27	- 31.41	- 21.56	- 21.19	+ 14.23	+ 2.43	+ 0.88	- 0.89	+ 2.38	- 1.00	- 49.80	+ 0.26	- 29.23	- 15.61

9.6 CONCLUSIONS

The effect of FA, *β*-CD and FA-*β*-CD composites on concrete durability was presented and discussed in this chapter. The durability study was based on permeability, sorptivity, porosity and chloride conductivity, some of the properties used to assess the durability of concrete. A decrease in permeability, sorptivity, porosity and chloride conductivity was observed for all the samples as curing age increased. The FA and FA-*β*-CD composites with 0.025% and 0.05% *β*-CD samples reduced the permeability and sorptivity in comparison to the control samples for both the 0.5-W/B and 0.4-W/B at both curing ages. The 0.4-W/B samples showed a better influence on the permeability (maximum 86.56% reduction for C50FA) compared to the 0.5-W/B (maximum 73.89% reduction for C50FA0.05CD) samples, while a better influence on sorptivity was observed for 0.5-W/B samples (maximum 41.56% reduction for C50FA0.05CD) compared to the 0.4-W/B (maximum 25.76% reduction for C30FA) samples. The positive effect of FA and FA-*β*-CD composite samples on concrete permeability and sorptivity, compared with the control samples is linked to their surface morphologies. The plain concrete with *β*-CD showed a better influence on porosity (maximum 27.34% reduction for C0.05CD and C0.1CD with 0.4-W/B) compared to the FA and FA-*β*-CD composites samples, and a better influence of FA and *β*-CD on porosity was observed in the case of the 0.4-W/B samples compared to the 0.5-W/B samples. The FA-*β*-CD composites reduced permeability, sorptivity and porosity properties of the 0.5-W/B pozzolanic concrete relative to the 0.4-W/B pozzolanic concrete. The CCI values of all the samples are below 0.75 mS/cm; therefore the increasing/decreasing influence of the FA, *β*-CD and FA-*β*-CD composite samples on the CCI of the control samples appeared insignificant.

9.7 REFERENCES

[1] Heede P.V., Gruyaert E., Belie N.D.: Transport properties of high-volume fly ash concrete: Capillary water sorption, water sorption under vacuum and gas permeability. Cement and Concrete Composites **32**, 749–756 (2010).

[2] Alexander M.G., Ballim Y., Mackechnie J.M.: Concrete durability index testing manual, Research monograph no. 4, Departments of Civil Engineering, University of Cape Town and University of the Witwatersrand (1999).

[3] Alexander M.G., Mackechnie J.R., Ballim Y.: Guide to the use of durability indexes for achieving durability in concrete structures, Research monograph no 2, published by the Department of Civil Engineering, University of Cape Town in collaboration of University of the Witwatersrand, 5-25 (2001).

[4] Alexander M. G.: Durability indexes and their use in concrete engineering, International RILEM Symposium on Concrete Science and Engineering: A Tribute to Arnon Bentur. Print-ISBN**:** 2-912143-46-2, e-ISBN**:** 2912143586, Publisher**:** RILEM Publications SARL, 9 – 22 (2004).

[5] Ramezanianpour A.A., Jovein H.B.: Influence of metakaolin as supplementary cementing material on strength and durability of concretes. Construction and Building Materials **30**, 470-479 (2012).

[6] Soroka I.: Portland cement paste and concrete, Published by the Macmillan Press Limited, ISBN 0-333-24231-9, pp. 30-34 (1979).

CHAPTER TEN

CONCLUSIONS AND RECOMMENDATIONS

10. 1 CONCLUSIONS

This study looked into the possibility of increasing the utilisation of fly ash (FA) in concrete technology. FA, being an industrial waste that is in abundance in South Africa and a source of environmental pollution is presently being used minimally in the construction industry. The study on its interaction with cyclodextrin (an enzymatic modification of starch) for possible increased usage in concrete operations was done. Different South African fly ashes were characterised and their compatibility with cyclodextrin to form a useful composite was studied by XRD, SEM and FT-IR. Composite samples were synthesized following two different procedures. Since these are novel composites, indicative tests were performed on strength (compressive and split tensile) and durability (oxygen permeability, sorptivity and porosity) on mortar/concrete made with FA (30% of cement by mass) and fly ash-β-cyclodextrin (FA-β-CD) composite, that further guided the research. Based on the indicative tests results, a possible optimum composite synthesis method and percentages of β-cyclodextrin (β-CD) in the mixtures were identified. These optimal parameters were used to study the effect of FA, β-CD and (FA-β-CD) composite on cement paste hydration (XRD, SEM and FT-IR), rheology (viscosity and setting time), concrete strength (compressive and split tensile) and concrete durability (oxygen permeability, sorptivity, porosity and chloride conductivity).

Based on the results presented in the preceding chapters, the following conclusions were made:

1. The four **South African Class F fly ashes** investigated have similar characteristics and exhibited similar structural changes with cyclodextrin. The structural changes of these fly ashes with cyclodextrin are shown by the

evidence of additional peaks in the XRD results between diffraction angles (2θ) 10^0 and 25^0, shift in FT-IR spectra frequencies and additional peak at approximately 1155 cm^{-1} attributed to O-Si-O bending vibration.

2. **Composite formation** was confirmed through the structural compatibility between fly ash and cyclodextrin. The new composite has additional peaks at the X-ray diffractogram and IR-spectra, also changes in surface morphologies, particle size and pore size compared to the original materials were observed.

3. **The indicative tests** showed that the FA-*β*-CD composite improved the flow of mortars and workability of concrete. The results showed that a higher content of *β*-CD (0.5%) in concrete has a detrimental effect on the workability and strength for both dry and solution mixtures. However, lower percentages of *β*-CD (0.1% and 0.2%) improved workability without reducing the cohesiveness of concrete, increased compressive strength at all ages compared to pozzolanic sample and increased split tensile strength at curing ages of 28 and 90 days when compared to the pozzolanic samples.

4. **The indicative tests** further revealed improved mortar/concrete durability with FA-*β*-CD composites at lower percentages (0.1% and 0.2%) of *β*-CD. The dry mix samples showed a better sorptivity and porosity compared to the solution mixed samples. The lower the *β*-CD in the composite, the better the positive effect it has on the durability. Based on these indicative tests, subsequent tests were performed on the lower contents of *β*-CD (0.025%, 0.05% and 0.1%), 30% and 50% FA and using the physical (dried) mixed composite synthesis method.

5. The effect of FA, *β*-CD and FA-*β*-CD composite on **cement paste hydration** showed that *β*-CD samples aid both early (from 7 days) and late hydration processes compared to control sample with the evidence of increased dissolution of C_3S and C_2S at the 7 days hydration period and higher formation of CH at the 90 days hydration period. The effect of *β*-CD on

pozzolanic reaction was revealed from the 28 days hydration period in the XRD results.

6. The **morphology** of the *β*-CD samples studied by **SEM** revealed a crystalline structure of portlandite (CH) at the 7 days hydration period for the C0.025CD samples compared to the control sample. The higher the *β*-CD content, the more the dissolution of the anhydrous phase of the cement paste was observed in the SEM morphology at the 7 days hydration period. The SEM results also revealed that at 90 days hydration period, *β*-CD and FA-*β*-CD composite samples had an improved denser surface and reduced continuous capillary pores when compared to the control, C30FA and C50FA samples.

7. The **FT-IR results** showed that *β*-CD aids the dissolution of C_3S clinker phase resulting in the greater and sharper intensity of Si-O asymmetric stretching band (ν_3) of samples containing *β*-CD compared to control sample at 24 hours and 7 days hydration periods. At 90 days, the FT-IR spectra of control, FA, *β*-CD and FA-*β*-CD composites samples were closely related.

8. The **viscosity test** performed on cement pastes with 0.6-W/B, 0.5-W/B and 0.4-W/B showed that the W/B has an effect on the viscosity of cement paste. The higher the W/B, the lower the viscosity observed for all samples. The FA, *β*-CD and FA-*β*-CD composites reduced the viscosity of the cement paste, with *β*-CD having a higher effect in reducing viscosity than FA. The lowest viscosity was observed with the FA-*β*-CD composites samples for all the W/B. The higher the FA and *β*-CD contents, the lower the viscosity observed.

9. The trend observed with **viscosity results** was also observed in setting times results. The higher the FA and *β*-CD contents, the lower the water required for consistency and the longer the setting times observed, with the FA-*β*-CD composites samples exhibiting longest setting times.

10. The effect of FA, *β*-CD and FA-*β*-CD composite on concrete **workability and strength** showed that, the higher the contents of FA and *β*-CD, as used in this study, the greater the workability of the concrete for both 0.5-W/B and 0.4-W/B mixtures. A progressive increase in both compressive strength and split tensile strength was observed for all the samples as curing age increased. The 0.4-W/B samples had higher compressive and split tensile strengths compared to the samples with 0.5-W/B at all curing ages. The C30FA sample, with 0.4W/B showed increase in compressive strength at 180 days curing age when compared with the control sample. On the other hand, the C50FA sample reduced the compressive strength at all curing ages with 19.84% reduction at 180 days curing age when compared with the control sample.

11. *β*-CD increased both compressive and **split tensile strengths** of the control, C30FA and C50FA samples with both the 0.5-W/B and 0.4-W/B. A greater influence of *β*-CD in increasing compressive strength was observed for sample with the 0.05% *β*-CD, while a greater influence of *β*-CD in increasing split tensile strength was observed for samples with 0.1% *β*-CD.

12. The effect of FA, *β*-CD and FA-*β*-CD composite on **concrete durability** showed a decrease in permeability, sorptivity, porosity and chloride conductivity for all the samples as curing age increased, for both 0.5-W/B and 0.4-W/B. The FA and FA-*β*-CD composite samples with 0.025% and 0.05% *β*-CD showed reduced permeability and sorptivity relative to the control sample, for both 0.5-W/B and 0.4-W/B samples, at both the 28 and 90 days curing ages.

13. The positive effect of FA and FA-*β*-CD composite samples on concrete **permeability and sorptivity** as compared with the control sample is linked to their surface morphologies. The plain concrete with *β*-CD showed a better influence on porosity than the FA and FA- *β*-CD composites samples. A better influence of FA and *β*-CD on porosity was observed with the 0.4-W/B

samples than with the 0.5-W/B samples. However, the FA-*β*-CD composites samples improved the permeability, sorptivity and porosity properties of the 0.5-W/B pozzolanic concrete better than pozzolanic concrete with 0.4W/B.

14. The **chloride conductivity index** (CCI) values of all the samples are below 0.75 mS/cm; therefore the increasing/decreasing influence of the FA, *β*-CD and FA-*β*-CD composite samples on the CCI of the control and pozzolanic samples appeared to be insignificant.

15. In **general**, concrete's hydration products were modified with FA – cyclodextrin composite, which boosted the performance of FA in concrete. The composite improved FA concrete's early compressive strength, permeability, sorptivity, porosity and chloride conductivity.

10.2 RECOMMENDATIONS

Based on the above conclusions, the following recommendations for further research, on the use of *β*-CD and FA-*β*-CD composite on plain and pozzolanic concrete, are deduced.

1. To incorporate FA-*β*-CD composite into concrete, it has to be used at lower percentages of FA and *β*-CD, optimum percentages for general improvement in strength and durability as seen in this study are 30% for FA and 0.05% for *β*-CD. A lower W/B of 0.4 and dried mixture composite synthesis method should be adopted.

2. For high strength concrete, where a reduced W/B is needed with improved workability, strength and durability properties, 0.05% *β*-CD can be incorporated into the mixture.

3. To standardize the use of *β*-CD and FA-*β*-CD composite on plain and pozzolanic concrete, further research needs to be done with different cement

types and other parameters related to the post hardening properties of concrete. Samples can also be exposed to some aggressive environments for number of days to which other samples were cured normally and checked for durability and reduction in strength.

4. Further research should be done on the effect of *β*-CD and FA-*β*-CD composite on self-compacting concrete.

APPENDIX A

DETAILED EXPERIMENTAL RESULTS

Table A.1: Indicative tests matrix

Tests	Sample sizes/type	Test ages	No of samples	Total	Test methods
Flow	Fresh mortar	After mixing	6	--	ASTM C 1437
Workability	Fresh concrete	After mixing	8	--	SANS 5862-1:2006
Compressive strength	100 mm cubes	7, 14, 28, 90 and 180 days	12 cubes/mix	96 cubes	SANS 5863: 2006
Split tensile strength	150mm x 300mm cylinders	14, 28 and 90 days	9 cylinders/mix	72 cylinders	SANS 6253: 2006
Oxygen permeability, sorptivity and porosity	100 mm cubes	14 and 28 days	2 cubes/mix (mortar) 4 cubes/mix (concrete)	48 cubes	Method described by Alexander et al (1999)

Total samples cast: 144 (100mm cubes), 72 (150mm x 300mm cylinders)

Table A.2: Actual tests matrix

Tests	Sample sizes/type	Test ages/type	No of samples	Total	Test methods
XRD	Hydrated samples	24 hours, 7, 28, 90 days	12/age	48	X-ray diffraction analysis
SEM	Hydrated samples	27, 28, 90 days	12/age	36	Scanning electron microscope
FT-IR	Hydrated samples	24 hours, 7, 28, 90 days	12/age	48	Fourier transform-infrared analysis
Viscosity	Fresh cement paste	0.6-W/B, 0.5-W/B and 0.4-W/B	12/W/B	36	VT-04F portable viscotester
Setting times	Fresh cement paste	Consistency samples	12	--	SANS 50196-3
Workability	Fresh concrete	After mixing (0.5-W/B and 0.4-W/B)	12/W/B	24	SANS 5862-1:2006
Compressive strength	100 mm cubes	7, 14, 28, 90 and 180 days (0.5-W/B and 0.4-W/B)	15 cubes/mix	360 cubes	SANS 5863: 2006
Split tensile strength	150mm x 300mm cylinders	14, 28, 90 and 180 days (0.5-W/B and 0.4-W/B)	12 cylinders/mix	288 cylinders	SANS 6253: 2006
Oxygen permeability, sorptivity, porosity and chloride conductivity	100 mm cubes	28 and 90 days (0.5-W/B and 0.4-W/B)	8 cubes/mix	192 cubes	Method described by Alexander et al (1999)

Total samples cast: 552 (100mm cubes), 288 (150mm x 300mm cylinders)

Table A.3: Compressive strength of samples at different curing ages for indicative samples

Samples	W/B	Slump mm	Com. Strength (7 days)				Com. Strength (14 days)				Com. Strength (28 days)				Com. Strength (90 days)				Com. Strength (180 days)			
			L1, (kN)	L2 (kN)	L3 (kN)	Av. S (MPa)	L1 (kN)	L2 (kN)	L3 (kN)	Av. S (MPa)	L1 (kN)	L2 (kN)	L3 (kN)	Av. S (MPa)	L1 (kN)	L2 (kN)	L3 (kN)	Av. S (MPa)	L1 (kN)	L2 (kN)	L3 (kN)	Av. S (MPa)
Control	0.5	50	388	388	343	**37.30**	426	443	400	**42.30**	520	518	519	**51.90**	525	521	521	**52.23**	526	530	528	**52.80**
FA-C	0.5	90	192	180	185	**18.57**	244	225	236	**23.50**	306	297	313	**30.53**	439	465	432	**44.50**	549	552	549	**55.00**
F-0.1CD-D	0.47	95	275	263	270	**26.93**	316	284	291	**29.70**	393	393	400	**39.50**	535	538	527	**53.33**	585	592	593	**59.00**
F-0.2CD-D	0.42	120	251	254	250	**25.17**	275	270	272	**27.23**	355	359	360	**35.80**	495	486	487	**48.90**	575	571	573	**57.30**
F-0.5CD-D	0.42	130	56	58	52	**5.53**	69	71	80	**7.33**	89	90	99	**9.27**	285	280	279	**28.13**	280	285	284	**28.30**
F-0.1CD-S	0.47	150	275	254	266	**26.50**	320	291	283	**29.80**	402	392	395	**39.6**	531	534	532	**53.23**	569	575	573	**57.23**
F-0.2CD-S	0.42	150	275	262	265	**26.73**	280	270	278	**27.60**	391	363	380	**37.80**	520	500	510	**51.0**	559	557	564	**56.0**
F-0.5CD-S	0.4	60	18	23	20	**2.03**	25	27	23	**2.50**	41	40	34	**3.83**	200	208	210	**20.6**	250	248	259	**25.23**

Table A.4: Split tensile strength of samples at different curing ages for indicative samples

Samples	Split Tensile Strength (14 days)				Split Tensile Strength (28 days)				Split Tensile Strength (90 days)			
	L1 (kN)	L2 (kN)	L3 (kN)	$F = \frac{2P}{\pi dl}$ (Mpa)	L1 (kN)	L2 (kN)	L3 (kN)	$F = \frac{2P}{\pi dl}$ (Mpa)	L1 (kN)	L2 (kN)	L3 (kN)	$F = \frac{2P}{\pi dl}$ (Mpa)
C	250	251	248	**3.53**	275	269	270	**3.84**	269	272	274	**3.84**
FA-C	183	185	180	**2.58**	192	204	200	**2.81**	241	238	245	**3.41**
F-0.1CD-D	181	183	179	**2.56**	240	232	233	**3.32**	312	310	310	**4.39**
F-0.2CD-D	165	170	160	**2.33**	212	215	220	**3.05**	275	278	280	**3.93**
F-0.5CD-D	18	20	18	**0.26**	44	40	42	**0.59**	150	152	158	**2.17**
F-0.1CD-S	188	186	185	**2.63**	235	230	243	**3.34**	306	308	310	**4.36**
F-0.2CD-S	170	166	172	**2.39**	195	182	190	**2.67**	270	272	274	**3.85**
F-0.5CD-S	15	13	18	**0.22**	21	25	22	**0.32**	149	145	150	**2.09**

Table A.5: Percentage increase in FA-*β*-CD composite samples compressive strength compared to pozzolanic sample compressive strength for indicative samples

	7 days	14 days	28 days	90 days	180 days
F-0.1CD-D	45.02%	26.38%	29.38%	19.84%	7.27%
F-0.1CD-S	42.70%	26.81%	29.71%	19.62%	4.05%
F-0.2CD-D	35.54%	15.87%	17.26%	9.89%	4.18%
F-0.2CD-S	43.94%	17.45%	23.81%	14.61%	1.81%

Table A.6: Percentage increase/decrease in FA-*β*-CD composite samples split tensile strength compared to pozzolanic sample split tensile strength for indicative samples

	14 days	28 days	90 days
F-0.1CD-D	-0.78%	18.15%	28.74%
F-0.1CD-S	1.94%	18.86%	27.86%
F-0.2CD-D	-9.69%	8.54%	15.25%
F-0.2CD-S	-7.36%	-4.98%	12.9%

Table A.7: Indicative durability (OPI, permeability, sorptivity and porosity) results of mortar samples at different curing ages

Samples	Days	OPI	Permeability, k (m/s)	Sorptivity ($mm/hr^{0.5}$)	Porosity (%)
MC	14	10.19	6.46E-11	5.69E+00	18.3
MC	28	10.20	6.25E-11	6.00E+00	17.4
MFA-C	14	10.04	9.13E-11	8.17E+00	20.7
MFA-C	28	10.26	5.35E-11	6.65E+00	19.0
M0.1D	14	10.28	4.40E-11	6.05E+00	13.8
M0.1D	28	10.49	3.10E-11	4.69E+00	12.5
M0.1S	14	10.40	3.40E-11	6.44E+00	14.2
M0.1S	28	10.50	3.00E-11	5.10E+00	13.1
M0.2D	14	10.27	5.30E-11	6.73E+00	14.4
M0.2D	28	10.46	3.49E-11	5.52E+00	13.0
M0.2S	14	10.47	3.21E-11	6.79E+00	15.0
M0.2S	28	10.53	2.92E-11	5.50E+00	14.7

Table A.8: Indicative durability (OPI, permeability, sorptivity and porosity) results of concrete samples at different curing ages

Samples	days	Sorptivity ($mm/hr^{0.5}$)	Porosity (%)
C	14	1.34E+01	13.8
C	28	8.83E+00	12.0
FA	14	1.18E+01	13.0
FA	28	9.90E+00	12.2
0.1D	14	9.92E+00	9.2
0.1D	28	7.00E+00	9.0
0.1S	14	1.12E+01	9.8
0.1S	28	8.70E+00	9.5
0.2D	14	1.02E+01	10.1
0.2D	28	9.26E+00	9.7
0.2S	14	1.15E+01	11.1
0.2S	28	9.60E+00	9.8

Table A.9: Initial and Final mass of 0.5-W/B concrete

Samples	Initial Concrete Mass			Concrete Mass (7 days)			Concrete Mass (14 days)			Concrete Mass(28 days)			Concrete Mass(90 days)			Concrete Mass (180 days)		
	m_1 (g)	m_2 (g)	m_3 (g)	m_1 (g)	m_2 (g)	m_3 (g)	m_1 (g)	m_2 (g)	m_3 (g)	m_1 (g)	m_2 (g)	m_3 (g)	m_1 (g)	m_2 (g)	m_3 (g)	m_1 (g)	m_2 (g)	m_3 (g)
Control (100% PC)	2417	2374	2394	2455	2420	2432	2455	2420	2432	2460	2425	2438	2460	2426	2439	2457	2425	2438
C30FA	2350	2348	2323	2383	2384	2354	2385	2386	2354	2395	2394	2364	2398	2398	2368	2397	2396	2365
C50FA	2274	2302	2352	2299	2324	2380	2308	2333	2388	2314	2339	2395	2317	2343	2398	2316	2343	2398
C0.025CD	2416	2347	2299	2451	2381	2334	2457	2388	2340	2459	2389	2343	2460	2390	2343	2460	2390	2344
C0.05CD	2360	2373	2322	2390	2410	2352	2396	2414	2356	2399	2418	2359	2400	2418	2359	2399	3418	2360
C0.1CD	2349	2341	2342	2372	2369	2372	2378	2375	2377	2382	2379	2380	2383	2380	2380	2381	2378	2380
C30FA0.025CD	2353	2373	2379	2376	2397	2402	2383	2404	2408	2387	2408	2413	2391	2413	2417	2390	2412	2416
C30FA0.05CD	2311	2353	2340	2339	2382	2368	2347	2389	2374	2351	2394	2379	2355	2398	2383	2354	2397	2382
C30FA0.1CD	2362	2371	2370	2381	2388	2388	2390	2398	2397	2395	2403	2403	2399	2407	2406	2399	2407	2406
C50FA0.025CD	2402	2396	2383	2427	2415	2398	2435	2424	2408	2442	2429	2414	2446	2433	2417	2444	2432	2417
C50FA0.05CD	2343	2344	2318	2369	2370	2345	2376	2376	2351	2378	2379	2353	2382	2381	2357	2380	2380	2356
C50FA0.1CD	2362	2352	2259	2411	2383	2294	2419	2391	2302	2423	2394	2306	2427	2397	2309	2425	2396	2307

Table A.10: Mass variation of 0.5-W/B concrete

Samples	Water absorption (7 days) Change in mass = *Final mass – Initial mass*				Water absorption (14 days) Change in mass = *Final mass – Initial mass*				Water absorption(28 days) Change in mass = *Final mass – Initial mass*				Water absorption(90 days) Change in mass = *Final mass – Initial mass*				Water absorption (180 days) Change in mass = *Final mass – Initial mass*			
	W.A 1 (g)	W.A 2 (g)	W.A 3 (g)	Av. Water absorbed	W. A 1 (g)	W.A 2 (g)	W.A 3 (g)	Av. Water absorbed	W.A 1 (g)	W.A 2 (g)	W.A 3 (g)	Av. Water absorbed	W.A 1 (g)	W.A 2 (g)	W.A 3 (g)	Av. Water absorbed	W. A1 (g)	W.A 2 (g)	W.A 3 (g)	Av. Water absorbed
Control (100% PC)	38	46	38	**40.67**	43	51	44	**46.00**	43	51	44	**46.00**	43	52	45	**46.67**	40	51	44	**45.00**
C30FA	33	36	31	**33.33**	35	38	31	**34.67**	45	46	41	**44.00**	48	50	45	**47.67**	47	48	42	**45.67**
C50FA	25	22	28	**25.00**	34	31	36	**33.67**	40	37	43	**40.00**	43	41	46	**43.33**	42	41	46	**43.00**
C0.025CD	35	34	35	**34.67**	41	41	41	**41.00**	43	42	44	**43.00**	44	43	44	**43.67**	44	43	45	**44.00**
C0.05CD	30	37	30	**32.33**	36	41	34	**37.00**	39	45	37	**40.33**	40	45	37	**40.67**	39	45	38	**40.67**
C0.1CD	23	28	30	**27.00**	29	34	35	**32.67**	33	38	38	**36.33**	34	39	38	**37.00**	32	37	38	**35.67**
C30FA0.025CD	23	24	23	**23.33**	30	31	29	**30.00**	34	35	34	**34.33**	38	40	38	**38.67**	37	39	37	**37.67**
C30FA0.05CD	28	29	28	**28.33**	36	36	34	**35.33**	40	41	39	**40.00**	44	45	43	**44.00**	43	44	42	**43.00**
C30FA0.1CD	19	17	18	**18.00**	28	27	27	**27.33**	33	32	33	**32.67**	37	36	36	**36.33**	37	36	36	**36.33**
C50FA0.025CD	25	19	15	**19.67**	33	28	25	**28.67**	40	33	31	**34.67**	44	37	34	**38.33**	42	36	34	**37.33**
C50FA0.05CD	26	26	27	**26.33**	33	32	33	**32.67**	35	35	35	**35.00**	39	37	39	**38.33**	37	36	38	**37.00**
C50FA0.1CD	49	31	35	**38.33**	57	39	43	**46.33**	61	42	47	**50.00**	65	45	50	**53.33**	63	44	48	**51.67**

Table A.11: Density of 0.5-W/B concrete

Samples	Initial Density (D) of concrete(kg/m^3) Volume = $0.001m^3$				Density of concrete (7 days)(kg/m^3) Volume = $0.001m^3$				Density of concrete (14 days)(kg/m^3) Volume = $0.001m^3$				Density of concrete (28 days)(kg/m^3) Volume = $0.001m^3$				Density of concrete (90 days)(kg/m^3) Volume = $0.001m^3$				Density of concrete (180 days)(kg/m^3) Volume = $0.001m^3$			
	m1 (g)	m2 (g)	m3 (g)	Av. D	m1 (g)	m2 (g)	m3 (g)	Av. D	m1 (g)	m2 (g)	m3 (g)	Av. D	m1 (g)	m2 (g)	m3 (g)	Av. D	m1 (g)	m2 (g)	m3 (g)	Av. D	m1 (g)	m2 (g)	m3 (g)	Av. D
Control (100% PC)	2417	2374	2394	**2395**	2455	2420	2432	**2436**	2455	2420	2432	**2436**	2460	2425	2438	**2441**	2460	2426	2439	**2442**	2457	2425	2438	**2440**
C30FA	2350	2348	2323	**2340**	2383	2384	2354	**2374**	2385	2386	2354	**2375**	2395	2394	2364	**2384**	2398	2398	2368	**2388**	2397	2396	2365	**2386**
C50FA	2274	2302	2352	**2309**	2299	2324	2380	**2334**	2308	2333	2388	**2343**	2314	2339	2395	**2349**	2317	2343	2398	**2353**	2316	2343	2398	**2352**
C0.025CD	2416	2347	2299	**2354**	2451	2381	2334	**2389**	2457	2388	2340	**2395**	2459	2389	2343	**2397**	2460	2390	2343	**2398**	2460	2390	2344	**2398**
C0.05CD	2360	2373	2322	**2352**	2390	2410	2352	**2384**	2396	2414	2356	**2389**	2399	2418	2359	**2392**	2400	2418	2359	**2392**	2399	3418	2360	**2726**
C0.1CD	2349	2341	2342	**2344**	2372	2369	2372	**2371**	2378	2375	2377	**2377**	2382	2379	2380	**2380**	2383	2380	2380	**2381**	2381	2378	2380	**2380**
C30FA0.025 CD	2353	2373	2379	**2368**	2376	2397	2402	**2392**	2383	2404	2408	**2398**	2387	2408	2413	**2403**	2391	2413	2417	**2407**	2390	2412	2416	**2406**
C30FA0.05C D	2311	2353	2340	**2335**	2339	2382	2368	**2363**	2347	2389	2374	**2370**	2351	2394	2379	**2375**	2355	2398	2383	**2379**	2354	2397	2382	**2378**
C30FA0.1CD	2362	2371	2370	**2368**	2381	2388	2388	**2386**	2390	2398	2397	**2395**	2395	2403	2403	**2400**	2399	2407	2406	**2404**	2399	2407	2406	**2404**
C50FA0.025 CD	2402	2396	2383	**2394**	2427	2415	2398	**2413**	2435	2424	2408	**2422**	2442	2429	2414	**2428**	2446	2433	2417	**2432**	2444	2432	2417	**2431**
C50FA0.05C D	2343	2344	2318	**2335**	2369	2370	2345	**2361**	2376	2376	2351	**2368**	2378	2379	2353	**2370**	2382	2381	2357	**2373**	2380	2380	2356	**2372**
C50FA0.1CD	2362	2352	2259	**2324**	2411	2383	2294	**2363**	2419	2391	2302	**2371**	2423	2394	2306	**2374**	2427	2397	2309	**2378**	2425	2396	2307	**2376**

Table A.12: Initial and Final mass of 0.4-W/B concrete

Samples	Initial Concrete Mass			Concrete Mass (7 days)			Concrete Mass (14 days)			Concrete Mass(28 days)			Concrete Mass(90 days)			Concrete Mass (180 days)		
	m1 (g)	m2 (g)	m3 (g)	m1 (g)	m2 (g)	m3 (g)	m1 (g)	m2 (g)	m3 (g)	m1 (g)	m2 (g)	m3 (g)	m1 (g)	m2 (g)	m3 (g)	m1 (g)	m2 (g)	m3 (g)
Control (100% PC)	2485	2493	2482	2514	2522	2512	2518	2525	2515	2518	2526	2515	2522	2531	2521	2520	2529	2519
C30FA	2467	2434	2413	2494	2464	2441	2499	2467	2444	2500	2468	2446	2504	2473	2452	2502	2471	2450
C50FA	2392	2386	2427	2418	2412	2455	2422	2415	2458	2422	2416	2458	2425	2421	2464	2414	2409	2452
C0.025CD	2444	2461	2471	2483	2497	2509	2484	2498	2510	2485	2499	2511	2489	2504	2515	2478	2492	2505
C0.05CD	2495	2482	2472	2523	2512	2499	2526	2515	2502	2526	2515	2502	2530	2519	2505	2518	2507	2493
C0.1CD	2446	2372	2471	2469	2402	2495	2471	2405	2497	2472	2405	2498	2475	2410	2503	2466	2399	2492
C30FA0.025CD	2409	2420	2489	2445	2448	2522	2450	2452	2527	2452	2454	2528	2455	2458	2531	2430	2432	2504
C30FA0.05CD	2423	2389	2443	2448	2424	2479	2452	2428	2483	2453	2430	2485	2456	2434	2488	2430	2407	2461
C30FA0.1CD	2392	2417	2435	2438	2477	2454	2441	2481	2458	2443	2483	2461	2446	2487	2463	2422	2461	2437
C50FA0.025CD	2357	2352	2332	2392	2400	2393	2397	2406	2399	2401	2410	2403	2404	2414	2407	2380	2390	2382
C50FA0.05CD	2405	2393	2430	2441	2423	2457	2446	2427	2460	2448	2430	2463	2450	2431	2465	2426	2408	2441
C50FA0.1CD	2408	2354	2395	2432	2379	2425	2437	2383	2430	2441	2388	2434	2444	2392	2438	2421	2368	2413

Table A.13: Mass variation of 0.4-W/B concrete

Samples	Water absorption (7 days) Change in mass = *Final mass – Initial mass*				Water absorption (14 days) Change in mass = *Final mass – Initial mass*				Water absorption (28 days) Change in mass = *Final mass – Initial mass*				Water absorption(90 days) Change in mass = *Final mass – Initial mass*				Water absorption (180 days) Change in mass = *Final mass – Initial mass*			
	W.A 1 (g)	W.A 2 (g)	W.A 3 (g)	Av. Water absorbed	W. A 1 (g)	W.A 2 (g)	W.A 3 (g)	Av. Water absorbed	W.A 1 (g)	W.A 2 (g)	W.A 3 (g)	Av. Water absorbed	W.A 1 (g)	W.A 2 (g)	W.A 3 (g)	Av. Water absorbed	W. A1 (g)	W.A 2 (g)	W.A 3 (g)	Av. Water absorbed
Control (100% PC)	29	29	30	**29.33**	33	32	33	**32.67**	33	33	33	**33.00**	37	38	39	**38.00**	35	36	37	**36.00**
C30FA	27	30	28	**28.33**	32	33	31	**32.00**	33	34	33	**33.33**	37	39	39	**38.33**	35	37	37	**36.33**
C50FA	26	26	28	**26.67**	30	29	31	**30.00**	30	30	31	**30.33**	33	35	37	**35.00**	22	23	25	**23.33**
C0.025CD	39	36	38	**37.67**	40	37	39	**38.67**	41	38	40	**39.67**	45	43	44	**44.00**	34	31	34	**33.33**
C0.05CD	28	30	27	**28.33**	31	33	30	**31.33**	31	33	30	**31.33**	35	37	33	**35.00**	23	25	21	**23.00**
C0.1CD	23	30	24	**25.67**	25	33	26	**28.00**	26	33	27	**28.67**	29	38	32	**33.00**	20	27	21	**22.67**
C30FA0.025CD	36	28	33	**32.33**	41	32	38	**37.00**	43	34	39	**38.67**	46	38	42	**42.00**	21	12	15	**16.00**
C30FA0.05CD	25	35	36	**32.00**	29	39	40	**36.00**	30	41	42	**37.67**	33	45	45	**41.00**	7	18	18	**14.33**
C30FA0.1CD	46	60	19	**41.67**	49	64	23	**45.33**	51	66	26	**47.67**	54	70	28	**50.67**	30	44	2	**25.33**
C50FA0.025CD	35	48	61	**48.00**	40	54	67	**53.67**	44	58	71	**57.67**	47	62	75	**61.33**	23	38	50	**37.00**
C50FA0.05CD	36	30	27	**31.00**	41	34	30	**35.00**	43	37	33	**37.67**	45	38	35	**39.33**	21	15	11	**15.67**
C50FA0.1CD	24	25	30	**26.33**	29	29	35	**31.00**	33	34	39	**35.33**	36	38	43	**39.00**	13	14	18	**15.00**

Table A.14: Density of 0.4-W/B concrete

Samples	Initial Density (D) of concrete(kg/m^3) Volume = 0.001m^3				Density of concrete (7 days)(kg/m^3) Volume = 0.001m^3				Density of concrete (14 days)(kg/m^3) Volume = 0.001m^3				Density of concrete (28 days)(kg/m^3) Volume = 0.001m^3				Density of concrete (90 days)(kg/m^3) Volume = 0.001m^3				Density of concrete (180 days)(kg/m^3) Volume = 0.001m^3			
	m1 (g)	m2 (g)	m3 (g)	Av. D	m1 (g)	m2 (g)	m3 (g)	Av. D	m1 (g)	m2 (g)	m3 (g)	Av. D	m1 (g)	m2 (g)	m3 (g)	Av. D	m1 (g)	m2 (g)	m3 (g)	Av. D	m1 (g)	m2 (g)	m3 (g)	Av. D
Control (100% PC)	2485	2493	2482	**2487**	2514	2522	2512	**2516**	2518	2525	2515	**2519**	2518	2526	2515	**2520**	2522	2531	2521	**2525**	2520	2529	2519	**2523**
C30FA	2467	2434	2413	**2438**	2494	2464	2441	**2466**	2499	2467	2444	**2470**	2500	2468	2446	**2471**	2504	2473	2452	**2476**	2502	2471	2450	**2474**
C50FA	2392	2386	2427	**2402**	2418	2412	2455	**2428**	2422	2415	2458	**2432**	2422	2416	2458	**2432**	2425	2421	2464	**2436**	2414	2409	2452	**2425**
C0.025CD	2444	2461	2471	**2459**	2483	2497	2509	**2496**	2484	2498	2510	**2497**	2485	2499	2511	**2498**	2489	2504	2515	**2503**	2478	2492	2505	**2492**
C0.05CD	2495	2482	2472	**2483**	2523	2512	2499	**2511**	2526	2515	2502	**2514**	2526	2515	2502	**2514**	2530	2519	2505	**2518**	2518	2507	2493	**2506**
C0.1CD	2446	2372	2471	**2430**	2469	2402	2495	**2455**	2471	2405	2497	**2458**	2472	2405	2498	**2458**	2475	2410	2503	**2463**	2466	2399	2492	**2452**
C30FA0.025CD	2409	2420	2489	**2439**	2445	2448	2522	**2472**	2450	2452	2527	**2476**	2452	2454	2528	**2478**	2455	2458	2531	**2481**	2430	2432	2504	**2455**
C30FA0.05CD	2423	2389	2443	**2418**	2448	2424	2479	**2450**	2452	2428	2483	**2454**	2453	2430	2485	**2456**	2456	2434	2488	**2459**	2430	2407	2461	**2433**
C30FA0.1CD	2392	2417	2435	**2415**	2438	2477	2454	**2456**	2441	2481	2458	**2460**	2443	2483	2461	**2462**	2446	2487	2463	**2465**	2422	2461	2437	**2440**
C50FA0.025CD	2357	2352	2332	**2347**	2392	2400	2393	**2395**	2397	2406	2399	**2401**	2401	2410	2403	**2405**	2404	2414	2407	**2408**	2380	2390	2382	**2384**
C50FA0.05CD	2405	2393	2430	**2409**	2441	2423	2457	**2440**	2446	2427	2460	**2444**	2448	2430	2463	**2447**	2450	2431	2465	**2449**	2426	2408	2441	**2425**
C50FA0.1CD	2408	2354	2395	**2386**	2432	2379	2425	**2412**	2437	2383	2430	**2417**	2441	2388	2434	**2421**	2444	2392	2438	**2425**	2421	2368	2413	**2401**

Table A.15: Compressive strength of 0.5-W/B concrete samples at different curing ages

Samples	W/B	Slump (mm)	Com. Strength (7 days)				Com. Strength (14 days)				Com. Strength (28 days)				Com. Strength (90 days)				Com. Strength (180 days)			
			L1 (kN)	L2 (kN)	L3 (kN)	Av. S (MPa)	L1 (kN)	L2 (kN)	L3 (kN)	Av. S (MPa)	L1 (kN)	L2 (kN)	L3 (kN)	Av. S (MPa)	L1 (kN)	L2 (kN)	L3 (kN)	Av. S (MPa)	L1 (kN)	L2 (kN)	L3 (kN)	Av. S (MPa)
Control (100% PC)	0.5	35	396	415	416	**40.9**	532	534	520	**52.87**	614	625	620	**61.97**	708	690	683	**69.37**	745	752	748	**74.83**
C30FA	0.5	45	219	219	214	**21.73**	390	395	405	**39.67**	431	434	442	**43.57**	583	590	585	**58.60**	690	695	700	**69.50**
C50FA	0.5	65	151	155	149	**15.17**	214	222	219	**21.83**	261	267	270	**26.60**	429	425	422	**42.53**	582	589	594	**58.83**
C0.025CD	0.5	95	432	436	437	**43.50**	540	562	552	**55.13**	610	608	615	**61.10**	689	690	692	**69.03**	739	740	745	**74.13**
C0.05CD	0.5	110	448	456	445	**44.97**	566	565	568	**56.63**	621	620	625	**62.20**	710	692	698	**70.00**	789	790	792	**79.03**
C0.1CD	0.5	180	395	397	416	**40.27**	534	540	535	**53.63**	596	600	602	**59.93**	700	698	697	**69.83**	776	772	770	**77.27**
C30FA0.025CD	0.5	100	279	307	283	**28.97**	440	437	434	**43.70**	487	491	493	**49.03**	626	624	622	**62.40**	742	740	738	**74.00**
C30FA0.05CD	0.5	160	277	289	279	**28.17**	470	475	469	**47.13**	520	525	522	**52.23**	655	658	660	**67.77**	765	767	766	**76.60**
C30FA0.1CD	0.47	145	324	342	333	**33.30**	466	462	464	**46.40**	515	518	516	**51.63**	636	640	638	**63.80**	754	760	758	**75.73**
C50FA0.025CD	0.47	100	196	200	203	**19.97**	258	257	257	**25.73**	320	322	325	**32.23**	460	462	459	**46.03**	645	640	639	**64.13**
C50FA0.05CD	0.45	105	218	222	220	**22.00**	296	300	298	**29.80**	431	436	433	**43.33**	510	508	515	**51.10**	691	690	695	**69.20**
C50FA0.1CD	0.45	160	215	210	211	**21.20**	264	266	261	**26.37**	395	392	390	**39.23**	498	492	498	**49.60**	664	661	660	**66.17**

Table A.16: Percentage increase/decrease in the compressive strength of C30FA, C50FA and β-CD samples compared to control sample (0.5-W/B)

	7 days	14 days	28 days	90 days	180 days
C30FA	-46.87%	-24.97%	-29.69%	-15.53%	-7.12%
C50FA	-62.91%	-58.71%	-57.08%	-38.69%	-21.38%
C0.025CD	6.36%	4.27%	-1.40%	-0.49%	-0.94%
C0.05CD	9.95%	7.11%	0.37%	0.91%	5.61%
C0.1CD	-1.54%	1.44%	-3.29%	0.66%	3.26%

Table A.17: Percentage increase/decrease in the compressive strength of FA-β-CD composites samples compared to control sample (0.5-W/B)

	7 days	14 days	28 days	90 days	180 days
C30FA0.025CD	-29.17%	-17.34%	-20.88%	-10.05%	-1.11%
C30FA0.05CD	-31.13%	-10.86%	-15.72%	-2.31%	2.37%
C30FA0.1CD	-18.58%	-12.24%	-16.69%	-8.03%	1.20%
C50FA0.025CD	-51.17%	-51.33%	-47.99%	-33.65%	-14.30%
C50FA0.05CD	-46.21%	-43.64%	-30.08%	-26.33%	-7.52%
C50FA0.1CD	-48.17%	-50.12%	-36.70%	-28.50%	-11.57%

Table A.18: Percentage increase in the compressive strength of FA-β-CD composite samples compressive strength compared to C30FA pozzolanic sample (0.5-W/B)

	7 days	14 days	28 days	90 days	180 days
C30FA0.025CD	33.32%	10.16%	12.53%	6.48%	6.48%
C30FA0.05CD	29.64%	18.81%	19.87%	15.65%	10.22%
C30FA0.1CD	53.24%	16.96%	18.50%	8.87%	8.96%

Table A.19: Percentage increase in the compressive strength of FA-β-CD composite samples compared to C50FA pozzolanic sample (0.5-W/B)

	7 days	14 days	28 days	90 days	180 days
C50FA0.025CD	31.64%	17.87%	21.17%	8.23%	9.01%
C50FA0.05CD	45.02%	36.51%	62.89%	20.15%	17.63%
C50FA0.1CD	39.75%	20.80%	47.48%	16.62%	12.48%

Table A.20: Compressive strength of 0.4-W/B concrete samples at different curing ages

Samples	W/B	Slump (mm)	Com. Strength (7 days)				Com. Strength (14 days)				Com. Strength (28 days)				Com. Strength (90 days)				Com. Strength (180 days)			
			L1 (kN)	L2 (kN)	L3 (kN)	Av. S (MPa)	L1 (kN)	L2 (kN)	L3 (kN)	Av. S (MPa)	L1 (kN)	L2 (kN)	L3 (kN)	Av. S (MPa)	L1 (kN)	L2 (kN)	L3 (kN)	Av. S (MPa)	L1 (kN)	L2 (kN)	L3 (kN)	Av. S (MPa)
Control (100% PC)	0.4	30	569	575	571	**57.17**	661	662	663	**66.20**	741	732	745	**73.93**	848	855	852	**85.17**	902	909	906	**90.57**
C30FA	0.4	40	387	388	383	**38.60**	470	471	475	**47.20**	574	578	578	**57.67**	825	822	828	**82.50**	935	932	940	**93.57**
C50FA	0.4	55	244	244	250	**24.60**	330	327	332	**32.97**	424	425	424	**42.43**	525	530	532	**52.90**	730	725	723	**72.60**
C0.025CD	0.4	40	592	590	595	**59.23**	670	665	671	**66.87**	775	772	770	**77.23**	860	865	868	**86.43**	909	910	906	**90.83**
C0.05CD	0.4	55	606	607	606	**60.63**	681	684	685	**68.33**	791	791	795	**79.23**	887	885	890	**88.73**	954	960	952	**95.53**
C0.1CD	0.4	135	596	598	600	**59.80**	670	675	672	**67.23**	788	783	784	**78.50**	874	870	872	**87.20**	932	927	929	**92.93**
C30FA0.025CD	0.4	55	389	395	384	**38.93**	472	475	479	**47.53**	600	610	605	**60.50**	856	855	850	**85.37**	952	945	943	**94.67**
C30FA0.05CD	0.4	70	404	408	400	**40.40**	498	508	505	**50.37**	634	640	642	**63.87**	880	878	874	**87.73**	966	970	961	**96.57**
C30FA0.1CD	0.4	180	395	400	398	**39.77**	483	488	501	**49.07**	625	620	615	**62.00**	864	859	863	**86.20**	959	956	959	**95.80**
C50FA0.025CD	0.4	80	232	225	228	**24.83**	341	344	348	**34.43**	462	466	465	**46.43**	571	569	568	**56.93**	766	769	766	**76.70**
C50FA0.05CD	0.4	115	265	267	269	**26.70**	372	376	377	**37.50**	489	485	483	**48.57**	598	600	595	**59.76**	792	790	795	**79.23**
C50FA0.1CD	0.4	200	250	254	253	**25.23**	354	355	359	**35.60**	471	475	474	**47.33**	575	582	580	**57.90**	775	778	779	**77.73**

Table A.21: Percentage increase in the compressive strength of C30FA, C50FA and *β*-CD samples compared to control sample (0.4-W/B)

	7 days	14 days	28 days	90 days	180 days
C30FA	-32.48%	-28.70%	-21.99%	-3.13%	3.31%
C50FA	-56.97%	-50.20%	-42.61%	-37.89%	-19.84%
C0.025CD	3.60%	1.01%	4.46%	1.48%	0.29%
C0.05CD	6.05%	3.22%	7.17%	4.18%	5.48%
C0.1CD	4.60%	1.56%	6.18%	2.38%	2.61%

Table A.22: Percentage increase/decrease in the compressive strength of FA-*β*-CD composites samples compared to control sample (0.4-W/B)

	7 days	14 days	28 days	90 days	180 days
C30FA0.025CD	-31.90%	-28.20%	-18.17%	0.23%	4.53%
C30FA0.05CD	-29.33%	-23.91%	-13.61%	3.01%	6.62%
C30FA0.1CD	-30.44%	-25.88%	-16.14%	1.21%	5.77%
C50FA0.025CD	-56.57%	-47.99%	-37.20%	-33.16%	-15.31%
C50FA0.05CD	-53.30%	-43.35%	-34.30%	-29.83%	-12.52%
C50FA0.1CD	-55.87%	-46.22%	-35.98%	-32.02%	-14.18%

Table A.23: Percentage increase in the compressive strength of FA-*β*-CD composite samples compared to C30FA pozzolanic sample (0.4-W/B)

	7 days	14 days	28 days	90 days	180 days
C30FA0.025CD	0.85%	0.70%	4.91%	3.48%	1.18%
C30FA0.05CD	4.66%	6.72%	10.75%	6.34%	3.21%
C30FA0.1CD	3.03%	3.96%	7.51%	4.48%	2.38%

Table A.24: Percentage increase in the compressive strength of FA-*β*-CD composite samples compared to C50FA pozzolanic sample (0.4-W/B)

	7 days	14 days	28 days	90 days	180 days
C50FA0.025CD	0.93%	4.43%	9.43%	7.62%	5.65%
C50FA0.05CD	8.54%	13.74%	14.47%	12.97%	9.13%
C50FA0.1CD	2.56%	7.98%	11.55%	9.45%	7.07%

Table A.25: Split tensile strength of 0.5-W/B concrete samples at different curing ages

Samples	Split Tensile Strength (14 days)				Split Tensile Strength (28 days)				Split Tensile Strength (90 days)				Split Tensile Strength (180 days)			
	L1 (kN)	L2 (kN)	L3 (kN)	$F = \frac{2P}{\pi dl}$ (MPa)	L1 (kN)	L2 (kN)	L3 (kN)	$F = \frac{2P}{\pi dl}$ (MPa)	L1 (kN)	L2 (kN)	L3 (kN)	$F = \frac{2P}{\pi dl}$ (MPa)	L1 (kN)	L2 (kN)	L3 (kN)	$F = \frac{2P}{\pi dl}$ (MPa)
Control (100% PC)	294	292	296	**4.16**	299	300	302	**4.25**	330	335	337	**4.72**	340	345	348	**4.87**
C30FA	209	215	210	**2.99**	239	242	244	**3.42**	284	288	289	**4.06**	352	350	355	**4.98**
C50FA	146	150	152	**2.11**	216	222	217	**3.09**	280	279	277	**3.94**	338	335	340	**4.78**
C0.025CD	291	293	290	**4.12**	298	305	304	**4.28**	340	342	344	**4.84**	350	358	355	**5.01**
C0.05CD	273	272	275	**3.87**	307	299	306	**4.30**	358	361	355	**5.06**	365	368	370	**5.20**
C0.1CD	278	285	282	**3.98**	310	312	309	**4.39**	365	364	362	**5.14**	378	377	372	**5.31**
C30FA0.025CD	203	200	201	**2.85**	225	227	229	**3.21**	300	306	310	**4.32**	360	365	365	**5.14**
C30FA0.05CD	203	205	208	**2.90**	232	235	237	**3.32**	315	322	320	**4.51**	370	374	377	**5.29**
C30FA0.1CD	227	222	221	**3.16**	257	258	260	**3.65**	330	333	335	**4.71**	382	385	388	**5.45**
C50FA0.025CD	159	162	160	**2.27**	210	215	212	**3.12**	282	285	281	**4.00**	345	348	345	**4.89**
C50FA0.05CD	164	165	164	**2.32**	220	224	221	**3.14**	298	306	305	**4.29**	358	360	362	**5.09**
C50FA0.1CD	191	194	190	**2.71**	240	242	239	**3.40**	315	320	322	**4.51**	365	370	372	**5.22**

Table A.26: Percentage increase/decrease in the split tensile strength of C30FA, C50FA and β-CD samples compared to control sample (0.5-W/B)

	14 days	**28 days**	**90 days**	**180 days**
C30FA	-28.13%	-19.53%	-13.98%	2.26%
C50FA	-49.28%	-27.29%	-16.53%	-1.85%
C0.025CD	-0.96%	0.71%	2.54%	2.87%
C0.05CD	-6.97%	1.18%	7.20%	6.78%
C0.1CD	-4.33%	3.29%	8.90%	9.03%

Table A.27: Percentage increase/decrease in the split tensile strength of FA-β-CD composites samples compared to control sample (0.5-W/B)

	14 days	**28 days**	**90 days**	**180 days**
C30FA0.025CD	-31.49%	-24.47%	-8.47%	5.54%
C30FA0.05CD	-30.29%	-21.88%	-4.45%	8.62%
C30FA0.1CD	-24.04%	-14.12%	-0.21%	11.91%
C50FA0.025CD	-45.43%	-26.59%	-15.25%	0.41%
C50FA0.05CD	-44.23%	-26.12%	-9.11%	4.51%
C50FA0.1CD	-34.86%	-20%	-4.45%	7.19%

Table A.28: Percentage increase/decrease in the split tensile strength of FA-β-CD composite samples compared to C30FA pozzolanic sample (0.5-W/B)

	14 days	**28 days**	**90 days**	**180 days**
C30FA0.025CD	-4.68%	-6.14%	6.40%	3.21%
C30FA0.05CD	-3.01%	-2.92%	11.08%	6.22%
C30FA0.1CD	5.69%	6.73%	16.01%	9.44%

Table A.29: Percentage increase in the split tensile strength of FA-β-CD composite samples compared to C50FA pozzolanic sample (0.5-W/B)

	14 days	**28 days**	**90 days**	**180 days**
C50FA0.025CD	7.58%	0.97%	1.52%	2.30%
C50FA0.05CD	9.95%	1.62%	8.88%	6.49%
C50FA0.1CD	28.44%	10.03%	14.47%	9.21%

Table A.30: Split tensile strength of 0.4-W/B concrete samples at different curing ages

Samples	Split Tensile Strength (14 days)				Split Tensile Strength (28 days)				Split Tensile Strength (90 days)				Split Tensile Strength (180 days)			
	L1 (kN)	L2 (kN)	L3 (kN)	$F = \frac{2P}{\pi dl}$ (MPa)	L1 (kN)	L2 (kN)	L3 (kN)	$F = \frac{2P}{\pi dl}$ (MPa)	L1 (kN)	L2 (kN)	L3 (kN)	$F = \frac{2P}{\pi dl}$ (MPa)	L1 (kN)	L2 (kN)	L3 (kN)	$F = \frac{2P}{\pi dl}$ (MPa)
Control (100% PC)	306	301	302	**4.29**	335	338	337	**4.76**	358	362	360	**5.09**	365	371	370	**5.21**
C30FA	231	238	236	**3.32**	296	300	299	**4.22**	346	350	352	**4.94**	377	374	375	**5.31**
C50FA	201	205	207	**2.89**	231	236	235	**3.31**	282	284	280	**3.99**	359	362	364	**5.12**
C0.025CD	293	290	294	**4.14**	310	315	312	**4.42**	358	352	355	**5.02**	382	380	379	**5.38**
C0.05CD	256	256	260	**3.64**	318	320	324	**4.54**	379	380	385	**5.39**	395	395	391	**5.57**
C0.1CD	266	268	265	**3.77**	330	336	335	**4.72**	368	372	370	**5.23**	383	388	392	**5.48**
C30FA0.025CD	249	252	250	**3.54**	316	310	312	**4.42**	355	359	354	**5.04**	384	388	391	**5.48**
C30FA0.05CD	258	262	260	**3.68**	320	322	318	**4.53**	372	369	368	**5.23**	392	396	399	**5.60**
C30FA0.1CD	276	282	275	**3.93**	335	330	336	**4.72**	389	390	391	**5.52**	405	410	415	**5.80**
C50FA0.025CD	210	212	215	**3.00**	240	238	244	**3.40**	287	290	296	**4.12**	370	375	371	**5.26**
C50FA0.05CD	225	228	230	**3.22**	248	254	250	**3.55**	314	320	313	**4.47**	389	395	388	**5.53**
C50FA0.1CD	232	233	235	**3.30**	266	264	260	**3.72**	332	329	331	**4.68**	408	415	410	**5.81**

Table A.31: Percentage increase/decrease in the split tensile strength of C30FA, C50FA and β-CD samples compared to control sample (0.4-W/B)

	14 days	**28 days**	**90 days**	**180 days**
C30FA	-22.61%	-11.34%	-2.95%	1.92%
C50FA	-32.63%	-30.46%	-21.61%	-1.73%
C0.025CD	-3.50%	-7.14%	-1.38%	3.26%
C0.05CD	-15.15%	-4.62%	5.89%	6.91%
C0.1CD	-12.12%	-0.84%	2.75%	5.18%

Table A.32: Percentage increase/decrease in the split tensile strength of FA-β-CD composites samples compared to control sample (0.4-W/B)

	14 days	**28 days**	**90 days**	**180 days**
C30FA0.025CD	-17.48%	-7.14%	-0.98%	5.18%
C30FA0.05CD	-14.22%	-4.83%	2.75%	7.49%
C30FA0.1CD	-8.39%	-0.84%	8.45%	11.32%
C50FA0.025CD	-30.07%	-28.57%	-19.06%	0.96%
C50FA0.05CD	-24.94%	-25.42%	-12.18%	6.14%
C50FA0.1CD	-23.08%	-21.85%	-8.06%	11.52%

Table A.33: Percentage increase in the split tensile strength of FA-β-CD composite samples compared to C30FA pozzolanic sample (0.4-W/B)

	14 days	**28 days**	**90 days**	**180 days**
C30FA0.025CD	6.63%	4.74%	2.02%	3.20%
C30FA0.05CD	10.84%	7.35%	5.87%	5.46%
C30FA0.1CD	18.37%	11.85%	11.74%	9.23%

Table A.34: Percentage increase in the split tensile strength of FA-β-CD composite samples compared to C50FA pozzolanic sample (0.4-W/B)

	14 days	**28 days**	**90 days**	**180 days**
C50FA0.025CD	3.81%	2.72%	3.26%	2.73%
C50FA0.05CD	11.42%	7.25%	12.03%	8.01%
C50FA0.1CD	14.98%	12.39%	17.29%	13.48%

Table A.35: Viscosity of 0.4-W/B Cement paste

SAMPLES	Initial	1 min	2 min	3 min	4 min	5 min	10 min	15 min	20 min	25 min	30 min	35 min	40 min
C	60	58	47	46	43	39	34	30	31	32	33	33	33
C30FA	59	54	49	45	40	39	30	24	24	27	32	32	32
C50FA	50	50	47	44	41	38	29	27	26	28	30	31	31
C0.025CD	46	42	40	39	38	37	34	33	30	31	31	31	31
C0.05CD	43	38	37	36	36	35	33	32	30	30	30	30	30
C0.1CD	34	32	30	29	29	29	28	27	28	28	29	30	30
C30FA0.025CD	35	34	33	32	33	34	33	32	31	29	29	32	32
C30FA0.05CD	25	25	24	24	25	26	27	28	28	28	28	28	28
C30FA0.1CD	19	18	17	17	17	18	19	20	22	22	23	23	23
C50FA0.025CD	27	27	28	29	30	31	32	32	32	32	32	32	32
C50FA0.05CD	23	24	25	26	26	27	28	28	28	28	28	28	28
C50FA0.1CD	17	16	16	17	17	17	19	20	21	21	21	21	21

Table A.36: Viscosity of 0.5-W/B Cement paste

SAMPLES	Initial	1 min	2 min	3 min	4 min	5 min	10 min	15 min	20 min
C	11.00	10.5	10.6	10.2	10.6	10.8	10.8	11.0	11.2
C30FA	8.8	8.8	8.0	7.9	8.0	8.2	8.7	9.0	9.2
C50FA	6.2	7.0	7.2	7.8	7.9	7.9	8.0	8.8	8.8
C0.025CD	7.2	7.2	7.5	7.6	7.5	7.7	7.7	8.0	8.2
C0.05CD	6.3	6.1	6.3	6.5	6.7	6.8	6.9	6.9	7.0
C0.1CD	6.1	6.0	6.2	6.3	6.3	6.4	6.6	6.9	6.9
C30FA0.025CD	5.6	5.9	6.0	6.2	6.5	6.7	7.0	7.1	7.4
C30FA0.05CD	4.4	4.3	4.5	4.8	5.3	5.9	6.0	6.2	6.4
C30FA0.1CD	4.0	3.9	4.1	4.3	4.5	4.6	5.8	6.0	6.2
C50FA0.025CD	3.9	3.7	4.0	4.2	4.4	4.6	5.5	5.9	6.0
C50FA0.05CD	2.9	2.8	3.1	3.4	3.6	3.8	4.5	4.9	5.3
C50FA0.1CD	2.9	2.8	3.0	3.1	3.3	3.4	3.7	4.0	4.2

Table A.37: Viscosity of 0.6-W/B Cement paste

SAMPLES	Initial	1 min	2 min	3 min	4 min	5 min	10 min	15 min	20 min
C	6.0	6.1	6.1	6.2	6.3	6.5	7.3	8.0	8.2
C30FA	4.6	4.8	4.6	4.8	4.9	4.9	6.0	6.9	7.3
C50FA	4.5	4.4	4.2	4.3	4.2	4.3	4.5	4.8	5.5
C0.025CD	5.2	5.5	5.3	5.6	5.9	6.0	6.2	7.0	7.9
C0.05CD	5.0	5.2	5.3	5.4	5.5	5.8	6.0	6.7	7.5
C0.1CD	4.9	5.2	5.2	5.2	5.3	5.5	5.8	6.5	7.2
C30FA0.025CD	4.5	4.4	4.5	4.5	4.6	4.8	6.0	6.4	7.0
C30FA0.05CD	3.7	3.6	3.8	4.0	4.2	4.4	5.8	6.4	6.9
C30FA0.1CD	3.3	3.1	3.3	3.4	3.6	3.7	4.6	5.9	6.8
C50FA0.025CD	4.4	4.2	4.3	4.4	4.4	4.5	4.5	4.6	4.8
C50FA0.05CD	2.8	3.3	3.1	3.2	3.2	3.3	3.5	3.7	4.0
C50FA0.1CD	2.7	2.6	2.7	2.7	2.8	2.8	2.9	3.1	3.5

Table A.38: Setting times results of cement paste

SAMPLES	% Consistency water	Initial set (mins)	Final set (mins)
Control (100% PC)	31.5	100	220
C30FA	29.2	250	541
C50FA	28.8	375	722
C0.025CD	29.3	395	801
C0.05CD	26.0	410	1097
C0.1CD	24.8	420	1158
C30FA0.025CD	26.1	428	1220
C30FA0.05CD	25.5	450	1295
C30FA0.1CD	24.4	475	1320
C50FA0.025CD	25.9	465	1260
C50FA0.05CD	24.4	692	1350
C50FA0.1CD	23.8	696	1420

Table A.39: Durability (OPI, permeability, sorptivity, porosity and chloride conductivity) results of actual concrete samples (0.5-W/B) at different curing ages

Samples	**OPI**		**Permeability, k (m/s)**		**Sorptivity (mm/hr$^{0.5}$)**		**Porosity (%)**		**Chloride conductivity (mS/cm)**	
	28 d	**90 d**	**28 d**	**90 d**	**28 d**	**90 d**	**28 d**	**90 d**	**28 d**	**90 d**
C	9.84	9.95	1.46E-10	1.13E-10	1.22E+01	1.09E+01	11.4	11.2	0.3687	0.1175
C30FA	9.95	10.16	1.13E-10	6.96E-11	1.08E+01	8.63E+00	12.7	11.3	0.1876	0.1209
C50FA	9.85	10.26	1.40E-10	5.46E-11	1.08E+01	8.00E+00	12.7	11.9	0.2085	0.1144
C0.025CD	9.73	9.96	1.85E-10	1.11E-10	1.10E+01	8.11E+00	9.9	9.1	0.2116	0.1338
C0.05CD	9.75	9.90	1.99E-10	1.26E-10	1.22E+01	1.10E+01	9.4	8.5	0.1458	0.1248
C0.1CD	Invalid	Invalid	Invalid	Invalid	1.68E+01	1.24E+01	8.8	8.3	0.1478	0.1232
C30FA0.025CD	10.21	10.24	6.12E-11	5.77E-11	9.17E+00	8.99E+00	11.6	11.0	0.1613	0.1297
C30FA0.05CD	9.99	9.99	1.03E-10	1.01E-10	1.03E+01	9.07E+00	11.7	11.4	0.2135	0.1258
C30FA0.1CD	Invalid	Invalid	Invalid	Invalid	1.04E+01	9.14E+00	10.6	10.2	0.1837	0.1421
C50FA0.025CD	10.07	10.40	8.54E-11	3.96E-11	8.17E+00	6.58E+00	12.1	11.0	0.1617	0.1311
C50FA0.05CD	10.25	10.53	5.65E-11	2.95E-11	9.62E+00	6.37E+00	11.3	11.2	0.1751	0.1153
C50FA0.1CD	9.10	Invalid	7.91E-10	Invalid	9.57E+00	8.59E+00	11.5	11.1	0.1851	0.1178

Table A.40: Durability (OPI, permeability, sorptivity, porosity and chloride conductivity) results of actual concrete samples (0.4-W/B) at different curing ages.

Samples	**OPI**		**Permeability, k (m/s)**		**Sorptivity (mm/hr$^{0.5}$)**		**Porosity (%)**		**Chloride conductivity (mS/cm)**	
	28 d	**90 d**	**28 d**	**90 d**	**28 d**	**90 d**	**28 d**	**90 d**	**28 d**	**90 d**
C	9.88	9.89	1.31E-10	1.28E-10	9.98E+00	9.86E+00	11.33	11.01	0.1916	0.1403
C30FA	9.99	10.43	1.03E-10	3.72E-11	7.80E+00	7.32E+00	12.1	8.6	0.1491	0.1329
C50FA	10.51	10.76	3.12E-11	1.72E-11	8.45E+00	8.11E+00	12.6	9.5	0.1955	0.1927
C0.025CD	9.77	10.03	1.71E-10	9.38E-11	1.00E+01	9.95E+00	9.8	8.7	0.1661	0.1656
C0.05CD	9.73	9.85	1.87E-10	1.41E-10	1.09E+01	1.04E+01	9.0	8.0	0.1854	0.1732
C0.1CD	Invalid	Invalid	Invalid	Invalid	1.42E+01	1.14E+01	8.7	8.0	0.1601	0.1562
C30FA0.025CD	10.28	10.42	5.22E-11	3.77E-11	9.99E+00	8.46E+00	11.0	10.6	0.1477	0.1309
C30FA0.05CD	9.95	10.06	1.11E-10	8.78E-11	9.47E+00	8.32E+00	11.3	10.6	0.1380	0.1348
C30FA0.1CD	Invalid	Invalid	Invalid	Invalid	1.81E+01	1.27E+01	10.3	9.7	0.1543	0.1219
C50FA0.025CD	9.96	10.08	1.10E-10	8.25E-11	9.57E+00	8.63E+00	12.7	12.4	0.1599	0.1359
C50FA0.05CD	10.15	10.23	7.93E-11	5.90E-11	1.04E+01	8.48E+00	12.9	11.7	0.1624	0.1535
C50FA0.1CD	Invalid	Invalid	Invalid	Invalid	1.14E+01	1.01E+01	11.6	10.9	0.1356	0.1184

Table A.41: Percentage increase/decrease in the permeability of C30FA, C50FA, *β*-CD and FA-*β*-CD composite samples compared to control sample (0.5-W/B)

	28 days	**90 days**
C30FA	-22.6027	-38.4071
C50FA	-4.10959	-51.6814
C0.025CD	26.71233	-1.76991
C0.05CD	36.30137	11.50442
C30FA0.025CD	-58.0822	-48.9381
C30FA0.05CD	-29.4521	-10.6195
C50FA0.025CD	-41.5068	-64.9558
C50FA0.05CD	-61.3014	-73.8938

Table A.42: Percentage increase in the permeability of FA-*β*-CD composite samples compared to C30FA pozzolanic sample (0.5-W/B)

	28 days	**90 days**
C30FA0.025CD	-45.8407	-17.0977
C30FA0.05CD	-8.84956	45.11494

Table A.43: Percentage increase in the permeability of FA-*β*-CD composite samples compared to C50FA pozzolanic sample (0.5-W/B)

	28 days	**90 days**
C50FA0.025CD	-39	-27.4725
C50FA0.05CD	-59.6429	-45.9707

Table A.44: Percentage increase/decrease in the permeability of C30FA, C50FA, *β*-CD and FA-*β*-CD composite samples compared to control sample (0.4-W/B)

	28 days	**90 days**
C30FA	-21.374	-70.9375
C50FA	-76.1832	-86.5625
C0.025CD	30.53435	-26.7188
C0.05CD	42.74809	10.15625
C30FA0.025CD	-60.1527	-70.5469
C30FA0.05CD	-15.2672	-31.4063
C50FA0.025CD	-16.0305	-35.5469
C50FA0.05CD	-39.4656	-53.9063

Table A.45: Percentage increase in the permeability of FA-*β*-CD composite samples compared to C30FA pozzolanic sample (0.4-W/B)

	28 days	**90 days**
C30FA0.025CD	-49.3204	1.344086
C30FA0.05CD	7.76699	136.0215

Table A.46: Percentage increase in the permeability of FA-*β*-CD composite samples compared to C50FA pozzolanic sample (0.4-W/B)

	28 days	**90 days**
C50FA0.025CD	252.5641	379.6512
C50FA0.05CD	154.1667	243.0233

Table A.47: Percentage increase/decrease in the sorptivity of C30FA, C50FA, *β*-CD and FA-*β*-CD composite samples compared to control sample (0.5-W/B)

	28 days	**90 days**
C30FA	-11.4754	-20.8257
C50FA	-11.4754	-26.6055
C0.025CD	-9.83607	-25.5963
C0.05CD	0	0.917431
C0.1CD	37.70492	13.76147
C30FA0.025CD	-24.8361	-17.5229
C30FA0.05CD	-15.5738	-16.789
C30FA0.1CD	-14.7541	-16.1468
C50FA0.025CD	-33.0328	-39.633
C50FA0.05CD	-21.1475	-41.5596
C50FA0.1CD	-21.5574	-21.1927

Table A.48: Percentage increase in the sorptivity of FA-*β*-CD composite samples compared to C30FA pozzolanic sample (0.5-W/B)

	28 days	**90 days**
C30FA0.025CD	-15.0926	4.171495
C30FA0.05CD	-4.62963	5.098494
C30FA0.1CD	-3.7037	5.909618

Table A.49: Percentage increase in the sorptivity of FA-*β*-CD composite samples compared to C50FA pozzolanic sample (0.5-W/B)

	28 days	**90 days**
C50FA0.025CD	-24.3519	-17.75
C50FA0.05CD	-10.9259	-20.375
C50FA0.1CD	-11.3889	7.375

Table A.50: Percentage increase/decrease in the sorptivity of C30FA, C50FA, *β*-CD and FA-*β*-CD composite samples compared to control sample (0.4-W/B)

	28 days	**90 days**
C30FA	-21.8437	-25.7606
C50FA	-15.3307	-17.7485
C0.025CD	0.200401	0.912779
C0.05CD	9.218437	5.476673
C0.1CD	42.28457	15.61866
C30FA0.025CD	0.1002	-14.1988
C30FA0.05CD	-5.11022	-15.6187
C30FA0.1CD	81.36273	28.80325
C50FA0.025CD	-4.10822	-12.4746
C50FA0.05CD	4.208417	-13.9959
C50FA0.1CD	14.22846	2.434077

Table A.51: Percentage increase in the sorptivity of FA-*β*-CD composite samples compared to C30FA pozzolanic sample (0.4-W/B)

	28 days	**90 days**
C30FA0.025CD	28.07692	15.57377
C30FA0.05CD	21.41026	13.661
C30FA0.1CD	132.0513	73.49727

Table A.52: Percentage increase in the sorptivity of FA-*β*-CD composite samples compared to C50FA pozzolanic sample (0.4-W/B)

	28 days	**90 days**
C50FA0.025CD	13.25444	6.411837
C50FA0.05CD	23.07692	4.562269
C50FA0.1CD	34.91124	24.53761

Table A.53: Percentage increase/decrease in the porosity of C30FA, C50FA, *β*-CD and FA-*β*-CD composite samples compared to control sample (0.5-W/B)

	28 days	**90 days**
C30FA	11.40351	0.892857
C50FA	11.40351	6.25
C0.025CD	-13.1579	-18.75
C0.05CD	-17.5439	-24.1071
C0.1CD	-22.807	-25.8929
C30FA0.025CD	1.754386	-1.78571
C30FA0.05CD	2.631579	1.785714
C30FA0.1CD	-7.01754	-8.92857
C50FA0.025CD	6.140351	-1.78571
C50FA0.05CD	-0.87719	0
C50FA0.1CD	0.877193	-0.89286

Table A.54: Percentage increase in the porosity of FA-*β*-CD composite samples compared to C30FA pozzolanic sample (0.5-W/B)

	28 days	**90 days**
C30FA0.025CD	-8.66142	-2.65487
C30FA0.05CD	-7.8740	0.884956
C30FA0.1CD	-16.5354	-9.73451

Table A.55: Percentage increase in the porosity of FA-*β*-CD composite samples compared to C50FA pozzolanic sample (0.5-W/B)

	28 days	**90 days**
C50FA0.025CD	-4.72441	-2.65487
C50FA0.05CD	-11.0236	-0.88496
C50FA0.1CD	-9.44882	-1.76991

Table A.56: Percentage increase/decrease in the porosity of C30FA, C50FA, *β*-CD and FA-*β*-CD composite samples compared to control sample (0.4-W/B)

	28 days	**90 days**
C30FA	6.796117	-21.8892
C50FA	11.20918	-13.7148
C0.025CD	-13.504	-20.9809
C0.05CD	-20.5649	-27.3388
C0.1CD	-23.2127	-27.3388
C30FA0.025CD	-2.91262	-3.72389
C30FA0.05CD	0	-3.72389
C30FA0.1CD	-9.09091	-11.8983
C50FA0.025CD	12.09179	12.62489
C50FA0.05CD	13.85702	6.26703
C50FA0.1CD	2.383054	-0.99909

Table A.57: Percentage increase in the porosity of FA-*β*-CD composite samples compared to C30FA pozzolanic sample (0.4-W/B)

	28 days	**90 days**
C30FA0.025CD	-9.09091	23.25581
C30FA0.05CD	-6.61157	23.25581
C30FA0.1CD	-14.876	12.7907

Table A.58: Percentage increase in the porosity of FA-*β*-CD composite samples compared to C50FA pozzolanic sample (0.4-W/B)

	28 days	**90 days**
C50FA0.025CD	0.793651	30.52632
C50FA0.05CD	2.380952	23.15789
C50FA0.1CD	-7.93651	14.73684

Table A.59: Percentage increase/decrease in the chloride conductivity of C30FA, C50FA, *β*-CD and FA-*β*-CD composite samples compared to control sample (0.5-W/B)

	28 days	**90 days**
C30FA	-49.1185	2.893617
C50FA	-43.45	-2.6383
C0.025CD	-42.6092	13.87234
C0.05CD	-60.4557	6.212766
C0.1CD	-59.913	4.851064
C30FA0.025CD	-56.2517	10.38298
C30FA0.05CD	-42.0938	7.06383
C30FA0.1CD	-50.1763	20.93617
C50FA0.025CD	-56.1432	11.57447
C50FA0.05CD	-52.5088	-1.87234
C50FA0.1CD	-49.7966	0.255319

Table A.60: Percentage increase in the chloride conductivity of FA-*β*-CD composite samples compared to C30FA pozzolanic sample (0.5-W/B)

	28 days	**90 days**
C30FA0.025CD	-14.0192	7.278743
C30FA0.05CD	13.80597	4.052936
C30FA0.1CD	-2.07889	17.53515

Table A.61: Percentage increase in the chloride conductivity of FA-*β*-CD composite samples compared to C50FA pozzolanic sample (0.5-W/B)

	28 days	**90 days**
C50FA0.025CD	-22.446	14.5979
C50FA0.05CD	-16.0192	0.786713
C50FA0.1CD	-11.223	2.972028

Table A.62: Percentage increase/decrease in the chloride conductivity of C30FA, C50FA, *β*-CD and FA-*β*-CD composite samples compared to control sample (0.4-W/B)

	28 days	**90 days**
C30FA	-22.1816	-5.27441
C50FA	2.035491	37.34854
C0.025CD	-13.309	18.03279
C0.05CD	-3.23591	23.44975
C0.1CD	-16.4405	11.33286
C30FA0.025CD	-22.9123	-6.69993
C30FA0.05CD	-27.9749	-3.92017
C30FA0.1CD	-19.4676	-13.1148
C50FA0.025CD	-16.5449	-3.13614
C50FA0.05CD	-15.2401	9.408411
C50FA0.1CD	-29.2276	-15.6094

Table A.63: Percentage increase in the chloride conductivity of FA-*β*-CD composite samples compared to C30FA pozzolanic sample (0.4-W/B)

	28 days	**90 days**
C30FA0.025CD	-0.93897	-1.50489
C30FA0.05CD	-7.44467	1.429646
C30FA0.1CD	3.487592	-8.2769

Table A.64: Percentage increase in the chloride conductivity of FA-*β*-CD composite samples compared to C50FA pozzolanic sample (0.4-W/B)

	28 days	**90 days**
C50FA0.025CD	-18.2097	-29.4759
C50FA0.05CD	-16.9309	-20.3425
C50FA0.1CD	-30.6394	-38.5573

APPENDIX B
XRD AND FT-IR PEAKS

Table B.1: XRD Peak identification of α and *β* cyclodextrin

Samples	2thetha(°)	Intensity (count)	d-spacing (Å)
β-CD	12.74	13662	6.93
	22.74	11172	3.91
	34.86	9065	2.57
α-CD	11.96	19986	7.40
	14.34	13753	6.16
	21.72	6341	4.0

Table B.2: XRD Peak identification of fly ashes (Chapter 3)

	2thetha(°)	Intensity (count)	d-spacing (Å)
Matla FA	16.40	691	5.39
	20.78	571	4.27
	26.56	3188	3.35
	35.22	1207	2.55
	40.79	1684	2.21
	60.58	1328	1.53
Majuba FA	16.45	952	5.38
	20.84	786	4.26
	26.67	4575	3.34
	35.27	1723	2.54
	40.84	2262	2.21
	60.65	1751	1.53
Lethabo FA	16.43	1183	5.39
	20.82	375	4.26
	26.28	2961	3.39
	35.23	2120	2.55
	40.83	2764	2.21
	60.62	2168	1.53
Kendal FA	16.43	960	5.38
	20.84	910	4.26
	26.65	5360	3.34

	35.25	1706	2.54
	40.84	2258	2.21
	60.62	1623	1.53

Table B.3: XRD Peak identification of FA- *β*-CD composite (Chapter 3)

	2thetha(^{o})	Intensity (count)	d-spacing (Å)
Matla/*β*-CD	12.67	63	6.99
	16.43	682	5.39
	20.78	614	4.27
	22.72	156	3.9
	26.60	3227	3.34
	40.81	1620	2.21
Majuba/*β*-CD	12.69	151	6.98
	16.45	944	5.39
	20.85	802	4.26
	22.77	133	3.9
	26.63	4694	3.34
	40.81	2204	2.21
Lethabo/*β*-CD	12.58	85	7.03
	16.42	1176	5.40
	20.80	411	4.27
	22.79	149	3.9
	26.24	3070	3.40
	40.79	2713	2.21
Kendal/*β*-CD	12.66	116	6.99
	16.45	933	5.39
	20.86	865	4.26
	22.71	132	3.9
	26.64	4753	3.35
	40.84	2180	2.21

Table B.4: XRD Peak identification of FA- *α*-CD composite and FA- *β*-CD composite (Chapter 4)

	2thetha(°)	Intensity (count)	d-spacing (Å)
FA	16.65	847	5.38
	20.85	724	4.25
	26.25	2016	3.39
	35.29	1398	2.54
	40.86	1903	2.21
	60.65	1473	1.53
90FA-10% α-CD	11.93	1077	7.41
	16.45	794	5.39
	21.71	786	4.09
	26.62	3027	3.35
	35.23	1422	2.55
	40.83	1894	2.21
	60.62	1288	1.53
90FA-10% *β*-CD	12.76	449	6.93
	16.45	796	5.38
	22.76	568	3.91
	26.63	3169	3.34
	35.27	1438	2.54
	40.84	1778	2.21
	60.63	1416	1.53
90FA-10% α-CD + H_2O	16.40	811	5.40
	20.78	637	4.26
	26.58	3815	3.35
	35.22	1314	2.55
	40.79	1811	2.21
	60.58	1265	1.53
90FA-10% *β*-CD + H_2O	16.40	770	5.40
	20.78	646	4.26
	26.56	3649	3.35
	35.22	1330	2.55
	40.79	1748	2.21
	60.58	1324	1.53

Table B.5: XRD Peak identification of cement paste samples hydrated for 24 hours (Chapter 6)

	2thetha(^{o})	Intensity (count)	d-spacing (Å)
C	18.3	236	4.86
	29.7	233	3.00
	32.8	326	2.73
	34.7	357	2.59
	41.6	121	2.17
	47.3	141	1.92
	52.0	116	1.76
	56.7	46	1.62
	62.6	84	1.48
C30FA	18.3	217	4.82
	26.5	63	3.35
	29.7	188	3.00
	32.8	194	2.71
	34.7	243	2.58
	41.6	88	2.16
	47.3	42	2.09
	52.0	103	1.76
	56.7	49	1.62
	62.6	15	1.48
C50FA	26.5	141	3.37
	29.7	213	3.01
	32.8	250	2.73
	34.7	227	2.59
	35.4	109	2.53
	41.6	94	2.17
	52.0	88	1.76
	62.6	61	1.48
C0.025CD	18.3	136	4.86
	29.7	288	3.01
	32.8	343	2.72
	34.7	354	2.59
	41.6	149	2.17
	47.3	128	1.92
	52.0	143	1.76
	56.7	61	1.62
	62.6	103	1.48
C0.05CD	11.9	145	7.45
	18.3	79	4.86

	29.7	343	3.00
	32.8	418	2.73
	34.7	417	2.56
	41.6	195	2.17
	47.3	73	1.92
	52.0	170	1.76
	56.7	79	1.62
	62.6	126	1.48
C0.1CD	11.9	68	7.45
	20.9	72	4.24
	29.7	355	3.01
	32.8	465	2.72
	34.7	543	2.59
	41.6	214	2.18
	47.3	62	1.92
	52.0	233	1.76
	56.7	102	1.62
	62.6	140	1.48
C30FA0.025CD	26.5	75	3.37
	29.7	238	3.01
	32.8	310	2.75
	34.7	248	2.59
	35.4	52	2.53
	41.6	111	2.17
	47.3	65	1.92
	52.0	143	1.76
	56.7	64	1.62
	62.6	83	1.48
C30FA0.05CD	11.9	126	7.46
	20.9	38	4.23
	29.7	74	3.36
	32.8	275	3.01
	34.7	374	2.73
	41.6	375	2.59
	47.3	191	2.17
	52.0	61	1.92
	56.7	168	1.76
	62.6	105	1.48
C30FA0.1CD	11.9	67	7.42
	20.9	65	4.22
	29.7	256	3.00
	32.8	363	2.72
	34.7	385	2.58

	41.6	219	2.17
	47.3	55	1.92
	52.0	194	1.76
	56.7	80	1.62
	62.6	113	1.48
C50FA0.025CD	11.9	29	7.53
	29.7	203	3.01
	32.8	275	2.73
	34.7	275	2.59
	35.4	98	2.53
	41.6	150	2.17
	52.0	107	1.76
	56.7	57	1.62
	62.6	76	1.48
C50FA0.05CD	11.9	128	7.46
	20.9	54	4.23
	29.7	248	3.01
	32.8	338	2.73
	34.7	341	2.59
	35.4	103	2.53
	41.6	166	2.17
	52.0	144	1.76
	56.7	78	1.62
	62.6	84	1.48
C50FA0.1CD	11.9	117	7.44
	18.3	251	3.01
	29.7	318	2.72
	32.8	353	2.59
	34.7	87	2.53
	41.6	168	2.17
	47.3	46	1.92
	52.0	147	1.76
	56.7	63	1.62
	62.6	89	1.48

Table B.6: XRD Peak identification of cement paste samples hydrated for 7 days (Chapter 6)

C	2thetha(^{o})	Intensity (count)	d-spacing (Å)
	18.2	340	4.87
	29.6	129	3.01
	32.4	150	2.76
	34.2	485	2.62
	47.2	162	1.93
C30FA	18.2	339	4.86
	26.4	78	3.36
	32.4	86	2.76
	34.2	396	2.62
C50FA	16.6	79	5.33
	18.2	282	4.86
	26.4	129	3.37
	32.4	66	2.77
	34.2	219	2.61
	41.0	129	2.20
	47.2	102	1.92
C0.025CD	18.2	402	4.86
	32.4	177	2.76
	34.2	477	2.62
	47.2	176	1.92
C0.05CD	18.2	327	4.85
	32.4	170	2.72
	34.2	392	2.61
	47.2	188	1.92
C0.1CD	18.2	269	4.86
	29.4	121	3.01
	32.4	219	2.77
	34.2	318	2.62
	41.0	74	2.17
	47.2	134	1.92
C30FA0.025CD	18.2	445	4.85
	26.4	86	3.89
	32.4	122	2.77
	34.2	387	2.61
	47.2	157	1.92
C30FA0.05CD	18.2	340	4.86
	32.4	97	2.76
	34.2	373	2.61

	41.0	68	2.20
	47.2	126	1.92
C30FA0.1CD	18.2	246	4.85
	26.4	61	3.36
	29.6	106	3.01
	32.4	117	2.76
	34.2	284	2.61
	47.2	112	1.92
C50FA0.025CD	16.6	88	5.33
	18.2	540	4.85
	34.2	198	2.62
	41.0	125	2.20
	47.2	97	1.92
C50FA0.05CD	16.6	77	5.34
	18.2	217	4.86
	26.4	127	3.37
	34.2	208	2.62
	41.0	111	2.20
	47.2	98	1.92
C50FA0.1CD	16.6	76	5.33
	18.2	154	4.87
	32.4	133	3.37
	34.2	158	2.76
	41.0	151	2.61

Table B.7: XRD Peak identification of cement paste samples hydrated for 28 days (Chapter 6)

	2thetha(^{o})	Intensity (count)	d-spacing (Å)
C	18.3	382	4.85
	32.4	107	2.76
	34.3	516	2.61
	47.3	190	1.92
	18.3	312	4.85
C30FA	32.4	83	2.76
	34.3	379	2.61
	47.3	120	1.92
	18.3	151	4.86

C50FA	26.4	126	3.37
	34.3	140	2.61
	18.3	338	4.85
C0.025CD	32.4	66	2.73
	34.3	382	2.61
	47.3	147	1.92
	18.3	322	4.85
C0.05CD	32.4	97	2.76
	34.3	334	2.62
	47.3	134	1.92
	18.3	224	4.85
C0.1CD	32.4	258	2.76
	34.3	362	2.61
	47.3	149	1.92
	18.3	301	4.86
C30FA0.025CD	32.4	87	2.76
	34.3	319	2.61
	47.3	146	1.92
	18.3	286	4.85
C30FA0.05CD	32.4	148	2.76
	34.3	340	2.61
	47.3	111	1.92
	18.3	260	4.85
C30FA0.1CD	34.3	335	2.61
	47.3	145	1.92
	16.6	119	5.33
C50FA0.025CD	18.3	209	4.85
	26.4	180	3.37
	34.3	191	2.61
	16.6	118	5.33
C50FA0.05CD	18.3	206	4.85
	26.4	172	3.37
	34.3	222	2.61
	47.3	97.8	1.92
	16.6	117	5.33
C50FA0.1CD	18.3	194	4.85
	26.4	187	3.37
	34.3	238	2.61

Table B.8: XRD Peak identification of cement paste samples hydrated for 90 days (Chapter 6)

	2thetha(^{o})	Intensity (count)	d-spacing (Å)
C	18.3	304	4.85
	34.3	439	2.60
	18.3	614	4.85
C30FA	34.3	99	2.59
	18.3	413	4.85
C50FA	34.3	470	2.61
	18.3	425	4.84
C0.025CD	34.3	346	2.61
	18.3	182	4.85
C0.05CD	34.3	272	2.61
	18.3	138	4.85
C0.1CD	34.3	145	2.61
	18.3	302	4.85
C30FA0.025CD	34.3	270	2.61
	18.3	207	4.85
C30FA0.05CD	34.3	267	2.61
	18.3	240	4.85
C30FA0.1CD	34.3	230	2.61
	18.3	640	4.85
C50FA0.025CD	34.3	144	2.61
	18.3	175	4.86
C50FA0.05CD	34.3	125	2.61
	18.3	123	4.85
C50FA0.1CD	34.3	140	2.61

Table B.9: FT-IR Peak identification of α and β cyclodextrin

	Wave number(cm^{-1})	Transmittance (%)
α-CD	3312	97
	2916	98
	1638	98
	1154	89
	1076	89
	1023	78
	998	79
	952	92

	710	99
β-CD	3316	68
	2928	83
	1657	65
	1550	90
	1220	68
	1152	58
	1078	49
	1025	16
	999	24
	775	16

Table B.10: FT-IR Peak identification of fly ashes (Chapter 3)

	Wave number(cm^{-1})	Transmittance (%)
Matla FA	2210	88
	1081	76
	842	82
Majuba FA	2235	85
	1086	75
Lethabo FA	2236	82
	1096	75
	796	77
Kendal FA	2180	86
	1074	82
	918	83

Table B.11: FT-IR Peak identification of FA- *β*-CD composite (Chapter 3)

	Wave number(cm^{-1})	Transmittance (%)
Matla/*β*-CD	1152	83
	1052	70
Majuba/*β*-CD	1154	87
	1060	78
Lethabo/*β*-CD	1155	81
	1084	70
Kendal/*β*-CD	1158	87
	1062	79

Table B.12: FT-IR Peak identification of FA- *β*-CD composite (Chapter 4)

	Wave number(cm^{-1})	Transmittance (%)
FA	1338	96
	1082	88
	763	93
FA-*β*-CD	1335	98
	1195	94
	1036	90
	772	95
FA-*β*-CD + H_2O	1160	100
	1036	95
FA-α-CD	1159	91
	1057	85
FA-α-CD + H_2O	1037	94

Table B.13: FT-IR Peak identification of hydration samples at 24 hours (Chapter 6)

	Wave number(cm^{-1})	Transmittance (%)
C	2945	98
	2174	95
	1999	95
	1416	93
	1119	96
	962	89
	876	90
	2183	94
C30FA	1446	95
	1116	93
	960	87
	917	88
	2186	94
C50FA	1439	96
	1100	90
	960	87
	2186	94
C0.025CD	1443	94
	1122	93
	951	85
	913	85

	2194	94
C0.05CD	1496	92
	1122	93
	877	84
	2196	93
C0.1CD	2000	93
	1442	95
	1142	94
	909	79
	2186	93
C30FA0.025CD	1447	94
	1113	91
	878	84
	2189	94
C30FA0.05CD	1441	95
	1115	90
	880	82
	2939	96
C30FA0.1CD	2529	96
	2174	93
	2000	93
	1483	96
	1116	92
	885	86
	2186	93
C50FA0.025CD	1443	95
	1103	88
	879	84
	2185	92
C50FA0.05CD	1105	89
	916	85
	2229	93
C50FA0.1CD	1122	88
	937	83

Table B.14: FT-IR Peak identification of hydration samples at 7 days (Chapter 6)

	Wave number(cm^{-1})	Transmittance (%)
C	3644	97
	1424	91
	1132	96
	949	88
	875	88
	3645	98
C30FA	1457	95
	953	84
	921	84
	1453	93
C50FA	976	84
	928	83
	2183	94
C0.025CD	1483	93
	1127	96
	963	87
	876	90
	2185	94
C0.05CD	1439	95
	1126	96
	962	88
	905	90
	2185	94
C0.1CD	1445	95
	1128	95
	958	86
	910	88
	2168	93
C30FA0.025CD	1997	93
	1485	94
	961	90
	874	92
	2170	94
C30FA0.05CD	1446	97
	1121	95
	961	88
	2184	93
C30FA0.1CD	1433	95
	1121	95

	958	89
	2186	93
C50FA0.025CD	1457	95
	1104	88
	879	84
	2176	93
C50FA0.05CD	1468	96
	1103	93
	966	87
	2179	92
C50FA0.1CD	1439	94
	1099	89
	965	84
	917	85

Table B.15: FT-IR Peak identification of hydration samples at 28 days (Chapter 6)

	Wave number(cm^{-1})	Transmittance (%)
C	2187	94
	1446	95
	1126	97
	962	88
	899	91
	2186	93
C30FA	1440	95
	963	86
	899	89
	2186	93
C50FA	1450	96
	964	84
	899	86
	2172	93
C0.025CD	1446	95
	1128	96
	962	86
	898	90
	2186	92
C0.05CD	1435	94
	1133	95

	961	95
	900	88
	2186	92
C0.1CD	1444	94
	1134	95
	962	92
	899	89
	2186	92
C30FA0.025CD	1444	95
	965	95
	898	89
	2186	93
C30FA0.05CD	1458	95
	963	83
	900	86
	2191	93
C30FA0.1CD	1461	95
	965	85
	903	87
	2187	94
C50FA0.025CD	1460	96
	965	86
	909	89
	2184	92
C50FA0.05CD	1454	95
	965	86
	905	88
	2188	94
C50FA0.1CD	1453	96
	964	85
	909	88

Table B.16: FT-IR Peak identification of hydration samples at 90 days (Chapter 6)

	Wave number(cm^{-1})	Transmittance (%)
C	3647	95
	2186	93
	1470	95
	963	84
	2186	92
C30FA	1483	95
	965	87
	2189	93
C50FA	1434	94
	965	85
	907	88
	3649	95
C0.025CD	2188	92
	1458	94
	963	83
	3651	97
C0.05CD	2198	94
	1453	96
	965	87
	3647	96
C0.1CD	2187	94
	1430	92
	963	84
	904	88
	2193	94
C30FA0.025CD	1453	96
	966	86
	2186	94
C30FA0.05CD	1457	96
	965	88
	2187	94
C30FA0.1CD	1456	96
	966	87
	903	90
	2199	95
C50FA0.025CD	1460	96
	967	86
	905	89
	2198	94

C50FA0.05CD	1460	96
	967	85
	904	88
	2187	94
C50FA0.1CD	1447	97
	966	87
	905	89